Identification of cisplatin resistance mechanisms and alternative treatment options for testicular germ cell tumors

Dissertation

zur

Erlangung des Doktorgrades (Dr. rer. nat.)

der

Mathematisch-Naturwissenschaftlichen Fakultät

der

Rheinischen Friedrich-Wilhelms-Universität Bonn

vorgelegt von

Kai Funke

aus

Göttingen

Bonn, 2023

Angefertigt mit Genehmigung der Mathematisch-Naturwissenschaftlichen Fakultät
der Rheinischen Friedrich-Wilhelms-Universität Bonn

1. Gutachter: Prof. Dr. Hubert Schorle
2. Gutachter: Prof. Dr. Oliver Gruß

Tag der Promotion: 12. Mai 2023
Erscheinungsjahr: 2023

Eidesstattliche Erklärung

Hiermit erkläre ich, dass diese Dissertation von mir selbst und ohne unerlaubte Hilfe angefertigt wurde. Es wurden keine anderen als die angegebenen Hilfsmittel benutzt. Ferner erkläre ich, dass die vorliegende Arbeit an keiner anderen Universität als Dissertation eingereicht wurde.

Teile dieser Arbeit wurden bereits in folgender Originalpublikation veröffentlicht:

[1] **Funke, K**.; Düster, R.; Wilson, P.D.-G.; Arévalo, L.; Geyer, M.; Schorle, H. Transcriptional CDK Inhibitors as Potential Treatment Option for Testicular Germ Cell Tumors. *Cancers* **2022**, *14, doi:*10.3390/cancers14071690.

Teile dieser Arbeit wurden in folgender eingereichten Originalpublikation (revidierte Version in Begutachtung, Stand 08.02.2023) behandelt:

[2] **Funke, K.**; Einsfelder, U.; Hansen, A.; Arévalo, L.; Schneider, S.; Nettersheim, D.; Stein, V.; Schorle, H. Genome-scale CRISPR screen reveals neddylation to contribute to cisplatin resistance of testicular germ cell tumors. *Br J Cancer*, ***revised version under revision, 2023***.

Die Publikation wurde am 06.04.2023 mit der DOI 10.1038/s41416-023-02247-5 im *Br J Cancer* veröffentlicht.

Bonn, 2023

_____

Kai Funke

List of Abbreviations

AFP	α-fetoprotein
ALDH	aldehyde dehydrogenase
APS	ammonium persulfate
ATM	ataxia telangiectasia mutated
ATR	ATM and RAD3-related
BEP	bleomycin, etoposide and cisplatin
BER	base excision repair
BRD	bromodomain
CAK	CDK-activating kinase complex
CAND1	cullin-associated NEDD8-dissociated protein 1
Cc	choriocarcinoma
CDK	cyclin dependent kinase
Cisplatin, CP	*cis*-Diamine platinum (II) dichloride
cm	centimeter
CRISPR	clustered regularly interspaced short palindromic repeats
CRL	cullin-RING ligase
CTD	carboxy-terminal domain
DAPI	6-Diamidino-2-phenylindole dihydrochloride
DDR	DNA damage response
DMEM	Dulbecco's Modified Eagle's Medium
DMF	N,N-dimethylformamide
DMSO	dimethyl sulfoxide
DNA	desoxyribonucleic acid
EC	embryonal carcinoma
EDTA	ethylene diamine tetra acetic acid
FBS	fetal bovine serum
GADD45	growth arrest and DNA-damage inducible 45
GCNIS	germ cell neoplasia *in situ*
GCT	germ cell tumor
GFP	green fluorescent protein
GO	gene ontology
h	hour(s)
HCG	human chorionic gonadotropin
HDAC	histone deacetylase
HMGB4	high-mobility-group box protein 4

HR	homologous recombination
IGCCCG	International Germ Cell Consensus Classification
IGFR1	insulin-like growth factor receptor 1
M	molar
MDM2	mouse double minute 2 homolog
min	minute
ml	milliliter
mM	millimolar
MMR	mismatch repair
mRNA	messenger RNA
MSI	microsatellite instability
mtDNA	mitochondrial DNA
NAE1	NEDD8 activating enzyme
NEDD8	neuronal precursor cell expressed developmentally down-regulated protein 8
NEDP1	NEDD8-specific protease 1
NELF	negative elongation factor
NER	nucleotide excision repair
NHEJ	nonhomologous end joining
nm	nanometer
nM	nanomolar
NOXA	phorbol-12-myristate-13-acetate-induced protein 1
NTT	normal testis tissue
PARP	poly (ADP-ribose) polymerase
PDGFRb	platelet-derived growth factor receptor b
PD-L1	programmed death ligand 1
PGC	primordial germ cell
PMS	N-methyl dibenzo pyrazine methyl sulfate
PROTAC	proteolysis targeting chimera
PTEFb	positive transcription elongation factor b
PUMA	p53 upregulated modulator of apoptosis
RBX	RING-box protein
RNA	ribonucleic acid
RNA Pol II	RNA polymerase II
ROS	reactive oxygen species
rpm	rounds per minute

RPMI	Roswell Park Memorial Institute medium
SAM	synergistic activation mediator
SDS	sodium dodecyl sulfate
sgRNA	single guide RNA
tCDK	transcriptional cyclin dependent kinase
TEMED	tetramethyl ethylenediamine
TCGA	The Cancer Genome Atlas
TGCT	testicular germ cell tumor
TLS	translesional synthesis
TME	tumor microenvironment
UBA3	ubiquitin-activating enzyme 3
UCHL3	ubiquitin C-terminal hydrolase isoenzyme 3
v/v	volume per volume
xg	relative centrifugal force
YST	yolk sac tumor
µg	microgram
µl	microliter
µm	micrometer
µM	micrometer

Table of Contents

List of Figures

List of Tables

Summary

Type II testicular germ cell tumors (TGCTs) are the most prevalent tumors in young men aged 18 to 35 years. TGCTs are classified as seminomas and non-seminomas. Embryonal carcinomas (EC), representing the cancer stem cell population of non-seminomas, can differentiate into yolk sac tumors (YST), choriocarcinomas (Cc) and teratomas. There are curation rates of 95% due to high sensitivity towards cisplatin-based chemotherapy. However, several patients develop cisplatin resistant tumors or drug intolerance facing poor prognosis due to lacking treatment alternatives. With this study I aimed to identify novel cisplatin resistance mechanisms and investigated the potential of different compounds for TGCT treatment.

Firstly, cyclin dependent kinase (CDK) inhibitors were investigated. While CDK inhibitors targeting the cell cycle have been studied extensively, no data were available describing transcriptional CDK (tCDK) inhibitors in TGCTs. tCDKs (CDK7, 8, 9 12, 13) are crucial for RNA polymerase II mediated mRNA transcription. Initially, the cytotoxic effects of Dinaciblib as well as Flavopiridol (both panCDK inhibitors), YKL-5-124 (CDK7), SY0351 (CDK7, 12, 13), THZ1 (CDK7, 12, 13), THZ531 (CDK12, 13), NVP2 (CDK9) and the CDK9 degrader THAL-SNS-032 were investigated on cisplatin resistant and cisplatin sensitive TGCT cell lines. Application of SY0351 and NVP2 showed very strong decrease in viability on the seminoma (TCam2) and EC (2102EP, NCCIT) cell lines as well as on the resistant sub cell lines (2102EP-R, NCCIT-R). YKL-5-124 treatment revealed a highly cytotoxic effect in 2102EP and 2102EP-R cells. The viability of the fibroblast cell line (MPAF) was not affected at all upon drug application. In 2102EP and TCam2 cells high levels of apoptosis induction as well as moderate cell cycle deregulation have been detected after NVP2, SY0351 and YKL-5-124 treatment. On mRNA level different cellular responses have been identified after NVP2 and SY0351 application while YKL-5-124 treated cells revealed a common response. NVP2 exposure of 2102EP and TCam2 cells resulted in deregulation of transcription and downregulation of mRNA processing, respectively. After YKL-5-124 application reduced mRNA processing and negative regulation of gene expression in 2102EP, TCam2 and MPAF cells was observable. The key findings after SY0351 exposure were upregulation of stress response and ubiquitin pathway deregulation. Thus, especially the cell line specific response after treatment with the highly potent inhibitors NVP2 and SY0351 suggests an opportunity for personalized therapy in seminomas and ECs.

Next, I aimed to identify cisplatin resistance mechanisms in TGCTs using a genome scale CRISPR/Cas9 activation screen in 2102EP and JAR (Cc) cell lines. Aside from already known factors involved in DNA damage repair and cell cycle regulation, overexpression of the neddylation pathway core component NAE1 resulting in overactivated neddylation has been found. Neddylation is a posttranslational modification which regulates stability, function and

localization of target proteins. The best characterized substrates of neddylation are cullins which are part of cullin-RING ligases (CRLs). Cullin neddylation activates the E3 ubiquitin ligase function of the CRL complex revealing polyubiquitination and subsequent proteasomal degradation of various substrates such as tumor suppressor proteins p21 and p27. Cisplatin resistance in TGCTs based on increased neddylation pathway activity could be validated by NAE1/GFP overexpression showing significantly decreased cisplatin sensitivity. Interestingly, NAE1 abundance is highest in TGCT tissues compared to other tumor entities and normal tissues. Thus, targeting the neddylation pathway seems to be a reasonable strategy. The covalent NAE1 inhibitor MLN4924 revealed strong cytotoxic effect in different TGCT cell lines. Most interestingly, MLN4924 application in combination with cisplatin significantly increased cytotoxicity compared to mono treatment in cisplatin sensitive and resistant cell lines. Further, combination treatment revealed G2/M-phase cell cycle arrest as well as strong apoptosis induction in 2102EP, JAR and TCam2 cells. Notably, MPAF fibroblast control cells were not affected all. Transcriptome analysis of 2102EP and JAR cells revealed elevated expression of apoptosis associated genes, deregulation of cell cycle and strong mesoderm/endoderm differentiation tendencies upon MLN4924 treatment in combination with cisplatin.

To conclude, NVP2, SY0351 as well as MLN4924 revealed not only strong cytotoxic effects on parental TGCT cell lines but also on cisplatin resistant cell lines. Thus, these compounds might be promising alternative treatment options for TGCT patients independent of chemotherapy resistance.

1. Introduction

1.1. Male germ cell development

The life of many living organisms such as mammals starts with the fertilization process which describes the fusion of highly specialized cells called gametes. These germ cells comprise male sperm as well as female oocytes carrying all genetic and epigenetic information necessary for the development of a new individual.

Development of germ cells is initiated during early embryogenesis. In humans, primordial germ cells (PGCs) are specified 2 weeks after fertilization in the nascent amnion [3,4]. Release of BMP4 and WNT3A promotes PGC formation from extraembryonic tissues surrounding the yolk sac [3–5]. High levels of WNT transactivate *EOMES* expression which further induces activation of the key factor, for PGC specification, *SOX17*. Interestingly, SOX17 was found to be crucial for activation of *BLIMP1* expression. BMP2 which is expressed in the extraembryonic mesoderm together with BMP4 is responsible for induction of *TFAP2C* expression. Together with SOX17 and BLIMP1 it forms an important transcription factor network which is responsible for specification and segregation of the first lineage from the epiblast upon implantation [4,6,7]. These factors repress the somatic cell differentiation program, enforce maintenance of pluripotency and regulate epigenetic reprogramming. 4 weeks after fertilization specified PGCs start migrating along the developing hindgut towards the genital ridges. During this process, PGCs arrest their cell cycle at G2-phase when induction of extensively imprinting erasure by demethylation and change of histone modifications at genome wide level occurs [3,8,9]. 4 to 6 weeks post embryo implantation the PGCs in the genital ridge resume proliferation and are now termed gonocytes which are characterized by expression of *MAGE-A4*, *DAZL*, *KIT*, *PLAP*, *POU5F1*, *TFAP2C*, *UTF1* as well as *VASA* [10,11]. Until birth gonocytes are prevented from mitosis by G0 cell cycle arrest. Up to 6 months after birth gonocytes differentiate into spermatogonia, subsequently staying dormant for the next 5 to 7 years. During puberty spermatogonia proliferate by mitosis and after following meiosis eventually differentiate into male gametes. The final maturation to spermatozoa occurs in a process called spermiogenesis [5].

1.2. Malignant germ cell development

Germ cell tumors (GCTs) are a heterogenous group of neoplasms with the highest incidence of more than 50% of all cases in young men aged 20-34 years [12,13]. During the last decade in western countries case numbers have been increased steadily emphasizing the importance to gain deep understanding of this malignancy [14]. There are only few validated risk factors for GCTs which makes it difficult to specify prevention measures. Proven factors increasing

the prevalence for GCTs are cryptorchidism, genetic predisposition, Klinefelter's syndrome and infertility [15,16]. Type I, II and III GCTs are classified according to genomic imprinting, developmental potential as well as anatomical site (**Figure 1**) [17].

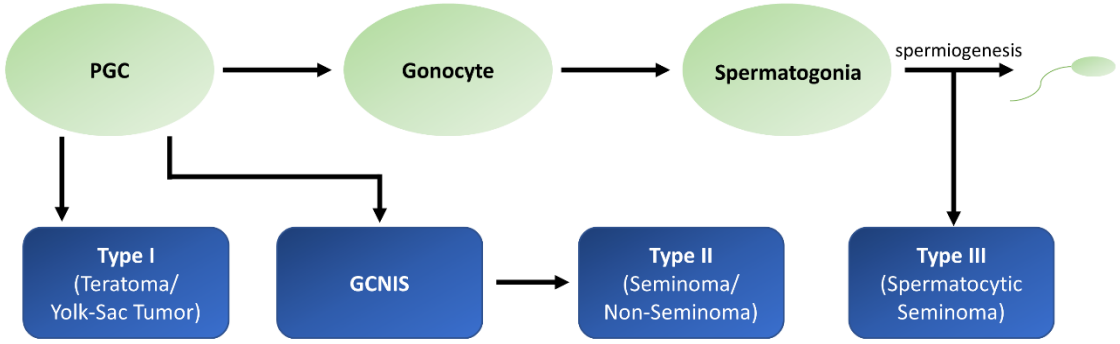

Figure 1: Type I, II and III GCT development. Modified from [9]. Type I GCTs are mainly present as teratoma or YST and directly arise from PGCs. Type II GCTs develop from a precursor lesion termed germ cell neoplasia *in situ* (GCNIS) which originates from an arrested PGC with acquired genetic or epigenetic aberration. These tumors occur as seminomas or non-seminomas. Type III GCTs arise during spermiogenesis.

1.2.1. Type I germ cell tumors

Type I GCTs are limited to young children with rare occurrence of 11.7 cases per million boys [18]. These tumors are usually present as non-seminomas which are differentiated into teratomas or yolk sac tumors (YSTs) [17]. A distinction is made between immature and mature teratomas based on the differentiation status [19]. Mature teratomas occur almost exclusively in infants, while mixed forms of immature and mature teratomas are often found in young adults [19,20]. In YSTs α-fetoprotein (AFP) was found to be highly expressed serving as robust biomarker [20]. Pediatric teratomas are in most cases benign and are treated by surgery with high overall survival. However, incomplete removal can result in YSTs which are prone to metastasize and therefore need to be treated with chemotherapy [17]. Type I GCTs are considered to arise directly from PGCs indicated by the presence of a partially abolished genomic imprinting pattern in the healthy and in the malignant cell type. [20]. It is believed, that failure of downregulation of pluripotency program after arrival at the genial ridge is a key factor for the malignant transformation [9] (**Figure 1**).

1.2.2. Type II germ cell tumors

Type II GCTs mainly emerge in the testes referred to as testicular germ cell tumors (TGCT). Only few patients show type II GCT occurrence along the body midline [9,17]. Type II TGCTs occur with a rate of 59 cases per million people [13] and represent the most prevalent tumors in young men aged 20 to 39 years [12]. This tumor entity arises from developmentally arrested

PGCs which failed to downregulate PGC and pluripotency associated genes presumably mediated by acquired genetic or epigenetic aberrations transforming into the precursor lesion termed germ cell neoplasia *in situ* (GCNIS) [21–23] (**Figure 1**). GCNIS cells asymptomatically stay dormant in the spermatogonial niche until late puberty [9]. When hormone and growth signaling is initiated by Sertoli and Leydig cells, GCNIS eventually proliferates and progresses into invasive type II TGCTs which are classified in seminomas and non-seminomas [24] (**Figure 2**). Seminomas display high morphological similarities with GCNIS and PGCs [17,25]. Further, transcriptomic analysis of PGCs, PGC like cells and seminoma derived TCam2 cells revealed close clustering of differentially expressed genes. In detail, a PGC-like expression pattern has been shown for the seminoma cells indicated by pluripotency (*LIN28A*, *POU5F*, *NANOG*, *TNAP*, *PRDM14*, *SALL4*), early germ cell (*PRDM1*, *cKIT*, *TFAP2C*, *DND1*, *CD38*) and late germ cell markers (*TDR5*, *TDRD9*, *TDRD12*, *RN17*, *PRAME*, *DDX43*) [17,26]. Interestingly, seminomas also express the key PGC-specifier *SOX17* which regulates the expression of *BLIMP1*, *TFAP2C* as well as *PRDM14*. These factors are important for repression of somatic genes as well as maintaining latent pluripotency [26,27]. Due to a high range of similarities with PGCs, seminomas are described as default pathway of GCNIS [17].

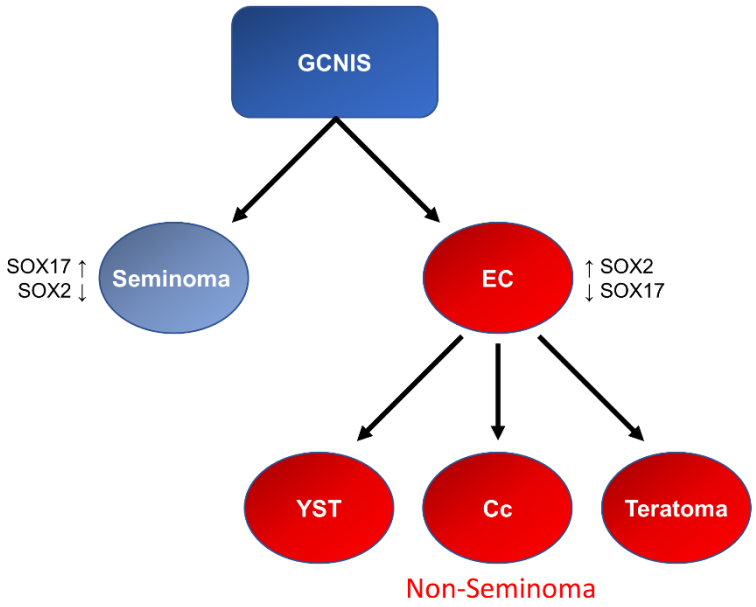

Figure 2: Schematic of type II TGCTs. Modified from [9]. Type II TGCTs arise from the precursor lesion GCNIS which eventually transforms into seminoma (high level of SOX17) or non-seminoma fate (EC, YST, Cc, teratoma). Totipotent ECs (high level of SOX2) are able to differentiate into YSTs, Ccs and teratomas.

The group of non-seminomas comprises embryonal carcinoma (EC), yolk sac tumor (YST), choriocarcinoma (Cc) and teratoma. ECs are considered as the non-seminoma cancer stem cell population displaying similarities to embryonic stem cells such as features of pluri- and totipotency [17,27]. Further, ECs are able to differentiate into all three germ layers and

extraembryonic tissues represented by YST, Cc and teratoma [17]. Notably, non-seminomas share expression of *NANOG* and *POU5F* (OCT3/4) expression with seminomas but additionally express *DNMT3B*, *DNMT3L*, *NODAL*, *CRIPTO*, *CD30* and *SOX2* [9,17,23,25]. OCT3/4 is a general marker which is highly expressed in all type II TGCT sub entities. In contrast, the expression of the transcription factors *SOX2* and *SOX17* in ECs as well as in seminomas, respectively, is a major difference which is exploited as biomarker to identify the respective tumor sub entity [25,28]. Of note, most type II TGCTs display a 12p gain which might be an important factor for invasiveness of TGCTs. The locus encodes for the pluripotency- and PGC-related genes *NANOG*, *GDF3* and *DPPA3* [17,29].

1.2.3. Type III germ cell tumors

Type III GCTs are benign spermatocytic seminomas (**Figure 1**). Due to specific pattern of imprinting which is similar to spermatogonia or spermatocytes it is believed that spermatocytic seminomas develop during spermiogenesis [9,17]. This tumor entity is usually only found in men older than 50 years with a very low incidence (0.3-0.8 cases per 1 million people) [17]. Type III GCTs can be cured in most cases by orchiectomy [17].

1.3. Treatment of type II TGCTs

TGCTs are diagnosed using physical examination, ultrasonography and determination of tumor markers like AFP, human chorionic gonadotropin (HCG) and lactate dehydrogenase (LDH). During first line treatment complete orchiectomy is performed. Tumor marker levels and histological reports of the removed testicle are used for tumor staging according to the guidelines of International Germ Cell Consensus Classification (IGCCCG), EAU and ESMO [30–35].

Seminomas and non-seminomas are classified in stage I to III. Stage I seminomas display curation rates of more than 99% independent of the treatment regimen. Thus, minimizing site effects is the major goal for this tumor type. Most commonly surveillance is considered as the best strategy. Only in few high risk tumors adjuvant chemotherapy including one carboplatin cycle is preferred [32]. Upon relapse highly effective radiotherapy can be applied in seminoma patients with very good response rates of around 70%. Stage II seminomas which come with metastases are treated with three to four cycles of bleomycin, etoposide and cisplatin (BEP) or radiotherapy [32]. In case of relapse, removal of the tumor by surgery followed by salvage chemotherapy would be the appropriate therapeutic option [31].

For stage I non-seminomas surveillance or one cycle of BEP is the preferred strategy. Due to extremely high platinum sensitivity of this tumor type, stage I non-seminomas display curation rates between 98 and 100% [32]. For relapsed tumors the IGCCCG guidelines recommend application of four cycles BEP followed by resection if residual tumor is present [31]. Stage II and III non-seminomas usually appear with metastases [31]. Patients are treated with three to four cycles of BEP [32]. Upon relapse, residual tumor tissue might be removed by surgery followed by treatment with salvage chemotherapy [31]. If second line salvage treatment fails, desperation surgery is often the only option [31].

Around 20% of patients with metastatic non-seminomas display cisplatin resistance [14,36,37]. Unfortunately, effective alternative therapies are rare. The only options are high-dose chemotherapy combined with a stem cell transplantation for reducing the side effects or desperation surgery [31,38]. Finally, an overall survival rate of only 50% is reached for these patients [38].

1.3.1. Cisplatin in TGCT treatment

The platinum (IV) complex was initially discovered as an inhibitor for bacterial proliferation by Rosenberg and colleagues in the 1960s [39]. Later, they analyzed the effect of cisplatin on tumor cells demonstrating a cytotoxic effect after treatment of Sarcoma tumor in Swiss white mice proven by significantly reduction of tumor size and long-term survival of the mice [40,41]. The establishment of cisplatin as an anticancer drug in humans followed in the 1970s resulting in highly effective chemotherapy. Especially the treatment of GCTs improved dramatically. The five year survival rate for TGCT patients increased from 72% in 1970−1973 to 91% in 1983−1985 [42].

On a molecular level the cytotoxic effect of cisplatin is based on a DNA damaging effect [43,44] (**Figure 3**). It has been shown that the passive compound influx into the cell is dependent on the copper transporter CTR1 [45]. In the cell cisplatin is converted into the pharmacologically active form by aquation which is the exchange of two chloride groups with water molecules. This conformation allows binding of cisplatin to purine DNA bases resulting in formation of inter- and intra-strand crosslinks. The DNA damages lead to transcription inhibition and reduced cell proliferation by cell cycle arrest. Next, the DNA lesion is either repaired or the cell initiates apoptosis [43,46]. Cisplatin cytotoxicity is also mediated by oxidative stress. Increased amount of reactive oxygen species (ROS) lead to mitochondrial dysfunction and DNA damage resulting in apoptosis [44,47].

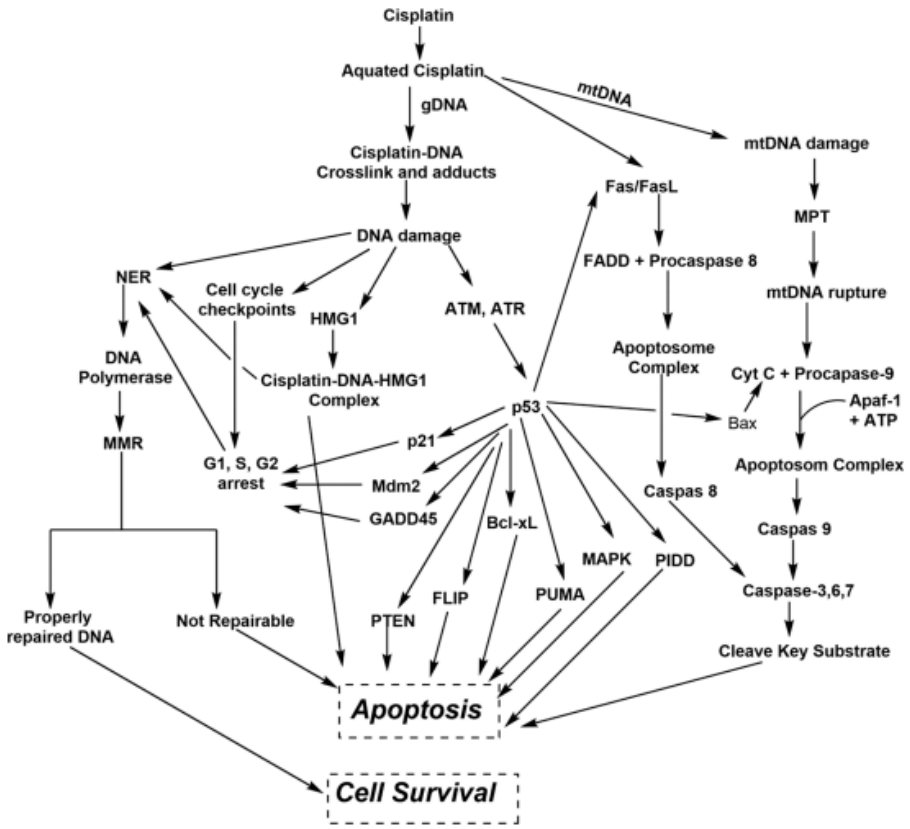

Figure 3: Cisplatin – mode of action in the cell. Reprinted from [46]. Cisplatin induces DNA damages resulting in activation of the DDR system. This leads to an activation of p53 which triggers apoptosis via different pathways (PTEN, PUMA, MAPK, Fas/FasL, etc.). Apoptosis is also induced, if the cell fails to repair the DNA lesions via the NER and the MMR system. Further, cisplatin causes mitochondrial DNA (mtDNA) damages which can result in caspase mediated apoptosis induction.

Further, the DNA damage response (DDR) system is crucial for cisplatin induced cytotoxicity. In particular, the cell is arrested in the cell cycle and induces different DNA repair systems/mechanisms: mismatch repair (MMR), nucleotide excision repair (NER), nonhomologous end joining (NHEJ) and homologous recombination (HR). Repeated DNA repair cycles can end up in formation of double strand breaks as well as activation of DNA damage response factors [44,48]. The protein kinases ATM (ataxia telangiectasia mutated), ATR (ATM and RAD3-related) and DNA-PKcs (DNA-dependent protein kinase catalytic subunit) are responsible for DDR induction. ATM is also responsible for activation of the tumor suppressor protein p53. Additionally, ATM mediated MDM2 (Mouse Double Minute 2 Homolog) phosphorylation revealing decreased poly-ubiquitination of p53 which is thereby stabilized [49–51]. Accumulation of p53 leads to increased expression of the cell cycle inhibitor p21 as well as GADD45 (growth arrest and DNA-damage inducible 45) which is an important factor for DNA repair initiation. Highly elevated levels of p53 trigger activation of pro-apoptotic Bcl-2 family members PUMA (p53 upregulated modulator of apoptosis) and NOXA (Phorbol-12-myristate-13-acetate-induced protein 1) as well as induction of the Fas/FasL pathway resulting in caspase mediated apoptosis [44,46]. p53 binding thereby prevents the anti-apoptotic

function of Bcl-xL (B-cell lymphoma-extra-large) as well as overexpression of *PTEN* supporting apoptosis [46].

Of note, the major cause of hypersensitive response of TGCTs towards cisplatin is based on almost absent error prone DNA repair mechanisms in germ cells which rather induce apoptosis to avoid passing on mutations to the germ line [52,53]. In detail, high-mobility-group box protein 4 (HMGB4), which plays an important role in avoiding NER-pathway repair by binding to cisplatin-DNA crosslinks, is predominantly expressed in the testes and contributes to cisplatin hypersensitivity [54]. Additionally, several NER-associated proteins such as ERCC1, XPF and XPA display only minor expression in TGCTs. Induced upregulation of ERCC1 and XPF revealed decreased cisplatin sensitivity suggesting that ERCC1-XPF axis is the limiting factor for NER repair pathway. Thus, low levels of ERCC1 as well as XPF are another crucial factor for hypersensitivity of TGCTs towards cisplatin [55,56]. Further, impaired DNA double strand repair indicated by low expression of Poly (ADP-ribose) polymerase (PARP) in TGCTs is important for the increased sensitivity [57]. P53 is a key player for the strong impact of cisplatin on TGCTs. It induces at the same time extrinsic apoptosis via transactivation of FAS receptor expression [58] and intrinsically activates expression of pro apoptotic proteins PUMA and NOXA [59]. Further, ECs were found to be even more sensitive to cisplatin compared to other tumor entities which correlates with exclusively high levels of the pluripotency factor OCT3/4 consequently repressing *CDKN1A* (p21) and upregulating *PUMA* as well as *NOXA* expression. Low abundance of p21 results in progression of cell cycle up to the G2/M checkpoint where the cells are arrested. Due to their inability to repair DNA damages, apoptosis is initiated [60]. G2/M phase cell cycle arrest is supported by overexpression of miRNA-302a in TGCTs upon cisplatin application. Despite high basal expression levels in TGCTs cisplatin application even further elevates miRNA-302a expression which is an important factor for hypersensitivity [61,62]. Another very interesting point is the epigenetic status of TGCTs. Seminomas are hypomethylated, ECs display intermediate methylation and the more differentiated teratomas reveal hypermethylation which correlates with the cisplatin sensitivity. Seminomas and ECs are highly sensitive while teratomas are less sensitive. The reason for elevated sensitivity under hypomethylated conditions might be explained by a more open and less dense packed DNA. This increases the accessibility for the damaging agent cisplatin as well as a stronger DNA damage response induced by an inherent transcriptional plasticity of this type of chromatin [63].

1.3.2. Cisplatin resistance in TGCT treatment

Therapeutic failure of TGCT treatment is often caused by cisplatin resistance. For better overview already known mechanisms contributing to cisplatin resistance are grouped into pre-

target, on-target, post-target and other mechanisms. Pre-target is defined by an effect inducing resistance before cisplatin binds to its actual target which is the DNA. On-target describes the impaired sensitivity directly associated with cisplatin-DNA adducts while the post-target mechanisms appear as downstream effects of signaling pathways activated by cisplatin-mediated DNA damage eventually leading to apoptosis. Altered pathways or factors disturbing the normal cisplatin response cascade leading to resistance are considered as other or off-target effects [44,63,64] (**Figure 4**). Of note, cisplatin resistance is multifactorial based on an interplay of various mechanisms [64].

In detail, already identified pre-target mechanisms are associated with decreased cisplatin levels in the cell. Resistance might be induced by decreased CTR1 expression and/or increased copper-transporting ATPases ATP7A/ATP7B expression resulting in reduced cisplatin influx and extended efflux [45]. Further, elevated detoxification by cytoplasmic scavengers such as glutathione and metallothionein which bind to cisplatin were found to contribute to cisplatin resistance [65,66]. The pre-target mechanisms are not considered to be the key factors in cisplatin resistance of TGCTs due to missing robust clinical evidence [64].

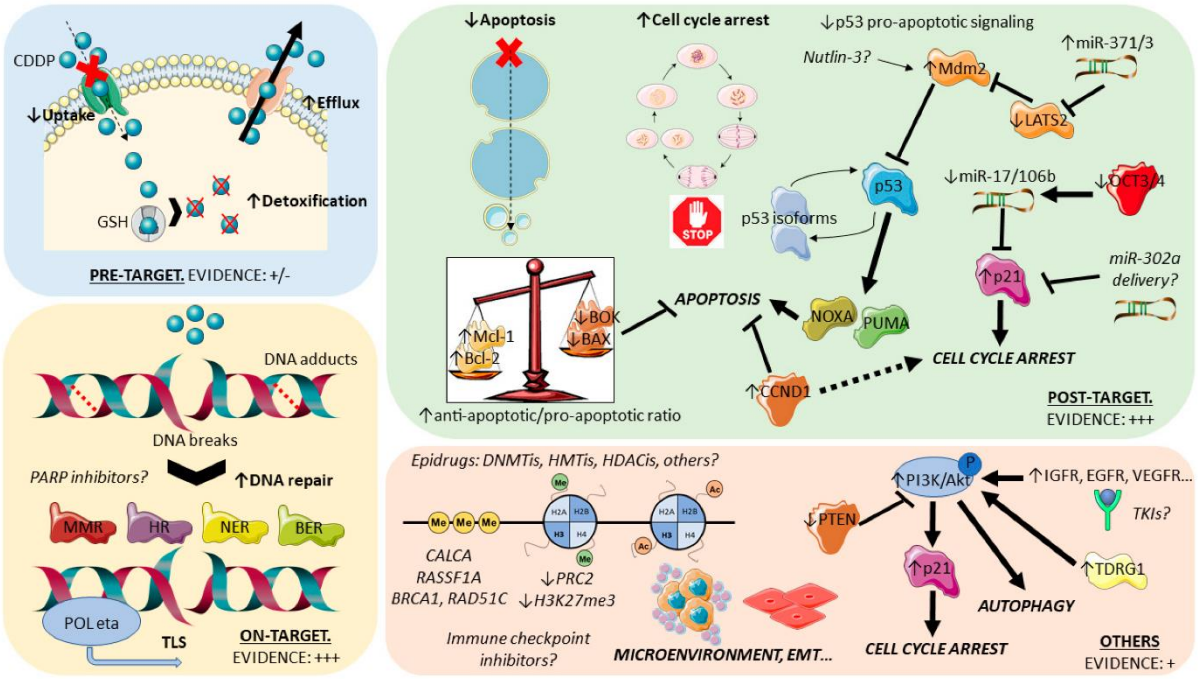

Figure 4: Cisplatin resistance mechanisms of TGCTs. Reprinted from [64]. Factors for cisplatin resistance are sub divided in pre-, on-, post-target and other mechanisms. Pre-target: Reduced drug uptake by downregulation of *CTR1* expression. Increased cellular drug efflux by upregulation of *ATP7A*/*ATP7B* expression. Detoxification by elevated levels of cytoplasmatic scavenger proteins such as glutathione. On-target: Highly activated DNA repair systems evade apoptosis initiation. Post-target: Increased *MDM2* expression causes p53 degradation subsequently preventing apoptosis. Others: Overactivation of PI3K/AKT pathway triggers p21 mediated cell cycle arrest.

On-target and post-target effects are studied comprehensively and more in detail. In cisplatin-resistant TGCTs improved DNA repair systems were observed [52] or DNA damages were

bypassed by increased expression of specific polymerases eventually evading apoptosis [67]. Defective MMR system, microsatellite instability (MSI) and BRAF mutations have been observed in resistant TGCTs. The MMR system cannot repair cisplatin induced DNA crosslinks but it is important for the detection of DNA-cisplatin adducts and subsequent induction of apoptosis cascade. Interestingly, BRAF mutations and MSI are associated with decreased expression of *MLH1* which is together with *MLH2* crucial for a functional MMR system [68,69]. Due to lack of these proteins the tumor cell is prone to bypass DNA-cisplatin adducts and progresses with DNA replication behind the lesion by activation of translesional synthesis (TLS) [70]. This process is guided by increased levels of specific DNA polymerases such as REV1, REV3, REV7 and POLH [71]. Another option for cisplatin resistance was demonstrated by Awuah *et al.* who performed knockout of HMGB4 which is important for shielding of DNA lesions to prevent NER. Thus, lack of HMGB4 triggers NER and prohibits apoptosis in TGCTs [54]. Another factor for increased chemoresistance might be the elevated expression of NER pathway compounds ERCC1 and XFP triggering cisplatin-DNA intrastrand crosslink repair [55].

Disruption of the p53/MDM2 axis as well as direct interference with apoptosis is implicated in the post-target group [72,73]. It has been found that overexpression of MDM2 which subsequently inactivates p53 is directly linked to cisplatin resistance due to prevention of PUMA and NOXA induced apoptosis [58]. In cisplatin resistant TGCT cells upregulation of the platelet-derived growth factor receptor b (PDGFRb) and its corresponding ligand PDGF-b was detected resulting in activation of the PDGFR/PI3K/AKT pathway. This leads to p21 phosphorylation as well as MDM2 activation. Thus, MDM2 inhibition of p53 prevents apoptosis induction while activated p21 accumulates in the cytoplasm triggering G1 phase cell cycle arrest [74,75]. More research is necessary regarding pro- and antiapoptotic factor ratios such as BOC/MCL1 and BAX/BCL2. Disbalance of these factors might also contribute to cisplatin resistance [64]. Highest level of insulin-like growth factor 1 receptor (IGFR1) was found in cisplatin resistant TGCT cells while knockdown re-sensitized the cells towards cisplatin [76]. Cell cycle regulation is another important factor for cisplatin resistance which has been demonstrated by overexpression of *CCND1* (CyclinD) [77].

Autophagy is characterized as off-target mechanism which is usually upregulated in cisplatin resistant tumors. Further, increased levels of survival factors like ERBB2 and heat shock protein 27 were found to contribute to cisplatin resistance [78]. The epigenetic methylation landscape has also been identified as an important factor. Promotors of genes such as *RASSF1A* and *HIC1* are hypermethylated in resistant non-seminomas [79]. In general, rather hypermethylated tumors like teratomas display resistance while hypomethylated seminomas are particularly sensitive [63]. Interestingly, differences in micro RNA expression have been

observed between resistant and sensitive tumors with high levels of miRNA371-373 in cisplatin resistant TGCTs. It is speculated that these micro RNAs interfere with the p53 mediated apoptosis signaling pathway [80]. Two recent studies investigated the role of chromosomal aberrations and genomic mutations in detail using a genome wide approach. Surprisingly, they showed that resistant TGCTs acquired significantly enriched copy number alterations (chromosomes 1, 4, and 18 deficiency, gains of chromosome 8), more single nucleotide polymorphisms as well as higher number of mutations [81,82]. The tumor microenvironment (TME) seems to be involved in resistance mechanisms as well. Interestingly, it could be shown that the more densely the tumor cells are packed in a 3D matrix the less cisplatin entered the cells resulting in decreased cisplatin sensitivity [83]. Further, the interaction between tumor infiltrating immune cells and cancer cells promotes tumor growth and progression [44]. Bad outcome has been observed in patients with TGCTs expressing high levels of programmed death ligand 1 (PD-L1). Due to PD-1/PD-L1 signaling the tumor cells are able to evade the immune response of the TME by inhibition of T-cell proliferation, downregulation of interleukin 2 production, etc. The highest levels of PD-L1 were observed in Ccs while declining levels are present in ECs, Teratomas, YSTs and lowest PD-L1 expression was found in seminomas [84]. Cancer stem cells are a small portion of cells in a tumor characterized by certain surface markers like CD24, CD44, CD133 and aldehyde dehydrogenases (ALDH). In mixed non-seminomas ECs represent the stem cell population. These tumor cells are the malignant counterpart to normal embryonic stem cells and have the ability to continue constant proliferation and to self-renew. Interestingly, elevated ALDH1A3 expression levels as well as increased aldehyde dehydrogenase activity was found in chemotherapy resistant EC cell lines [44,83].

Taken together, all these mechanisms such as reduced CTR1 mediated cisplatin influx, elevated efflux by ATP7A/ATP7B transporters, increased detoxification, improved DNA damage repair, DNA damage bypass, alterations in apoptosis signaling pathways, epigenetic changes as well as TME, etc. contribute to cisplatin resistance in TGCTs. This clearly emphasizes the fact that cisplatin resistance is multifactorial with many different contributing mechanisms. Thus, it is highly important to identify all possible factors involved in that process.

1.3.3. Alternative treatment options

Due to lacking clinical approved alternatives to chemotherapy in cisplatin resistant TGCTs different compounds such as epigenetic drugs, immunotherapy, other single agents or combination treatment with cisplatin are studied in preclinical and clinical trials [44]. The main target of immune system directed drugs is the PD-1/PD-L1 interaction. In different phase II clinical trials treatment of refractory TGCTs with PD-1/PD-L1 inhibitors like Pembrolizumab or

Avelumab did not reveal any significant antitumoral effect [85,86]. Another interesting approach on TGCT cell lines with bispecific antibodies (Catumaxomab) which specifically bind the tumor cells and recruit T-cells as well as natural killer cells revealed promising initial results. The antibody binds to the surface protein EpCAM which is highly expressed in TGCT cell lines but almost absent in a Sertoli cell line and in fibroblasts. Binding of CD3 and due to the Fc domain toxic effector cells are attracted [87].

Several epigenetic drugs like JQ1 (BRD2, BRD4, BRDT inhibitor), Romidepsin (HDAC1, 2 inhibitor), Quisinostat (HDAC1 inhibitor), MZ-1 (BRD2, BRD4, BRDT degrader), JIB-04 (KDM5A, JARID1A inhibitor) displayed promising effects in TGCT treatment in cisplatin sensitive and resistant tumor cells *in vitro* and/or *in vivo* [88–91]. The second-generation DNA methyltransferase inhibitor Guadecitabine was successfully investigated in pre-clinical and clinical studies. *In vivo* experiments in a xenografted mouse model revealed high sensitivity of cisplatin resistant EC cells towards the inhibitor which was mediated by altered transcription resulting in activation of immune response associated pathways and p53 targets as well as downregulation of pluripotency. Moreover, the cisplatin resistant cells were re-sensitized by the treatment [92]. Additionally, Guadecitabine was investigated in combination with cisplatin in a clinical phase I study in patients with relapsed cisplatin resistant TGCTs. The overall response rate in patients was 23% while the clinical benefit rate revealed 46% indicating a therapeutic proceeding in at least several cases [93]. Another interesting target for refractory TGCT treatment is the ALDH which is overexpressed in all TGCT subtypes. *In vitro* and *in vivo* models demonstrated the therapeutic potential of the ALDH inhibitor Disulfiram [83]. The compound is under investigation in combination with cisplatin in a clinical phase II study for patients with refractory TGCTs (NCT03950830).

Further, single agent therapeutics or in combination with cisplatin have been investigated in pre-clinical and clinical studies with different outcomes. The microtubule inhibitor Cabazitaxel revealed only modest therapeutic benefit in a clinical study [94] while the mTOR inhibitor Everolimus failed in treatment of refractory TGCTs [95]. Pazopanib which is a tyrosine kinase inhibitor was investigated in patients with relapsed and cisplatin resistant TGCTs revealing only minimal beneficial effects [96]. Other drugs targeting PARP which is involved in base excision repair (BER) of cisplatin induced DNA damages. Two PARP inhibitors were studied in clinical trials. Olaparib mono treatment or Veliparib in combination with Gemcitabine and carboplatin revealed low efficacy in patients with refractory TGCTs [97,98]. CD30, which is notably expressed in ECs, has been identified as an additional target for tumor directed treatment. Interestingly, maintained CD30 expression after initial chemotherapy is correlated with a poorer outcome. In this context the CD30 antibody–drug (monomethyl auristatin E) conjugate Brentuximab Vedotin was investigated in TGCT cell lines revealing strong

cytotoxicity as well as an anti-tumor bystander effect of CD30 negative cells cocultured with CD30 positive ECs mimicking mixed non-seminomas [99]. Based on these promising effects Brentuximab Vedotin was investigated in clinical studies revealing partially beneficial effects for CD30 positive TGCT treatment [100,101].

Further, CDK inhibitors are an interesting compound group which turned out to potentially support TGCT treatment. The cell cycle associated CDK inhibitors Palbociclib and Ribociclib targeting CDK4 and 6 were investigated in pre-clinical studies and clinical trials [102,103]. TGCT cell lines derived from different entities (seminoma, EC, Cc) as well as cisplatin resistant sub cell lines revealed very promising results for Palbociclib treatment in combination with Ribociclib [102]. In contrast application of Palbociclib in retinoblastoma positive teratoma patients revealed only moderate beneficial anti-tumoral effects [103]. CDK inhibitors are covered in detail in chapter 1.6.

Various treatment approaches targeting CD30, cell cycle CDKs, PARP, mTOR pathway, tyrosine kinases, ALDH, DNMT or the immune system tried to overcome cisplatin resistance in TGCT. Despite promising pre-clinical results most clinical trials revealed only limiting drug effectivity in the patients calling for further research to find novel treatment options for TGCTs.

1.4. TGCT models

To investigate TGCTs *in vitro* different cell culture models are available. Non-seminomas are represented by several cell lines which are EC cell lines such as 2102EP, NCCIT as well as NT2/D1 and the choriocarcinoma cell line JAR. The TCam2 cell line resembles seminomas [9]. NCCIT and 2102EP are derived from a mixed non-seminoma displaying pluripotency and nullipotence features, respectively. The pluripotency stem cell markers *SOX2*, *POU5F*, *NANOG*, *TRA-1-60*, *TRA-1-81* as well as *ALPL* (alkaline phosphatase) are expressed in NCCIT and 2102EP cells. Interestingly, exposure of retinoic acid drives NCCIT cells into mesoderm, endoderm and ectoderm differentiation modeling teratoma growth while 2102EP cells lack the differentiation ability. Xenografted NCCIT cells in nude mice grow as mixed non-seminoma. In contrast, the nullipotent 2102EP cells remain their EC character. Morphologically, both cell lines grow in a uniform monolayer forming high density clusters [9,104,105]. NT2/D1 cells displayed similar morphology. This cell line is clonally developed from the NTERA-2 cell line which resembles a pluripotent EC. Retinoic acid treatment induces neuronal cell differentiation *in vitro* [106]. The JAR cell line is derived from a Cc and grows *in vitro* as well as *in vivo* as Cc [9,107].

The only model available for seminomas is the TCam2 cell line which displays expression of TGCT and early germ cell markers such as *TFAP2C*, *LIN28*, *NANOG* and *POU5F* and

characteristic seminoma markers *SOX17*, *KIT* as well as *PRDM1* [9]. TCam2 cells are shaped flat and polygonal and contain a large cytoplasm [108].

Different cisplatin resistant TGCT (2102EP-R, NCCIT-R, NT2/D1-R) cell lines are available generated in a long term approach by several cycles using escalating doses of cisplatin revealing significantly increased tolerance [109]. These lines have been used in different compound studies [89,91,102,109] as well as transcriptomic [81] and proteomic approaches [110] for characterization of cisplatin resistance.

1.5. The plasticity of type II TGCTs

The transformation of GCNIS in seminomas and non-seminomas as well as further non-seminoma differentiation in teratoma, Cc and YST has been observed in a mouse model as well as in patients [111]. Interestingly, the application of *TGFβ1*, *EGF* and *FGF4* revealed *in vitro* conversion of the seminoma model cell line TCam2 in a mixed non-seminoma or choriocarcinoma like fate [112]. Further, TCam2 cells injected in testis of nude mice remained in seminoma state, while in brain and in the flank the injected TCam2 cells developed into an EC-like fate. This indicates the importance of the tumor microenvironment [113].

To investigate the role of SOX2 during seminoma reprogramming, SOX2 deficient TCam2 cells were xenografted into the flank of nude mice revealing seminoma growth as well as a subpopulation which differentiated into a mixed non-seminoma like cell fate. Thus, SOX2 seems to be crucial for seminoma to EC conversion but is dispensable for seminoma differentiation [114].

Taken together, these fate transitions demonstrate the strong plasticity of TGCTs *in vitro*, *in vivo* and in patients.

1.6. Cyclin dependent kinase inhibitors

Cyclin dependent kinases (CDKs) are crucial for intracellular processes. The CDKs are subdivided in cell cycle CDKs 1, 2, 4 and 6 as well as transcriptional CDKs (tCDKs) 7, 8, 9, 12 and 13. tCDKs are crucial for RNA polymerase II (RNA Pol II) mediated transcription initiation, pausing release, elongation and termination (**Figure 5**) [115,116]. In detail, the pre-initiation complex, formed by RNA Pol II and several transcription factors, is recruited by the mediator complex (CDK8/cyclin c/mediator) to enhancer regions of the target gene [116,117]. Next, CDK7 partners with cyclin H as well as MAT1 forming the CDK-activating kinase complex (CAK) mediating specific phosphorylation of carboxy-terminal domain (CTD) of RNA Pol II thereby initiating the RNA Pol II directed transcription process by promotor escape [115,118].

Immediately after recruiting the capping machinery and adding the 5' mRNA cap, transcription interruption of RNA Pol II transcription is implemented [119,120]. The promoter-proximal pausing is important for precise processing of mRNA and assembly of the elongation complex.

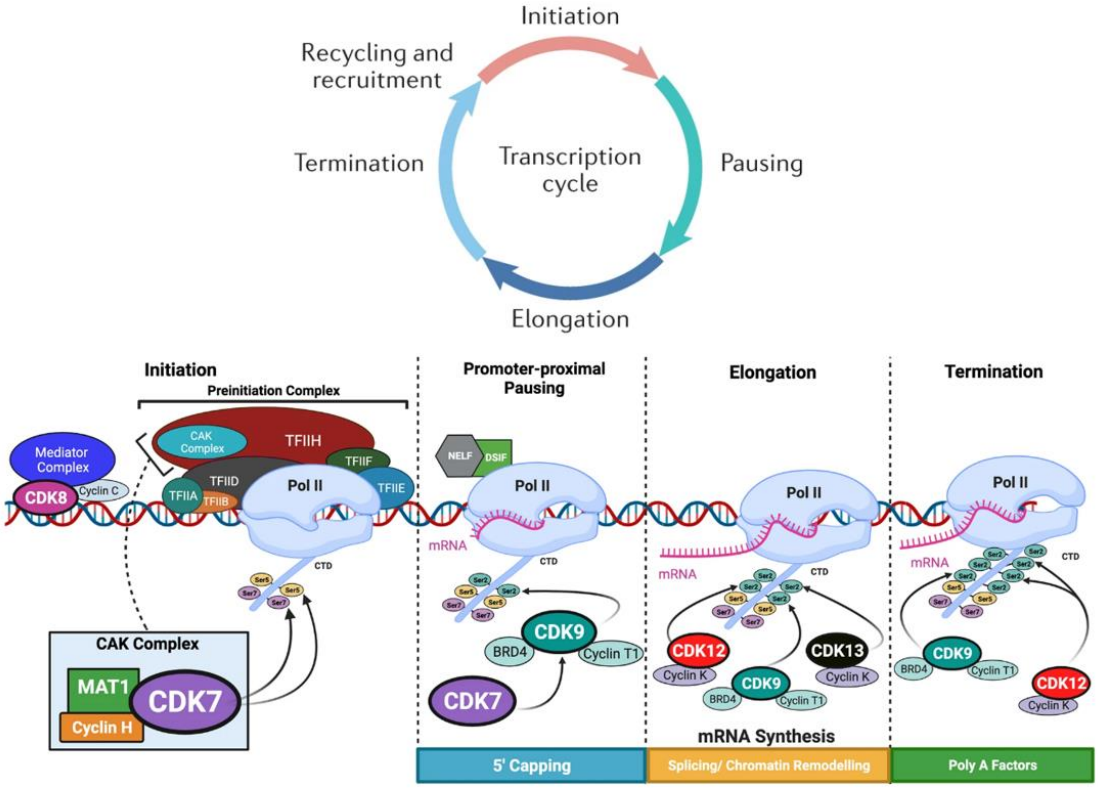

Figure 5: RNA polymerase II-based transcription cycle is mediated by tCDKs. Modified from [115,116]. The RNA polymerase II transcription cycle is divided into four sections (initiation, pausing, elongation and termination). In the initiation phase, the preinitiation complex, including RNA polymerase II, is recruited by the mediator complex to the transcription start site. Next, the CAK complex establishes a specific phosphorylation pattern at the CTD of RNA polymerase II resulting in promoter release and transcription initiation. After addition of the 5' mRNA cap, transcription is paused to ensure precise mRNA processing and assembly of the elongation complex. Pause release is triggered by PTEFb mediated phosphorylation of NELF and phosphorylation of CTD of RNA polymerase II. During mRNA elongation phase CDK12 and CDK13 introduce further CTD phosphorylation of RNA polymerase II ensuring full length mRNA transcription. Termination of transcription is mediated by PTEFb and CDK12.

Pause release is mediated by CDK7 based activation due to phosphorylation of CDK9 partnering with cyclin T forming the positive transcription elongation factor b (PTEFb) [115,121,122]. Selective phosphorylation at CTD of Pol II and negative elongation factor (NELF) by PTEFb promotes pause release as well as transcription elongation of mRNA [118,123]. Especially, CDK7 mediated CTD phosphorylation pattern of RNA Pol II induces epigenetic alterations by SETD1A/B histone H3K4 methyltransferase crucial for pre-mRNA splicing. Further, CDK7 activity was identified to be important for mRNA splicing in general by regulation of various splicing and RNA processing factors [115,124]. Kinase function of CDK12 and 13 are activated by binding to cyclin K. Both CDKs introduce a specific RNA Pol II phosphorylation pattern at the CTD thereby avoiding intronic and alternative polyadenylations important for assuring the synthesis of full-length mRNA [115,125,126]. Aside from

CDK12/cyclin K, the PTEFb plays an important role in the mRNA transcription termination by establishing deposition of histone H2B monoubiquitylation controlled by CTD phosphorylation. Further, CDK9 was shown to activate the nuclear 5′-to-3′ exoribonuclease Xrn2 and other factors important for 3'end processing and transcription termination [116,127].

CDK inhibitors have been identified as promising therapeutic options for a variety of tumor entities. While cell cycle CDK inhibitors for TGCT treatment have already been studied extensively in pre-clinical and clinical trials, data about transcriptional CDK inhibitors are rare [102,128,129].

The first generation pan-CDK inhibitor (CDK1, 2, 4, 6, 7, 9) Flavopiridol has been studied in a variety of tumor types such as leukemia, lymphoma, gastric cancer, prostate cancer, etc. [129]. The compound was found to cause apoptosis in non-seminoma cell lines NT2/D1, 2102EP as well as NCCIT *in vitro* [130]. A clinical phase I trial with refractory germ cell tumor patients was conducted resulting in a limited and very patient-specific response to Flavopiridol administration [131]. *In vitro* investigation of Dinaciclib, a second generation pan CDK inhibitor targeting CDK1, 2, 5, 9, 12 and 13 revealed apoptosis induction in ovarian cancer and displayed a synergistic effect when applied in combination with cisplatin [132]. Further, Dinaciclib was analyzed in a clinical phase II study demonstrating a good drug compatibility but showing no benefit over regular treatment regimens in patients with advanced breast cancer [133]. Another phase II and a phase III trial revealed promising results of chronic lymphocytic leukemia patients treated with Dinaciclib [134,135].

During the last years, development of highly specific CDK inhibitors rapidly progressed enabling researchers to get deeper insights in the role of CDKs during transcription as well as implementation as novel therapeutics for cancer. A milestone in CDK inhibitor design was THZ1 a CDK7, 12 and 13 specific inhibitor which was found to be effective in a broad range of cancer treatment [129]. Based on THZ1, the highly selective CDK12, 13 inhibitor THZ531 was developed [136]. THZ531 was shown to induce apoptosis in Jurkat T-cell acute lymphoblastic leukemia and neuroblastoma cells due to decreased phosphorylation at CTD of RNA Pol II and suppression of DDR-associated gene expression such as *BRACA1*, *ERCC4*, etc. [126], termed a “BRACAness” phenotype. Induced downregulation of DNA damage repair in tumor cells is predestined to be combined with DNA damaging agents for effective treatment such as the PARP inhibitor Olaparib. THZ531 and Olaparib have been shown to synergistically induce cell death in multiple myeloma cells [137].

With SY0351, developed from THZ1, an inhibitor with elevated CDK7 selectivity was introduced [138]. The compound revealed significant anti-cancer activity in different AML xenografts [138] and was important for understanding the CDK7 mediated activation of CDK9, 12 and 13 during RNA Pol II based transcription [139].

Since all compounds derived from THZ1 displayed cross reactions a highly specific CDK7 inhibitor was missing until YKL-5-124 was discovered. YKL-5-124 consists of a covalent THZ1 linker combined with a PAK4 inhibitor scaffold and was demonstrated to be selective to CDK7 without inhibitory activity towards CDK12 and 13. Of note, in HAP1 cells (chronic myeloid leukemia) YKL-5-124 triggers cell death only in combination with a CDK12, 13 inhibitor [140].

NVP2 an ATP competitive inhibitor displayed sub-nanomolar CDK9 selectivity while affinity towards other CDKs was 1000 times lower. CDK9 inhibition by NVP2 caused decreased RNA Pol II mediated transcription levels due to prevention of RNA Pol II pausing release in MOLT4 cells (acute lymphoblastic leukemia) as well as induction of apoptosis [122]. Thus, NVP2 has great potential as powerful antitumor agent. Interestingly, it is also a CDK9 degrader available. THAL-SNS-032 belongs to the class of proteolysis-targeting chimera (PROTAC) which describes a compound composed of an E3 ubiquitin ligase recruiting ligand, a linker molecule and a ligand binding to the target protein. After polyubiquitination the target protein undergoes proteasomal degradation. THAL-SNS-032 was applied to MOLT4 cells also revealing apoptosis. Of note, in comparison to NVP2 it was demonstrated that the degrader induced a delayed but sustained cellular response [122].

A variety of transcriptional CDK inhibitors have been designed, improved and investigated as potential novel therapeutics revealing tremendous potential in cancer treatment which makes these compounds also extremely interesting for an application in TGCTs.

1.7. Neddylation

Neddylation is based on a multistep conjugation cascade transferring the ubiquitin like small molecule NEDD8 (neuronal precursor cell expressed developmentally down-regulated protein 8) to a substrate (**Figure 6**). The modification of target proteins by NEED8 is essential for their function, stability and localization. [141]. Initially, NEDD8 is processed by NEDD8-specific protease 1 (NEDP1) as well as ubiquitin C-terminal hydrolase isoenzyme 3 (UCHL3) [142]. After maturation, NEDD8 is activated by a heterodimer, with E1 ligase function, comprising NAE1 (NEDD8 activating enzyme) and ubiquitin-activating enzyme 3 (UBA3), upon ATP consumption. During this step NEDD8 is bound to AMP and further conjugated to the E1 complex. Next, NEDD8 is transferred to an E2 ligase (UBE2M or UBE2F) and further conjugated to a substrate specific NEDD8-E3 ligase. A variety of E3 ligases for NEDD8 transfer has been identified such as RING-box protein 1 (RBX1) and RING-box protein 2 (RBX2), DCN-like proteins, MDM2, etc.

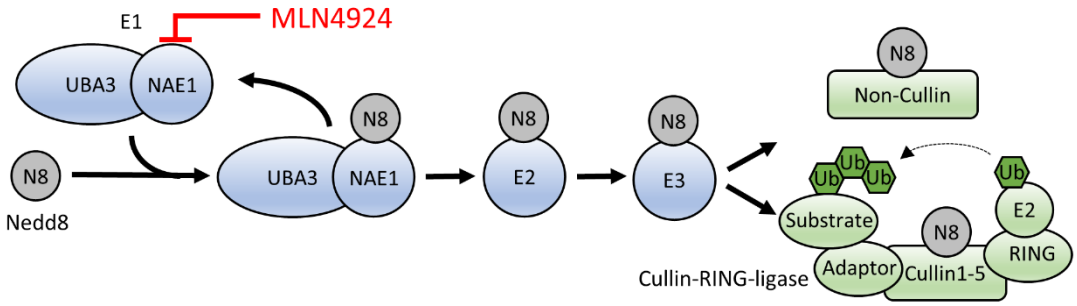

Figure 6: Schematic of the neddylation pathway. Reprinted from [2]. NEDD8 is conjugated to an E1 ligase and transferred in a canonical manner via E2 and E3 ligase to specific substrates. These substrates are divided in cullins and non-cullins. Cullin 1-5 are subunits of the CRLs. This complex displays ubiquitin E3 ligase function which is activated by neddylation. The neddylation cascade can be interrupted by covalent binding of the MLN4924 inhibitor to NAE1.

The substrates of the neddylation pathway are grouped in cullins and non-cullins. While the cullins are very well characterized, little is known about the non-cullin class [141,143]. Only few non-cullins such as tumor suppressor p53, E2F transcription factors, NFκB signaling interfering factors, EGFR, effector caspase drICE, etc. are described. Neddylation seems to be involved in modulation of transcription and translation, receptor tyrosine kinase signaling as well as DNA damage response [144]. Cullin1, 2, 3, 4A, 4B 5, 7 and 9 represent the second group of neddylation substrates. NEDD8 is conjugated to cullins via the E3 ligases RBX1 or RBX2. Cullins are a crucial subunit of cullin-RING ligases (CRL) which function as ubiquitin E3 ligases. Due to conformation change by neddylation, Cullin-associated NEDD8-dissociated protein 1 (CAND1) is released thereby activating the CRL [141,142]. Specific substrates bound by the CRL complex are polyubiquitylated and further degraded by the proteasome. This process is essential for the cell since 20% of protein degradation is processed via this pathway maintaining the proteome balance [141,143]. Several substrates have already been identified such as cell cycle inhibitors (p21, p27, Wee1), proteins involved in apoptotic pathways (Caspase8, NOXA), DNA damage repair (DDB1, DDB2) and chromatin remodeling proteins (CDT1) [145,146]. Since many tumor suppressors are degraded via the CLR proteasome pathway, neddylation is considered to promote cancer development and progression. Overactivation of neddylation was found in various entities such as pancreatic [147], lung [148] and breast cancer [149] highlighting the neddylation cascade as a promising target for cancer treatment. Application of the NAE1 inhibitor MLN4924 (Pevonedistat) induced cell cycle arrest and initiated an apoptotic response due to accumulation of p53, Wee1, p21, p27, etc. [147–149]. Interestingly, treatment of pancreatic cancer cells with MLN4924 increased sensitivity towards cisplatin indicating an additive effect of both compounds [147]. So far, the safety, tolerability and potency of MLN4924 in cancer therapy has been investigated in 40 clinical trials (https://www.clinicaltrials.gov/).

1.8. Genome scale CRISPR/Cas9 activation screen

For investigation of drug resistance factors, new druggable targets, essential genes for specific cellular processes, etc. genome scale CRISPR/Cas9 based screens turned out to be very effective [150,151]. The activation screen described by Joung *et al.* [152] is based on the synergistic activation mediator complex (SAM) system inducing overactivation of endogenous genes on a genome scale level mediated by a comprehensive collection (library) of single guide RNAs (sgRNAs). The sgRNAs are crucial for recruitment of the dCas9 enzyme to the target gene. The peculiarity of the SAM gain of function screen is the dCas9-VP64 fusion protein with inactive endonuclease function, the sgRNA library with two RNA MS2 binding loops and the MS2-P65-HSF1 construct. The transactivation domain VP64 attracts further transcription factors. In addition, the sgRNA MS2 binding loops recruit the MS2 aptamers which are fused to two further transcription factors. All together revealing robust activation of downstream gene expression [152].

1.9. Aim of the thesis

The aim of the thesis was the identification of novel cisplatin resistance factors in TGCTs as well as the investigation of alternative treatment options in this tumor entity. To address these problems, I elucidated the cytotoxic potential of a panel of transcriptional CDK inhibitors on cisplatin resistant and sensitive TGCTs in a cell culture model. The cellular impact on the cells as well as the molecular response were further investigated in detail using FACS apoptosis/cell cycle analysis and 3’mRNA sequencing.

In a second approach I performed a genome scale CRISPR/Cas9 based activation screen to generate cisplatin resistant TGCT cells which were further analyzed to identify candidate genes responsible for the induced resistance revealing an important effect of an overactivated neddylation pathway. It was further aimed to study the effect of neddylation pathway inhibition by NAE1 inhibitor MLN4924 trying to restore sensitivity towards cisplatin.

These approaches will help to provide a basis and contribute to improved options for TGCT treatment focusing on alternative options for treatment of cisplatin resistant tumors as well as drugs with less severe side effects compared to chemotherapeutics.

2. Materials and Methods

2.1. Materials

2.1.1. Cell Lines

Cell line	Description	Standard culture medium	Source
2102EP	Non-seminoma, EC	DMEM, 10% FBS, 2 mM L-glutamine, 100 units/mL penicillin G, 100 µg/mL streptomycin	Prof. Dr. L. Looijenga, Princess Máxima Center for Pediatric Oncology, Utrecht, The Netherlands
2102EP-R	cisplatin resistant subline derived from 2102EP	DMEM, 10% FBS, 2 mM L-glutamine, 100 units/mL penicillin G, 100 µg/mL streptomycin	PD Dr. F. Honecker, ZeTup Silberturm, St. Gallen, Switzerland
NCCIT	Non-seminoma, EC	DMEM, 10% FBS, 2 mM L-glutamine, 100 units/mL penicillin G, 100 µg/mL streptomycin	Prof. Dr. L. Looijenga, Princess Máxima Center for Pediatric Oncology, Utrecht, The Netherlands
NCCIT-R	cisplatin resistant subline derived from NCCIT	DMEM, 10% FBS, 2 mM L-glutamine, 100 units/mL penicillin G, 100 µg/mL streptomycin	PD Dr. F. Honecker, ZeTup Silberturm, St. Gallen, Switzerland
NT2/D1	Non seminoma, EC	DMEM, 10% FBS, 2 mM L-glutamine, 100 units/mL penicillin G, 100 µg/mL streptomycin	Prof. Dr. L. Looijenga, Princess Máxima Center for Pediatric Oncology, Utrecht, The Netherlands
NT2/D1-R	cisplatin resistant subline derived from NT2/D1	DMEM, 10% FBS, 2 mM L-glutamine, 100 units/mL penicillin G, 100 µg/mL streptomycin	PD Dr. F. Honecker, ZeTup Silberturm, St. Gallen, Switzerland
JAR	Non-seminoma, CC	DMEM, 10% FBS, 2 mM L-glutamine, 100 units/mL penicillin G, 100 µg/mL streptomycin	ATCC, Manassas, VA, USA
TCam2	Seminoma	RPMI, 10% FBS, 2 mM L-glutamine, 100 units/mL penicillin G, 100 µg/mL streptomycin	Prof. Dr. Hubert Schorle, Developmental Pathology, Pathology, University Hospital Bonn
FS1	Sertoli cell line	DMEM, 20% FBS, 2 mM L-glutamine, 100 units/mL penicillin G, 100 µg/mL streptomycin	Dr. Valerie Schumacher, Nephrology Research Center, Boston, USA
HEK293T	Human embryonic kidney cell line, expression of the SV40 large T antigen	DMEM, 10% FBS, 2 mM L-glutamine, 100 units/mL penicillin G, 100 µg/mL streptomycin, 1 mM sodium pyruvate, 0.7 mM non-essential amino acids solution	PD Dr. M. Peitz, Institute of Reconstructive Neurobiology, Bonn University, Bonn, Germany

Cell line	Description	Standard culture medium	Source
MPAF	Human adult fibroblast cells	DMEM, 10% FBS, 2 mM L-glutamine, 100 units/mL penicillin G, 100 µg/mL streptomycin, 1 mM, 0.7 mM non-essential amino acids solution	PD Dr. M. Peitz, Institute of Reconstructive Neurobiology, Bonn University, Bonn, Germany

2.1.2. Bacteria

Name	Genotype	Manufacturer
E. coli Endura ElectroCompetent Cells	*rec*A13 *sup*E44 *ara*-14 *gal*K2 *lac*Y1 *pro*A2 *rps*L20(StrR) *xyl*-5 λ– *leu mtl*-1 F– *mcr*B *mrr hsd*S20(*r*B–, *m*B–)	BioCat GmbH, Heidelberg, Germany
E. coli TOP 10, One Shot™, Chemically competent	F- *mcrA* Δ(*mrr-hsd*RMS-*mcr*BC) Φ80*lac*ZΔM15 Δ *lac*X74 *rec*A1 *ara*D139 Δ(*araleu*)7697 *gal*U *gal*K *rps*L (StrR) *end*A1 *nup*G	Thermo Fisher Scientific, Waltham, USA

2.1.3. Chemicals and reagents

Product	Manufacturer
2-Mercaptoethanol	Merck, Darmstadt, Germany
6-Diamidino-2-phenylindole dihydrochloride (DAPI)	AppliChem, Darmstadt, Germany
7AAD	BioLegend, San Diego, CA USA
Acetic acid	AppliChem, Darmstadt, Germany
Aceton	VWR, Darmstadt, Germany
Acrylamide Mix	Roth, Karlsruhe, Germany
Albumin fraction V (BSA)	AppliChem, Darmstadt, Germany
Ammonium persulfate (APS)	Carl Roth, Karlsruhe, Germany
Ampicillin	AppliChem, Darmstadt, Germany
CDK inhibitors: YKL-5-124, SY0351, THZ1, THZ531, NVP2, Dinaciclib, Flavopiridol	Provided by Matthias Geyer, Institute of Structural Biology, University of Bonn
CDK PROTAC THAL-SNS-032	Provided by Matthias Geyer, Institute of Structural Biology, University of Bonn

Product	**Manufacturer**
cis-Diamineplatinum(II) dichloride (Cisplatin)	Merck, Darmstadt, Germany
cOmplete™ ULTRA Tablets, Mini Protease Inhibitor Cocktail	Roche, Basel, Suisse
Dimethyl sulfoxide (DMSO)	Merck, Darmstadt, Germany
Ethanol	VWR, Darmstadt, Germany
Ethidium bromide (Etbr) solution	Carl Roth, Karlsruhe, Germany
Ethylene diamine tetra acetic acid (EDTA)	Merck, Darmstadt, Germany
GeneRuler™ 1 kb DNA ladder	Thermo Fisher Scientific, Waltham, USA
GeneRuler™ 100 bp DNA ladder	Thermo Fisher Scientific, Waltham, USA
Glucose	AppliChem, Darmstadt, Germany
Glycine	Carl Roth, Karlsruhe, Germany
Halt™ Phosphatase Inhibitor Cocktail	Thermo Fisher Scientific, Waltham, USA
Halt™ Protease-Inhibitor-Cocktail (100x)	Thermo Fisher Scientific, Waltham, USA
Hoechst-33342	Merck, Darmstadt, Germany
Hydrochloric acid (HCl)	VWR, Darmstadt, Germany
Isopropanol	AppliChem, Darmstadt, Germany
Lenti-X concentrator	Takara BIO INC., Kusatsu, Shiga, Japan
Methanol	VWR, Darmstadt, Germany
MLN4924 (Pevonedistat)	Selleckchem, Huston, TX, USA
N,N-Dimethylformamide (DMF)	AppliChem, Darmstadt, Germany
N-methyl dibenzopyrazine methyl sulfate (PMS)	Merck, Darmstadt, Germany
Nonfat dried milk powder	AppliChem, Darmstadt, Germany
Oligonucleotide (Primer)	Merck, Darmstadt, Germany
PageRuler Prestained Protein Ladder	Thermo Fisher Scientific, Waltham, USA
PageRuler Prestained Protein Ladder	Thermo Fisher Scientific, Waltham, USA
PE Annexin V	BioLegend, San Diego, CA USA
Phosphate buffered saline (PBS) tablets	AppliChem, Darmstadt, Germany
Polybrene	Thermo Fisher Scientific, Waltham, USA
Ponceau S	Merck, Darmstadt, Germany
Potassiumacetate	AppliChem, Darmstadt, Germany
RNaseA	AppliChem, Darmstadt, Germany
Roti-Load 1, reducing, 4 x concentrated	Carl Roth, Karlsruhe, Germany

Product	Manufacturer
Rotiphorese Gel 30 (acrylamide stock solution)	Carl Roth, Karlsruhe, Germany
Sodium acetate	Merck, Darmstadt, Germany
Sodium Chloride (NaCl)	Merck, Darmstadt, Germany
Sodium dodecyl sulfate (SDS)	Merck, Darmstadt, Germany
Sodium hydroxide (NaOH)	VWR, Darmstadt, Germany
Sodium acetate	Merck, Darmstadt, Germany
Tetramethyl ethylenediamine (TEMED)	VWR, Darmstadt, Germany
Transporter™ 5 Transfection Reagent	Polysciences, Inc., Warrington, USA
Tris hydrochloride	Carl Roth, Karlsruhe, Germany
Tris-HCl	Roth, Karlsruhe, Germany
Tween 20	AppliChem, Darmstadt, Germany
UltraPure™ agarose	Invitrogen™, Thermo Fisher Scientific, Waltham, USA
Water, nuclease free	Thermo Fisher Scientific, Waltham, USA
XTT (sodium salt)	Merck, Darmstadt, Germany

2.1.4. Kits

Kit	Manufacturer
CellTiter-Glo® Luminescent Cell Viability Assay	Promega, Mannheim, Germany
NEBNext® High-Fidelity 2X PCR Master Mix	New England Biolabs GmbH, Frankfurt am Main, Germany
NucleoBond® Xtra Maxi Plus	Macherey-Nagel, Düren, Germany
Pierce™ BCA Protein Assay Kit	Thermo Fisher Scientific, Waltham, USA
Quick DNA Midi Prep Plus Kit	Zymo Research, Irvine, CA, US
RNeasy Mini Kit	Qiagen, Hilden, Germany
SuperSignal™ Western Blot Femto	Thermo Fisher Scientific, Waltham, USA
WESTAR NOVA 2.0	Cyanagen, Bologna, Italy

2.1.5. Buffers and recipes

Buffer/Solution	Recipe/supplier
Annexin Binding buffer	BioLegend, San Diego, CA USA
Ammonium persulfate (APS) 10%	10% (w/v) ammonium persulfate in H2O
BSA-Blocking solution for immunoblotting	5% (w/v) BSA in PBST
DNA loading Dye, 6x	Thermo Fisher Scientific, Waltham, USA
LB agar	10 g tryptone, 5 g NaCl, 5 g yeast extract, 15 g agar; ad 1 l H2O, autoclaved
LB medium (5 x)	50 g tryptone; 50 g NaCl; 25 g yeast extract; pH 7.0 with NaOH, ad 1 l H2O, autoclaved
Milk-Blocking solution for immunoblotting	5% (w/v) non-fat milk powder in PBST
M-PER Mammalian Protein Extraction Reagent	Thermo Fisher Scientific, Waltham, USA
PBST	200 ml 10 x PBS; 1 ml Tween 20; ad 2000 ml H2O
Plasmid DNA isolation buffer P1	50 mM, 10 mM EDTA; 25 mM Tris-HCl, pH 8.0
Plasmid DNA isolation buffer P2	200 mM NaOH; 1% SDS
Plasmid DNA isolation buffer P3	60 ml 5 M potassium acetate, 28.5 ml H2O, 11.5 ml acetic acid
Ponceau S staining solution	1 g Ponceau S, 5 ml acetic acid, ad 100 ml H2O
RIPA buffer	Cell signaling, Danvers, MA, USA
SDS Polyacrylamide gel	12% Separation Gel: 1.6 ml H2O, 2.0 ml Rotiphorese Gel 30, 1.3 ml 1.5 M Tris (pH 8.8), 50 µl 10% SDS, 50 µl 10% APS, 2 µl TEMED Stacking Gel (4%): 2.1 ml H2O, 500 µl Rotiphorese Gel 30, 380 µl 1.0 M Tris (pH 6.8), 30 µl 10% SDS, 30 µl 10% APS, 3 µl TEMED
S.O.C. medium (recovery medium *E. coli* TOP 10)	Thermo Fisher Scientific, Waltham, USA
Tris-acetate-EDTA-buffer (TAE), 50 x	2 M Tris base, 50 mM EDTA, 1 M acetic acid
Tris-EDTA (TE) buffer, pH 8.0, low EDTA	AppliChem, Darmstadt, Germany
Western blot stripping buffer	3.125 ml Tris-HCl (1.5 M, pH 8.8); 390 µl β-mercaptoethanol; 5 ml 20% SDS, ad 50 ml H2O

Buffer/Solution	Recipe/supplier
Western Blot transfer buffer (10X)	20 mM Tris; 192 mM glycine; 0.1% (w/v) SDS; 20% (v/v) MeOH
Western Blot transfer buffer (1X)	700 ml H2O, 200 ml methanol, 100 ml Western Blot transfer buffer (10X)

2.1.6. Consumables

Consumable	Manufacturer
Whatman Paper	Macherey-Nagel, Düren, Germany
Cell Culture Dishes (55 cm^2, 143 cm^2)	VWR, Darmstadt, Germany
Cell Culture Flasks, Filter Cap, CELLSTAR® (T25, T75)	Greiner bio-one, Frickenhausen, Germany
Cell Culture Flasks, Filter Cap, Nunc™ EasYFlask™ (T225)	Thermo Fisher Scientific, Waltham, USA
Cell Culture, Multiwell Plates (6-, 12-, 24-, 96-well-plate)	TPP, Trasadingen, Austria
Cell Culture Multiwell Plate, 96 well clear-bottom black	Thermo Fisher Scientific, Waltham, USA
Cryogenic vials 1 ml, external thread	Thermo Fisher Scientific, Waltham, USA
Cryogenic vials 2 ml, internal thread	Greiner bio-one, Frickenhausen, Germany
Eppendorf tubes (1.5 ml, 2 ml)	Eppendorf, Hamburg, Germany
FACS tubes	BD Biosciences, Heidelberg, Germany
Filter tips (10 µl, 100 µl, 1000 µl)	Nerbe Plus, Winsen/Luhe, Germany
Microplates, U-bottom, transparent, 96-well	VWR, Darmstadt, Germany
Multiply®-µStrip Pro	Sarstedt, Nürnbrecht, Germany
Parafilm M®	Pechiney Plastic Packaging, Menasha, USA
PCR® strip tubes	Axygen Scientific, Union City, USA
Petri dishes	Greiner bio-one, Frickenhausen, Germany
Pipette tips (10 µl, 100 µl, 1000 µl)	Greiner bio-one, Frickenhausen, Germany
Polypropylene tubes CELLSTAR® (15 ml, 50 ml)	Corning, Amsterdam, Netherlands
Roti-PVDF membrane	Carl Roth, Karlsruhe, Germany
Costar® Stripettes (5 ml, 10 ml, 25 ml)	Greiner bio-one, Frickenhausen, Germany
Sterile filters, 0.2 µm	Corning Incorporated, Corning, USA
Sterile filters, 0.45 µm Surfactant-free cellulose acetate membrane (SFCA)	Corning Incorporated, Corning, USA

Consumable	Manufacturer
Syringe Omnifix® (10 ml, 20 ml, 50 ml)	B. Braun, Melsungen, Germany

2.1.7. Cell culture accessories

Medium/reagent	Manufacturer
0,05% Trypsin-EDTA	Thermo Fisher Scientific, Waltham, USA
Blasticidin S HCl solution	Santa Cruz, Dallas, USA
Dimethyl Sulfoxide (DMSO)	AppliChem, Darmstadt, Germany
Dulbecco's Modified Eagle's Medium (DMEM) high glucose	Thermo Fisher Scientific, Waltham, USA
Fetal Bovine Serum (FBS)	Merck, Darmstadt, Germany
Hygromycin B solution	Santa Cruz, Dallas, USA
L-Glutamine 200 mM	Thermo Fisher Scientific, Waltham, USA
Non-essential amino acids	Thermo Fisher Scientific, Waltham, USA
Penicillin/Streptomycin (P/S)	Thermo Fisher Scientific, Waltham, USA
Phosphate-Buffered Saline (PBS)	Thermo Fisher Scientific, Waltham, USA
Roswell Park Memorial Institute (RPMI) medium	Thermo Fisher Scientific, Waltham, USA
Sodium Pyruvate	Merck, Darmstadt, Germany

2.1.8. Equipment

Equipment	Manufacturer
Agarose gel chamber	Peqlab, Erlangen, Germany
Balance BP211S	Sartorius, Göttingen, Germany
Balance PT 120	Sartorius, Göttingen, Germany
BioVortex V1	Peqlab, Erlangen, Germany
Cell culture hood BSB 6A	Gelaire, Sydney, Australia
Cell culture hood Safety cabinet HERAsafe®	Kendro, Langenselbold, Germany
Centrifuge 5417R	Eppendorf, Hamburg, Germany
Centrifuge 5424	Eppendorf, Hamburg, Germany
Centrifuge Biofuge fresco	Thermo Fisher Scientific, Waltham, USA
Centrifuge Galaxy-Mini	VWR, Darmstadt, Germany
Centrifuge Heraeus™ Megafuge™ 16	Thermo Fisher Scientific, Waltham, USA
Centrifuge Heraeus™ Multifuge™ 3 S-R	Thermo Fisher Scientific, Waltham, USA

Equipment	**Manufacturer**
Consort EV 243 power supply	Sigma-Aldrich, St. Louis, USA
Gel Documentation System GEL iX20 Imager	Intas Science Imaging Instruments GmbH, Gottingen, Germany
Incubator Heracell 240i	Thermo Fisher Scientific, Waltham, USA
Incubator Shaker Innova 4000	Eppendorf, Hamburg, Germany
Incubator UM200	Memmert, Schwabach, Germany
Magnetic stirrer MR 3001	Heidolph, Schwabach, Germany
Microplate Luminometer Centro LB 960	Berthold Detection Systems, Pforzheim
Microplate Reader iMark	Bio-Rad Laboratories, Hercules, USA
Microscope Axiovert 40C	Zeiss, Jena, Germany
Microscope Labovert FS	Leica Microsystems, Wetzlar, Germany
Multichannel Pipet	Eppendorf, Hamburg, Germany
Neubauer Improved cell counting chamber	Brand, Wertheim, Germany
PAGE Handcast System Mini-PROTEAN® Tetra Handcast system	Bio-Rad Laboratories, Hercules, USA
pH-Meter	Schott Instruments, Mainz, Germany
Pipette controller Accu-Jet® Pro	Brand, Wertheim, Germany
Pipettes (10 µl, 100 µl, 1000 µl)	Eppendorf, Hamburg, Germany
SDS-PAGE System Mini-PROTEAN® Tetra Cell	Bio-Rad Laboratories, Hercules, USA
Sonicator Bioruptor®	Diagenode, Seraing, Belgium
Spectrophotometer Nano Drop 1000	Thermo Fisher Scientific, Waltham, USA
Thermal cycler 2720	Applied Biosystems® by Thermo Fisher Scientific Inc., Carlsbad, USA
Thermomixer compact	Eppendorf, Hamburg, Germany
Vortex-Genie® 2	Scientific Industries, New York, USA
Waterbath TW8	Julabo, Seelbach, Germany
Waterbath WNE 45	Memmert, Schwabach, Germany
Western Blot Imaging System ChemiDoc MP	Bio-Rad Laboratories, Hercules, USA
Western Blot Transfer System Trans-Blot® Turbo™	Bio-Rad Laboratories, Hercules, USA

2.1.9. Primers

Primer for amplification and preparation of sgRNA library for NGS according to Joung *et al.* 2017 [152]. A unique barcode (bold letters) was included in the reverse primers for pooled sequencing run. Oligonucleotides were synthesized by Merck, Darmstadt, Germany.

Name	**Sequence (5`->3`)**
NGS-Lib-Fwd-1	AATGATACGGCGACCACCGAGATCTACACTCTTTCCCTACACGACGCTCTTCCGATCTTAAGTAGAGGCTTTATATATCTTGTGGAAAGGACGAAACACC
NGS-Lib-Fwd-2	AATGATACGGCGACCACCGAGATCTACACTCTTTCCCTACACGACGCTCTTCCGATCTATCATGCTTAGCTTTATATATCTTGTGGAAAGGACGAAACACC
NGS-Lib-Fwd-3	AATGATACGGCGACCACCGAGATCTACACTCTTTCCCTACACGACGCTCTTCCGATCTGATGCACATCTGCTTTATATATCTTGTGGAAAGGACGAAACACC
NGS-Lib-Fwd-4	AATGATACGGCGACCACCGAGATCTACACTCTTTCCCTACACGACGCTCTTCCGATCTCGATTGCTCGACGCTTTATATATCTTGTGGAAAGGACGAAACACC
NGS-Lib-Fwd-5	AATGATACGGCGACCACCGAGATCTACACTCTTTCCCTACACGACGCTCTTCCGATCTTCGATAGCAATTCGCTTTATATATCTTGTGGAAAGGACGAAACACC
NGS-Lib-Fwd-6	AATGATACGGCGACCACCGAGATCTACACTCTTTCCCTACACGACGCTCTTCCGATCTATCGATAGTTGCTTGCTTTATATATCTTGTGGAAAGGACGAAACACC
NGS-Lib-Fwd-7	AATGATACGGCGACCACCGAGATCTACACTCTTTCCCTACACGACGCTCTTCCGATCTGATCGATCCAGTTAGGCTTTATATATCTTGTGGAAAGGACGAAACACC
NGS-Lib-Fwd-8	AATGATACGGCGACCACCGAGATCTACACTCTTTCCCTACACGACGCTCTTCCGATCTCGATCGATTTGAGCCTGCTTTATATATCTTGTGGAAAGGACGAAACACC
NGS-Lib-Fwd-9	AATGATACGGCGACCACCGAGATCTACACTCTTTCCCTACACGACGCTCTTCCGATCTACGATCGATACACGATCGCTTTATATATCTTGTGGAAAGGACGAAACACC
NGS-Lib-Fwd-10	AATGATACGGCGACCACCGAGATCTACACTCTTTCCCTACACGACGCTCTTCCGATCTTACGATCGATGGTCCAGAGCTTTATATATCTTGTGGAAAGGACGAAACACC

Name	Sequence (5`->3`)
NGS-Lib-SAM-Rev-3 (2102EP$^{MPHv2/SAMv2}$)	CAAGCAGAAGACGGCATACGAGAT**GAAGAAGT**GTGACTGGAGTTCAGACGTGTGCTCTTCCGATCTGCCAAGTTGATAACGGACTAGCCTT
NGS-Lib-SAM-Rev-4 (JAR$^{MPHv2/SAMv2}$)	CAAGCAGAAGACGGCATACGAGAT**GTCTGATG**GTGACTGGAGTTCAGACGTGTGCTCTTCCGATCTGCCAAGTTGATAACGGACTAGCCTT

2.1.10. Antibodies

All antibodies were applied in Western Blot analyses.

Antibody	Order no.	Host species	Dilution	Company
CDK10	36106S	Rabbit	1:500	Cell signaling, Danvers, MA, USA
CDK12	ABE1861	Rabbit	1:500	Merck, Darmstadt, Germany
CDK13	ABIN6130965	Rabbit	1:1000	Antibodies-online.com (01/2022)
CDK7	PA5-34791	Rabbit	1:1000	Invitrogen, Waltham, MA, USA
CDK9	2316T	Rabbit	1:1000	Cell signaling, Danvers, MA, USA
GFP	sc9996	Mouse	1:1000	Santa Cruz, Dallas, USA
H2A.X pS139 (γH2A.X)	ab11174	Rabbit	1:2000	Abcam, Cambridge, UK
NAE1	14321S	Rabbit	1:1000	Cell signaling, USA
P27 Kip1	3686S	Rabbit	1:1000	Cell signaling, USA
β-Actin	a5441	Mouse	1:25000	Merck, Darmstadt, Germany
Rabbit HRP	P0447	Goat	1:2000	Agilent Technologies (Dako), USA
Mouse-HRP	P0260	Rabbit	1:1000	Agilent Technologies (Dako), USA

2.1.11. Plasmids

Plasmid	Plasmid components	Depositor
Human CRISPR Activation Library (SAMv2)	70290 different sgRNAs for gene activation, dCas9 VP64 fusion protein, blasticidin resistance	Human CRISPR activation pooled library (SAMv2) was a gift from Feng Zhang (Addgene #1000000078)
lentiMPHv2	MS2-P65-HSF1 activator helper complex, hygromycin resistance	lentiMPH v2 was a gift from Feng Zhang (Addgene plasmid # 89308)
pLV-NAE1-GFPSpark	Overexpression of NEA1/GFP fusion protein	Sino Biological, Beijing, China
pMD2.G	VSV-G envelope expressing plasmid	pMD2.G was a gift from Didier Trono (Addgene plasmid # 12259)
psPAX2	Lentiviral packaging plasmid	psPAX2 was a gift from Didier Trono (Addgene plasmid # 12260)

2.1.12. Software and databases

Name	Purpose	Source
Bioconductor v3.13	Software packages for R-based analysis of omics data	https://www.bioconductor.org/ [153]
Bionavigator software	Analysis of peptide chip array	Pamgene, ‘s-Hertogenbosch, The Netherlands
Biopython	Python tools for computational molecular biology	https://biopython.org/ [154,155]
Citavi 6	Reference program	Swiss Academic Software GmbH
FastQC v0.11.9	Investigating raw data quality of 3’mRNA sequencing data	https://www.bioinformatics.babraham.ac.uk/projects/fastqc [156]
FlowJo™v10.8	Evaluation of FACS generated data	BD Biosciences, Heidelberg, Germany
Gene ontology	Enrichment analysis on gene/protein sets	www.geneontology.org [157]
HISAT2.1	Mapping of 3’mRNA sequencing data to a genome	http://daehwankimlab.github.io/hisat2/ [158]

Name	Purpose	Source
KEGG Pathway database	Enriched pathway analyses	https://www.genome.jp/kegg/pathway.html [159]
Microsoft Office 2016 (Word, Excel, Power Point)	Word and data processing as well as presentation software	Microsoft, Redmond, WA, USA
NCBI pubmed	Bibliographic database	www.ncbi.nlm.nih.gov/pubmed/
Python 2.7	Programming language	https://www.python.org/ [160]
R v4.0.4	Programming language and	https://www.r-project.org/ [161]
Reactome	Pathway database	https://reactome.org [162]
R-Studio v1.4.1106	R based integrated development environment	https://www.rstudio.com/ [163]
STRING	Analyse and predict protein-protein interactions	https://string-db.org [164]
StringTie 1.3.3	Quantification and annotation of mapped 3'mRNA sequencing data	https://ccb.jhu.edu/software/stringtie/ [165]
TrimGalore v0.6.1	Trimming of 3'mRNA sequencing data	https://www.bioinformatics.babraham.ac.uk/projects/trim_galore/ [166]
Venny 2.1	Create Venn diagram representing the overlap of different datasets	http://bioinfogp.cnb.csic.es/tools/venny/ [167]

2.2. Methods

2.2.1. Cell culture

Cells were cultivated in standard cell culture medium (see 2.1.1) in a sub-confluent condition at 37 °C and 7.5% CO_2. Passaging was performed 2 to 3 times a week. In detail, cells were washed with PBS, incubated with Trypsin-EDTA for 5 min at 37 °C and resuspended in cell culture medium. One part of the cell suspension was transferred into a new cell culture flask for further cultivation.

2.2.2. XTT cell viability assay

Cells were seeded in 96-well cell culture plates at a density of $3x10^3$ cells/well in 100 µl cell culture medium. The next day, treatment with CDK inhibitors, MLN4924, cisplatin, MLN4924/cisplatin combination, or corresponding solvent control was performed. All CDK inhibitors as well as MLN4924 were dissolved in DMSO while cisplatin was solubilized in DMF. Viability of the cells was determined at different time points between day 0 and day 7. XTT-salt was dissolved in DMEM/RPMI (0.6 mg/ml) and supplemented with 1.25 mM PMS. 50 µl of the XTT solution were added to each well, incubated at 37 °C for 4 h. Subsequently, absorbance was measured in an iMark Microplate Reader (450 nm vs. 650 nm). For each condition at least three technical replicates were measured.

2.2.3. FACS apoptosis analysis (AnnexinV PE/7AAD/DAPI)

Cells were seeded in 6-well cell culture plates ($1.5x10^5$ cells/well) and treated with CDK-inhibitors, MLN4924, cisplatin, MLN4924/cisplatin combination or with the corresponding solvent (DMF/DMSO). Next, cells were harvested using Trypsin-EDTA, washed twice with PBS and resuspended in 100 µl Annexin V binding buffer. For cell staining 4 µl PE AnnexinV/4 µl 7AAD (CDK inhibitors treated samples) or 4 µl PE AnnexinV/5µg/ml DAPI (MLN4924/cisplatin treated samples) were added. After incubation for 15 min in the dark at 37 °C, measurement was performed at FACS Canto and analyzed with BD FACSDiva software™.

2.2.4. FACS cell cycle analysis

After treatment of cells in 6-well cell culture plate format cells were harvested, washed and resuspended in 300 µl PBS. For permeabilization ice cold methanol was added dropwise to a concentration of 70% v/v, incubated for 2 h at 4 °C and subsequently washed twice with PBS. Cells were resuspended in staining solution (2 µg/mL Hoechst-33342, 50 µg/mL RNaseA in

PBS) and incubated for 30 min at 37 °C. FACS Canto was used to determine DNA content. Evaluation was carried out utilizing the BD FACSDiva software™.

2.2.5. Lentivirus Production

Depending on the scale of virus production, HEK293T cells were seeded in 10 cm cell culture dishes ($7x10^6$ cells) or T225 cell culture flasks ($2.1x10^7$ cells). Next day, a transfection mix (**Table 1**) containing DMEM, pMD2.G and psPAX2 helper plasmids as well as a plasmid containing the target DNA (e.g., pLV-NAE1-GFPSpark) was prepared. After addition of transporter-5 transfection reagent the mixture was incubated for 10 min. The transfection mixture was combined with HEK293T medium and added to the HEK293T cells. After 2 days, virus containing cell culture supernatant was collected, filtered (0.45 µm pore size, SFCA membrane), aliquoted and stored at -80 °C.

Table 1: Components for virus production

Component	Amount per 10 cm dish	Amount per T225
DMEM	167 µl	651 µl
pMD2.G	0.88 µg	3.4 µg
psPAX2	1.75 µg	6.8 µg
Target DNA	3.51 µg	13.6 µg
Transporter-5 transfection reagent	50.3 µl	195 µl
HEK293T medium	10 ml	25 ml

2.2.6. Generation of clonal NAE1 overexpression cell lines

For lentivirus production HEK293T cells were transfected with pMD2.G, psPAX2 and pLV-NAE1-GPFSpark coding for NAE1/GFP fusion protein (see 2.2.5). Lenti-X concentrator was used for 50x virus concentration according to the manufacturer's manual. To generate overexpression cell lines, 2102EP and JAR cells were seeded in 6-well cell culture plates ($0.5x10^5$ cells/well) and transduced with lentiviral particles. To enhance lentivirus efficiency cell culture medium was supplemented with 10 µg/ml polybrene. Remaining virus particles were washed out after 24 h with PBS. After expansion for 6 days, cells were harvested, resuspended in PBS containing 1.5% FBS and filtered through cell strainers to select for single cells (40 µm for 2102EP and 70 µm for JAR). Next, DAPI (5 µg/ml) staining was performed. To generate clonal $2102EP^{NAE1/GFP}$ and $JAR^{NAE1/GFP}$ cell lines, single cell FACS sorting (BD FACS ARIA III/BD FACS Melody) for DAPI negative (alive)/GFP (NAE1) positive cells was applied. Single cells were collected in 96-well plates and expanded.

2.2.7. Generation of MS2-P65-HSF1 Helper Cell Lines

MS2-P65-HSF1 lentiviral particles were generated as described in chapter 2.2.5. 400 µl of virus containing supernatant were used for transduction of 2102EP and JAR cells. To select for cells (2102EP^{MPHv2}, JAR^{MPHv2}) which integrated the MS2-P65-HSF1 encoding DNA hygromycin b treatment (250 µg/ml) was carried out for 7 days.

2.2.8. Genome scale CRISPR/Cas9 transcriptional activation screen

The transcriptional activation screen was performed as described earlier by Joung *et al.* [152]. Endura ElectroCompetent cells were used for SAMv2 plasmid library amplification. To investigate sgRNA coverage NGS (NextSeq™ 550) and Python-/Biopython-based analysis were carried out [154,155,160]. SAMv2 library lentiviral particles were produced according to chapter 2.2.5 in T225 cell culture flasks. For virus concentration the Lenti-X concentrator was applied as described in the manufacturer's manual. To determine the virus titer, 2102EP and JAR cells were seeded in a 6-well cell culture plate (10^5 cells/well), supplemented with polybrene (10 µg/ml) to facilitate virus/cell interaction and transduced with different volumes of virus (0, 15.63, 31.25, 62.5, 125 or 250 µl) by centrifugation at 1500 xg, 32 °C for 30 min. After 48 h, 1500 cells/condition were seeded in each well of 96-well cell culture plates as quadruplicates. Antibiotic selection (5 µg/ml blasticidin S HCl) was performed on two of the four replicates until all cells in the non-transduced control died. Subsequently, the viability was determined using the CellTiter-Glo™ Luminescent Cell Viability Assay Kit as described in the manufacturer's manual. Multiplicity of infection was calculated for each condition by referring the antibiotic treated samples to the untreated samples.

Table 2: Cell numbers for genome scale CRISPR/Cas9 activation screen

Cell line	Library	Library size (sgRNAs)	Cell number for coverage of 100% [1)]	Cells for trans-duction	Coverage in the screen [%]	Cell number for gDNA isolation [2)]
2102EP^{MPHv2}	SAMv2	70290	$1.17x10^8$	$1.18 x10^8$	100.9	$3.54x10^7$
JAR^{MPHv2}	SAMv2	70290	$1.17x10^8$	$1.2x10^8$	102.6	$3.61x10^7$

1) Coverage of 100% at MOI of 0.3 and 500 cells/sgRNA

2) To maintain coverage of 100% gDNA had to be isolated from 500 cells/sgRNA

For SAMv2 library transduction 2102EP^{MPHv2} and JAR^{MPHv2} helper cell lines were seeded in 6-well cell culture plates (10^6 cells/well). Library size and corresponding cell numbers to reach 100% coverage are given in **Table 2**. Next day, the cells were supplemented with polybrene.

Transduction by centrifugation (1500 xg, 32 °C, 30 min) was performed at low MOI of 0.3 with the SAMv2 library lentivirus. After 2 days, the cells were transferred to 15 cm cell culture dishes. Cisplatin treatment was started on the next day and continued until all cells in the wild type control died. Medium containing cisplatin was changed every 2nd/3rd day. Cells surviving this treatment regimen were recovered and expanded in normal cell culture medium. To confirm acquired cisplatin resistance 2102EP$^{MPHv2/SAMv2}$, JAR$^{MPHv2/SAMv2}$, 2102EP^{WT} as well as JAR^{WT} cells were reseeded in 6-well cell culture plates and again exposed to cisplatin. Resulting cell viability was detected via brightfield microscopy.

For candidate gene identification, genomic DNA was isolated from 2102EP$^{MPHv2/SAMv2}$ as well as JAR$^{MPHv2/SAMv2}$ cells, sgRNA encoding DNA regions were amplified with specific bar code labeled primers using NEBNext® High-Fidelity 2X PCR Master Mix and analyzed via NGS on the NextSeq 550™ device. Bioinformatic analysis was carried out as described by Joung *et al.* [152] applying the *count_spacers.py* algorithm in Python/Biopython [154,155,160] to identify candidate genes and corresponding read count. All candidate genes displaying a read count >10,000 were analyzed using STRING 11.5 protein interaction database [164]. Overrepresented networks were further investigated for enriched pathways by Reactome database analysis tool [162].

2.2.9. Transformation

Chemically competent *E.coli* Top10 bacteria were thawed on ice. Plasmid DNA (1 µg) was added to 40 µl of bacteria and incubated for 30 min on ice. Next, heat shock was performed by keeping the cells for 1 min at 42 °C and subsequently on ice for 2 min. Afterwards, bacteria solution was supplemented with 400 µl recovery medium and incubated at 37 °C for 1 h at a shaking incubator (250 rpm). 50 µl of the transformation mix were spread on a LB agar plate containing 100 µg/ml ampicillin. Bacteria were grown overnight at 37 °C.

2.2.10. Plasmid Isolation

Colonies were picked from the LB agar plates (2.2.9) and incubated overnight in 3 ml liquid LB medium supplemented with ampicillin (100 µg/ml) at 200 rpm and 37 °C. 2 ml of the suspension were centrifuged at 13000 rpm for 1 min. The pellet was resuspended in 150 µl P1 buffer including RNaseA (100 µg/ml). Next, 300 µl of buffer P2 were added. The solution was carefully mixed. After addition of 150 µl buffer P3 and subsequent mixing a white sediment precipitated. Next, centrifugation was performed for 10 min at 14000 rpm. The clear supernatant was transferred to a new 1.5 ml reaction tube and 2 volumes ice cold ethanol were

added. For plasmid DNA precipitation the suspension was kept at -20 °C for 20 min and subsequently centrifuged for 2 min at 13000 rpm at 4 °C. Afterwards, the supernatant was removed and the pellet was air dried. Finally, the pellet was resuspended in 50 µl TE-buffer at 55 °C in a shaking incubator. DNA concentration was determined spectrophotometrically via a NanoDrop 1000 by measuring the absorbance at 260 nm.

2.2.11. Maxi prep

1 ml of the bacteria culture from 2.2.10 were used to inoculate 250 ml LB medium supplemented with ampicillin (100 µg/ml). The bacterial suspension was incubated at 37 °C, on a shaking incubator overnight. For large scale purification of plasmids, the NucleoBond® Xtra Maxi Plus kit was used according to the manufacturer's manual.

2.2.12. Sterile DNA precipitation

100 µl plasmid DNA were combined with 300 µl cold ethanol and 10 µl sodium acetate (3 M). DNA precipitation was performed at -80 °C for 30 min. Next, the suspension was centrifuged at 13000 xg, for 15 min at 4 °C. The pellet was washed twice with 70% ethanol (5 min, 12000 xg, 4 °C). After the second washing step the supernatant was completely removed and the pellet was air dried. Finally, the DNA was dissolved in 100 µl TE-buffer for 1 h at 55 °C on a shaking incubator. DNA concentration was determined using a NanoDrop 1000 device measuring the absorbance at 260 nm.

2.2.13. Agarose gel electrophoresis

DNA fragments were separated according to their size by agarose gel electrophoresis. Agarose was dissolved in 100 ml TAE buffer by boiling. Next, 10 µl of 0.07% ethidiumbromide were added for visualization of the DNA. Samples were mixed with 6x loading dye and loaded in the pockets of a polymerized agarose gel. After electrophoresis at 90 V for 30 to 60 min ethidium bromide bound DNA was detected by UV exposure (256 nm) resulting in red orange light emission.

2.2.14. RNA Isolation

For RNA isolation, cells were harvested using trypsin-EDTA. The cell pellet was washed twice with PBS by centrifugation at 12000 rpm for 5 min. RNA isolation was performed using the

RNeasy Mini Kit according to the manufacturer's instructions. The RNA concentration and purity were determined spectrophotometrically at 260 nm with a NanoDrop 1000 device. A 260 nm/280 nm ratio between 1.8 and 2.2 is accepted as an indicator for high purity RNA.

2.2.15. 3'mRNA sequencing

Cells were seeded in 6-well cell culture plates and treated for 1 h or 24 h with CDK inhibitors/solvents or for 2 days with MLN4924/cisplatin/combination or corresponding solvent. Total RNA was isolated as described in chapter 2.2.14. To determine RNA integrity (RIN) Nano 6000 Assay kit with the Agilent Bioanalyzer 2100 system was used. Samples with RIN >7 which is considered to be good quality were used for RNA sequencing analysis. The RNA quality control, library preparation (QuantSeq 3'-mRNA Library Prep) and RNA sequencing were carried out by the Core Facility Next Generation Sequencing (University of Bonn) using an Illumina HiSeq 2500 V4 (generating >10 million 50bp 3'-end reads per sample). Next, FastQC was applied to investigate raw data quality [156], for sequence trimming TrimGalore was used [166] and HISAT2.1 [158] was applied to map the trimmed sequences to the human genome (GRCh38.p13). StringTie 1.3.3 application [165] was used for quantification and annotation of transcripts. The python script preDE.py included in the StringTie package was applied for generation of a DEseq2 compatible data table. Further analysis was conducted in R/Bioconductor [153,161] embedded in R-studio environment [163]. For calculation of differential expressed genes with an adjusted p-value <0.05 (Benjamini-Hochberg method) the DESeq2 1.16.1 package [168] was used. Differential expression data were further investigated using STRING 11.5 database [164], integrated Gene Ontology [157,169] Reactome [162] and KEGG pathway [159] analysis tools.

2.2.16. Protein isolation

Treated or untreated cells were lysed in RIPA buffer supplemented with cOmplete ULTRA Tablets protease inhibitor and subsequent sonication. Cell debris were pelleted by centrifugation at 13,000 xg, for 15 min at 4 °C. Protein containing supernatant was collected and stored at -20 °C or -80 °C. For determination of protein concentration, the Pierce™ BCA Protein Assay kit was used according to the manufacturer's manual.

2.2.17. SDS-PAGE and Western blot analysis

Protein samples (see chapter 2.2.16) were supplemented with 4xRotiLoad and denatured for 10 min at 95 °C. Typically 20 µg of proteins were loaded in each pocket of a 12% SDS-polyacrylamide gel. An additional pocket was loaded with 5 µl PageRuler prestained protein ladder. Proteins were separated according to their molecular weight by gel electrophoresis. Next, proteins were transferred from the SDS-gel onto a PVDF membrane (pore size of 0.45 µm) using the semi-dry Trans Blot Turbo blotting chamber. To confirm successful transfer, the PVDF membrane was stained with Ponceau S solution. After washing the membrane with PBST, blocking in 5% BSA/PBST or in 5% milk/PBST was carried out for 1 h at RT. Next, the membrane was incubated with the target specific primary antibody overnight at 4 °C. After washing the membrane 3x for 10 min in PBST solution incubation with a species specific HRP-linked secondary antibody was performed for 1 h at RT. Again, the membrane was washed 3x for 10 min with PBST. To detect the signal the membrane was moistened with an enhanced chemiluminescence substrate (WESTAR NOVA 2.0/SuperSignal™ Western Blot Femto) and subsequently imaged at the ChemiDoc MP imaging system. If a second protein had to be detected bound antibodies were removed from the membrane by incubation in stripping buffer for 30 min at 60 °C. Subsequently, the membrane was washed 3x with ddH_2O, 3x with PBST and further processed as described above.

2.2.18. Peptide Chip Array

This method has been described before [170]. In brief, cells were treated with CDK inhibitors or corresponding DMSO control in 6-well cell culture plates for 1 h/24 h. Cells were lysed using M-PER Mammalian Protein Extraction Reagent, supplemented with Halt™ Phosphatase Inhibitor Cocktail as well as Halt™ Protease-Inhibitor Cocktail. After centrifugation at 13,000 xg, 4 °C for 15 min, supernatant was transferred to a new 1.5 ml reaction tube, snap frozen in liquid nitrogen and stored at -80 °C. On a Pamstation, serine and threonine kinase activity were examined in protein samples. Assay buffer containing 400 µM ATP was used to dilute the lysates before incubation on an immobilized peptide array. Detection of phosphorylated peptides followed a two-step process comprising a primary antibody against the phosphorylated serine or threonine residues and a secondary antibody labeled with FITC dye for fluorescence-based readout. Signal intensity correlates with phosphorylation frequency. Upstream kinases were identified according to the phosphorylation pattern of the immobilized substrates. The bioinformatic evaluation was performed by Pamgene application specialists using the Bionavigator software.

3. Results

TGCTs can be cured in most patients due to high sensitivity towards cisplatin [44,52]. However, apart from severe side effects, patients with cisplatin-resistant TGCTs are facing a very poor prognosis due to the lack of further treatment options [38]. Therefore, it is important to identify cisplatin resistance factors as well as alternative therapeutic options with less side effects independent of cisplatin sensitive or resistant tumors.

3.1. The role of transcriptional CDK inhibitors in TGCTs

Different CDK inhibitors were identified as potential options for cancer treatment. Especially drugs targeting cell cycle CDKs have been studied extensively [128,129]. The three CDK4/6 inhibitors Abemaciclib, Palbociclib and Ribociclib are already FDA approved for clinical treatment of advanced breast cancer [129]. Interestingly, Palbociclib and Ribociclib have also been shown to effectively reduce viability of TGCTs [102]. Nevertheless, there is further need for investigation of CDK inhibitors in TGCT treatment to identify the optimal treatment option with a minimum of side effects. Therefore, I first investigated the effect of CDK inhibitors on TGCTs with a strong focus on compounds targeting transcriptional CDKs.

3.1.1. CDKs are expressed in TGCTs

Initially, to confirm the expression of CDKs in TGCTs, I performed a meta-analysis of microarray data generated previously [108,171]. The expression of *CDK1-13* in TGCT/control cell lines and tissues was investigated. Interestingly, *CDK1*, *2*, *4* and *7* were highly expressed in TCam2, 2102EP, NCCIT, FS1 and MPAF cells (**Figure 7A**). Expression was also observed for *CDK5*, *6*, *9*, *10*, *11A*/*B*, *12* and *13* in all cell lines tested. *CDK3* and *8* were only expressed to a very low extend. Surprisingly, MPAF cells displayed lowest expression levels for many CDKs compared to other TGCT cell lines. *CDK1*, *4*, *7* and *9* were highly expressed in GCNIS, seminoma, EC, teratomas, mixed non-seminomas and normal testicular tissues (NTT) (**Figure 7B**). Expression of *CDK2*, *3*, *5*, *6*, *8*, *10*, *11A*/*B*, *12* and *13* was also found in all analyzed tissues. To determine CDK protein levels, I performed western blot revealing high CDK7, 9, 10 and medium CDK12, 13 levels in 2102EP, NCCIT, TCam2 and FS1 cell line (**Figure 7C**). In MPAF cells only CDK7 protein seemed to be highly expressed while low CDK9, 10, 12, 13 levels were detected. CDK7 double bands represented phosphorylated and unphosphorylated isoforms. Taken together, these findings demonstrated substantial *CDK7*, *9*, *10*, *12*, *13* mRNA and protein expression and therefore were viewed as potential targets for TGCT treatment.

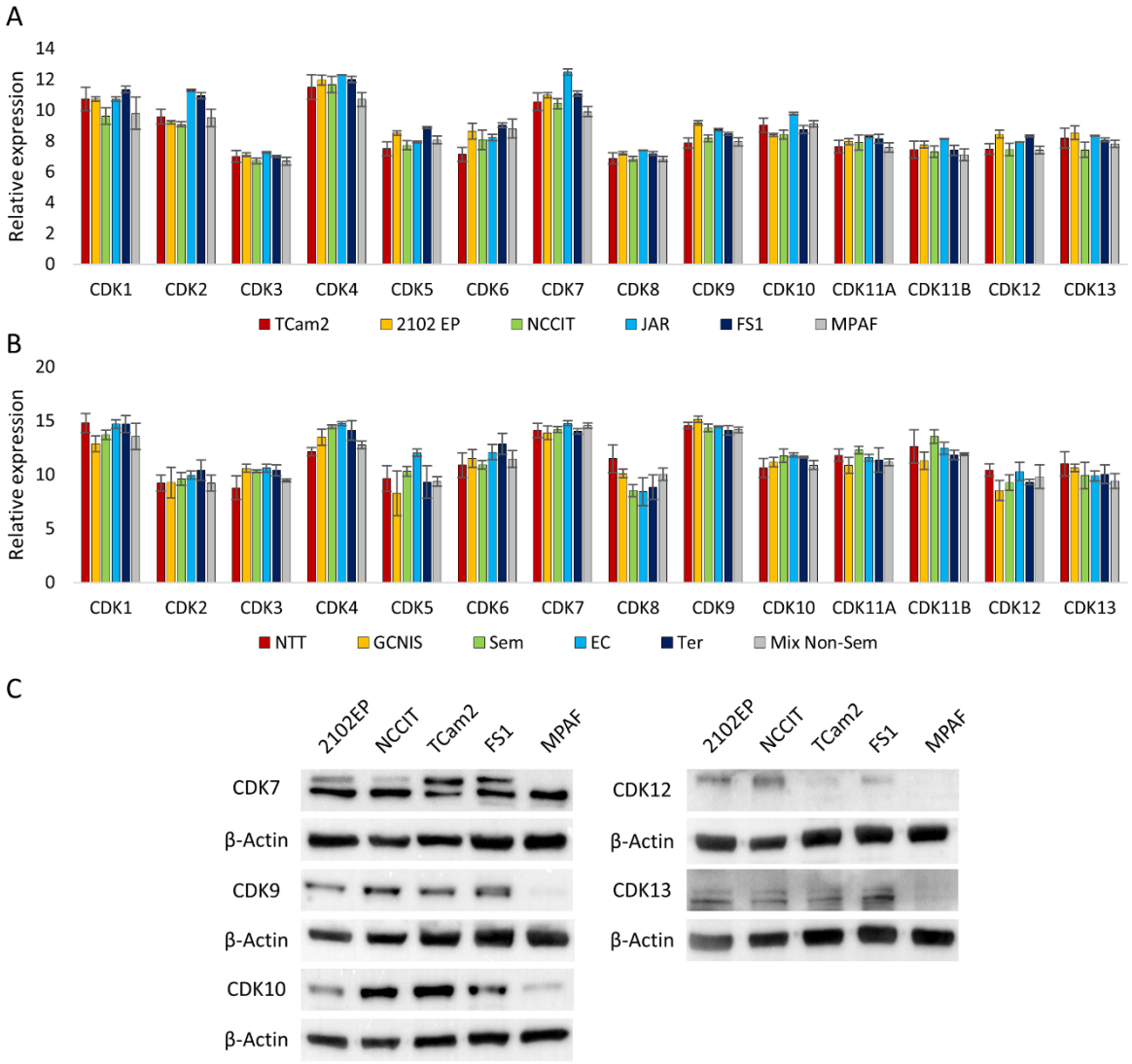

Figure 7: Expression of CDKs in TGCT and control cell lines. Modified from [1]. (**A**) Meta-analysis of CDK RNA expression levels of Illumina microarray data in TCam2, 2102EP, NCCIT, FS1 and MPAF cells. CDKs with relative expression >7 were considered expressed. (**B**) CDK expression on RNA level in tumor- (GCNIS, seminomas (Sem), EC, teratoma (Ter), mixed non-seminomas (Mixed Non-Sem)) and normal testicular tissues (NTT) derived from meta-analysis of Affymetrix microarray. CDKs with relative expression >10 were considered expressed. (**C**) CDK7, 9, 10, 12, 13 protein expression in 2102EP, NCCIT, TCam2, FS1 and MPAF cells detected via western blot analysis.

3.1.2. CDK inhibitors reduce viability in TGCT cell lines

Next, I investigated the effect of 7 different CDK inhibitors (YKL-5-124, S0351, NVP2, THZ531, THZ1, Dinaciclib and Flavopiridol) and a CDK9 degrader (THAL-SNS-032) (**Table 3**) on the viability of TGCT cisplatin sensitive, cisplatin resistant and control cell lines via XTT assay (**Figure 8**, **Figure 9**).

Table 3: CDK inhibitors/degrader and corresponding targets

Compound	Inhibitor/degrader	Targets
Flavopiridol	inhibitor	CDK1, 2, 4, 6, 7, 9
Dinaciclib	inhibitor	CDK1, 2, 5, 9, 12, 13
YKL-5-124	inhibitor	CDK7
THZ1	inhibitor	CDK7, 12, 13
SY0351	inhibitor	CDK7, 12, 13
THZ531	inhibitor	CDK12, 13
NVP2	inhibitor	CDK9
THAL-SNS-032	degrader	CDK9

The strongest effect was observed after 24 to 72 h NVP2 (CDK9 inhibitor) and SY0351 (CDK7, 12, 13 inhibitor) treatment which induced significantly decreased viability already at a concentration of 10 nM for 2102EP, 2102EP-R, NCCIT, NCCIT-R, TCam2 as well as FS1 cells. A similar effect was observable for YKL-5-124 (CDK7 inhibitor) treatment at 50 nM. Especially, the 2102EP and 2102EP-R cell lines seemed to be more sensitive towards the drug compared to the other cell lines. The CDK12, 13 inhibitor THZ531 induced only significantly decreased viability at 100 nM in the non-seminoma cell lines (2102EP, 2102EP-R, NCCIT, NCCIT-R) and at 500 nM in the seminoma (TCam2) as well as in the Sertoli cell line (FS1). Application of THZ1 (CDK7, 12, 13 inhibitor) resulted already at a concentration of 50 nM in significantly decreased viability in 2102EP, 2102EP-R, NCCIT and NCCIT-R cells. TCam2 and FS1 cells were only affected at 500 nM treatment. The pan CDK inhibitor Dinaciclib (CDK1, 2, 5, 9, 12, 13) turned out to be the most potent compound due to significantly decreased viability at 1 nM (2102EP, 2102EP-R, NCCIT, NCCIT-R and TCam2) and 50 nM (FS1). In 2102EP, 2102EP-R, NCCIT and NCCIT-R cell lines Flavorpiridol (CDK1, 2, 4, 6, 7, 9) induced effective reduction of viability at 50 nM while TCam2 as well as FS1 cells were only affected at 100/500 nM. The CDK9 degrader THAL-SNS-032 displayed strong effect on 2102EP, NCCIT and TCam2 cells at 100 nM but not on FS1 cells. Interestingly, MPAF cells were not or only affected to a low extend by the different CDK inhibitors/CDK degrader highlighting the therapeutic potential of this class of drugs.

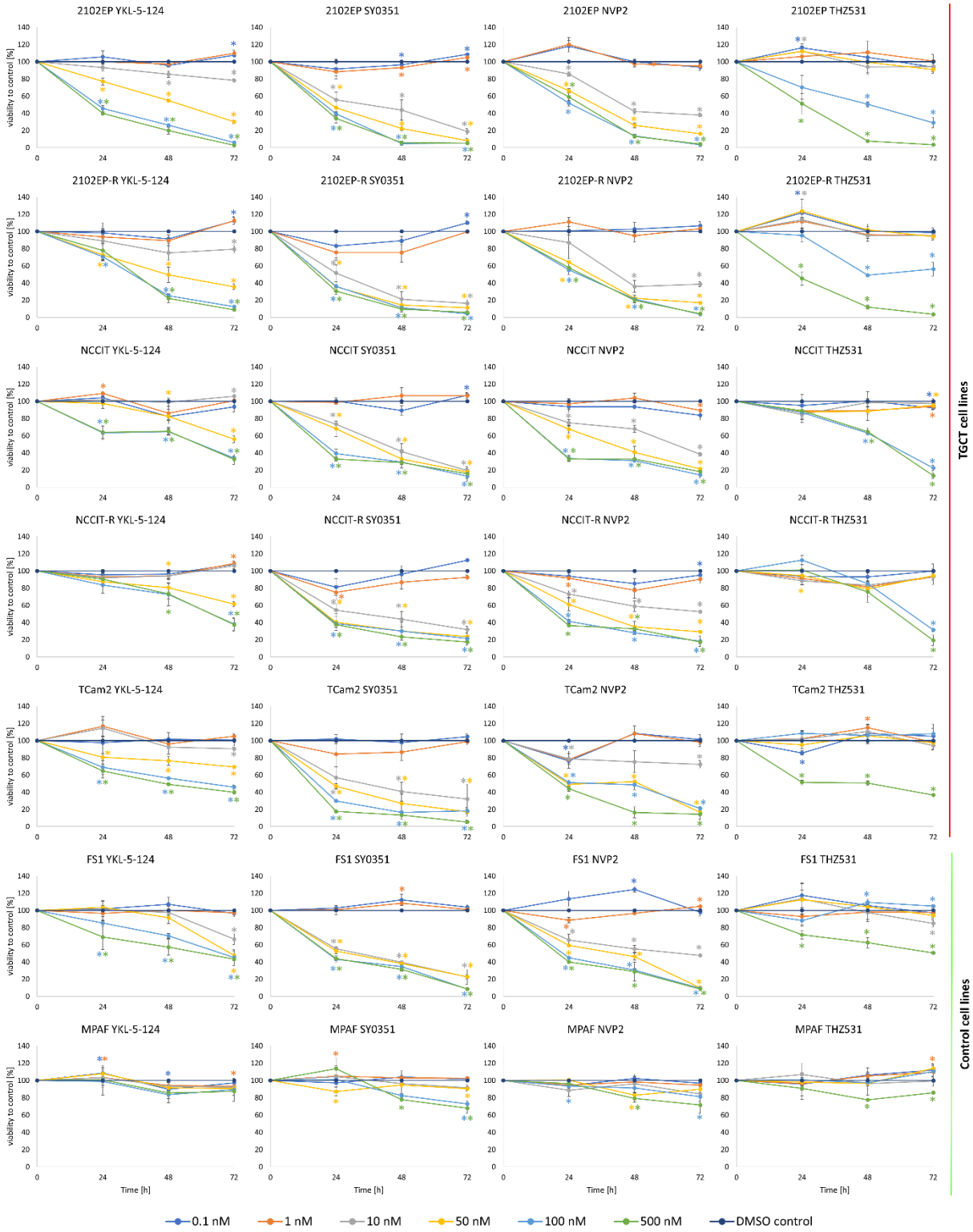

Figure 8: Viability of TGCT and control cells after YKL-5-124, SY0351, NVP2 and THZ531 treatment. Modified from [1]. Cisplatin sensitive as well as cisplatin resistant TGCT cell lines and control cells were treated with YKL-5-124, SY0351, NVP2, THZ531 or DMSO. After 24, 48 and 72 h cell viability was measured via XTT assay. CDK inhibitor treated groups were referred to control group. Asterisks indicate significant difference between treated group and control group ($p<0.05$) determined by two tailed student's t-test. Different CDK inhibitor concentrations are indicated by the color code. n=3-7.

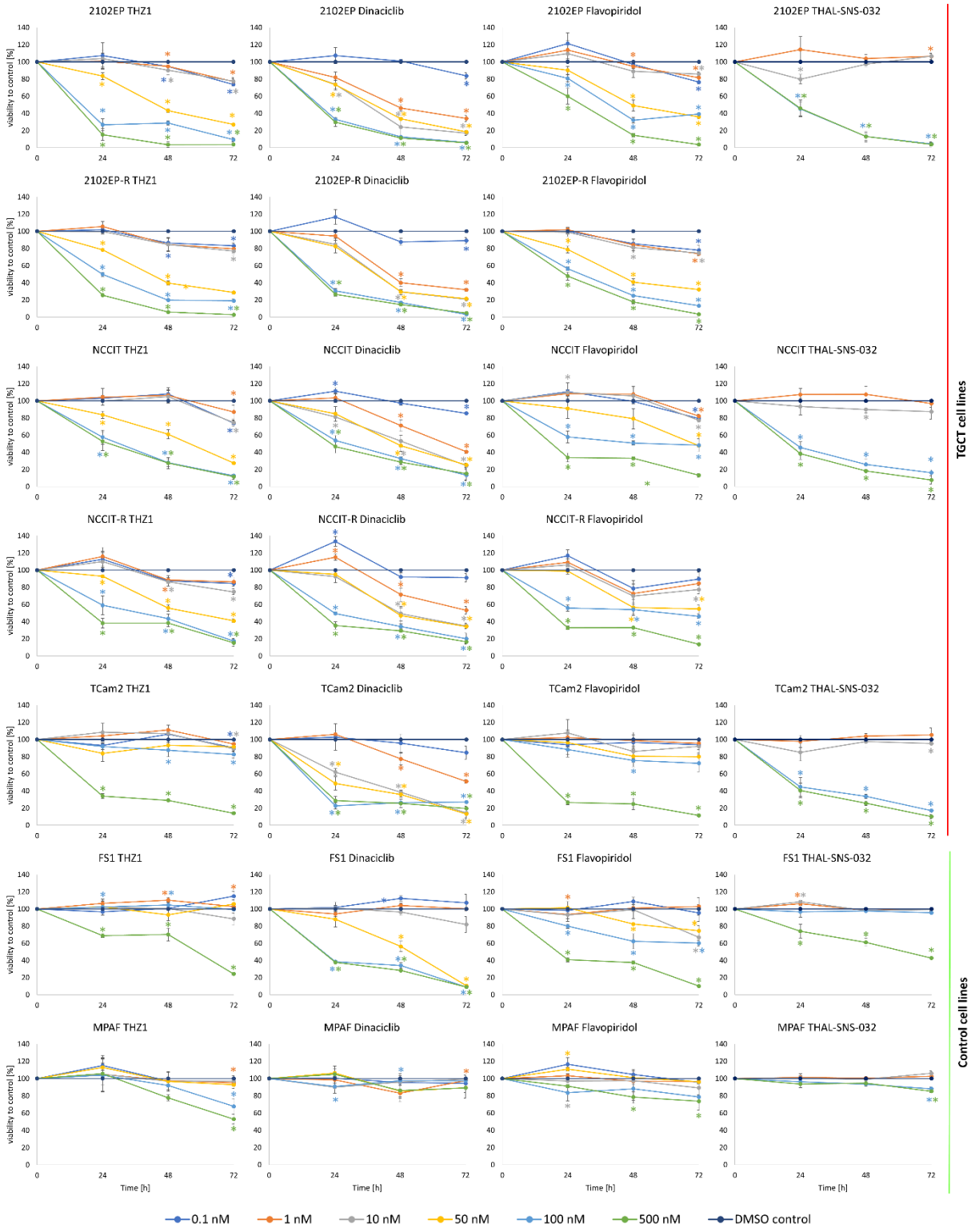

Figure 9: Viability of TGCT and control cells after THZ1, Dinaciclib, Flavopiridol and THAL-SNS-032 treatment. Modified from [1]. Cisplatin sensitive as well as cisplatin resistant TGCT cell lines and control cells were treated with THZ1, Dinaciclib, Flavopiridol, THAL-SNS-032 or DMSO. After 24, 48 and 72 h cell viability was determined via XTT assay. CDK inhibitor/PROTAC treated groups were referred to control group. Asterisks indicate significant difference between treated group and control group ($p<0.05$) calculated by two tailed student's t-test. Different CDK inhibitor/PROTAC concentrations are indicated by the color code. n=3-7

To compare the cytotoxic potential of the compounds IC_{50} values were calculated (**Table 4**). The highest potency was observed for Dinaciclib with IC_{50} values between 0.8 and 4.3 nM after 72 h treatment of TGCT cell lines. Very high potency was also detectable after 2102EP, 2102EP-R, NCCIT and FS1 cell treatment for 72 h with NVP2 (IC_{50}: 6.1 to 8.6 nM). SY0351 was found with very low IC_{50} concentrations (IC_{50}: 6.4 to 9.0 nM) in 2102EP, 2102EP-R, NCCIT, TCam2 and FS1 indicating very high potency as well. Flavopiridol (IC_{50}: 7.5 to 272.7 nM) and THZ1 (IC_{50}: 6.7 to >1000 nM) displayed very high to low drug potency after 72 h of 2102EP, 2102EP-R, NCCIT, NCCIT-R, TCam2 and FS1 cell lines, indicating strong cell line specific cytotoxicity. IC_{50} values after YKL-5-124 were especially low in 2102EP (72 h IC_{50}: 17.2 nM) and 2102EP-R (72 h IC_{50}: 23.6 nM) cells suggesting a high selectivity for these cell lines. THZ531 revealed high potency in 2102EP/NCCIT cells (72 h IC_{50}: 74.5/96.9 nM), moderate potency in 2102EP-R/NCCIT-R cells (72 h IC_{50}: 163.9/137.2 nM) and low potency in TCam2/FS1 cells (72 h IC_{50}: both >1000 nM). Interestingly, for all inhibitors IC_{50} values for MPAF control cells were >1000 nM after 24, 48 and 72 h suggesting very low sensitivity towards CDK inhibitors. Taken together, these data indicate specific cytotoxic effect of CDK inhibitors/degrader on TGCTs while somatic cells are unaffected.

Table 4: IC50 values of CDK inhibitor treated TGCT and control cells. Modified from [1]. Values were calculated based on the XTT viability data (**Figure 8, Figure 9**) by logarithmic regression (**Appendix Figure 1** - **Appendix Figure 8**). Color code indicates very high drug potency (green, IC_{50} <10 nM), high drug potency (yellow, IC_{50} between 10 and 100 nM), moderate drug potency (red, IC_{50} between 100 and 1000 nM) and low drug potency (white, IC_{50} >1000 nM).

	IC_{50} [nM]							
	NVP2	**SY0351**	**YKL-5-124**	**THZ531**	**THZ1**	**Dina-ciclib**	**Flavo-piridol**	**THAL-SNS-032**
2102EP 24h	502.7	38.7	317.6	>1000	95.6	76.8	>1000	164.15
2102EP 48h	10.5	7.5	43.6	179.6	26.3	3.4	39.94	39.51
2102EP 72h	6.1	6.7	17.2	74.5	6.7	0.8	18.01	34.82
2102EP-R 24h	884.1	15.9	>1000	>1000	235.3	102.2	>1000	
2102EP-R 48h	11.2	3.4	30.5	227.5	16.3	2.0	21.85	
2102EP-R 72h	8.6	6.4	23.6	163.9	9.9	1.1	7.56	
NCCIT 24h	90.6	104.5	>1000	>1000	>1000	593.5	710.47	149.39
NCCIT 48h	40.7	19.1	>1000	>1000	92.9	21.8	21.85	50.62
NCCIT 72h	6.5	9.0	121.1	96.6	9.3	1.5	34.07	30.09
IC_{50} < 10nM			10nM < IC_{50} < 100nM			100nM < IC_{50} < 1000nM		

	IC_{50} [nM]							
	NVP2	**SY0351**	**YKL-5-124**	**THZ531**	**THZ1**	**Dina-ciclib**	**Flavo-piridol**	**THAL-SNS-032**
NCCIT-R 24h	103.7	24.9	>1000	>1000	929.4	314.8	638.83	
NCCIT-R 48h	17.1	14.0	>1000	>1000	145.0	19.6	106.83	
NCCIT-R 72h	12.2	11.6	178.1	137.2	16.2	4.3	43.28	
TCam2 24h	215.7	21.6	>1000	>1000	>1000	35.1	>1000	139.83
TCam2 48h	60.0	8.9	>1000	>1000	>1000	11.5	581.81	76.70
TCam2 72h	16.1	8.6	263.4	>1000	847.0	1.6	272.74	39.57
FS1 24h	98.2	85.4	>1000	>1000	>1000	392.6	>1000	>1000
FS1 48h	33.5	30.1	>1000	>1000	>1000	85.7	695.75	>1000
FS1 72h	8.9	7.7	95.2	>1000	>1000	14.3	91.47	>1000
MPAF 24h	>1000	>1000	>1000	>1000	>1000	>1000	>1000	>1000
MPAF 48h	>1000	>1000	>1000	>1000	>1000	>1000	>1000	>1000
MPAF 72h	>1000	>1000	>1000	>1000	>1000	>1000	>1000	>1000
IC_{50} < 10nM			10nM < IC_{50} < 100nM			100nM < IC_{50} < 1000nM		

3.1.3. NVP2, SY0351, YKL-5-124 and THZ531 induce apoptosis and cell cycle arrest in TGCT cell lines

For further investigations, I decided to focus on the CDK9 inhibitor NVP2 and the CDK7, 12, 13 inhibitor SY0351 because of their very high potency in TGCT cell lines, YKL-5-124 (CDK7 inhibitor) which displayed high cytotoxicity towards 2102EP cell lines and THZ531 (CDK12, 13 inhibitor) showing a low cytotoxic effect towards FS1 cells. Next, apoptosis (**Figure 10**, **Appendix Figure 9**) and cell cycle analysis (**Figure 11**, **Appendix Figure 10**) were performed in 2102EP, NCCIT, TCam2, FS1 and MPAF cells.

To investigate apoptosis induction after CDK inhibitor treatment of TGCT cell lines FACS-based apoptosis analysis was conducted (**Figure 10**). Very strong apoptosis which was up to 5.6-fold higher than in DMSO control was detected in 2102EP and NCCIT cells treated with low concentrations of NVP2 (10 nM) or SY0351 (10 nM) for 48 h. Elevated levels of apoptotic cells have also been observed in TCam2 and FS1 cells. MPAF cells revealed even 48 h after treatment lower levels of apoptosis (1.7- to 2.4-fold change).

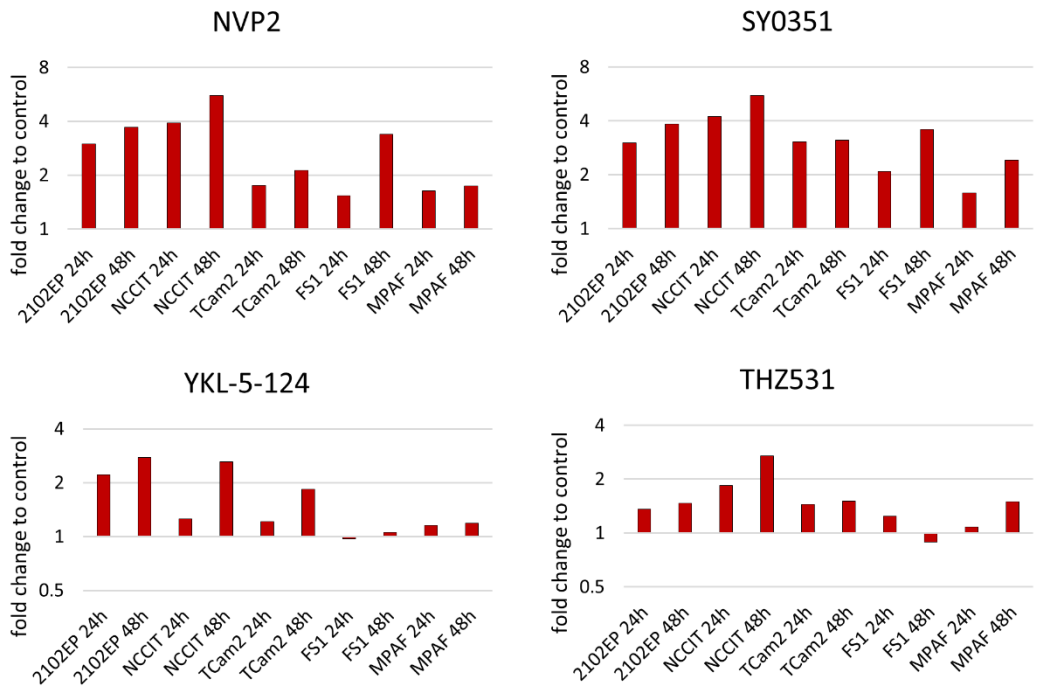

Figure 10: Apoptosis induction after CDK inhibitor treatment of TGCT cell lines. Modified from [1]. After treatment of 2102EP, NCCIT, TCam2, FS1 and MPAF cells with NVP2 (10 nM), SY0351 (10 nM), YKL-5-124 (100 nM), THZ531 (100 nM) and DMSO control (0.0002%) for 24/48 h FACS-based apoptosis analysis (PE AnnexinV/7AAD) was performed. Fold change to control was calculated according to data in **Appendix Figure 9**.

YKL-5-124 (100 nM) treatment did not induce apoptosis in the control cell line FS1 and MPAF cells. 2102EP, NCCIT and TCam2 cells revealed an apoptotic response after 48 h of YKL-5-124 exposure (up to 2.8-fold change), indicating a tumor cell line specific response. Interestingly, the apoptosis rate was already more than 2-fold higher in 2102EP cells compared to DMSO control treated cells after 24 h of YKL-5-124 treatment covering the findings from the XTT viability assay of high 2102EP sensitivity towards the CDK7 inhibitor. THZ531 resulted only in low levels of apoptosis between 1.3- and 2.7-fold change in 2102EP, NCCIT as well as TCam2 cells. In general, NVP2, SY0351 and YKL-5-124 displayed strong apoptosis induction in 2102EP as well as NCCIT cell lines while TCam2, FS1 and MPAF cells were less sensitive towards the treatment.

Since the drugs interfere with cell proliferation, cell cycle distribution of 2102EP, NCCIT, TCam2, FS1 and MPAF cells after 20 h of NVP2, SY0351, YKL-5-124 and THZ531 treatment was investigated (**Figure 11**/**Appendix Figure 10**). Overall, all compounds only induced mild changes in the cell cycle after 20 h of treatment.

In detail, NVP2 and SY0351 treatments revealed accumulation of 2102EP as well as NCCIT cells in the G1 phase and reduction of cell fraction in S-phase. TCam2 cells also displayed reduced number of cells in S-phase but similar increase of cells in G1 as well as G2/M-phase. Cell cycle of FS1 and MPAF cells was only disturbed to a very low extend.

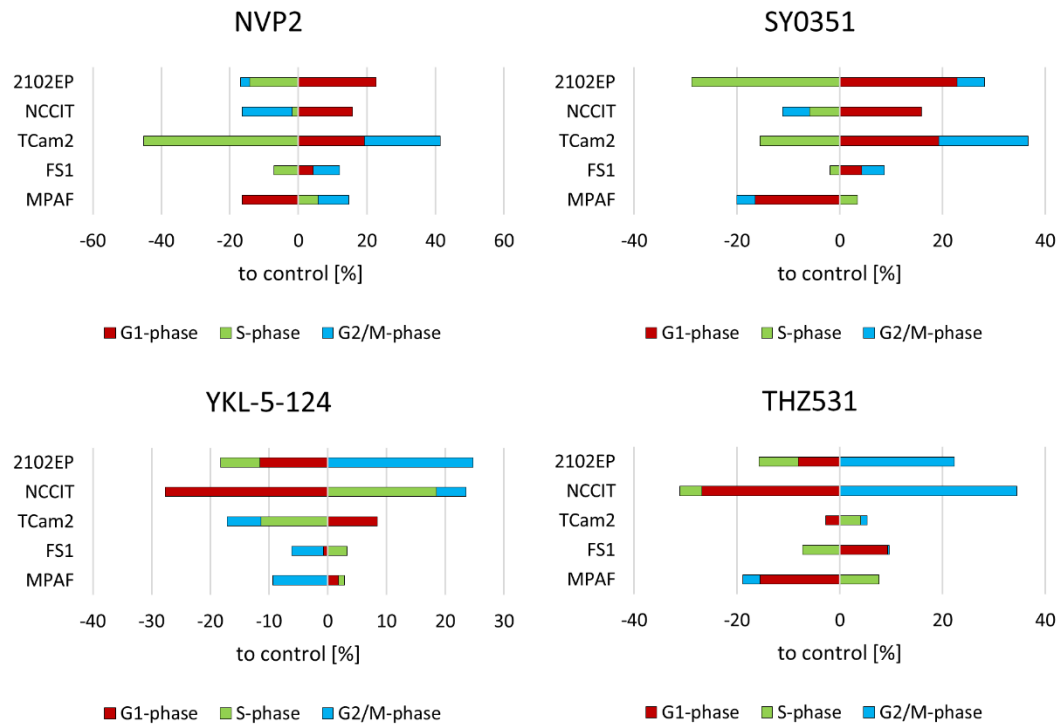

Figure 11: CDK inhibition disturbed the cell cycle of TGCT cell lines. Modified from [1]. Hoechst FACS-based cell cycle analysis of 2102EP, NCCIT, TCam2, FS1 and MPAF cell lines treated with NVP2 (10 nM), SY0351 (10 nM), YKL-5-124 (100 nM), THZ531 (100 nM) and DMSO (0.0002%) for 20 h. Change of cell fraction in cell cycle phases were referred to DMSO control (see **Appendix Figure 10**).

YKL-5-124 initiated accumulation of 2102EP cells in G2/M-phase while NCCIT cells revealed increased cell number in S-phase. In TCam2, FS1 as well as MPAF cells minor changes in cell cycle distribution were found. After 20 h of THZ531 treatment accumulation of cells in G2/M-phase and slight reduction of S-phase cell fraction was observable in 2102EP as well as NCCIT. For TCam2, FS1 as well as MPAF cells, cell cycle was only affected to a very low extend. To sum up, application of NVP2, SY0351, YKL-5-124 and THZ-531 revealed disturbed cell cycle causing cell accumulation in G1 or G2/M-phase in 2102EP, NCCIT and TCam2 cells while only minor effects were observed in the control cell lines FS1 and MPAF.

3.1.4. Elucidating the molecular effects of NVP2, SY0351, YKL-5-124 and THZ531

To investigate the impact of NVP2, SY0351, YKL-5-124 and THZ53 on global gene expression, 3'mRNA-sequencing of treated 2102EP, TCam2 and MPAF cells was performed. Interestingly, after 1 h and 24 h of NVP2, SY0351 and THZ531 application between 0 and 17 differentially expressed genes overlapped in 2102EP, TCam2 and MPAF cells indicating a cell line specific response to the different compounds (**Figure 12**).

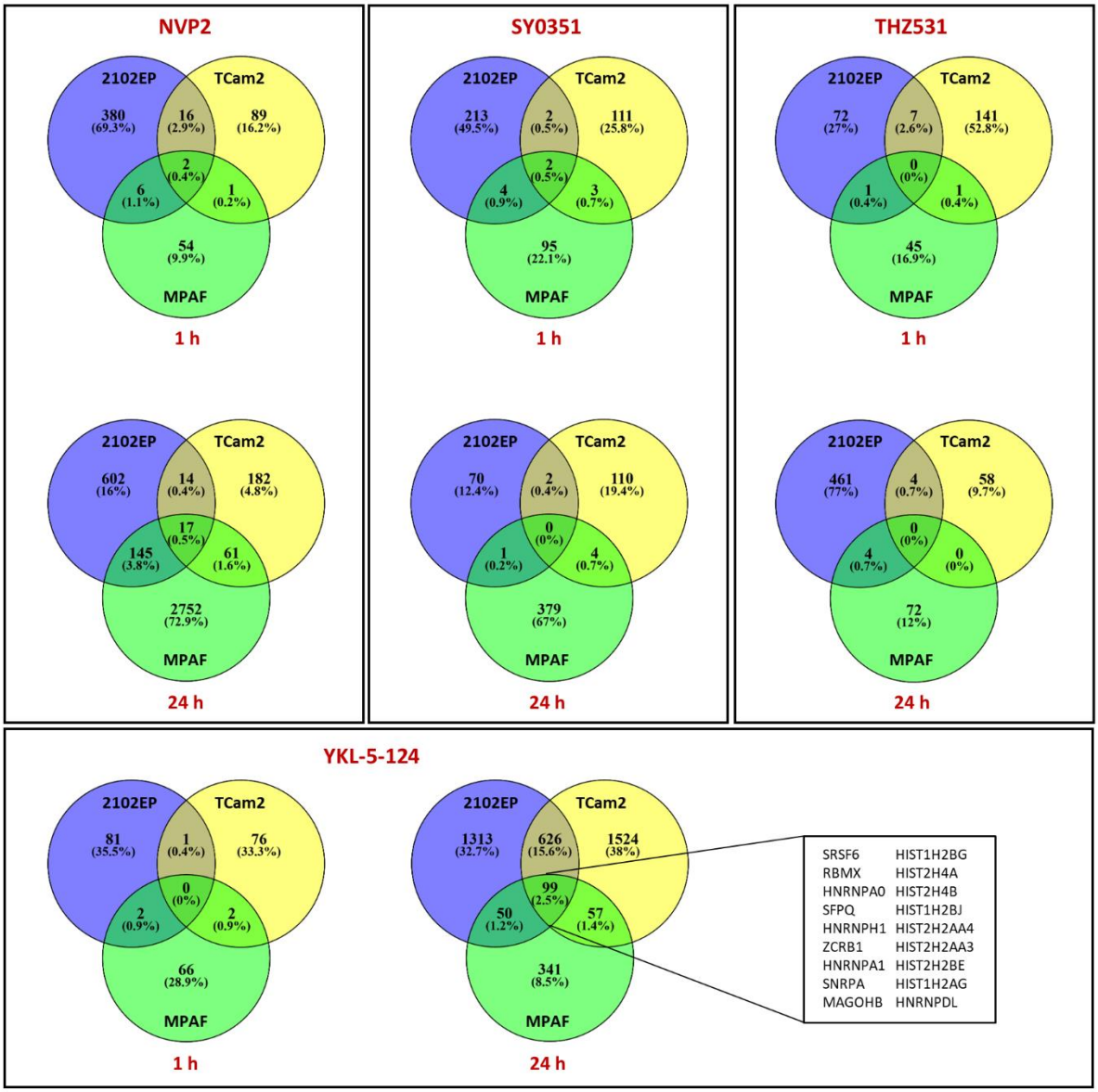

Figure 12: Common differentially expressed genes identified by 3'mRNA-Sequencing analysis after CDK inhibitor treatment. Modified from [1]. After NVP2, SY0351, THZ531 and YKL-5-124 treatment for 1 or 24 h the transcriptome was analyzed using 3'mRNA sequencing. Venn diagrams display overlap of differentially expressed genes for the different cell lines, inhibitors and time points.

Surprisingly, YKL-5-124 treatment of 2102EP, TCam2 and MPAF for 24 h revealed 99 common differentially expressed genes, amongst others comprising 8 different genes for histone variants. Histone mRNAs typically end in a 3'stem loop rather than being polyadenylated. Therefore, the high upregulation most likely indicates defective 3'-end processing resulting in incorporation of cryptic polyA sites mediated by CDK7 inhibition [118]. This suggests false positive histone mRNA enrichment in 3'mRNA sequencing analysis.

Further, YKL-5-124 treatment (**Figure 13A**) revealed a compact STRING interaction network including 11 genes like *HNRNP* family members *HSPA8*, *SFPQ*, *MAGOHB*, *RBMX*, *SNRPA*, *SRSF6* as well as *ZCRB1* (**Figure 13B**). GO analysis of the network members suggested downregulation of mRNA splicing and mRNA processing (**Figure 13C**) mediated by YKL-5-124 treatment.

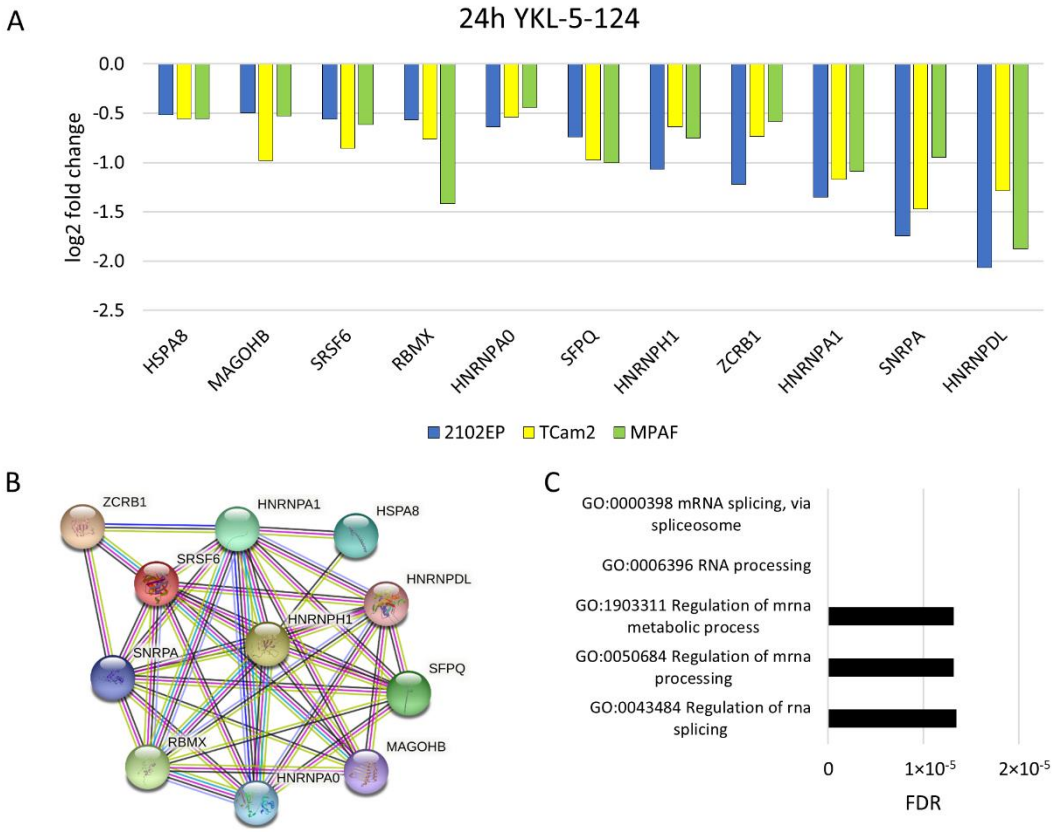

Figure 13: YKL-5-124 treatment induces a common molecular response in 2102EP, TCam2 and MPAF. Modified from [1]. 2102EP, TCam2 and MPAF cells were treated for 24 h with YKL-5-124 (100 nM) or DMSO control (0.0002%) and subsequently analyzed by 3'mRNA-sequencing. (**A**) Log2 fold change of common differentially downregulated genes, (**B**) corresponding STRING interaction network and (**C**) gene ontology analysis. *n=3.*

Next, I had a closer look on cell line specific effects induced by YKL-5-124 treatment (**Figure 14A**). Immediate early genes such as *EGR* and transcription factor subunit *JUN* were downregulated after treated for 1 h. In addition, lower *ASPH*, *POLR2E*, *CTDP1*, *LY6E* as well as *PLAUR* transcript abundancy was detected revealing enriched GO terms associated with downregulation of RNA polymerase II transcription activity (**Figure 14B**) and a STRING interaction network (**Figure 14C**). MPAF cells exposed for 24 h to YKL-5-124 displayed differentially downregulated genes like *E2F1*, *E2F2*, *CCNA*, *CCNE2*, *CDT1* etc. (**Figure 14D**) clustering together in a STRING interaction network (**Figure 14E**). According to GO analysis these genes are responsible for cell cycle progression (**Figure 14F**) suggesting cell cycle arrest after more than 24 h of YKL-5-124 treatment.

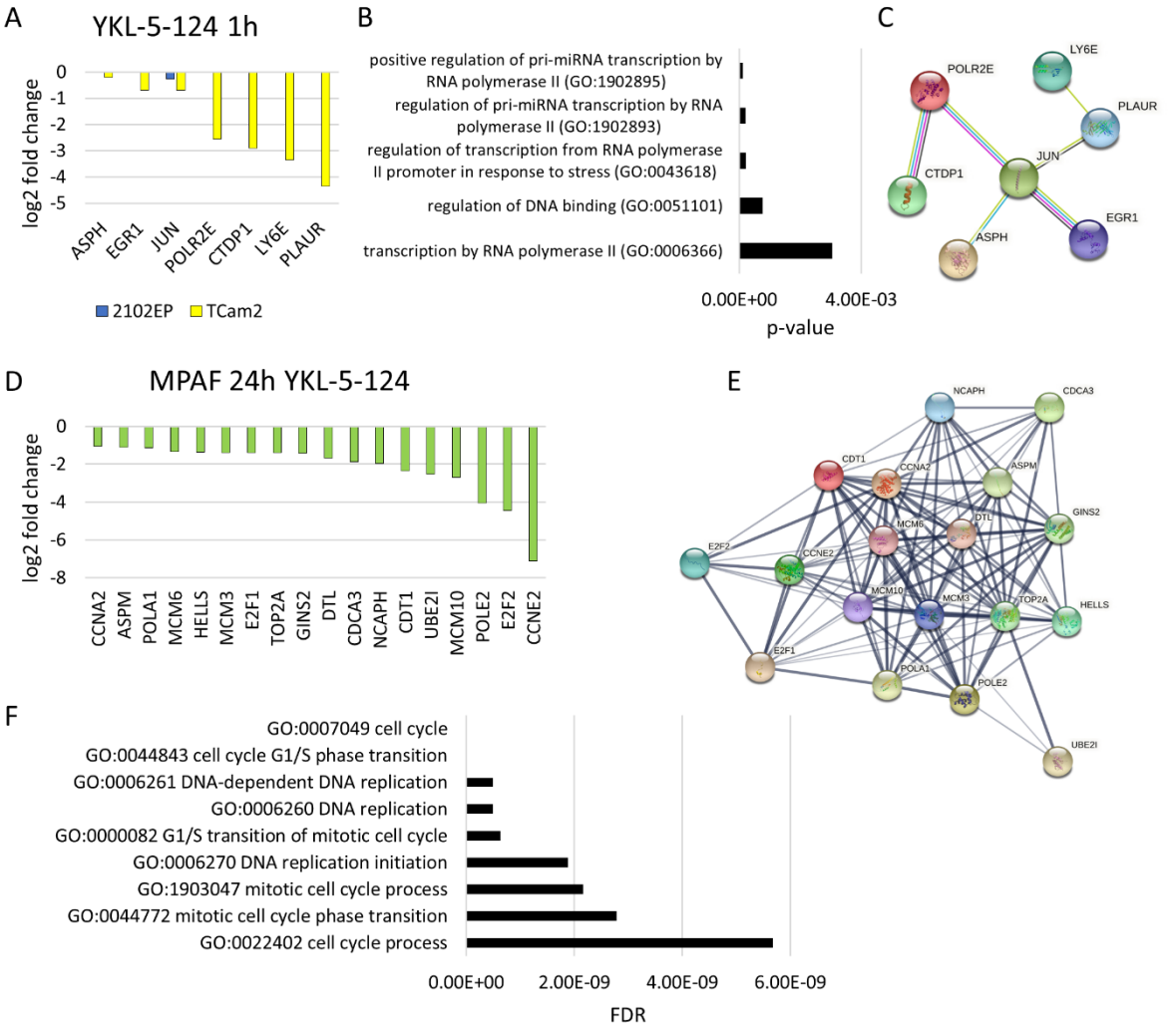

Figure 14: Elucidating YKL-5-124 cell line specific molecular effects. Modified from [1]. (**A**) Differentially downregulated genes after 1 h of YKL-5-124 treatment in TCam2 and 2102EP cells (**B**) associated with RNA polymerase II function (GO analysis) and corresponding (**C**) STRING interaction network. (**D**) 24 h treatment of MPAF cells with YKL-5-124 revealed differentially downregulated genes (**E**) forming a STRING interaction network and (**F**) GO terms associated with the cell cycle. *n=3.*

Transcriptome analysis of NVP2 revealed differentially deregulated genes after 1 h of treatment. *PCBP4*, *MED12*, *CCNY* and *CDKN1A* forming a STRING interaction network were found to be upregulated and according to GO analysis associated with induction of cell cycle arrest (**Figure 15A**). Transcripts of *SOX2*, *JUNB*, *NFKBIA*, *JUN*, *TRIB1*, *IRF1*, *DDIT*, *EGR1* and *FOSB* were found to be less abundant also forming a complex STRING interaction network related to decreased RNA Polymerase II specific DNA-binding transcription activator activity. 24 h of NVP2 treatment revealed increased mRNA levels of PRAME (*PRAMEF8*, *9*, *11, 14, 26*), methyl-CpG-binding domain protein 3-like (*MBD3L2*, *MBD3L3*, *MBD3L5*) and TRIM (*TRIM43*, *48*, *49*, *49C*) family members (**Figure 15B**). GO analysis suggested negative regulation of transcription, increased DNA-methylation-dependent heterochromatin assembly and ubiquitination activity, respectively.

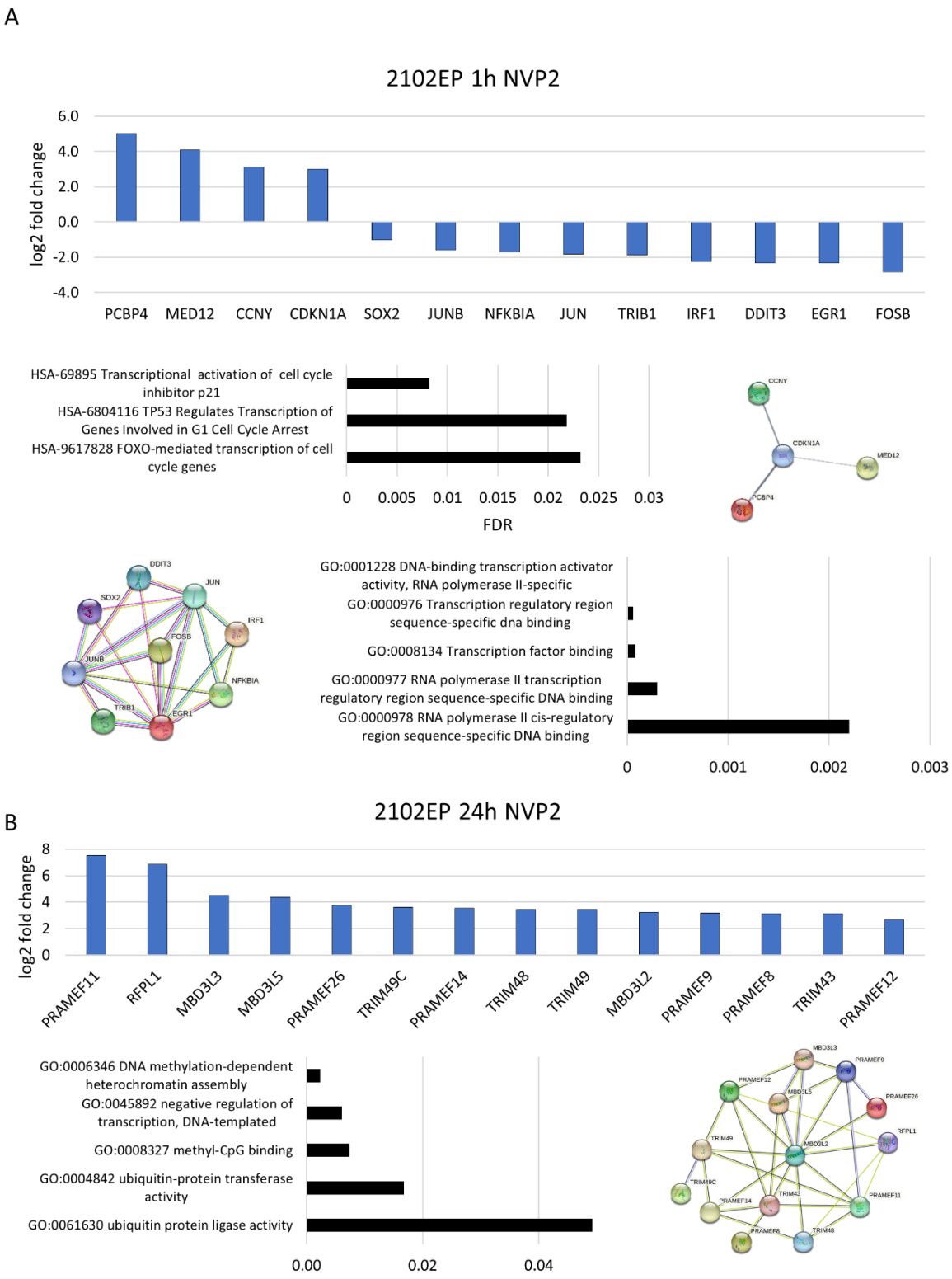

Figure 15: NVP2 treatment induced 2102EP cell line specific molecular response. Modified from [1]. (**A**) 3'mRNA sequencing analysis after NVP2 treatment for 1 h of 2102EP cells revealed differentially expressed genes, which were investigated by STRING interaction network and GO analysis. (**B**) Differentially expressed genes in 2102EP cells after 24 h of NVP2 treatment and corresponding GO and STRING interaction analysis. *n=3.*

In NVP2 treated TCam2 cells (1 h) deregulation of apoptotic process and RNA Polymerase II based transcription in response to stress was found based on downregulation of *DUSP4*,

NFKBIA, *CBX4*, *DDIT3*, *JUN*, *DUSP6* and *EGR1* (**Figure 16A**). 24 h of treatment revealed a highly significant STRING interaction network with differentially downregulated genes (*LSM3*, *SRSF7*, *SNRPB*, *HNRNPC*, *HNRNPH1*, *ALYREF*, *MAGOHB*, *SRSF6*, *HNRNPA1* and *SF3B1*) which are responsible for decreased RNA processing activity (**Figure 16B**).

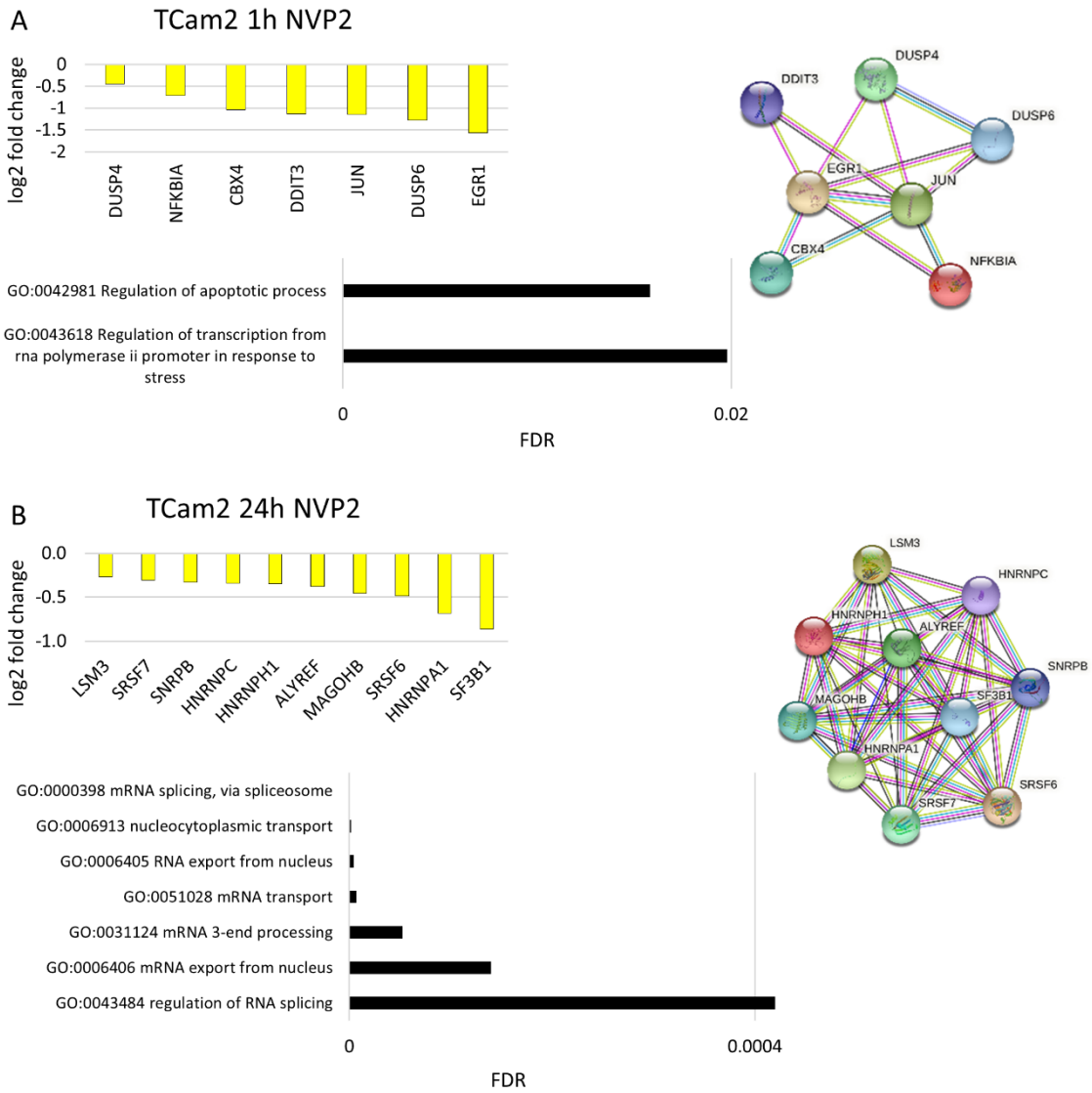

Figure 16: TCam2 cell line displayed a specific molecular response after NVP2 treatment. Modified from [1]. Differentially expressed genes 1 h (**A**) as well as 24 h (**B**) of NVP2 treatment in TCam2 cells and corresponding STRING interaction networks including GO analysis. *n=3.*

In 2102EP and TCam2 cells, already after 1 h exposure to the CDK9, 12, 13 inhibitor SY0351 differentially deregulated genes forming STRING interaction networks could be detected (**Figure 17A**/**B**). In 2102EP increased transcript abundance of *ASB6*, *RNF7*, *UBE2E1*, *NAE1* and *MAP3K14*, *GLI1*, *ENDOG*, *CASP2*, etc. were found which are associated with elevated ubiquitination and response to stress combined with apoptosis induction, respectively. After 1 h of SY0351 treatment of TCam2 cells differentially downregulated genes such as eukaryotic translation initiation factors *EIF3C*, *EIF2S1* and *EIF5A* as well as apoptosis-inhibiting factors

XIAP, *CFLAR* were detected. Reactome pathway analysis of these factors revealed decreased RNA transport and downregulation of apoptosis induction. MPAF cells treated for 24 h displayed deregulation of immediate early genes like *EGR1*, *FOS* and *JUNB* (**Figure 17C**). Together with *AHR*, *CDKN1A* and *DUSP* these genes reveal a STRING interaction network associated with decreased transcription factor AP-1 and RNA Pol II activity.

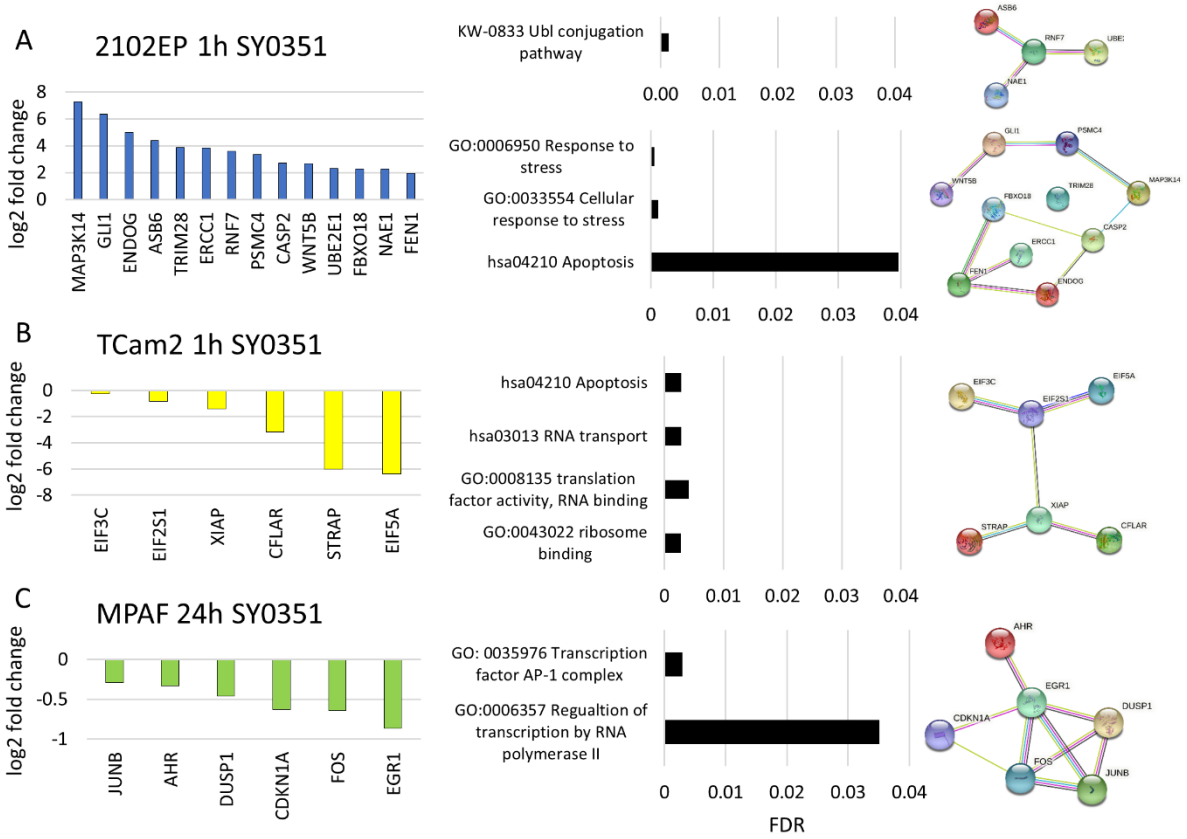

Figure 17: Transcriptome analysis of SY0351 treated 2102EP, TCam2 and MPAF cells. Modified from [1]. After SY0351/DMSO control treatment of (**A**) 2102EP/ (**B**) TCam2 cells for 1 h and (**C**) MPAF cells for 24 h 3'mRNA sequencing analysis was performed. Differentially expression was determined and GO as well as STRING interaction analysis were applied. *n=3.*

THZ531 treated 2102EP cells (24 h) revealed increased RNA degradation and poly(A)-specific ribonuclease activity indicated by elevated mRNA levels of *PAN2*, *BTG2*, *PABPC1* and *PARN* (**Figure 18A**). In TCam2 cells after 1 h of SY0351 exposure 26S-proteasomal subunits *PSMD7*, *PSMD13* and *PSME4* as well as further proteasome-associated transcripts (*RAD23A*, *UBA1*, *NACC1*) were found to be differentially downregulated suggesting decreased protein ubiquitination and consequently lower levels of proteasomal activity (**Figure 18B**).

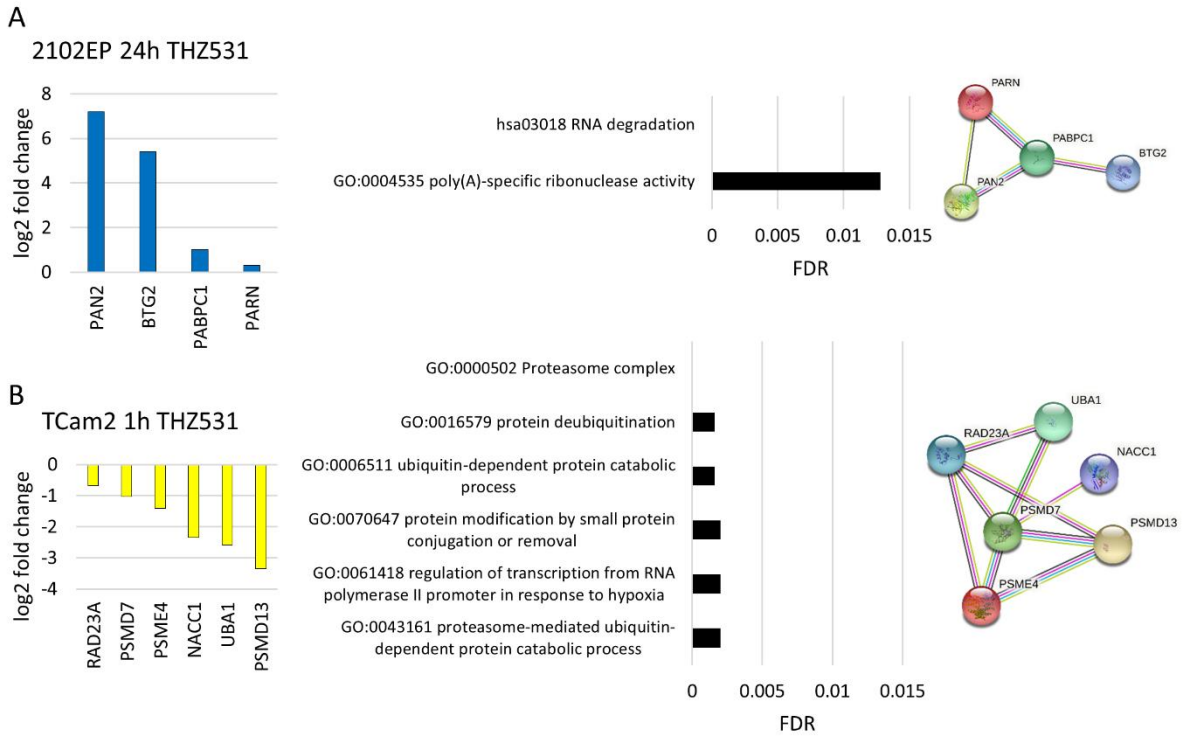

Figure 18: Investigation of molecular effect on RNA level after THZ531 treatment. Modified from [1]. Differentially gene expression, GO and STRING interaction network analysis were performed after THZ531 treatment of (**A**) 2102EP cells for 24 h and (**B**) TCam2 cells for 1 h. *n=3.*

In order to generate a more detailed understanding of the molecular pathways affected upon YKL-5-124, NVP2 and THZ531 treatment, I performed a peptide microarray to investigate the serine/threonine kinase activity (**Figure 19A-C**).

After 1 h of YKL-5-124 treatment, death-associated protein kinase 3 (DAPK3) was identified as the top upregulated kinase in 2102EP cells confirming the earlier mentioned potential of specific and strong induction of apoptosis (**Figure 19A**). TCam2 cells revealed only mild changes in differential serine/threonine kinase activity on a global point of view which is in line with the low effect of YKL-5-124 on the seminoma cell line.

In contrast, NVP2 treatment of 2102EP cells for 1 h resulted in elevated phosphorylation activity of stress-related and pro-apoptotic kinases (p38α, JNK1, JNK 2, JNK 3) (**Figure 19B**). This supports the strong effect of the compound which has been detected in XTT viability assay and FACS based apoptosis analysis. Interestingly, CDK15 (PFTAIRE2) activity was enhanced, which is in accordance with the observed upregulation of the corresponding cyclin *CCNY* on mRNA level. Exposure of 24 h revealed high activity of PIM1, PIM2, PIM3 responsible for antagonization of p21 activity, thereby preventing G1 phase cell cycle arrest.

Figure 19: Altered serine/threonine kinase activity in CDK inhibitor treated TGCT cell lines. Reprinted from [1]. Top differential kinases (treated group vs. DMSO control) were rank-ordered in kinase score blots. 2102EP and TCam2 cells were treated for 1 h/24 h with (**A**) YKL-5-124 (100 nM), (**B**) NVP2 (10 nM) or (**C**) THZ531 (100nM). Proteins were isolated and subsequently analyzed by microarray peptide assay (PAM Gene). For all conditions *n=2*.

2102EP cells treated with THZ531 (1 h) displayed DNA repair induction (CK1 delta), elevated growth signaling (ERK1, ERK2) as well as cell cycle progression (CDK6) (**Figure 19C**). After 24 h, global downregulation of serine/threonine kinase activity was observable. PI3K-AKT pathway members p70S6K and AKT1, AKT2 as well as protein kinase A which is involved in energy metabolism were identified as kinases with strongest downregulated activity. In contrast to 2102EP cells, TCam2 cell line treated for 1 h with THZ531 revealed downregulation of CDK2, ERK1, ERK2 and CDK9 activity. After 24 h, a global downregulation of kinase activity was detected in TCam2 cells comparable to the effect observed in 2102EP cells. In detail,

kinase activity of CDK1, CDK5, CDK9, CDK11 as well as stress-activated Protein Kinase 2b (p38) were reduced.

To sum up, I identified various CDK inhibitors revealing a strong cytotoxic effect, apoptosis and disturbed cell cycle progression in TGCT cell lines without affecting the fibroblast control cell line. Transcriptome analysis of SY0351, NVP and THZ531 application displayed cell line specific effects while YKL-5-124 treated 2102EP, TCam2 and MPAF cells resulted in many common differentially deregulated genes suggesting a similar response mechanism.

3.2. Elucidating molecular mechanisms of cisplatin resistance in TGCTs

As mentioned before, chemotherapy resistance of TGCTs is a very important issue since no effective alternative treatment is available yet [38]. So, on the one hand site it is very important to put effort in research for novel treatment options as shown in section 3.1 and on the other side it is crucial to identify cisplatin resistance mechanisms thereby addressing the problem from different sites. Thus, I next applied a genome scale CRISPR/Cas9 activation screen to generate cisplatin resistant TGCT cells and identify candidate genes (**Figure 20**).

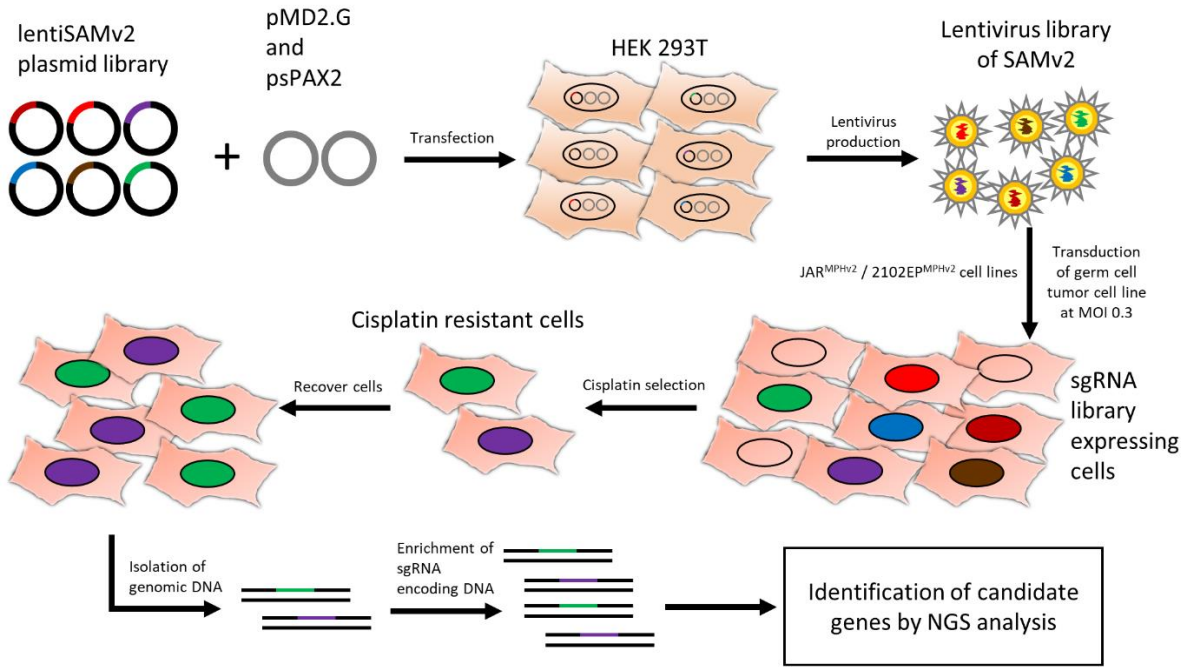

Figure 20: Schematic of the genome scale CRISPR/Cas9 activation screen. Modified from [2]. The screen is based on the lentiSAMv2 plasmid library which encodes for 70290 different sgRNAs and a dCas9-VP64 fusion protein. The library was transfected together with two helper plasmids (pMD2.G and psPAX2) into HEK293T cells in order to produce lentiviral particles. The lentivirus was used to transduce MS2-p65-HSF1 expressing JAR^{MPHv2} and 2102EP^{MPHv2} cells to generate genome scale overexpression cell populations. These cells were treated with cisplatin. Surviving cells, which were considered as cisplatin resistant, were recovered and expanded in standard cell culture medium. Next, genomic DNA was isolated, enrichment of sgRNA encoding DNA region and NGS were performed. Candidate genes were identified by bioinformatic evaluation of the sequencing data.

3.2.1. Genome scale CRISPR/Cas9 activation screen – library amplification

Initially, lentiSAMv2 plasmid library amplification in Endura electro competent cells and subsequent isolation as well as purification was conducted. To determine sgRNA coverage in the amplified library, NGS analysis was performed revealing normal distribution of sgRNAs when plotting the count against the frequency with a skew ratio below 6 and a coverage of more than 99.9% important for data quality and genome scale range (**Figure 21A/B**). Based on these results it can be assumed that each gene in the genome is targeted with a high probability in the following screen.

A

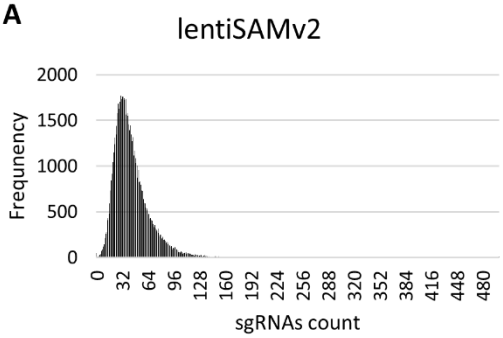

B

	lentiSAMv2
Detected sgRNAs [count]	70248
Detected sgRNAs [%]	99.93
Undetected sgRNAs [count]	49
Undetected sgRNAs [%]	0.07
Skew ratio of top 10% to bottom 10%	3.4
Guides total	70297
Reads total	3079894

Figure 21: Quality check of lentiSMAv2 plasmid library. Reprinted from [2]. (**A**) NGS was performed on the amplified and purified lentiSAMv2 plasmid library to investigate the sgRNA distribution. (**B**) Bioinformatic analysis was performed according to Joung *et. al.* [152].

3.2.2. Generation of cisplatin resistant cells by genome scale CRISPR/Cas9 activation screen

Next, the lentiSAMv2 plasmid library was used for lentivirus production. In order to activate each gene in the genome with a high statistical probability at least once more than $1.17x10^8$ $2102EP^{MPHv2}$ and JAR^{MPHv2} cells were transduced with SAMv2 lentiviral particles. Resulting $2102EP^{MPHv2/SAMv2}$ and $JAR^{MPHv2/SAMv2}$ as well as corresponding wild type cells were treated for 9 to 14 days with cisplatin and were subsequently allowed to recover in cell culture medium without cisplatin (**Figure 22A/B**). During the treatment both transduced and wild type cells displayed decreased cell number. While in the wild type samples all cells died after 14 days,

several 2102EP$^{MPHv2/SAMv2}$ as well as JAR$^{MPHv2/SAMv2}$ cells survived and re-initiated proliferation indicating cisplatin resistance.

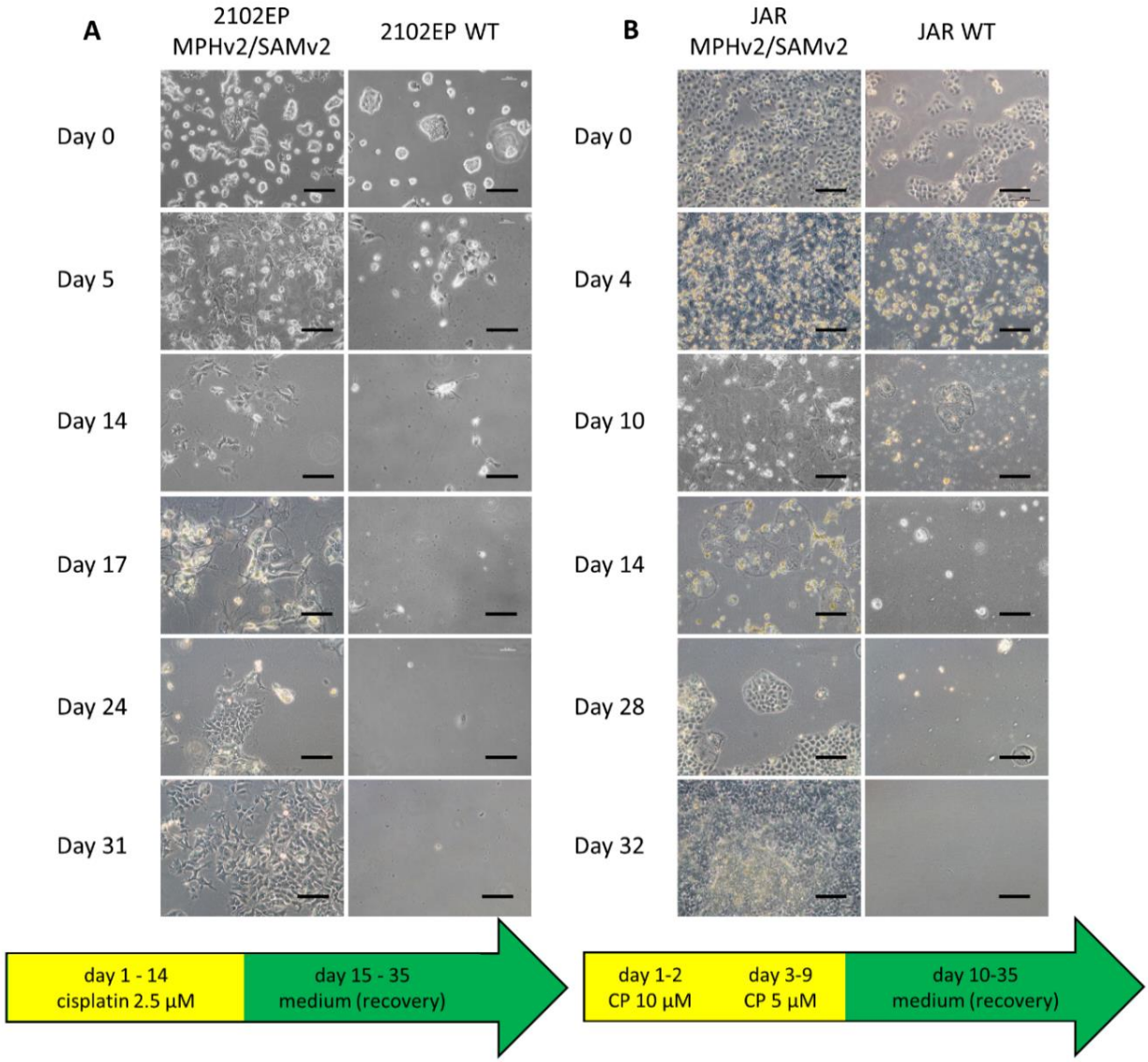

Figure 22: Cisplatin treatment of 2102EP$^{MPHv2/SAMv2}$ and JAR$^{MPHv2/SAMv2}$ cells. Reprinted from [2]. After library transduction (**A**) 2102EP$^{MPHv2/SAMv2}$ and (**B**) JAR$^{MPHv2/SAMv2}$ cells, cisplatin regimens were applied followed by a recovery phase in standard cell culture medium. 2102EP^{WT} and JAR^{WT} cells were treated accordingly. Differences between WT and overexpression cells in viability/proliferation were observed using bright filed microscopy. Scale bar: 100 µm.

To confirm cisplatin resistance, surviving 2102EP$^{MPHv2/SAMv2}$ and JAR$^{MPHv2/SAMv2}$ cells as well as wild type control cells were seeded and re-treated with cisplatin for 14 days (**Figure 23A/B**). Evaluation by brightfield imaging revealed increased survival of 2102EP$^{MPHv2/SAMv2}$/JAR$^{MPHv2/SAMv2}$ cells indicating cisplatin resistance. Control cells died during the cisplatin treatment.

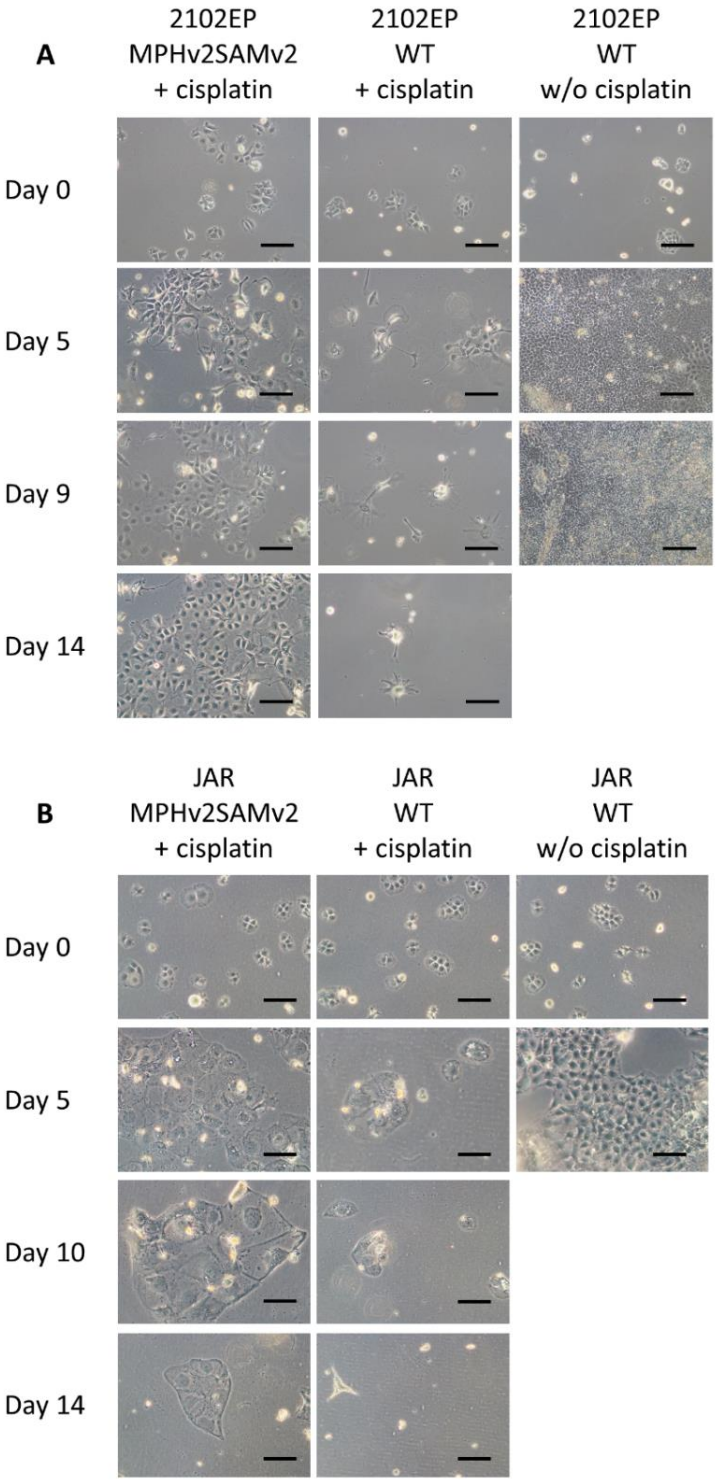

Figure 23: Validation of cisplatin resistant cells surviving the genome scale CRISPR/Cas9 activation screen. Reprinted from [2]. (**A**) 2102EP$^{MPHv2/SAMv2}$ as well as (**B**) JAR$^{MPHv2/SAMv2}$ cells (2.5x10^4 cells per well of a 6 well cell culture plate) were re-treated with 2.5 µM and 5 µM cisplatin, respectively. 2102EP^{WT} and JAR^{WT} cells were either exposed to the same conditions or kept in standard cell culture medium without cisplatin. Cell viability and proliferation differences between the cell lines and the conditions were highlighted by bright filed microscopy. Scale bar: 100 µm.

3.2.3. Identification of candidate genes for cisplatin resistance

For amplification of the sgRNA encoding region from the gDNA which was isolated from cisplatin resistant 2102EP$^{MPHv2/SAMv2}$ and JAR$^{MPHv2/SAMv2}$ cells PCR was used. To identify candidate genes the PCR products were analyzed via NGS and bioinformatic evaluation according to Joung *et al.* [152] (**Figure 24A**). Only three candidate genes (*DDB1*, *TK1*, *TRAP1*) were found to be common in 2102EP$^{MPHv2/SAMv2}$ and JAR$^{MPHv2/SAMv2}$ cells indicating rather cell line specific cisplatin resistance mechanisms (**Figure 24B**). STRING interaction analysis revealed a network for JAR$^{MPHv2/SAMv2}$ candidate genes including *TRAP1*, *CDC37*, *DDB1*, *NAE1*, *POLE4*, *NUP133*, *TK1* and *SGOL2* (**Figure 24C**). For 2102EP$^{MPHv2/SAMv2}$ a smaller network with *DDB1*, *TRAP1* and *AKT3* was identified. Next, Reactome pathway analysis on these networks resulted in terms associated with cell cycle, DNA repair and neddylation. Since disturbed cell cycle and altered DNA repair have already been described as cisplatin resistance mechanism in TGCTs [172], I further focused on neddylation. Interestingly, the neddylation associated gene *DDB1* was found upregulated in both samples (2102EP$^{MPHv2/SAMv2}$/JAR$^{MPHv2/SAMv2}$) while overexpression of the neddylation master regulator *NAE1* was only detected in JAR$^{MPHv2/SAMv2}$ cells.

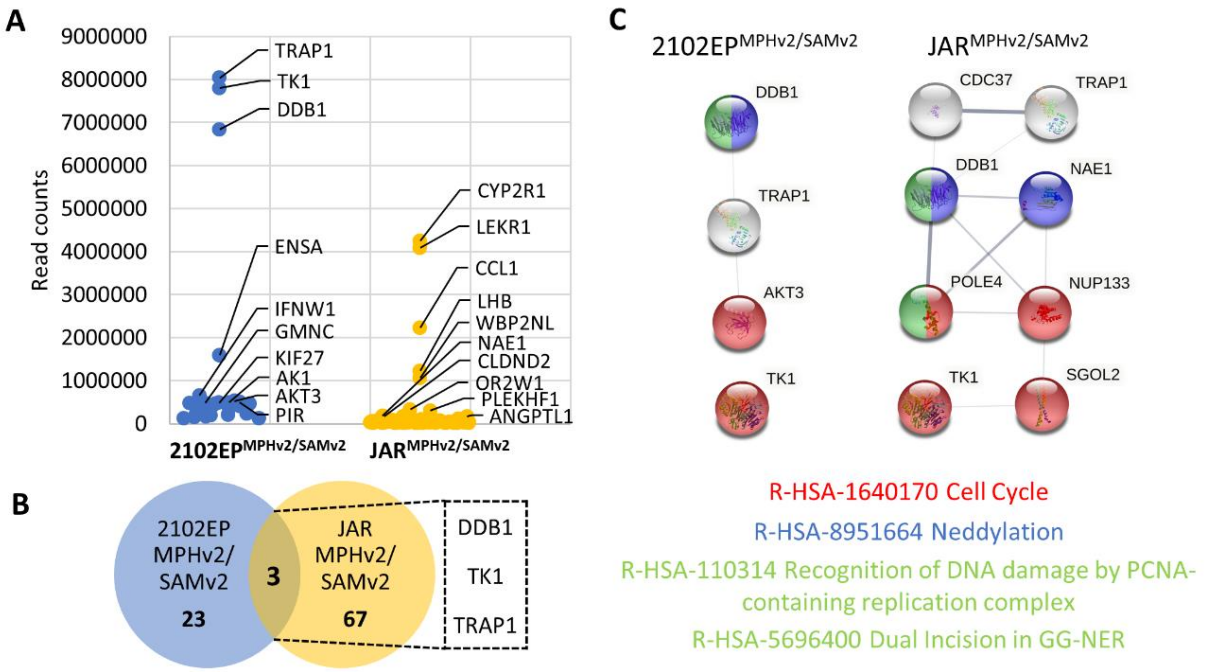

Figure 24: Identification of candidate genes responsible for cisplatin resistance. Modified from [2]. (**A**) NGS analysis of sgRNA encoding gDNA from 2102EP$^{MPHv2/SAMv2}$ as well as JAR$^{MPHv2/SAMv2}$ cells revealed a list of candidate genes. Genes are depicted with read count >10000. (**B**) Venn diagram displaying overlap analysis of candidate genes derived from 2102EP$^{MPHv2/SAMv2}$ and JAR$^{MPHv2/SAMv2}$ cells. (**C**) STRING interaction and Reactome pathway analysis of candidate genes.

3.2.4. NAE1 overexpression revealed cisplatin resistance in TGCT cell lines

To test, whether upregulation of *NAE1* mediates cisplatin resistance in TGCT cell lines, I generated transgenic cell lines overexpressing *NAE1*. For this purpose, a CMV promotor driven NAE1/GFP fusion construct (pLV-NAE1-GFPSpark) was used. After lentivirus production 2102EP and JAR cells were transduced. For derivation of monoclonal cell lines, FACS sorting was performed to select for GFP positive and DAPI negative cells which were collected separately (one cell per well) and expanded. **Figure 25A/B** shows GFP positive cells after transduction, in the single cells and post sorting indicating successful transfection and overexpression of the NAE1/GFP fusion protein.

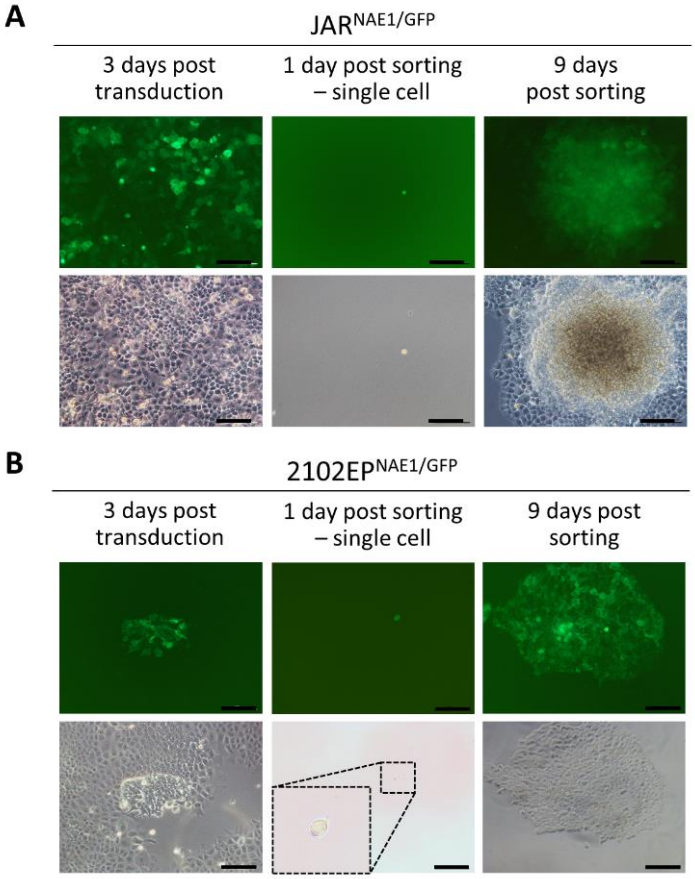

Figure 25: Generation of clonal NAE1 overexpression cell lines. Modified from [2]. (**A**) JAR^{WT} and (**B**) 2102EP^{WT} cells were transduced with a transgenic NAE1/GFP overexpression construct. Clonal cell lines were generated by FACS-based single cell sorting for positive GPF and negative DAPI (alive cells) signal. Single cells were further cultured and expanded. Fluorescence and brightfield microscopy were utilized to follow clonal cell line generation. Scale bar 100 µm.

NAE1 overexpression was validated by western blot analysis (**Figure 26A/B**). Protein lysates from JAR$^{NAE1/GFP}$ line 2, 3, 5, 2102EP$^{NAE1/GFP}$ line 1, 2, 3 and corresponding wild type cell lines showed bands for NAE1 at 60 kDa. The transgenic samples clearly displayed additional NAE1/GFP fusion protein bands detected with NAE1 and GFP antibody at 87 kDa. The GFP bands observable at 27 kDa were most likely indicative for cleaved fusion protein.

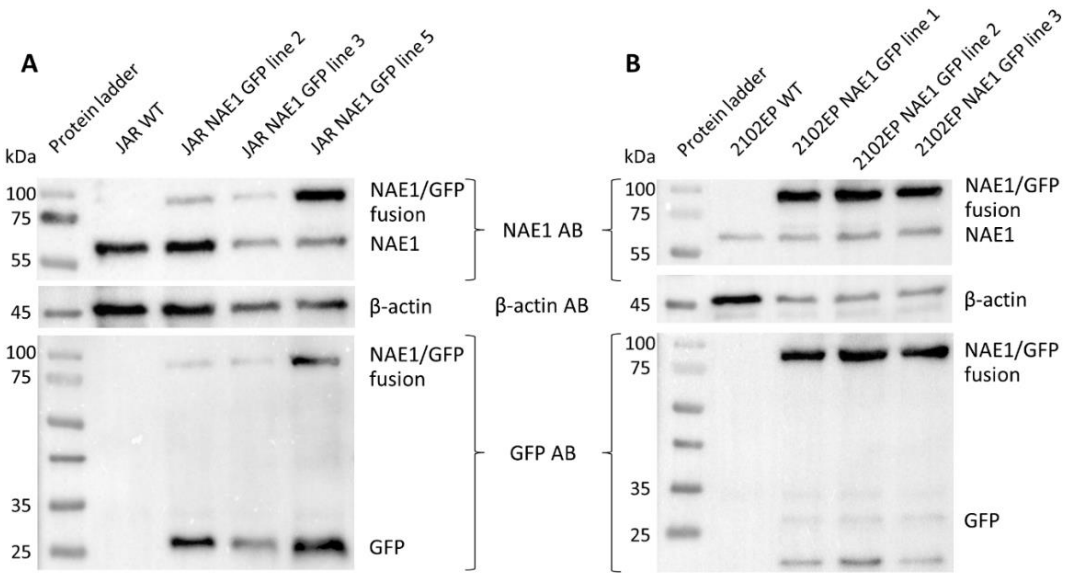

Figure 26: Validation of clonal JARNAE1/GFP and 2102EPNAE1/GFP lines. Modified from [2]. Western Blot analysis from (**A**) JAR$^{NAE1/GFP}$ and (**B**) 2102EP$^{NAE1/GFP}$ protein lysates for NAE1, GFP as well as β-actin (loading control).

Next, JAR$^{NAE1/GFP}$ clone 2, 3, 5, 2102EP$^{NAE1/GFP}$ clone 1, 2, 3, JAR^{WT} and 2102EP^{WT} cells were seeded and treated for 9 days with cisplatin. *NAE1/GFP* overexpression cell lines showed a significantly higher viability compared to the wild type cell lines strongly suggesting that expression of NAE1 induces cisplatin resistance (**Figure 27A/B**). Surprisingly, the effect was even stronger in the 2102EP$^{NAE1/GFP}$ lines with up to 600% increased viability compared to the JAR$^{NAE1/GFP}$ lines where the viability was elevated up to 200%.

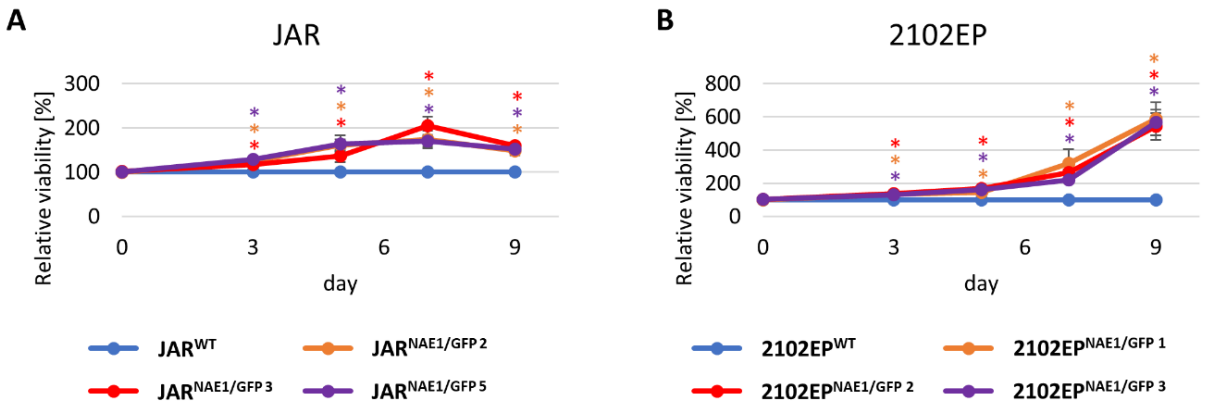

Figure 27: Investigation of cisplatin resistance in clonal JAR$^{NAE1/GFP}$ and 2102^{EP}NAE1/GFP lines. Modified from [2]. (**A**) JAR$^{NAE1/GFP}$ line 2, 3, 5, (**B**) 2102EP$^{NAE1/GFP}$ line 1, 2, 3 and corresponding WT cell lines were seeded in 96-well cell culture plates. Treatment was performed with cisplatin (JAR: 5 µM/2102EP: 2.5 µM) or solvent control. (DMF). Viability of the cells was measured at day 3, 5, 7 and 9 via XTT assay. At each time point treated samples were normalized to control DMF samples and referred to the WT sample.

3.2.5. NAE1 is expressed in TGCT cell lines and tissues

Since the results from the CRISPR/Cas9 activation screen revealed overactivation of the neddylation pathway as a potential mechanism of CP resistance, I sought to analyze expression levels of *NAE1* in TGCT cell lines and tissues. Meta analysis of microarray data [171] revealed high mRNA expression of *NAE1* in 2102EP, NCCIT, JAR and TCam2 cell lines while lower expression was observable in MPAF fibroblast cells (**Figure 28A**). A similar pattern was detectable on protein level. Western blot analysis revealed strong NAE1 abundance in 2102EP, 2102EP-R, NCCIT, NCCIT-R, NT2/D1, NT2/D1-R, JAR and TCam2 cells (**Figure 28B**). For MPAF cells only a faint band indicating low levels of NAE1 protein were observable.

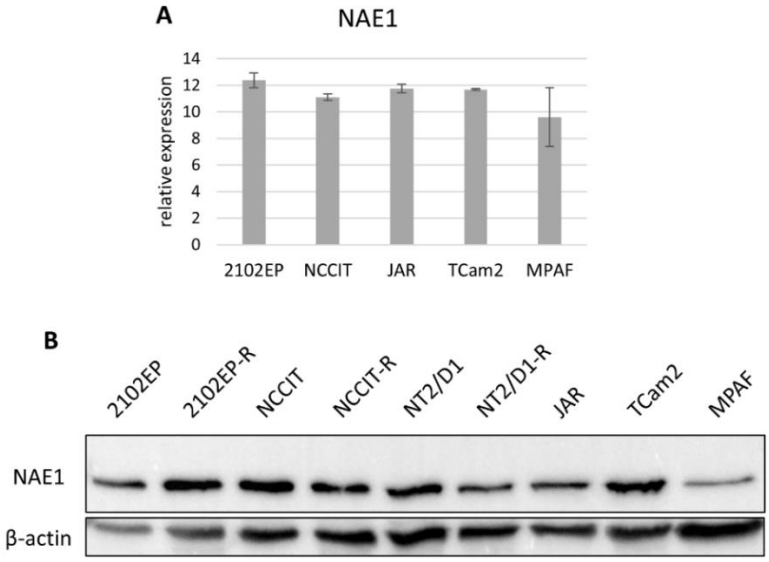

Figure 28: *NAE1* expression in TGCT cell lines. Modified from [2]. (**A**) Meta analysis of Illumina microarray data [171] for *NAE1* expression on mRNA level in 2102EP, NCCIT, JAR, TCam2 and MPAF cells. *NAE1* with relative expression >7 was considered expressed. (**B**) Western Blot analysis for NAE1 protein levels and β-actin levels (loading control) in 2102EP, 2102EP-R, NCCIT, NCCIT-R, NT2/D1, NT2/D1-R, JAR, TCam2 and MPAF cells.

Expression of *NAE1* on RNA level was highest in tumor tissues (CIS, Seminoma, EC, Teratoma, Mixed Non-Seminoma) and lower in normal testis tissue as learned from meta data analysis of Affymetrix tissue microarray [108] (**Figure 29A**). Interestingly, Firebrowse analysis showed increased *NAE1* levels in tissues of various tumor entities compared to the respective normal tissue (**Figure 29C**). Surprisingly, the overall *NAE1* expression levels were found to be highest in TGCT tissue. Comparing the The Cancer Genome Atlas (TCGA) TGCT cohort with GTEX Testis cohort (normal testis tissue) revealed differences in the expression of several NAE1 isoforms (**Figure 29B**).

To sum up, high expression of *NAE1* in TGCT cell lines and tissues has been detected. In the genome scale CRISPR/Cas9 activation screen and in the overexpression cell lines, NAE1 has been shown to induce cisplatin resistance. Thus, not high expression but only overexpression of *NAE1* triggers cisplatin resistance in TGCT cell lines. Interestingly, lower expression of

NAE1 was detected in the fibroblast control cell line as well as in normal testis tissue compared to the TGCT cell lines and tissues. Accordingly, TGCT cells might have a stronger dependency on the neddylation pathway. These findings suggest NAE1 as a potential target for TGCT therapy.

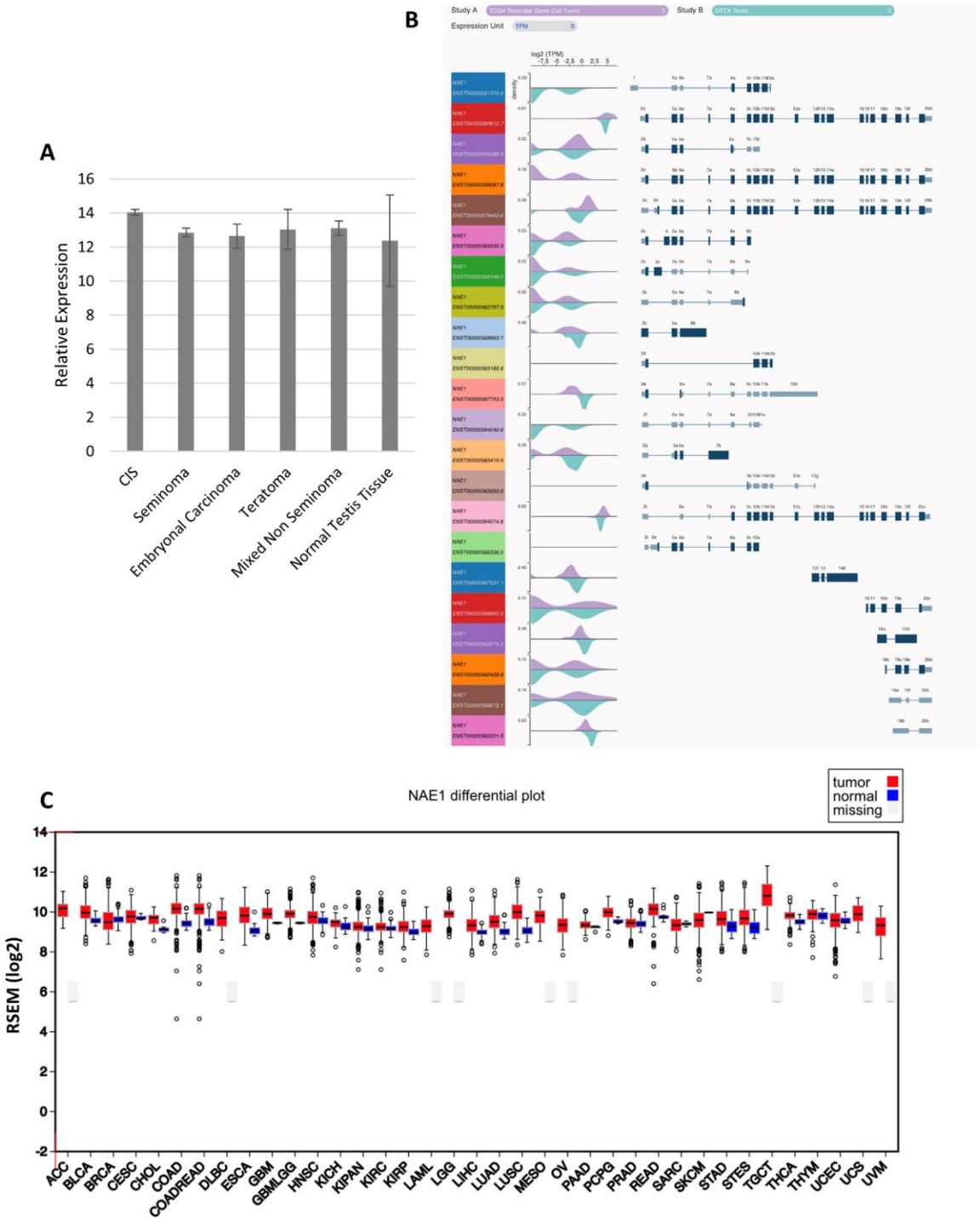

Figure 29: Investigation of NAE1 expression in TGCT and normal tissues. Reprinted from [2]. (**A**) Meta-analysis of Affymetrix microarray data [108] of *NAE1* expression in carcinoma *in situ* (CIS), seminoma, EC, teratoma, mixed non-seminoma and normal testis tissue (*n=3/4*). *NAE1* with relative expression >10 was considered expressed. Data represent average of biological replicates ± SD. (**B**) UCSC Xena browser-mediated analysis of *NAE1* isoform expression on TCGA TGCT cohort in comparison to GTEX Testis control group. (**C**) *NAE1* expression in various tumor and normal tissues derived from Firebrowse analysis based on TCGA database.

3.2.6. Additive cytotoxic effect of NAE1 inhibition in combination with cisplatin treatment

Since overexpression of *NAE1* resulted in cisplatin resistance, I asked whether inhibition of neddylation would increase cisplatin sensitivity. To address this question, different cell lines (2102EP, 2102EP-R, NCCIT, NCCIT-R, NT2/D1, NT2/D1-R, JAR, TCam2 and MPAF cells) were treated with NAE1 inhibitor MLN4924, cisplatin or a combination of both drugs (**Figure 30A-I**).

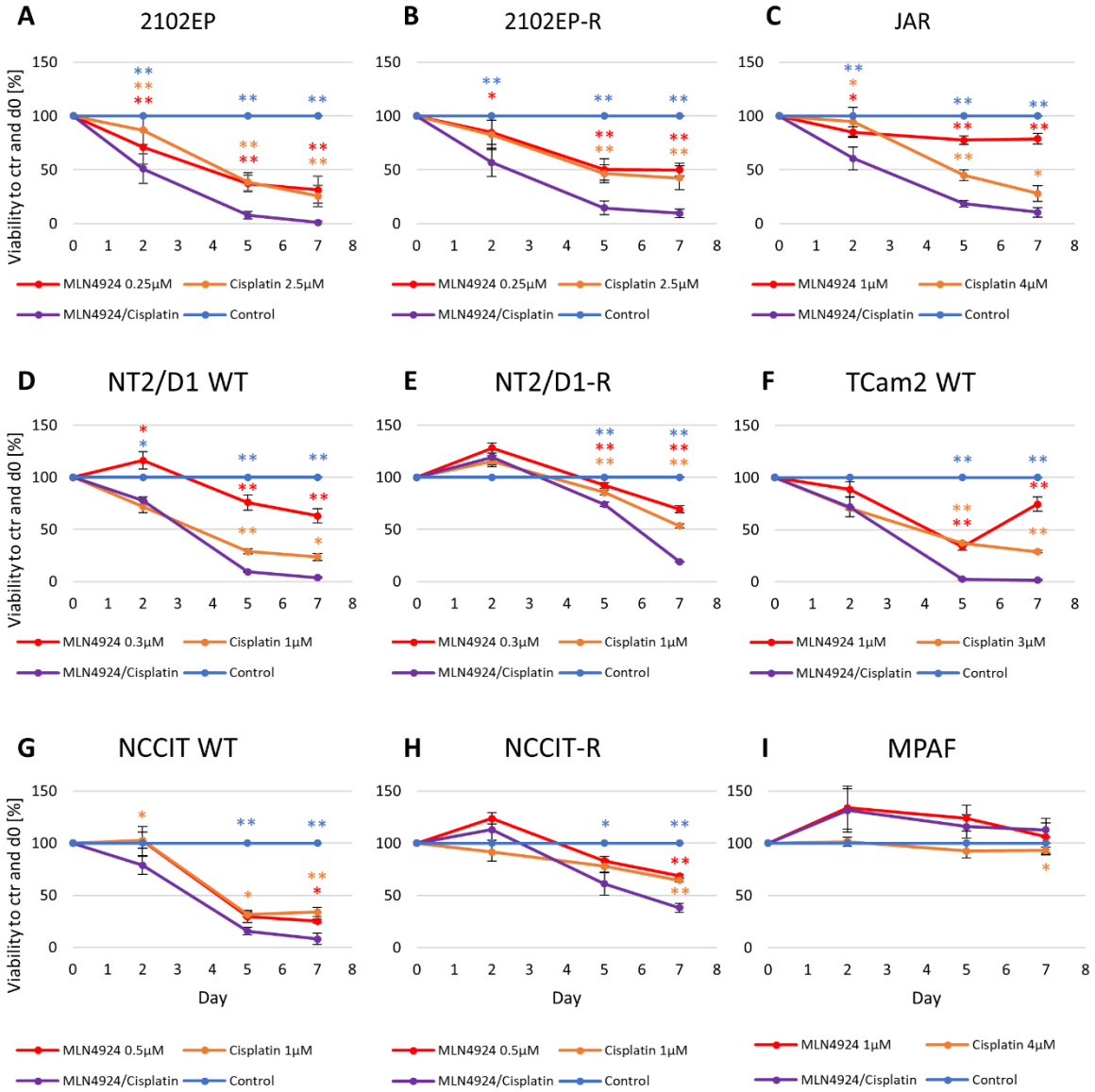

Figure 30: Cisplatin/MLN4924 and combination treatment of TGCT cell lines. Modified from [2]. (**A**) 2102EP, (**B**) 2102EP-R, (**C**) JAR, (**D**) NT2/D1, (**E**) NT2/D1-R, (**F**) TCam2, (**G**) NCCIT, (**H**) NCCIT-R and (**I**) MPAF cells were treated up to 7 days with indicated concentrations of MLN4924 only, cisplatin only, a combination of both compounds, DMSO, DMF or DMSO/DMF combination. Viability was determined at day 0, 2, 5 and 7 using the XTT assay. Treated samples were normalized to solvent controls and referred to day 0. Asterisks indicate significant difference between MLN4924/cisplatin combination group and mono therapy as well as control group (* p<0.05, ** p<0.01). *n=3-5*.

In the TGCT cell lines reduced viability was found from 5 days of cisplatin or MLN4924 treatment. Of note, the viability of the TGCT cell lines was significantly stronger decreased by

combination treatment (MLN4924 and cisplatin) compared to the MLN4924 only, cisplatin only and solvent (control) treatment for 7 days (MLN4924 only/cisplatin only/combination: 2102EP 32/26/1%, NT2/D1 63/24/4%, NCCIT 25/34/8%, JAR 79/28/11%, TCam2 75/29/2%). This suggests an additive cytotoxic effect of neddylation inhibition in combination with cisplatin. Surprisingly, even cisplatin resistant cell lines revealed significantly stronger decreased viability after application of MLN4924 in combination with cisplatin (MLN4924 only/ cisplatin only/ combination at day 7: 2102EP-R 50/43/10%, NT2/D1-R 70/54/19%, NCCIT-R 69/65/38%). Importantly, MPAF control cells were not affected from any treatment condition (MLN4924 only/ cisplatin only/ combination at day 7: 106/93/112%) even at the highest concentrations of MLN4924 and cisplatin as applied in the TGCT cells.

To investigate the mode of action of cisplatin and MLN4924, I analyzed the known downstream targets γH2A.X as well as p27, respectively. Cisplatin causes DNA damages thereby inducing expression of γH2A.X [173,174]. p27 accumulation was already shown as a robust marker for neddylation inhibition [141,175]. Western blot analyses of 2102EP, JAR and TCam2 cells which were treated for 48 h with MLN4924 only clearly displayed accumulation of p27 whereas cisplatin treatment induced strong accumulation of γH2A.X levels (**Figure 31A-C**). Interestingly, after combination treatment with MLN4924 and cisplatin increased levels of both proteins γH2A.X and p27 were detected in 2102EP, JAR and TCam2 cells. Thus, cisplatin induced DNA damage in combination with MLN4924 mediated neddylation inhibition seemed to trigger a stronger cytotoxic response compared to single drug treatment.

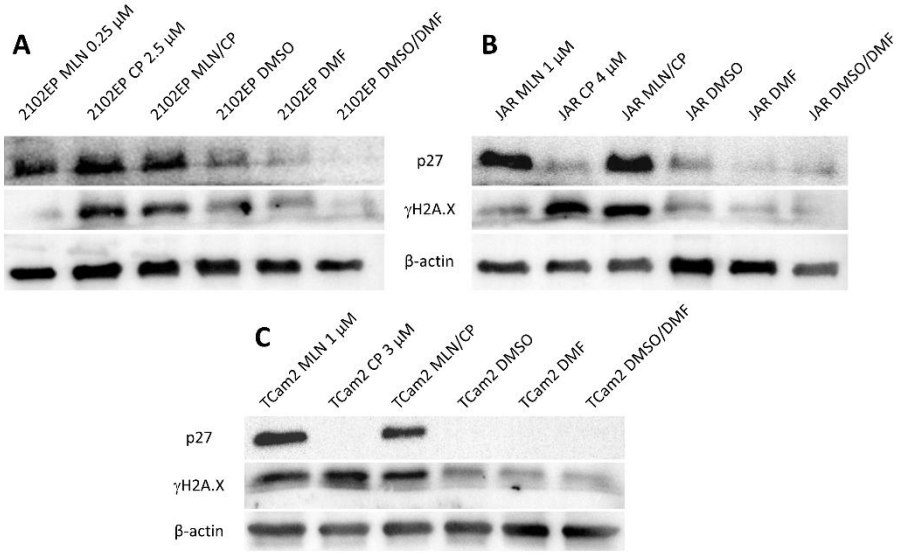

Figure 31: Western blot analysis of MLN4924/cisplatin/combination treated cells. Modified from [2]. (**A**) 2102EP, (**B**) JAR and (**C**) TCam2 cells were treated for 48 h with indicated concentrations of MLN4924, cisplatin, a combination of both drugs or the corresponding solvent (DMSO, DMF, DMSO/DMF). Subsequently, protein extraction, SDS-PAGE, Western Blot analysis and p27, γH2A.X as well as β-actin (loading control) detection were performed.

3.2.7. Inhibition of neddylation in combination with cisplatin induces strong apoptotic response in TGCT cell lines

To further investigate the cellular response to the treatment, apoptosis analysis was performed. After 2 and 5 days of MLN4924 or cisplatin treatment, induction of apoptosis was observable in 2102EP (up to 2.6-fold) and JAR (up to 4.2-fold) cells while in TCam2 (up to 1.9-fold) cells apoptosis induction was detectable at day 5 (**Figure 32**). Interestingly, in TGCT cell lines combination treatment elicited significantly higher induction of apoptosis (exposure 2 days/5 days: 2102EP 3.2/3.5-fold, JAR 1.7/5.5-fold, TCam2 2.4/3.9-fold). Only combination treatment for 2 days in JAR cells revealed increased apoptosis level compared to JAR cisplatin treated cells which was not significant. For MPAF control cells minimal increase of apoptosis was observable after 2 days and 5 days of mono or combination treatment (fold change between 0.9 and 1.3). Thus, apoptosis induction was clearly detectable in TGCT cell lines after treatment and importantly, the additive potential of MLN4924/cisplatin combination application could be validated.

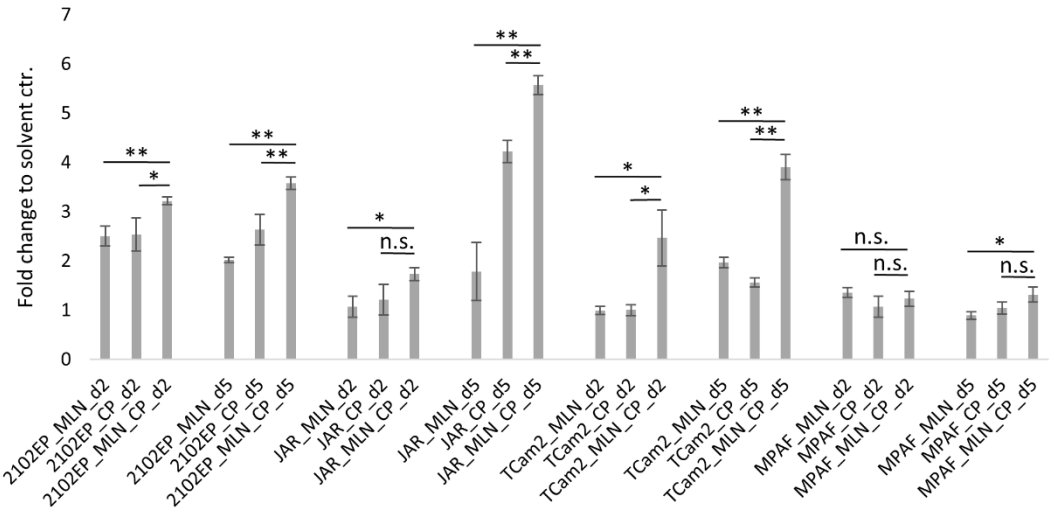

Figure 32: Apoptosis analysis of MLN4924/cisplatin/combination treated cells. Modified from [2]. The treatment was performed with MLN4924 (2102EP: 0.25 µM, JAR/TCam2/MPAF: 1 µM), cisplatin (2102EP 2.5 µM, TCam2 3 µM, JAR/MPAF 4 µM) and combination of both compounds (same concentrations as MLN4924 and cisplatin only) for 2 and 5 days. Apoptosis was determined using FACS based PE Annexin V/DAPI analysis. Treated samples were referred to the solvent (DMSO and DMF) samples representing the fold change of apoptotic cells. Asterisks indicate significant difference between samples with mono drug application and combination treatment (n.s. not significant, * $p<0.05$, ** $p<0.01$). (*n*=3).

3.2.8. Neddylation inhibition and cisplatin treatment triggered G2/M-phase cell cycle arrest in TGCT cell lines

Next, I investigated the effect of neddylation inhibition as well as cisplatin treatment on the cell cycle to get further insights in the cellular response. After 24 and 48 h of MLN4924/cisplatin/combination treatment, in 2102EP and JAR cells significantly decreased cell numbers were detected in G1 phase and significantly elevated number of cells in G2/M-

phase (**Figure 33**). The strongest cell accumulation of almost 80% in G2/M-phase was detected in JAR cells after combination treatment for 48 h. Interestingly, highly significant decreased number of cells has been found in S-phase after treatment of 2102EP cells for 48 h with cisplatin and combination treatment. In JAR cells exposure of MLN4924/cisplatin/combination revealed significantly lower number of cells in S-phase. TCam2 cells displayed only minor changes in cell cycle after 24 h of MLN4924/cisplatin/combination treatment. After 48 h exposure to the drugs there was a highly significant increase in the number of G2/M-phase cells and a significantly decreased cell number in G1-phase. The delayed effect in TCam2 cells might be caused by the lower doubling time compared to 2102EP and JAR cells. The mildest effects were observable in MPAF cells where almost no changes in the cell cycle distribution were detected. Taken together, in 2102EP, JAR and TCam2 cells G2/M-phase cell cycle arrest was initiated by all three treatment conditions (MLN4924/cisplatin/combination) latest after 48 h while almost no cell cycle alteration was found in MPAF cells.

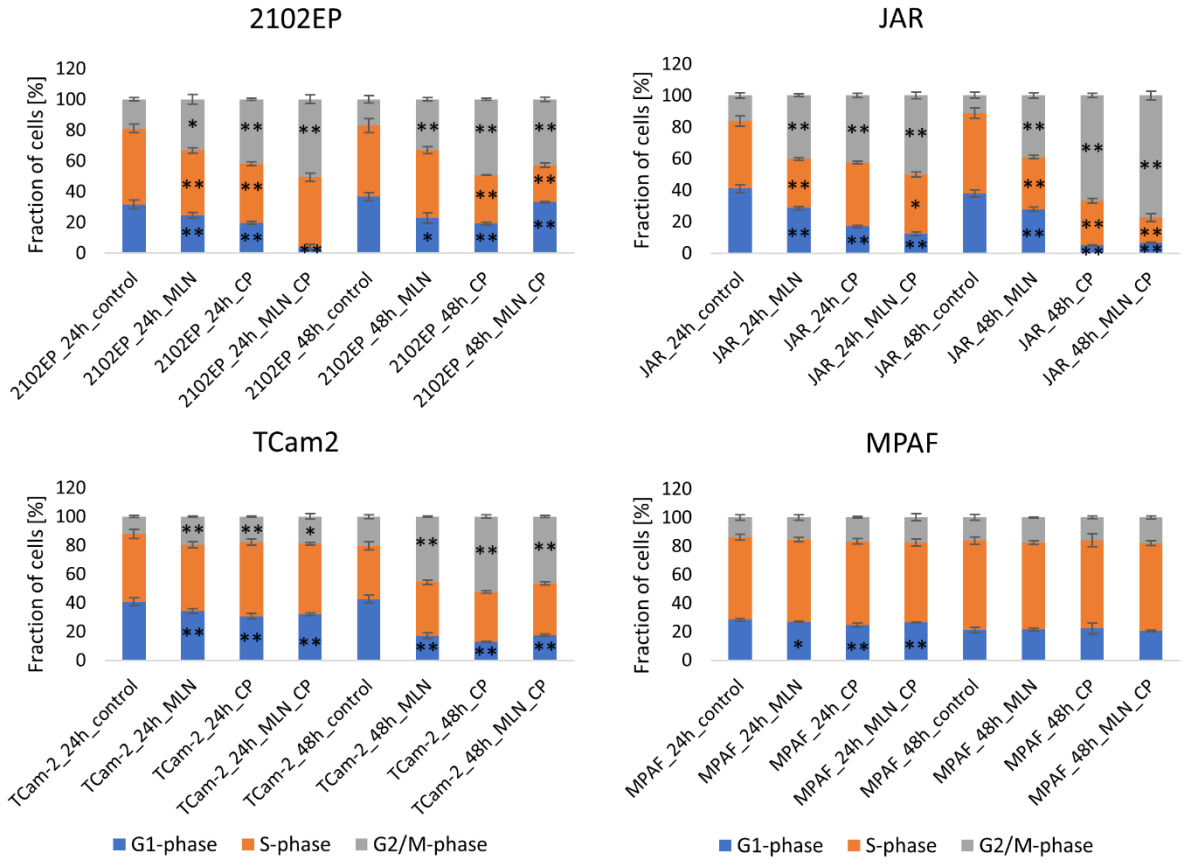

Figure 33: Cell cycle analysis of MLN4924/cisplatin/combination treated cells. Modified from [2]. MLN4924 (2102EP: 0.25 µM, JAR/TCam2/MPAF: 1 µM), cisplatin (2102EP 2.5 µM, TCam2 3 µM, JAR/MPAF 4 µM) and combination (same concentrations as applied in mono application) treatment as well as DMSO/DMF application (control) was performed for 24 h and 48 h. For FACS-based cell cycle analysis cells were stained with Hoechst-33342 and analyzed for DNA content. Significance was calculated between treated and control group for each cell cycle phase using the two-tailed student's t-test. Asterisks indicate significant difference (* $p<0.05$, ** $p<0.01$). *n*=3.

3.2.9. Elucidating the impact of neddylation inhibition and cisplatin treatment on the transcriptome in 2102EP and JAR cell lines

In order to explore the molecular effects of MLN4924 mediated inhibition of neddylation, the effects of cisplatin as well as the molecular response towards the combination treatment, transcriptome analysis was performed. 2102EP and JAR cells were treated for 48 h with MLN4924/cisplatin/combination and analyzed via 3'mRNA sequencing.

Increased apoptosis level after MLN4924/cisplatin/combination treatment found by FACS analysis (see chapter 3.2.7) were confirmed on transcriptomic level for 2102EP (**Figure 34A-C**, **Appendix Figure 11A-C**) and JAR cells (**Figure 35A-C**, **Appendix Figure 12A-C**). STRING analyses on differentially expressed transcripts with higher abundance revealed interaction networks associated with GO terms apoptosis and cell death. In 2102EP cells exposed to the combination treatment, according to the differentially expression of the top 10 upregulated genes, the strongest fold changes were observed suggesting that the additive cytotoxic effect was also detectable on a molecular level. Interestingly, *Keratin17* was the top differentially upregulated gene in the combination treated sample (log2 fold change: 9.9). This gene was also found to be upregulated to a lower extend after MLN4924 only (log2 fold change: 5.7) and cisplatin only (log2 fold change: 6.8) treatment.

In the JAR cells the additive cytotoxic effect was even more striking. Upon MLN4924 and cisplatin mono treatment only small STRING interaction networks, including 10 differentially upregulated genes each, associated with apoptosis and cell death were found. Combination treatment revealed a robust network including 47 different transcripts with higher abundance involved in cell death and apoptosis.

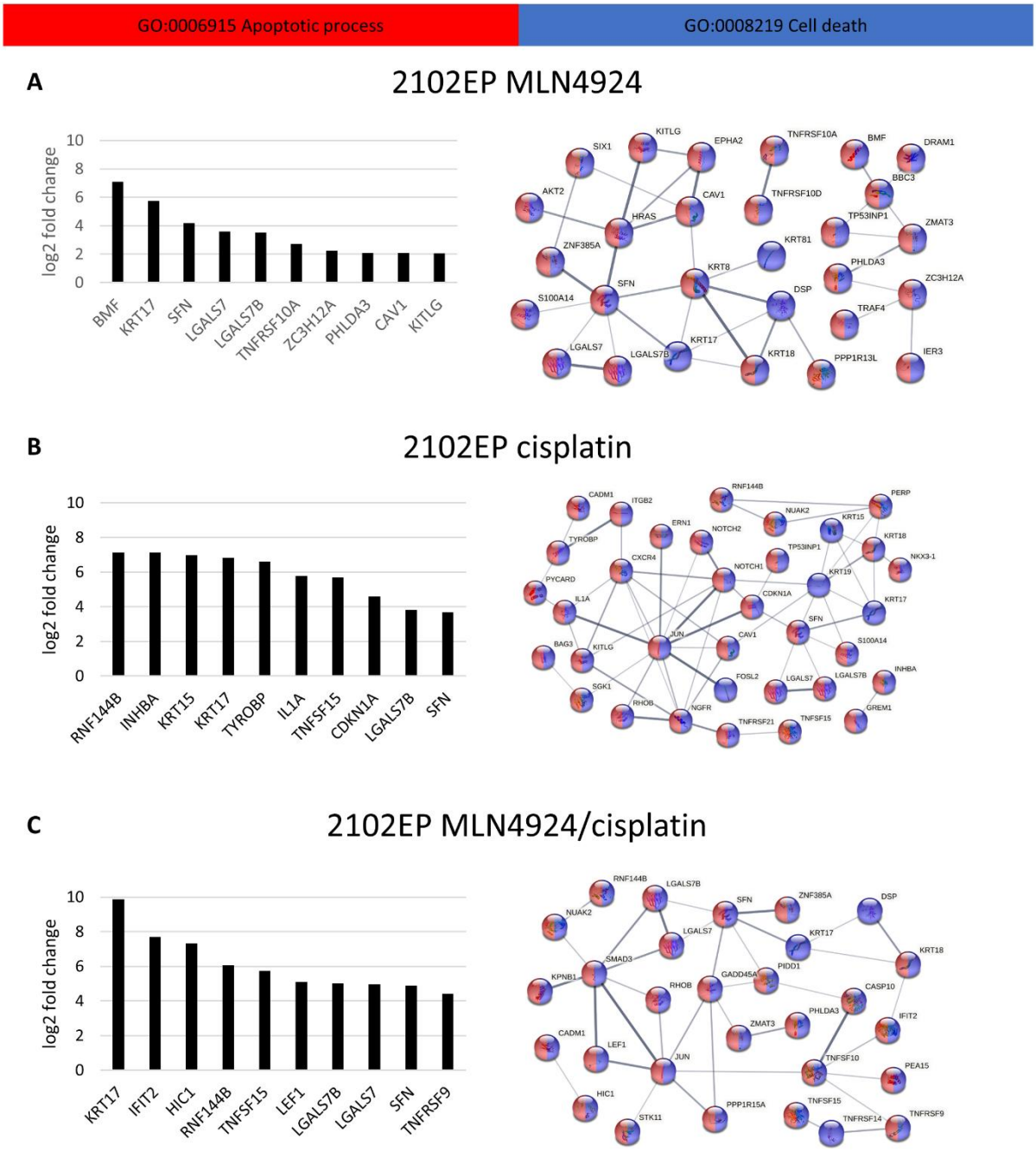

Figure 34: Transcriptome analysis revealed apoptosis and cell death after neddylation inhibition and cisplatin treatment in 2102EP cells. Modified from [2]. Treatment of 2102EP cells was performed for 48 h with (**A**) MLN4924 (0.25 µM), (**B**) cisplatin (2.5 µM), (**C**) MLN4924/cisplatin combination (0.25 µM + 2.5 µM) as well as corresponding solvent (DMSO/DMF/DMSO+DMF). 3'mRNA sequencing results were investigated by STRING interaction and GO analysis. Top 10 differentially upregulated genes with log2 fold changes of the corresponding STRING interaction network are displayed. *n*=3.

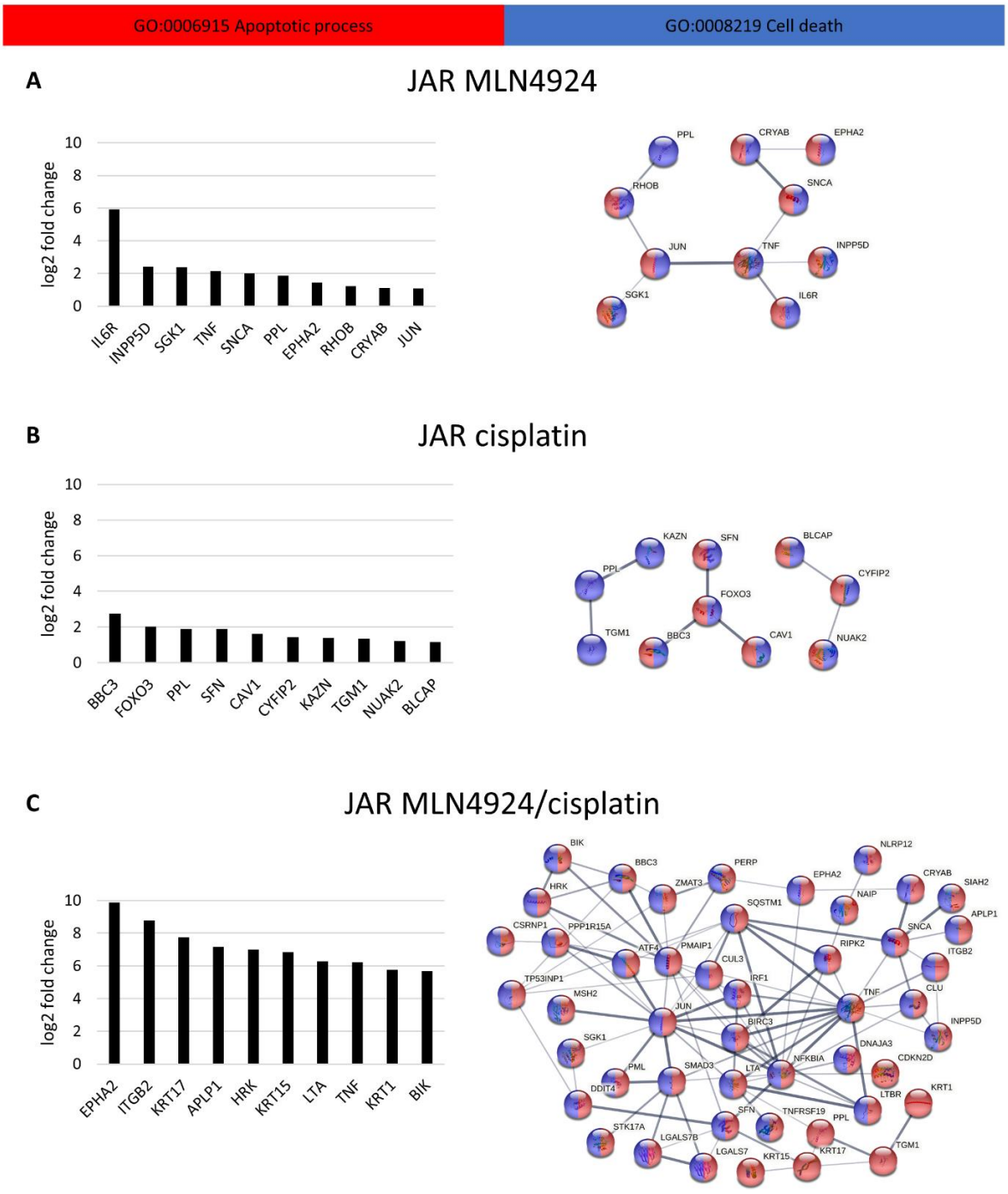

Figure 35: Transcriptome analysis revealed apoptosis and cell death after neddylation inhibition and cisplatin treatment in JAR cells. Modified from [2]. 3'mRNA sequencing of JAR cells was performed after (**A**) MLN4924 (1 µM), (**B**) cisplatin (4 µM), (**C**) MLN4924/cisplatin combination (1 µM + 4 µM) and solvent treatment for 48 h. Log2 fold change of top 10 differentially upregulated genes associated with apoptosis/cell death, identified by STRING interaction and GO analysis, is displayed. *n*=3.

Next, I analyzed the transcriptomics data regarding cell cycle related transcripts. 2102EP cells revealed small STRING networks upon MLN4924 only/cisplatin only (10/8 genes) treatment including differentially upregulated genes associated with cell cycle arrest and negative cell cycle regulation (**Figure 36A-C**). Again, an additive effect induced by combination treatment was observable indicated by a STRING network with strongly increased number of 21

differentially upregulated genes including important factors such as *GPER1*, *SFN*, etc. responsible for negative cell cycle regulation. Interestingly, expression of the important cell cycle regulator *CDKN1A* was upregulated in cisplatin treated sample pinpointing towards cell cycle arrest.

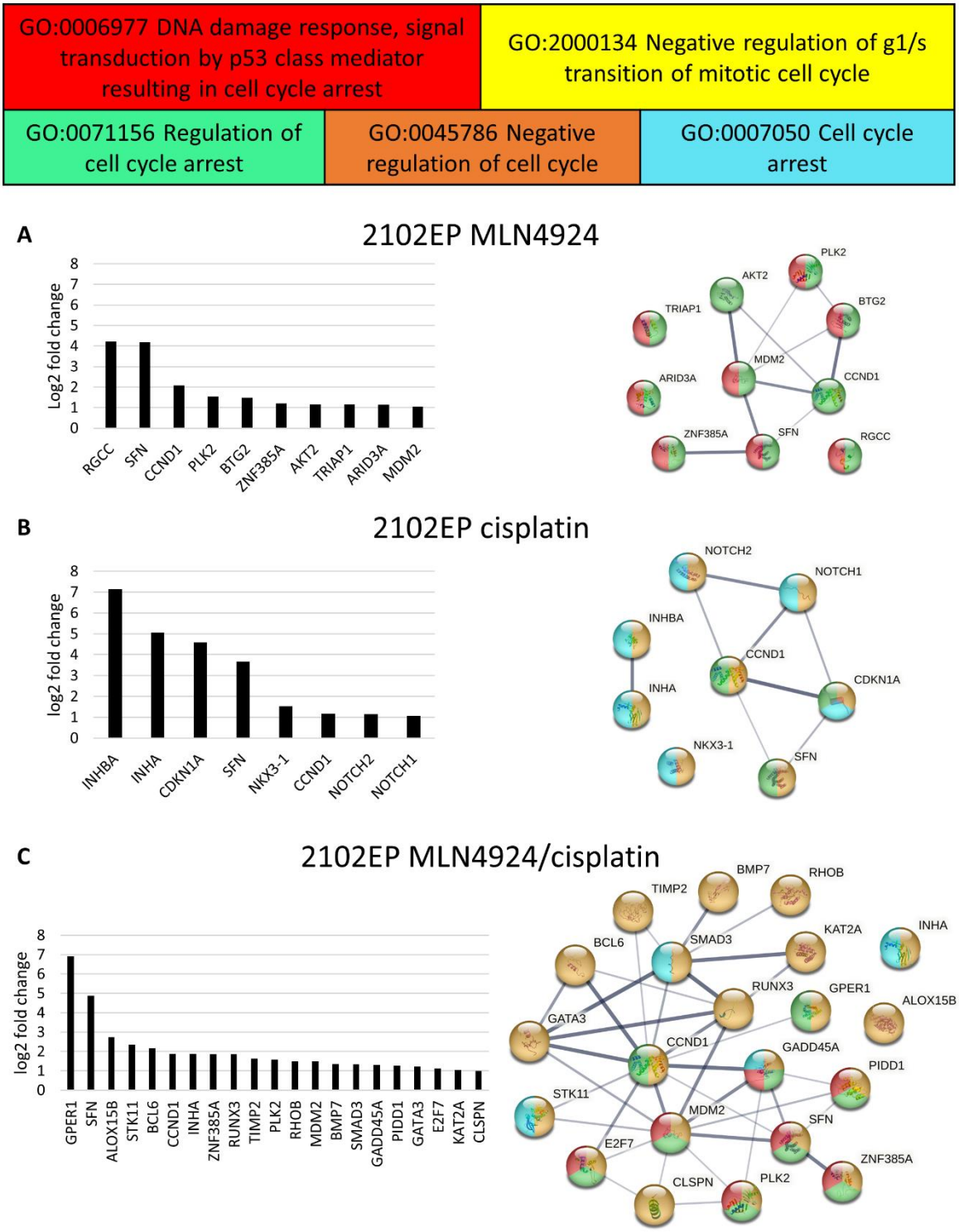

Figure 36: Transcriptome analysis revealed cell cycle arrest in 2102EP cells due to inhibition of neddylation and cisplatin treatment. Reprinted from [2]. 3'mRNA sequencing analysis after 48 h of (**A**) MLN4924, (**B**) cisplatin and (**C**) combination treatment of 2102EP cells. STRING interaction networks involved in GO terms associated with cell cycle arrest are displayed. Log2 Fold change of network members are shown. *n*=3

Surprisingly, analysis of differentially downregulated genes in terms of cell cycle transition/cell cycle process in 2102EP cells displayed a compact STRING interaction network upon MLN4924 treatment involving *CCNA1, TUBB4B, KIFC1, BUB3*, etc. (**Figure 37A**). This finding indicates inhibition of cell cycle progression also after MLN4924 mono treatment. Cisplatin treated cells revealed only 4 differentially lower abundant transcripts associated with cell cycle (**Figure 37B**) while combination treatment again displays most differentially downregulated genes indicative of the additive effect of MLN4924 application in combination with cisplatin (**Figure 37C**).

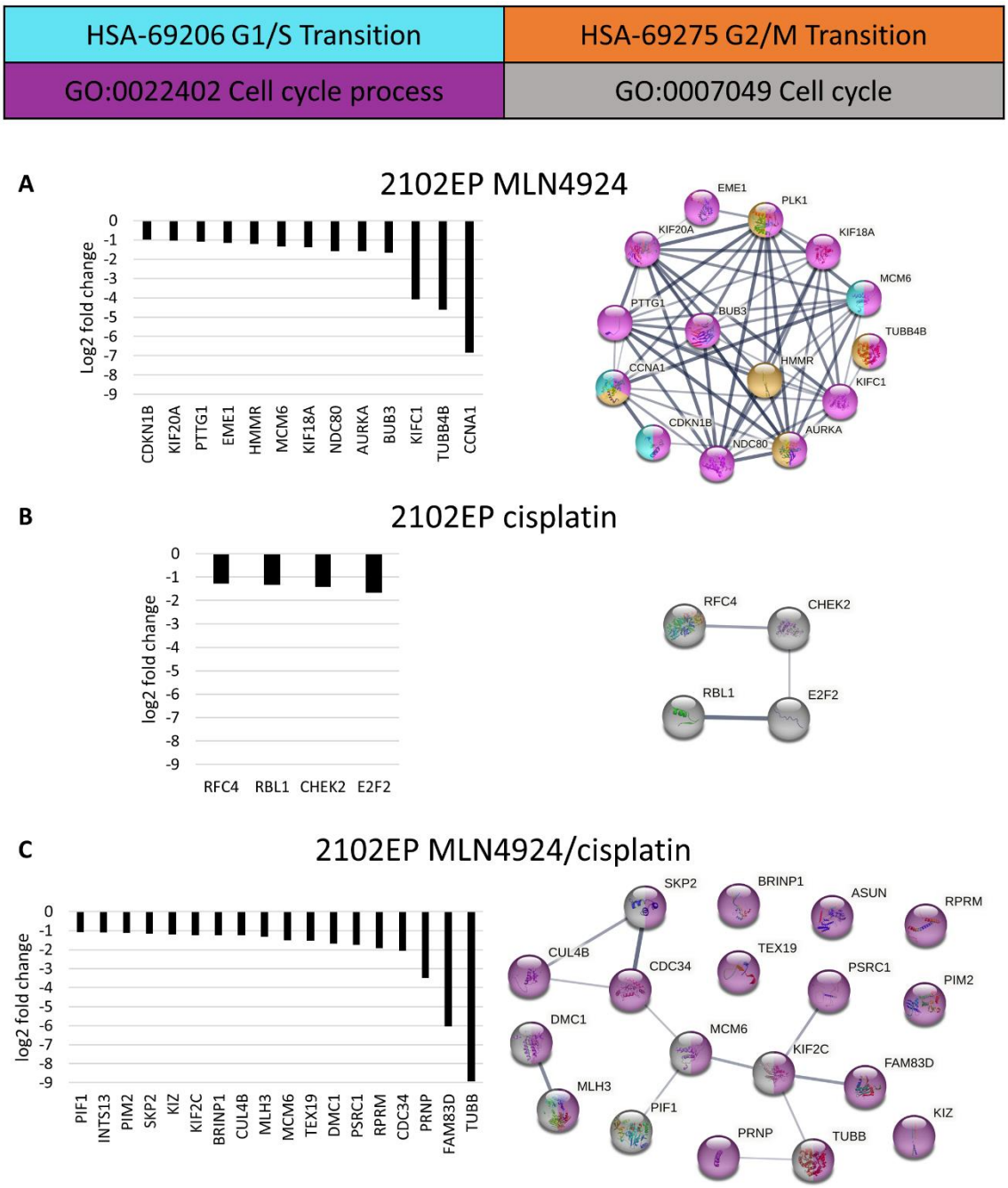

Figure 37: MLN4924 and cisplatin treatment were associated with downregulation of cell cycle process in 2102EP cells. Reprinted from [2]. 3'mRNA sequencing after 48 h of (**A**) MLN4924 (0.25 µM), (**B**) cisplatin (2.5 µM) and (**C**) combination treatment revealed differentially downregulated genes associated with cell cycle progression (STRING interaction and GO analysis). *n*=3

In the JAR cell line, only few genes associated with cell cycle arrest were differentially upregulated upon MLN4924 and combination treatment (**Figure 38A-C**). Interestingly, increased transcript abundancy of cell cycle inhibitor *CDKN2D* was found in JAR cells treated with MLN4924 and MLN4924/cisplatin. Despite no transcripts were found after cisplatin application associated with negative cell cycle regulation, there was an additive effect in the combination treatment observable revealing higher fold change and more differentially upregulated genes compared to mono therapy.

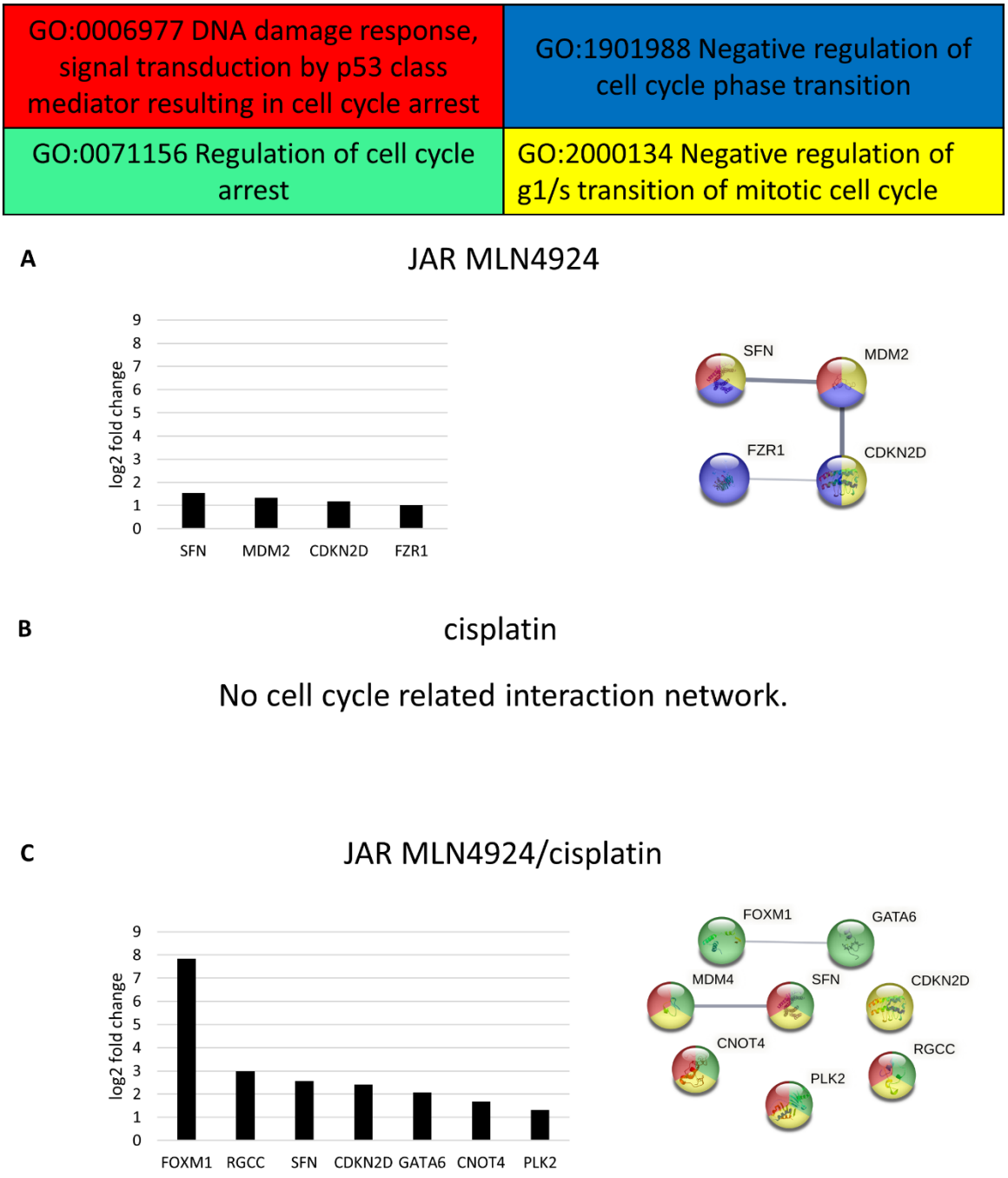

Figure 38: Transcriptome analysis of MLN4924/cisplatin/combination treated JAR cells associated to cell cycle arrest. Reprinted from [2]. 3'mRNA sequencing analysis of JAR cells treated with (**A**) MLN4924 (1 µM), (**B**) cisplatin (4 µM) and (**C**) combination of both drugs for 48 h. STRING interaction network and corresponding differentially upregulated genes associated to cell cycle arrest (GO analysis) are displayed. *n*=3.

Investigation of the differentially downregulated genes after JAR cell treatment gave more relevant insights about molecular mechanisms related to downregulation of the cell cycle (**Figure 39A-C**). Initial analysis of JAR cells upon MLN4924/cisplatin/combination treatment revealed 10/12/31 differentially downregulated genes associated with cell cycle process indicating as mentioned above an additive effect of MLN4924 application together with cisplatin.

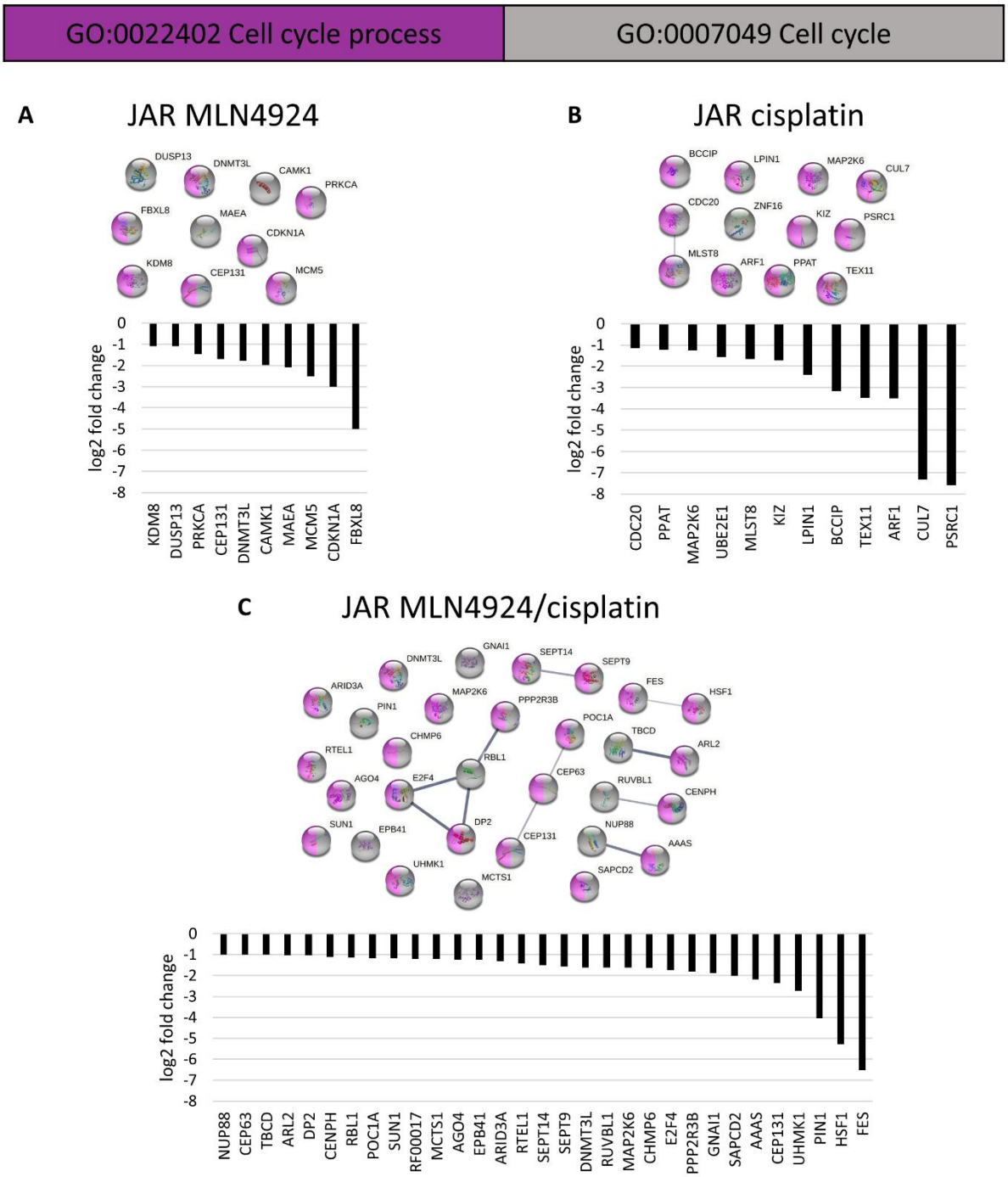

Figure 39: MLN4924 and cisplatin treatment were associated with downregulation of cell cycle process in JAR cells. Reprinted from [2]. 3'mRNA sequencing after 48 h of (**A**) MLN4924 (1 µM), (**B**) cisplatin (4 µM) and (**C**) combination treatment revealed differentially downregulated genes associated with cell cycle progression (STRING interaction and GO analysis). *n*=3

Notably, further investigation of the transcriptomics data strongly pinpointed towards cell differentiation upon MLN4924/cisplatin/combination treatment of 2102EP and JAR cells (**Figure 40A/B**, **Appendix Figure 13A-C**, **Appendix Figure 14A-C**). Interestingly, in 2102EP cells all three conditions resulted in highly increased transcript abundancy of important differentiation markers such as *HAND1*, *CDX2*, *CLDN1* and *SOX15*. While after mono therapy several mesoderm and endoderm marker genes were upregulated, combination treatment revealed a trend towards mesoderm development by increased transcript abundancy of *HAND1*, *IKZF3*, *LEF1*, *LHX1*, *T*, *CHRD*, *SECTM1*, etc. In JAR cells exposed to MLN4924 only few meso-/endoderm marker genes were found with elevated transcript abundancy. Combination treatment resulted in upregulation of 9 endoderm (*SMAD3*, *GATA6*, *DUSP5*, *LAMB3*, *COL12A1*, *DUSP4*, *COL7A1*, *MIXL1* and *ITGB2*) and 9 mesoderm marker genes (*TWSG1*, *EPB41L5*, *TBX3*, *FOXC1*, *AMH*, *TCF15*, *TXNRD1*, *EPHA2* and *SMAD3*).

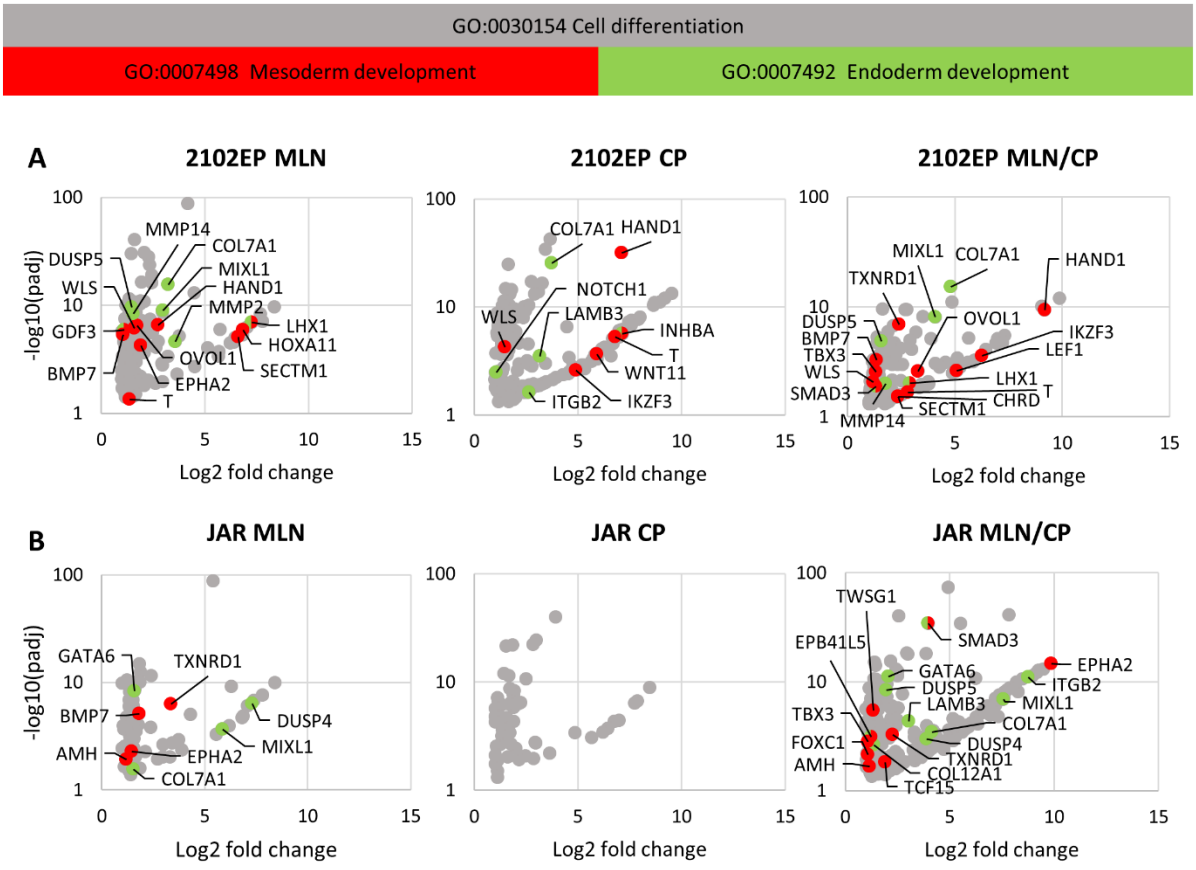

Figure 40: NAE1 inhibition and cisplatin treatment revealed cell differentiation of 2102EP and JAR cells on transcriptome level. Reprinted from [2]. (**A**) 2102EP as well as (**B**) JAR cells were exposed to MLN4924 (2102EP: 0.25 µM; JAR: 1 µM), cisplatin (2102EP: 2.5 µM; JAR 4 µM) and MLN4924/cisplatin combination (same concentrations as applied in the mono treatments) for 48 h. Gene ontology analysis revealed clusters of differentially upregulated genes associated with cell differentiation (grey dots), mesoderm (red dots) or endoderm development (green dots). *n*=3

Since, I found elevated transcript abundancy of genes associated with cell differentiation, I further analyzed the 3'mRNA-sequencing data for transcription factors and pluripotency

markers. Interestingly, 2102EP cells exposed to MLN4924 and MLN4924/cisplatin combination revealed STRING interaction networks composed of differentially downregulated transcription factors and core pluripotency markers such as SOX2, *SOX21* and *HESX1* (only deregulated in MLN4924/cisplatin sample) indicating loss of pluripotency (**Figure 41A/B**).

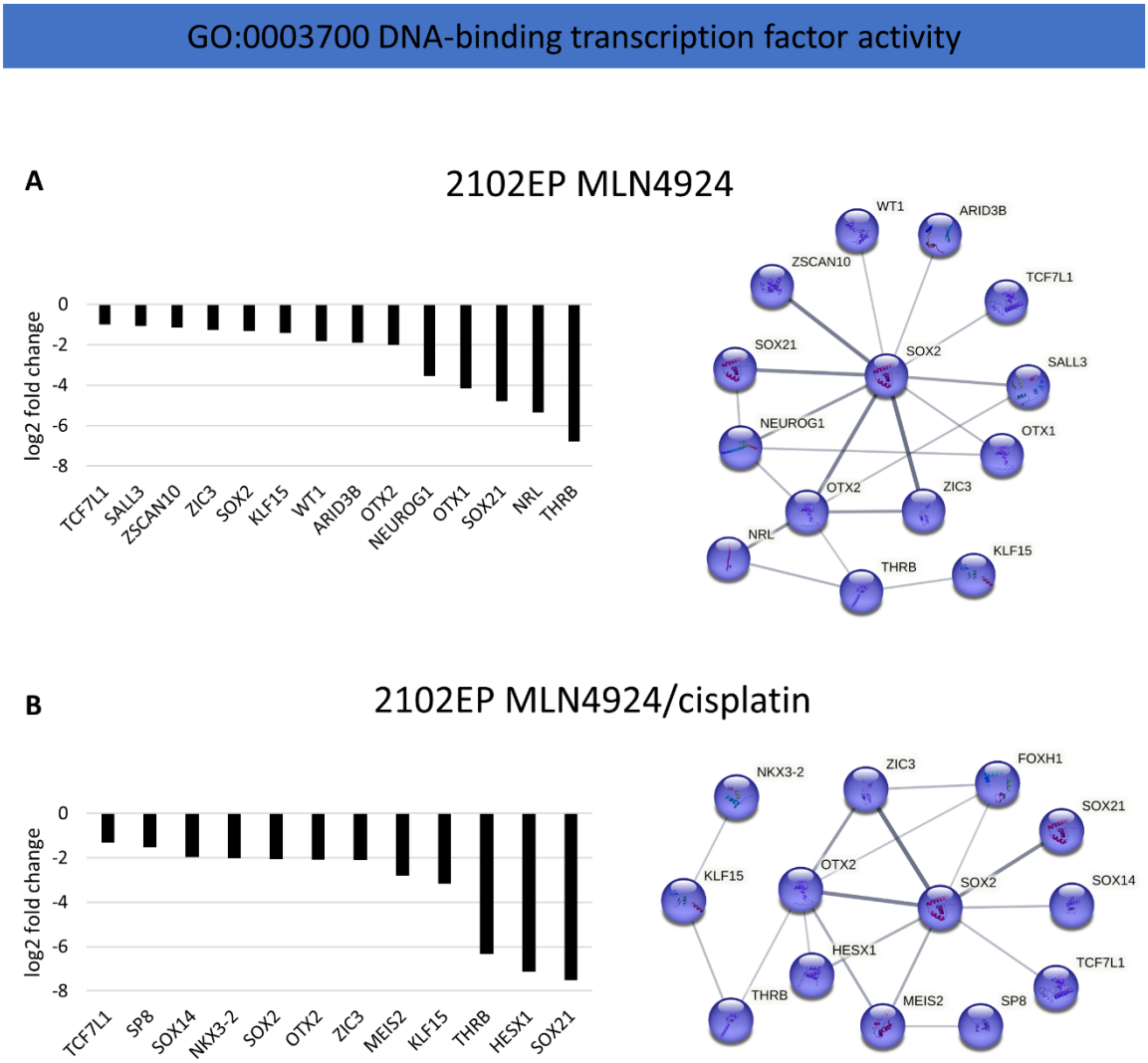

Figure 41: Reduced transcript abundancy of pluripotency factors in 2102EP cells after NAE1 inhibition and combination treatment with cisplatin. Reprinted from [2]. Transcriptome analysis of 2102EP cells treated with (**A**) MLN4924 (0.25 µM) or (**B**) MLN4924/cisplatin (0.25 µM/2.5 µM) displayed transcription factor associated (GO analysis) STRING interaction networks of differentially downregulated genes.

In contrast to 2102EP cells, JAR cells displayed only several differentially downregulated transcription factors after MLN4924 and combination treatment like *USF2*, *KLF15*, *HSF1*, etc. indicating global downregulation of transcription (**Figure 42A/B**).

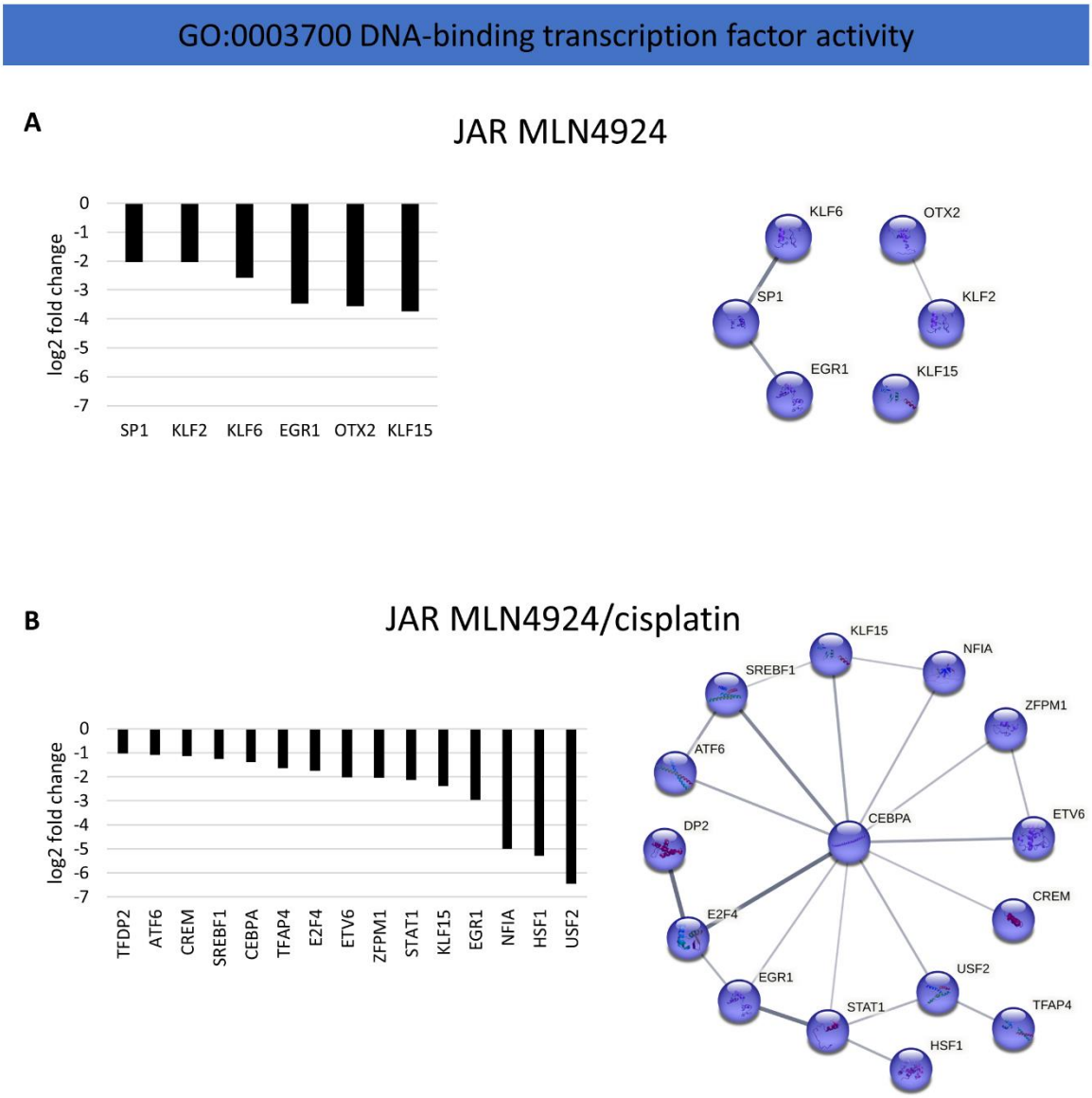

Figure 42: Reduced transcript abundancy of transcription factors in 2102EP cells after NAE1 inhibition and combination treatment with cisplatin. Reprinted from [2]. Transcriptome analysis of JAR cells treated with (**A**) MLN4924 (1 µM) or (**B**) MLN4924/cisplatin (1 µM/4 µM) displayed transcription factor associated (GO analysis) STRING interaction networks of differentially downregulated genes.

To sum up, the transcriptomic analyses revealed further insights in the molecular response of 2102EP and JAR cells treated with MLN4924/cisplatin/combination. Increased transcript abundance associated with apoptosis induction and cell cycle arrest after treatment were found. Further, the results suggested mesoderm and endoderm differentiation. For 2102EP cells downregulation of pluripotency related transcripts was detectable. Most important, all effects were stronger after combination treatment compared to cisplatin or MLN4924 only application indicating again the above-mentioned additive effect of both drugs.

4. Discussion

TGCTs can usually be treated very well by surgery and cisplatin-based chemotherapy reaching curation rates of around 95%. However, several patients develop chemotherapy resistant tumors during first line treatment or during relapse. Due to further lacking treatment options many patients can only be treated by salvage therapy facing very poor prognosis and low survival rates [14,36,37]. Thus, this study aimed to address the question of cisplatin resistance mechanisms as well as alternative therapeutics for TGCT treatment.

4.1. Transcriptional CDK inhibitors as an alternative treatment option for TGCTs

Since identification of CDKs as targets for cancer treatment, a variety of CDK inhibitors have been designed. Especially the cell cycle CDK inhibitors have been investigated extensively revealing a combination of Palbociclib and Ribociclib as promising treatment option in TGCTs [102]. However, compounds targeting the transcriptional CDKs in TGCTs have been poorly studied, yet. Due to promising therapeutic results of several transcriptional CDK inhibitors in other tumor entities such as AML, CLL, lymphoma, multiple myeloma, gastric cancer, prostate cancer, ovarian cancer, etc. [129,132,137] I investigated the potential of the two pan CDK inhibitors Flavopiridol and Dinaciclib, the tCDK inhibitors NVP2, SY0351, YKL-5-124, THZ1 and THZ531 as well as the CDK9 degrader THAL-SNS-032 on TGCT cell lines. For this study I used cisplatin sensitive (NCCIT, 2102EP, TCam2) as well as cisplatin resistant cell lines (NCCIT-R, 2102EP-R) resembling ECs (NCCIT, NCCIT-R, 2102EP, 2102EP-R) and seminomas (TCam2). Interestingly, all applied inhibitors displayed a strong reduction in viability of cisplatin sensitive and cisplatin resistant TGCT cell lines. Further investigation of cellular effects after NVP2, YKL-5-124 and SY0351 treatment demonstrated potent induction of apoptosis and cell cycle deregulation in 2102EP, NCCIT and TCam2 cells indicating strong cytotoxic effects of the compounds. In contrast THZ531 was found to induce strong cell cycle disturbance only in the EC cell lines 2102EP and NCCIT as well as moderate apoptosis in NCCIT cells. On a molecular level I discovered a rather cell line specific response of cells treated with SY0351, NVP2 and THZ531 demonstrating the reaction of different entities opening up novel specified treatment options for seminomas and non-seminomas. YKL-5-124 application resulted in a more common answer in cell lines representing different entities [1].

Treatment of the Sertoli cell derived control cell line FS1 with the different CDK inhibitors/degrader displayed strong to moderate cytotoxicity indicating side effects in the healthy testis tissue. Of note, Fibroblast derived MPAF cells were not or only very limited affected due to the CDK inhibitor/degrader treatment indicating very low side effects to other somatic tissues in the body and revealing great potential for TGCT treatment [1]. Only the testicular application of the CDK7, 12 and 13 inhibitor THZ1, studied in a mouse model, revealed impaired spermiogenesis [176]. The effect of THAL-SNS-032, NVP2, Flavopiridol,

Dinaciclib, SY0351, YKL-5-124 and THZ531 on heathy tissues as well as spermatogenesis remains elusive. Further *in vivo* studies are necessary to evaluate possible side effects more in detail.

Surprisingly, the treatment of 2102EP, TCam2 and the MPAF cells revealed a partially common molecular response only after YKL-5-124 treatment while THZ531, SY0351 and NVP2 induced different reactions on a transcriptomic level (**Figure 43**). In THZ531 treated (1 h) TCam2 cells decreased ubiquitin pathway activity as well as lower levels of corresponding proteasomal degradation were observed while 2102EP cells revealed increased poly(A) RNA degradation after 24 h of THZ531 application based on the GO analysis of the differential expression data. Previously published studies highlighted the diminished DNA repair capability induced by CDK12 and 13 inhibition or depletion. Lack of functional CDK12 and 13 results in deregulated intronic polyadenylation which is in turn necessary for functional expression of HR repair associated genes [125,126,136]. Despite disturbed RNA processing the data I generated did not display any alterations in DNA damage repair gene expression. Thus, in TGCT cells the response mechanism towards THZ531 treatment seems to be altered compared to other tumor entities (breast, prostate, ovarian, hepatocellular cancer) [177] which might be the explanation for the low cytotoxicity in the cell lines tested here. This emphasizes the unique role of germ cells and TGCTs. Of note, in germ cells DNA lesions are naturally not repaired but the cells undergo apoptosis in order to prevent passing on mutations to the germ line [52].

Interestingly, after 1 h of SY0351 (CDK7, 12, 13 inhibitor) application in 2102EP cells elevated ubiquitin pathway activity as well as increased transcript abundancy of genes associated with stress response were found. Here, I speculate that this is an explanation for the strong cytotoxic impact of the compound detectable in the XTT viability assays as well as in the apoptosis analysis. Further, accumulation of NCCIT, 2102EP and TCam2 cells in G1 or G2/M-phase have been observed after 20 h of drug exposure which is covered by previously generated data [140]. It has been shown that the inhibition of CDK7 impairs activation of CDK1, 2 and 4 by phosphorylation which are crucial for cell cycle progression arresting the cell in G1 or G2/M-cell cycle phase [140]. MPAF cells display very low sensitivity to the drug by overcoming the deregulation of immediate early genes, preventing cell cycle arrest and exhibiting only weak apoptosis induction.

After 1 h of treatment, the CDK7 specific inhibitor YKL-5-124 which shows very low off target affinity towards other CDKs [140] induced reduction of RNA Pol II mediated transcription and associated with that decreased abundance of immediate early gene transcripts in TCam2 cells. Interestingly, when Olson *et al.* developed and characterized YKL-5-124 they found only little changes in the phosphorylation status of RNA Pol II CTD [140]. Thus, decreased RNA Pol II

mediated transcription might be a primary effect in the TCam2 cell line which the cells overcome by a rescue mechanism controlled by CDK9, 12, and 13. It has been shown that CDK7 and CDK9, 12 as well as 13 display redundant functions in CTD phosphorylation of RNA Pol II [140].

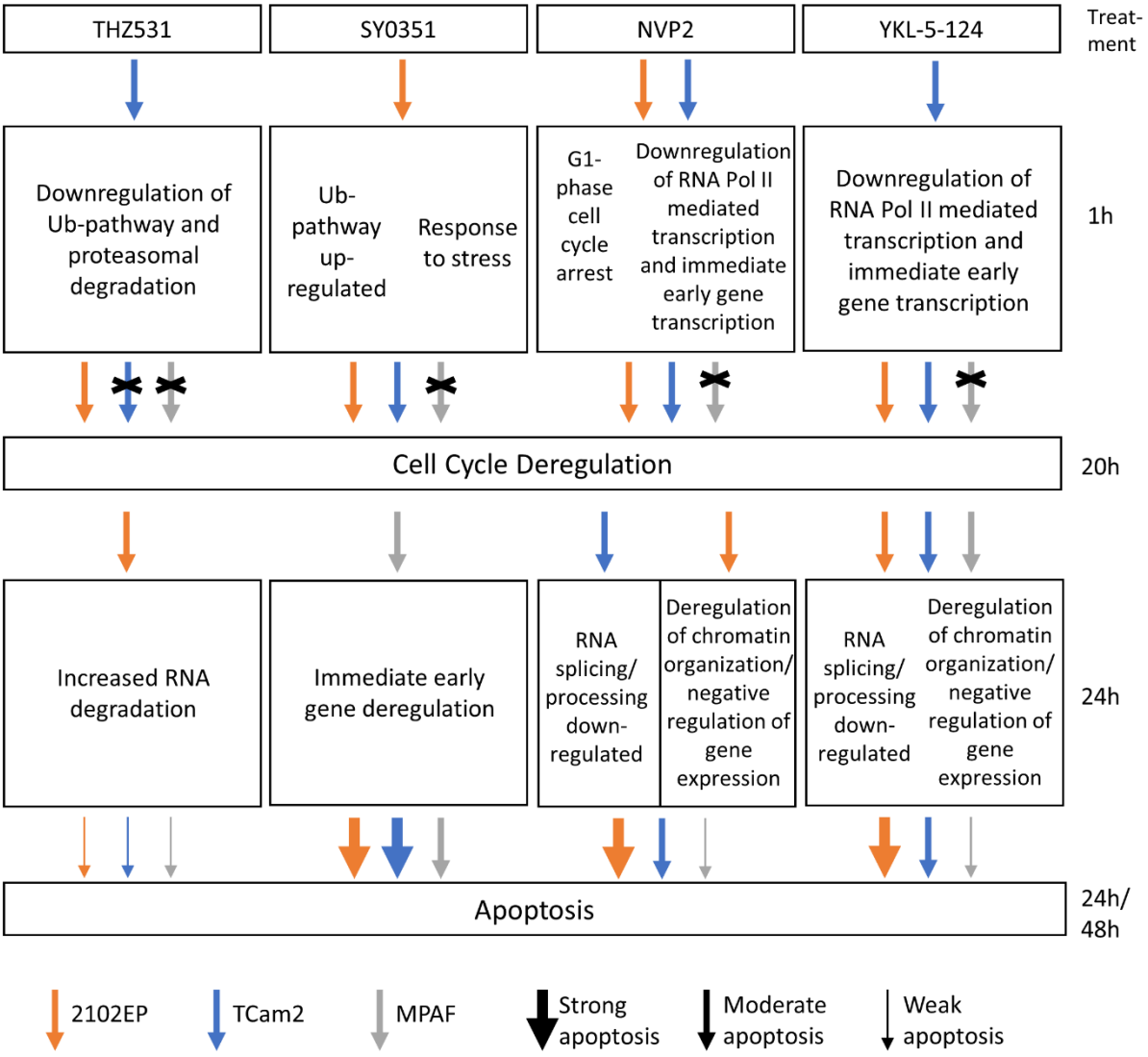

Figure 43: Schematic of THZ531, SY0351, NVP2 and YKL-5-124 effect in 2102EP, TCam2 and MPAF cells. Reprinted from [1].

2102EP, TCam2 and MPAF cells treated for 24 h with the YKL-5-124 inhibitor revealed a huge number of commonly deregulated genes which partially cluster together according to STRING interaction analysis. Detailed GO analysis suggested decreased RNA splicing/processing, disturbed chromatin organization and downregulated gene expression. CDK7 is considered as key regulator of transcription due to its function in the universal transcription factor TFIIH and as part of the CAK complex responsible for CDK9, 12 and 13 activity regulation by phosphorylation [118]. Interestingly, the importance of CDK7 as a major factor for splicing has already been shown in the human leukemia cell line HL60 treated with SY0351 [139]. Here,

splicing deregulation was not found in SY0351 treated cells but only in 2102EP, TCam2 and MPAF cells exposed to YKL-5-124 and in TCam2 cells treated with NVP2 for 24 h. Notably, NVP2 functions as an ATP-competitive CDK9 inhibitor, whereas YKL-5-124 suppresses CDK7 activity, avoiding the phosphorylation of CDK9. Aside from CAK mediated activation of substrates involved in the splicing process these results imply possible canonical activation of CDK9 induced by CDK7 resulting in CTD phosphorylation of RNA Pol II important for normal splicing activity. The importance of implementation of a specific phosphorylation pattern at the CTD of RNA Pol II has been shown in different studies [178,179]. Treatment of TCam2 cells with NVP2 for 24 h revealed downregulation of several important mRNA splicing, processing and transportation factors such as SF3B1, SRSF6, SRSF7, etc. The role of CDK9 as a crucial factor for transcription elongation and termination as well as the importance to interact with the splicing factor SF3B1 was emphasized in a recent article [179].

Unexpectedly, YKL-5-124 treated seminoma (TCam2) and EC cells (2102EP, NCCIT) revealed modest to strong apoptosis induction, respectively, while MPAF control cells were unaffected. Other research articles described YKL-5-124 treatment of chronic myeloid leukemia and small cell lung cancer cell lines revealing rather cell cycle arrest than apoptosis [140,180], leading to the conclusion that in most tumor entities in addition to a specific CDK7 inhibition a further compound is required for effective treatment. However, in EC cells strong apoptosis and cell cycle arrest, recognized by downregulation of several genes associated with cell cycle progression, have been observed due to CDK7 specific YKL-5-124 inhibitor exposure. Thus, YKL-5-124 might be a very potent and effective alternative treatment especially due to the high cytotoxicity in ECs compared to other tumor entities and even more important compared to fibroblasts. The CDK7, 12 and 13 inhibitor SY0351 resulted in strong apoptosis induction and cell cycle deregulation in TCam2 and 2102EP cells revealing a broader application spectrum. In MPAF control cells the compound caused only minor cytotoxic effects. Interestingly, the greatest potential of CDK7 inhibition is achieved with synergistically acting agents such as nutlin-3, 5-fluorouracil or a CDK12/13 inhibitor as shown in colon and ovarian cancer [181,182]. Further, clinical studies have been performed using highly CDK7 specific inhibitors CT7001 as well as SY-5609 alone or in combination with other compounds in advanced solid tumors (https://clinicaltrials.gov/) with identifiers NCT04247126 and NCT03363893. Hence, some of these drugs might also be efficient in TGCTs and should be further investigated.

Application of NVP2 and THAL-SNS-032 allowed a closer study of the intracellular CDK9 function. Despite different modes of action such as CDK9 inhibition (NVP2) and CDK9 degradation, both compounds induced strong reduction in viability in 2102EP and NCCIT cells while moderate decrease in viability was observed for TCam2 cells. Thus, CDK9 seems to play

an important role in the survival and proliferation of TGCTs. Further, strong and moderate apoptosis was detected for TCam2 and 2102EP cells exposed to NVP2 (10 nM) after 24/48 h supported by the peptide microarray data revealing elevated kinase activity of proapoptotic factors JNK1, 2 and 3 after 1 h NVP2 exposure. Interestingly, treatment of leukemia cells triggered apoptosis already after 6 h with a 25 fold higher NVP2 concentration [122]. On a molecular level after 1 h of NVP2 treatment 2102EP and TCam2 cells displayed G1-phase cell cycle arrest indicated by increased transcript abundance of cell cycle inhibitor p21 as well as reduced RNA Pol II mediated transcription which led also to differentially downregulated levels of immediate early gene expression such as *EGR1*, *FOSB*, *JUN* and *JUNB*. Since CDK9 is a crucial subunit for P-TEF activation, which is important for transcription elongation, inhibition of CDK9 activity is known to correlate with reduced full length gene expression [122]. Further, an accumulation of TCam2 cells in G2/-phase and 2102EP cells in G1-phase were found after 20 h of NVP2 application. This correlates with upregulated p21 expression driving the cells in G1- or G2-phase cell cycle arrest [183].

The molecular response after 24 h of NVP2 treatment was exclusively cell line related. In 2102EP cells a network comprising differentially upregulated MBD3L, PRAME as well as TRIM family members was identified. MBD3L and PRAME proteins might be responsible for epigenetic changes by DNA methylation and thereby induction of heterochromatin formation resulting in overall decreased transcription. TRIM related proteins are involved in labeling substrates with ubiquitin for proteasomal degradation. The exact mechanism how these proteins contribute to apoptosis induction in 2102EP cells remains elusive. In TCam2 cells characteristic response towards CDK9 inhibition including downregulation of RNA processing and splicing was observable [178,179]. The overall effect of NVP2 treatment seemed to be most potent in EC cells and less effective in seminomas while fibroblast control cells were hardly affected.

Notably, in 2102EP and TCam2 cells increased CDK15 (PFTAIRE2) phosphorylation activity has been detected in the peptide kinase assay after 1 h of NVP2 application. The corresponding cyclin Y was shown to be differentially upregulated on mRNA level in 2102EP cells. The active CDK15/cyclin Y complex is considered to play a role in prevention of cell death mediated by TNF-related apoptosis-inducing ligands (TRAIL) [184]. I further identified increased kinase activity of PIM1, 2 and 3 after 24 h of NVP2 treatment in 2102EP cells. Despite the importance of these oncogenic kinases for cell growth and migration [185] apoptosis was induced after 24/48 h indicating a rescue mechanism of the cells which ultimately fails.

4.2. Elucidating the role of neddylation in cisplatin resistance of TGCTs

Despite identification of several cisplatin resistance targets in TGCTs the major breakthrough is still absent [44,64]. Therefore, in the second part of this study I performed a genome scale CRISPR/Cas9 activation screen in JAR and 2102EP cells to identify further factors of cisplatin resistance. Thus, an overactivated neddylation pathway mediated by increased NAE1 abundance has been identified as a novel factor contributing to cisplatin resistance. These findings were validated in clonal *NAE1* overexpression cell lines (**Figure 44**). In order to investigate whether neddylation inhibition increased sensitivity of TGCT cells towards cisplatin the covalent NAE1 inhibitor MLN4924 was applied. Interestingly, combination treatment with cisplatin and MLN4924 revealed significantly reduced viability compared to mono therapy in different TGCT cell lines. The additive effect has also been observed in 2102EP, JAR and TCam2 cell lines for apoptosis induction and G2/M-phase cell cycle arrest. Elevated γH2A.X and p27 levels were discovered after cisplatin or MLN4924 mono therapy, respectively, validating the expected function of MLN4924 and cisplatin in cells. Of note, after combination treatment both p27 and γH2A.X displayed high abundance. Transcriptome analysis confirmed apoptosis induction and cell cycle deregulation on RNA level. Further, strong tendency towards cell differentiation after combination treatment was identified in both 2102EP and JAR cell lines while downregulation of pluripotency markers has only been detected in 2102EP cells. Most important high cytotoxicity of combination treatment was also observable in resistant TGCT cell lines indicating a re-sensitizing effect towards cisplatin while MPAF control cell line was not affected by any of the treatment regimens at all [2].

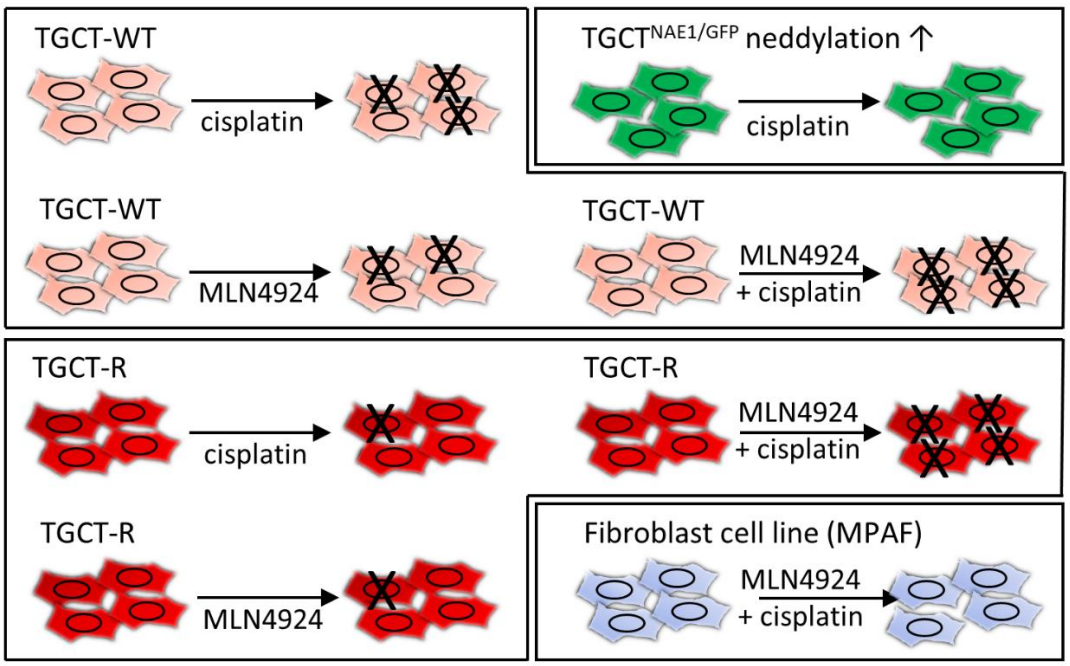

Figure 44: Effects of neddylation overexpression and neddylation inhibition alone or in combination with cisplatin. Modified from [2]. TGCT-WT, TGCT-R and Fibroblast cells revealed different viability after cisplatin or MLN4924 mono treatment and combination treatment.

Here I applied a genome scale CRISPR/Cas9 activation screen in 2102EP and JAR cells to identify cisplatin resistance factors in TGCTs. Cisplatin resistant clones revealed overactivation of cell cycle and DNA damage repair associated genes such as *AKT3* and *POLE4*. Interestingly, these factors have already been described in literature in the context of cisplatin resistance [44,56,64,186]. High abundance of PI3K/AKT pathway member AKT3 is important for cell survival and cell proliferation avoiding apoptosis and cell cycle arrest by MDM2 as well as p21 phosphorylation, respectively [44,64]. As a subunit of DNA polymerase ε POLE4 is involved in various DNA repair mechanisms (e.g. DNA double strand break repair, base excision repair, nucleotide excision repair) and in proof reading, promoting genome integrity [56,186]. Due to the finding of already described genes contributing to cisplatin resistance the screen was considered as reliable and to deliver robust results. Cisplatin resistant 2102EP$^{MPHv2/SAMv2}$ and JAR$^{MPHv2/SAMv2}$ cells derived from the screen revealed upregulation of *NAE1* as a novel factor. Due to absence of information about deregulated *NAE1* expression in the context of cisplatin resistance in TGCTs the neddylation pathway was investigated in detail. In general, upregulation of neddylation pathway is considered to play an important role in carcinogenesis and tumor progression as shown in breast, liver and lung cancer [147–149]. Interestingly, in pancreatic cancer elevated NAE1 levels correlated with increase of cisplatin resistance [147]. The screen further revealed *DDB1* overexpression as a potential candidate gene. Aside from DNA repair involvement, DDB1 is a member of the cullin4-RING ligase complex taking the adapter function which connects the cullin4 with the substrate [187]. In ovarian cancer *Cul4*/*DDB1* overexpression has been outlined as an important cisplatin resistance factor. Notably, knockdown of cullin4 increased cisplatin sensitivity [188]. Thus, NAE1 mediated activation and overexpression of neddylation pathway component *Cul4* as well as the corresponding substrate *DDB1* might also play an important role in cisplatin resistance of TGCTs. Here, I already validated increased cisplatin resistance in clonal 2102EP$^{NAE1/GFP}$ and JAR$^{NAE1/GFP}$ overexpression cell lines. These initial findings highlighted the neddylation pathway as a promising target for TGCT treatment.

Additionally, overactivation of candidate genes such as *SGOL2*, *TK1* and *TRAP1* were identified in cisplatin resistant 2102EP$^{MPHv2/SAMv2}$ and JAR$^{MPHv2/SAMv2}$ cells derived from the genome scale screen. Interestingly, *SGOL2*, *TK1* and *TRAP1* have not been described in the context of cisplatin resistance in TGCTs, yet. However, elevated expression of *SGOL2*, *TK1* and *TRAP1* is known to trigger carcinogenesis and tumor progression in different entities [189–192]. High abundance of TK1 after first line chemotherapy was identified as tumor marker indicating poor outcome in breast, lung and ovarian cancer [189]. SGOL2 displays oncogenic character in hepatocellular carcinoma cells [190]. Knockdown of the mitochondrial heat shock protein TRAP1 in lung cancer cells promoted cisplatin sensitivity while overactivation of *TRAP1* expression prevented cisplatin induced apoptosis by reduction of ROS production as shown

for osteosarcoma, colorectal, prostate and lung cancer [191,192]. Based on these previous findings I suggest that elevated SGOL2 and TK1 levels also further enhance tumor progression in TGCTs thereby contributing to cisplatin resistance. Thus, *SGOL2*, *TK1* and *TRAP1* are interesting factors that can be exploited as prognostic markers and might be useful for targeted therapy in chemotherapy resistant TGCT cells.

As mentioned above, increased neddylation mediated by elevated *NAE1* expression was found to induce cisplatin resistance in TGCTs. In order to investigate the effect of reduced neddylation activity on cisplatin resistant and sensitive cells I applied the NAE1 inhibitor MLN4924 alone or in combination with cisplatin. Interestingly, in different TGCT cell lines a significantly decreased viability was detectable after combination treatment compared to mono treatment. The same effect has been shown in a mouse model with xenografted pancreatic cancer cells. After MLN4924 and cisplatin combination treatment the tumor volume was significantly reduced and apoptosis induction was dramatically increased compared to mono treatment [147]. In my study, significantly elevated levels of apoptosis as well as G2/M-phase cell cycle arrest were observable after MLN4924/cisplatin combination treatment in 2102EP, JAR and TCam2 cells. Interestingly, cisplatin treatment as well as combination treatment revealed accumulation of the histone modification γH2A.X which is the direct response to DNA double strand breaks. Accumulation of p27 after MLN4924 and combination treatment pointed towards cell cycle arrest. Strong abundance of γH2A.X and p27 after combination treatment also indicated the strong additive effect which was observed before. Apoptosis in TGCTs is induced by cisplatin causing DNA inter- and intrastrand crosslinks resulting in DNA double strand breaks revealing increased levels of γH2A.X, subsequent G2/M-phase cell cycle arrest and apoptosis induction mediated by PUMA, NOXA as well as caspases [56,172]. Interestingly, in esophageal squamous cell carcinoma as well as lung cancer exposure to the neddylation inhibitor revealed p21, p27 and Wee1 protein accumulation which are responsible for initiation of G2/M-phase cell cycle arrest and subsequent apoptosis induction [148,193]. Thus, my results are in line with earlier findings regarding cell cycle and apoptosis induction after MLN4924 and cisplatin treatment.

Transcriptome analysis of 2102EP and JAR cells after MLN4924, cisplatin or MLN4924/cisplatin treatment revealed strong differential upregulation of *Keratin17* which is based on the gene ontology analysis involved in apoptosis initiation. In pancreatic cancer increased levels of *Keratin17* have been shown to reduce CyclinD1 and increase Caspase3 protein levels thereby initiating cell cycle arrest as well as apoptosis, respectively [194]. Together with the here generated data this suggests a contribution in cell cycle deregulation and apoptosis in TGCTs as well.

After MLN4924 mono treatment and combination treatment of 2102EP cells mRNA sequencing analysis revealed reduction of *SOX21* and the key EC factor *SOX2* indicating negative regulation of pluripotency. Simultaneously, in 2102EP and JAR cells several differentiation-associated transcripts were found to be strongly upregulated upon MLN4924 and cisplatin combination treatment. In 2102EP cells *CDX2* and *HAND1* transcripts revealed highly enriched abundance while in JAR cells only modest upregulation of both genes was detectable. High levels of SOX2 in EC cells normally activate SOX21 which further represses CDX2 [195]. Thus, downregulation of *SOX2* results in *CDX2* expression and thereby initiates differentiation. Interestingly, a deeper look into differentially upregulated genes associated with differentiation revealed clear induction of mesoderm formation (13 genes) including key markers such as *HAND1* and *LEF1*. In a previous study treatment of NCCIT cells with the BRD2, 4 and T inhibitor JQ1 also resulted in a similar phenotype including downregulation of pluripotency and induction of mesoderm differentiation [89]. Terminal tumor differentiation can be beneficial due to minimized metastatic and progressive potential. This has been shown for ECs treated with the differentiation agents thioridazine and salinomycin displaying heavily reduced carcinogenicity [196]. Interestingly, even for the choriocarcinoma derived cell line JAR 4 mesoderm- (*BMP7*, *TXNRD1*, etc.) and 4 endoderm-associated genes (*MIXL1*, *DUSP4*, etc.) were found to be upregulated upon MLN4924 treatment. This was very unexpected due to the absence of pluripotency and EC markers which might indicate a direct conversion from extraembryonic into endoderm/mesoderm fate avoiding an EC like intermediate state. Reprogramming of seminoma to an EC-like and mixed non-seminoma fate has been demonstrated before [111–113]. The reprogramming of JAR cells again highlights the strong innate plasticity of TGCTs.

Neddylation mediated cisplatin resistance might be classified as pre- or post-target mechanism since it has not been described yet whether *NAE1* is already overexpressed before cisplatin treatment or whether neddylation induction is acquired upon treatment resulting in cisplatin resistance. The underlying mechanism is based on elevated neddylation activity resulting in enhanced cullin neddylation which leads to increased CRL activity. CRLs are important for polyubiquitination of tumor suppressor substrates such as Wee1, p21 and p27 thereby preventing cell cycle arrest and apoptosis induction [141]. Interestingly, inhibition of neddylation using MLN4924 results in accumulation of these tumor suppressors inducing cell cycle arrest and apoptosis [141].

Cisplatin in combination with MLN4924 has also been investigated in other tumor entities such as pancreatic cancer and esophageal squamous cell carcinoma where cytotoxic effects were observed for concentrations between 0.2 to 1 µM [147,193] which is in the same range compared to the TGCT cell lines. In this study, I highlighted the potential of neddylation

inhibition by MLN4924 for combination treatment with cisplatin in sensitive TGCT cell lines and displayed the re-sensitizing effect of NAE1 inhibition in cisplatin resistant cells as a promising novel treatment option. Interestingly, in TGCT tissues the NAE1 expression was higher compared to other tumor entities and normal tissues which renders these cells probably most sensitive towards neddylation pathway interference. Especially, the highly cytotoxic effect in TGCT cell lines together with unaffected fibroblasts makes the drug combination very valuable. The MLN4924 inhibitor is currently investigated in 40 clinical trials (https://www.clinicaltrials.gov/) in various tumor entities. As soon as the drug is approved an off-label use for TGCT therapy might be a promising option.

5. Conclusion

Treatment of chemotherapy resistant TGCTs remains a huge problem due to lacking alternative treatment options. In this study cisplatin resistance mechanisms were further investigated and alternative treatment options were evaluated.

CDK inhibitors are known to be a potent treatment option in various tumor entities. Here, I analyzed a panel of pan CDK and tCDK inhibitors as well as a CDK9 degrader. Especially, the CDK9 inhibitor NVP2 as well as the CDK7, 12 and 13 inhibitor SY0351 revealed very promising results at low nanomolar concentrations. The compounds displayed strong cytotoxicity in seminomas, ECs and cisplatin resistant TGCT cell lines while the fibroblast control cell line was hardly affected. Thus, NVP2 and SY0351 might be effectively used in a broad spectrum of TGCT therapy. The CDK7 specific inhibitor YKL-5-124 showed a very strong cytotoxicity in 2102EP and 2102EP-R cells while other cell lines were affected to a lower extend which indicates a narrow but highly specific and precise window for YKL-5-124 application. The molecular response of different cell lines representing different entities varied upon NVP2, SY0351 and YKL-5-124 treatment. Thus, it seems to be important to exactly determine the tumor composition (seminoma, EC, teratoma, Cc, YST) to choose a precise and personalized treatment strategy.

In order to determine cisplatin resistance mechanisms a genome scale CRISPR/Cas9 activation screen was performed. This screen revealed amongst already known factors novel candidate genes such as *NAE1* which is the core component of the neddylation pathway. Overactivated neddylation significantly contributed to cisplatin resistance in TGCTs. However, the exact mechanism remains elusive. I speculate that according to the generated data the NAE1/cullin4-RING ligase axis might be very important in resistant cells. To investigate this hypothesis, upregulation of *Cul4* and subsequent reaction towards cisplatin exposure should be analyzed. Further, proteomics analysis upon *Cul4* overexpression would be interesting to identify substrates which are degraded by increased Cul4-RING ligase activity.

The same question remains elusive for MLN4924 application. This drug inhibits the neddylation cascade at the very beginning which makes it difficult to pinpoint a certain sub pathway responsible for apoptosis induction. Thus, it would be interesting to target the different cullins and perform a viability analysis as well as proteomics analysis to determine whether one of these pathways is responsible for the strong cytotoxic effect. However, there is also a huge number of non-cullin substrates which are altered in function, stability and location during neddylation suppression. Nevertheless, application of MLN4924 especially in combination with cisplatin displayed a very potent and significantly stronger cytotoxic effect compared to mono treatment in cisplatin sensitive and cisplatin resistant TGCT cell lines. Importantly, NAE1

expression was found to be highest in TGCTs. Thus, this treatment regimen is a promising alternative in TGCT treatment independent of chemotherapy resistance.

In order to further investigate the potential of YKL-5-124, NVP2, SY0351 and MLN4924, TGCT cells xenografted in nude-mice would be helpful to study cytotoxic effects on the tumor as well as side effects of the compounds *in vivo*. In the next step clinical studies could be performed to investigate tolerability and effectivity of these drugs in patients. Alternatively, as soon as the drugs are clinically approved for treatment of other tumor entities, a possible off-label use might be considered.

6. Bibliography

1. Funke, K.; Düster, R.; Wilson, P.D.-G.; Arévalo, L.; Geyer, M.; Schorle, H. Transcriptional CDK Inhibitors as Potential Treatment Option for Testicular Germ Cell Tumors. *Cancers* **2022**, *14, doi:*10.3390/cancers14071690.

2. Funke, K.; Einsfelder, U.; Hansen, A.; Arévalo, L.; Schneider, S.; Nettersheim, D.; Stein, V.; Schorle, H. Genome-scale CRISPR screen reveals neddylation to contribute to cisplatin resistance of testicular germ cell tumors. *Br J Cancer*, ***revised version under revision, 2023***.

3. Tang, W.W.C.; Kobayashi, T.; Irie, N.; Dietmann, S.; Surani, M.A. Specification and epigenetic programming of the human germ line. *Nat. Rev. Genet.* **2016**, *17*, 585–600, doi:10.1038/nrg.2016.88.

4. Sasaki, K.; Nakamura, T.; Okamoto, I.; Yabuta, Y.; Iwatani, C.; Tsuchiya, H.; Seita, Y.; Nakamura, S.; Shiraki, N.; Takakuwa, T.; et al. The Germ Cell Fate of Cynomolgus Monkeys Is Specified in the Nascent Amnion. *Dev. Cell* **2016**, *39*, 169–185, doi:10.1016/j.devcel.2016.09.007.

5. Neto, F.T.L.; Bach, P.V.; Najari, B.B.; Li, P.S.; Goldstein, M. Spermatogenesis in humans and its affecting factors. *Semin. Cell Dev. Biol.* **2016**, *59*, 10–26, doi:10.1016/j.semcdb.2016.04.009.

6. Kojima, Y.; Sasaki, K.; Yokobayashi, S.; Sakai, Y.; Nakamura, T.; Yabuta, Y.; Nakaki, F.; Nagaoka, S.; Woltjen, K.; Hotta, A.; et al. Evolutionarily Distinctive Transcriptional and Signaling Programs Drive Human Germ Cell Lineage Specification from Pluripotent Stem Cells. *Cell Stem Cell* **2017**, *21*, 517-532.e5, doi:10.1016/j.stem.2017.09.005.

7. Kobayashi, T.; Zhang, H.; Tang, W.W.C.; Irie, N.; Withey, S.; Klisch, D.; Sybirna, A.; Dietmann, S.; Contreras, D.A.; Webb, R.; et al. Principles of early human development and germ cell program from conserved model systems. *Nature* **2017**, *546*, 416–420, doi:10.1038/nature22812.

8. Meyenn, F. von; Reik, W. Forget the Parents: Epigenetic Reprogramming in Human Germ Cells. *Cell* **2015**, *161*, 1248–1251, doi:10.1016/j.cell.2015.05.039.

9. Nettersheim, D.; Jostes, S.; Schneider, S.; Schorle, H. Elucidating human male germ cell development by studying germ cell cancer. *Reproduction* **2016**, *152*, R101-13, doi:10.1530/REP-16-0114.

10. Pauls, K.; Schorle, H.; Jeske, W.; Brehm, R.; Steger, K.; Wernert, N.; Büttner, R.; Zhou, H. Spatial expression of germ cell markers during maturation of human fetal male gonads:

an immunohistochemical study. *Hum. Reprod.* **2006**, *21*, 397–404, doi:10.1093/humrep/dei325.

11. Stukenborg, J.-B.; Kjartansdóttir, K.R.; Reda, A.; Colon, E.; Albersmeier, J.P.; Söder, O. Male germ cell development in humans. *Horm. Res. Paediatr.* **2014**, *81*, 2–12, doi:10.1159/000355599.
12. Hayes-Lattin, B.; Nichols, C.R. Testicular Cancer: A Prototypic Tumor of Young Adults. *Seminars in Oncology* **2009**, *36*, 432–438, doi:10.1053/j.seminoncol.2009.07.006.
13. National Cancer Institute. Cancer Stat Facts SEER. Testicular Cancer. Available online: https://seer.cancer.gov/statfacts/html/testis.html (accessed on 5 September 2022).
14. Oing, C.; Seidel, C.; Bokemeyer, C. Therapeutic approaches for refractory germ cell cancer. *Expert Rev. Anticancer Ther* **2018**, *18, doi:*10.1080/14737140.2018.1450630.
15. Bonouvrie, K.; van der Werff Ten Bosch, J.; van den Akker, M. Klinefelter syndrome and germ cell tumors: review of the literature. *Int. J. Pediatr. Endocrinol.* **2020**, *2020*, 18, doi:10.1186/s13633-020-00088-0.
16. Fukawa, T.; Kanayama, H.-O. Current knowledge of risk factors for testicular germ cell tumors. *Int. J. Urol.* **2018**, *25*, 337–344, doi:10.1111/iju.13519.
17. Oosterhuis, J.W.; Looijenga, L.H.J. Testicular germ-cell tumours in a broader perspective. *Nat. Rev. Cancer* **2005**, *5, doi:*10.1038/nrc1568.
18. Weil, B.R.; Billmire, D.F. Management of Germ Cell Tumors in Pediatric Patients. *Surg. Oncol. Clin. N. Am.* **2021**, *30*, 325–338, doi:10.1016/j.soc.2020.11.011.
19. Harms, D.; Zahn, S.; Göbel, U.; Schneider, D.T. Pathology and molecular biology of teratomas in childhood and adolescence. *Klin. Padiatr.* **2006**, *218*, 296–302, doi:10.1055/s-2006-942271.
20. Mosbech, C.H.; Rechnitzer, C.; Brok, J.S.; Rajpert-De Meyts, E.; Hoei-Hansen, C.E. Recent advances in understanding the etiology and pathogenesis of pediatric germ cell tumors. *J. Pediatr. Hematol. Oncol.* **2014**, *36*, 263–270, doi:10.1097/MPH.0000000000000125.
21. Berney, D.M.; Looijenga, L.H.J.; Idrees, M.; Oosterhuis, J.W.; Rajpert-De Meyts, E.; Ulbright, T.M.; Skakkebaek, N.E. Germ cell neoplasia in situ (GCNIS): evolution of the current nomenclature for testicular pre-invasive germ cell malignancy. *Histopathology* **2016**, *69*, 7–10, doi:10.1111/his.12958.

22. Skakkebaek, N.E.; Berthelsen, J.G.; Giwercman, A.; Müller, J. Carcinoma-in-situ of the testis: possible origin from gonocytes and precursor of all types of germ cell tumours except spermatocytoma. *Int. J. Androl.* **1987**, *10*, 19–28, doi:10.1111/j.1365-2605.1987.tb00161.x.

23. Hoei-Hansen, C.E.; Nielsen, J.E.; Almstrup, K.; Sonne, S.B.; Graem, N.; Skakkebaek, N.E.; Leffers, H.; Rajpert-De Meyts, E. Transcription factor AP-2gamma is a developmentally regulated marker of testicular carcinoma in situ and germ cell tumors. *Clin. Cancer Res.* **2004**, *10*, 8521–8530, doi:10.1158/1078-0432.CCR-04-1285.

24. Baroni, T.; Arato, I.; Mancuso, F.; Calafiore, R.; Luca, G. On the Origin of Testicular Germ Cell Tumors: From Gonocytes to Testicular Cancer. *Front. Endocrinol. (Lausanne)* **2019**, *10*, 343, doi:10.3389/fendo.2019.00343.

25. Jong, J. de; Stoop, H.; Gillis, A.J.M.; van Gurp, R.J.H.L.M.; van de Geijn, G.-J.M.; Boer, M. de; Hersmus, R.; Saunders, P.T.K.; Anderson, R.A.; Oosterhuis, J.W.; et al. Differential expression of SOX17 and SOX2 in germ cells and stem cells has biological and clinical implications. *J. Pathol.* **2008**, *215*, 21–30, doi:10.1002/path.2332.

26. Irie, N.; Weinberger, L.; Tang, W.W.C.; Kobayashi, T.; Viukov, S.; Manor, Y.S.; Dietmann, S.; Hanna, J.H.; Surani, M.A. SOX17 is a critical specifier of human primordial germ cell fate. *Cell* **2015**, *160*, 253–268, doi:10.1016/j.cell.2014.12.013.

27. Jostes, S.V.; Fellermeyer, M.; Arévalo, L.; Merges, G.E.; Kristiansen, G.; Nettersheim, D.; Schorle, H. Unique and redundant roles of SOX2 and SOX17 in regulating the germ cell tumor fate. *Int. J. Cancer* **2020**, *146*, 1592–1605, doi:10.1002/ijc.32714.

28. Nonaka, D. Differential expression of SOX2 and SOX17 in testicular germ cell tumors. *Am. J. Clin. Pathol.* **2009**, *131*, 731–736, doi:10.1309/AJCP7MNCNBCRN8NO.

29. Sheikine, Y.; Genega, E.; Melamed, J.; Lee, P.; Reuter, V.E.; Ye, H. Molecular genetics of testicular germ cell tumors. *Am. J. Cancer Res.* **2012**, *2*, 153–167.

30. Koši Kunac, A.; Gnjidić, M.; Antunac Golubić, Z.; Gamulin, M. Treatment of germ cell testicular cancer. *Acta Clin. Croat.* **2020**, *59*, 496–504, doi:10.20471/acc.2020.59.03.14.

31. EAU Guidelines. Edn. presented at the EAU Annual Congress Amsterdam 2022., ISBN 978-94-92671-16-5.

32. Oldenburg, J.; Berney, D.M.; Bokemeyer, C.; Climent, M.A.; Daugaard, G.; Gietema, J.A.; Giorgi, U. de; Haugnes, H.S.; Huddart, R.A.; Leão, R.; et al. Testicular seminoma and non-seminoma: ESMO-EURACAN Clinical Practice Guideline for diagnosis, treatment and follow-up. *Ann. Oncol.* **2022**, *33*, 362–375, doi:10.1016/j.annonc.2022.01.002.

33. International Germ Cell Consensus Classification: a prognostic factor-based staging system for metastatic germ cell cancers. International Germ Cell Cancer Collaborative Group. *J. Clin. Oncol.* **1997**, *15*, 594–603, doi:10.1200/JCO.1997.15.2.594.

34. Beyer, J.; Collette, L.; Sauvé, N.; Daugaard, G.; Feldman, D.R.; Tandstad, T.; Tryakin, A.; Stahl, O.; Gonzalez-Billalabeitia, E.; Giorgi, U. de; et al. Survival and New Prognosticators in Metastatic Seminoma: Results From the IGCCCG-Update Consortium. *J. Clin. Oncol.* **2021**, *39*, 1553–1562, doi:10.1200/JCO.20.03292.

35. Gillessen, S.; Sauvé, N.; Collette, L.; Daugaard, G.; Wit, R. de; Albany, C.; Tryakin, A.; Fizazi, K.; Stahl, O.; Gietema, J.A.; et al. Predicting Outcomes in Men With Metastatic Nonseminomatous Germ Cell Tumors (NSGCT): Results From the IGCCCG Update Consortium. *J. Clin. Oncol.* **2021**, *39*, 1563–1574, doi:10.1200/JCO.20.03296.

36. Oing, C.; Lorch, A. The role of salvage high-dose chemotherapy in relapsed male germ cell tumors. *Oncol. Res. Treat.* **2018**, *41*.

37. Oing, C.; Giannatempo, P.; Honecker, F.; Oechsle, K.; Bokemeyer, C.; Beyer, J. Palliative treatment of germ cell cancer. *Cancer Treatment Reviews* **2018**, *71*, 102–107, doi:10.1016/j.ctrv.2018.10.007.

38. Bagrodia, A.; Lee, B.H.; Lee, W.; Cha, E.K.; Sfakianos, J.P.; Iyer, G.; Pietzak, E.J.; Gao, S.P.; Zabor, E.C.; Ostrovnaya, I.; et al. Genetic Determinants of Cisplatin Resistance in Patients With Advanced Germ Cell Tumors. *J. Clin. Oncol.* **2016**, *34*, 4000–4007, doi:10.1200/JCO.2016.68.7798.

39. Rosenberg, B.; Renshaw, E.; Vancamp, L.; Hartwick, J.; Drobnik, J. Platinum-induced filamentous growth in Escherichia coli. *J. Bacteriol.* **1967**, *93*, 716–721, doi:10.1128/jb.93.2.716-721.1967.

40. Rosenberg, B.; Vancamp, L.; Trosko, J.E.; Mansour, V.H. Platinum compounds: a new class of potent antitumour agents. *Nature* **1969**, *222*, 385–386, doi:10.1038/222385a0.

41. Rosenberg, B.; Vancamp, L. The successful regression of large solid sarcoma 180 tumors by platinum compounds. *Cancer Res.* **1970**, *30*, 1799–1802.

42. Ries, L.; Young, J.; Keel, G.; Eisner, M.; Lin, Y.; Horner, M. *Seer survival monograph: Cancer survival among adults: U.S. SEER Program, 1988-2001, Patient and Tumor Characteristics.;* Bibliogov: Bethesda, MD.

43. Rocha, C.R.R.; Silva, M.M.; Quinet, A.; Cabral-Neto, J.B.; Menck, C.F.M. DNA repair pathways and cisplatin resistance: an intimate relationship. *Clinics (Sao Paulo)* **2018**, *73*, e478s, doi:10.6061/clinics/2018/e478s.

44. Országhová, Z.; Kalavska, K.; Mego, M.; Chovanec, M. Overcoming Chemotherapy Resistance in Germ Cell Tumors. *Biomedicines* **2022**, *10, doi:*10.3390/biomedicines10050972.

45. Ishida, S.; Lee, J.; Thiele, D.J.; Herskowitz, I. Uptake of the anticancer drug cisplatin mediated by the copper transporter Ctr1 in yeast and mammals. *PNAS* **2002**, *99*, 14298–14302, doi:10.1073/pnas.162491399.

46. Ghosh, S. Cisplatin: The first metal based anticancer drug. *Bioorg. Chem.* **2019**, *88*, 102925, doi:10.1016/j.bioorg.2019.102925.

47. Brozovic, A.; Ambriović-Ristov, A.; Osmak, M. The relationship between cisplatin-induced reactive oxygen species, glutathione, and BCL-2 and resistance to cisplatin. *Crit. Rev. Toxicol.* **2010**, *40*, 347–359, doi:10.3109/10408441003601836.

48. Lord, C.J.; Ashworth, A. The DNA damage response and cancer therapy. *Nature* **2012**, *481*, 287–294, doi:10.1038/nature10760.

49. Awasthi, P.; Foiani, M.; Kumar, A. ATM and ATR signaling at a glance. *J. Cell Sci.* **2016**, *129*, 1285, doi:10.1242/jcs.188631.

50. Blackford, A.N.; Jackson, S.P. ATM, ATR, and DNA-PK: The Trinity at the Heart of the DNA Damage Response. *Mol. Cell* **2017**, *66*, 801–817, doi:10.1016/j.molcel.2017.05.015.

51. Weber, A.M.; Ryan, A.J. ATM and ATR as therapeutic targets in cancer. *Pharmacol. Ther.* **2015**, *149*, 124–138, doi:10.1016/j.pharmthera.2014.12.001.

52. Bloom, J.C.; Loehr, A.R.; Schimenti, J.C.; Weiss, R.S. Germline genome protection: Implications for gamete quality and germ cell tumorigenesis. *Andrology* **2019**, *7*, 516–526, doi:10.1111/andr.12651.

53. Vries, G. de; Rosas-Plaza, X.; van Vugt, M.A.T.M.; Gietema, J.A.; Jong, S. de. Testicular cancer: Determinants of cisplatin sensitivity and novel therapeutic opportunities. *Cancer Treatment Reviews* **2020**, *88*, 102054, doi:10.1016/j.ctrv.2020.102054.

54. Awuah, S.G.; Riddell, I.A.; Lippard, S.J. Repair shielding of platinum-DNA lesions in testicular germ cell tumors by high-mobility group box protein 4 imparts cisplatin hypersensitivity. *Proc. Natl. Acad. Sci. U. S. A.* **2017**, *114*, 950–955, doi:10.1073/pnas.1615327114.

55. Welsh, C.; Day, R.; McGurk, C.; Masters, J.R.W.; Wood, R.D.; Köberle, B. Reduced levels of XPA, ERCC1 and XPF DNA repair proteins in testis tumor cell lines. *Int. J. Cancer* **2004**, *110*, 352–361, doi:10.1002/ijc.20134.

56. Usanova, S.; Piée-Staffa, A.; Sied, U.; Thomale, J.; Schneider, A.; Kaina, B.; Köberle, B. Cisplatin sensitivity of testis tumour cells is due to deficiency in interstrand-crosslink repair and low ERCC1-XPF expression. *Mol Cancer* **2010**, *9*, 248, doi:10.1186/1476-4598-9-248.

57. Mego, M.; Cierna, Z.; Svetlovska, D.; Macak, D.; Machalekova, K.; Miskovska, V.; Chovanec, M.; Usakova, V.; Obertova, J.; Babal, P.; et al. PARP expression in germ cell tumours. *J. Clin. Pathol.* **2013**, *66*, 607–612, doi:10.1136/jclinpath-2012-201088.

58. Koster, R.; Timmer-Bosscha, H.; Bischoff, R.; Gietema, J.A.; Jong, S. de. Disruption of the MDM2-p53 interaction strongly potentiates p53-dependent apoptosis in cisplatin-resistant human testicular carcinoma cells via the Fas/FasL pathway. *Cell Death Dis.* **2011**, *2*, e148, doi:10.1038/cddis.2011.33.

59. Gutekunst, M.; Oren, M.; Weilbacher, A.; Dengler, M.A.; Markwardt, C.; Thomale, J.; Aulitzky, W.E.; van der Kuip, H. p53 hypersensitivity is the predominant mechanism of the unique responsiveness of testicular germ cell tumor (TGCT) cells to cisplatin. *PLoS ONE* **2011**, *6*, e19198, doi:10.1371/journal.pone.0019198.

60. Gutekunst, M.; Mueller, T.; Weilbacher, A.; Dengler, M.A.; Bedke, J.; Kruck, S.; Oren, M.; Aulitzky, W.E.; van der Kuip, H. Cisplatin hypersensitivity of testicular germ cell tumors is determined by high constitutive Noxa levels mediated by Oct-4. *Cancer Res.* **2013**, *73*, 1460–1469, doi:10.1158/0008-5472.CAN-12-2876.

61. Palmer, R.D.; Murray, M.J.; Saini, H.K.; van Dongen, S.; Abreu-Goodger, C.; Muralidhar, B.; Pett, M.R.; Thornton, C.M.; Nicholson, J.C.; Enright, A.J.; et al. Malignant germ cell tumors display common microRNA profiles resulting in global changes in expression of messenger RNA targets. *Cancer Res.* **2010**, *70*, 2911–2923, doi:10.1158/0008-5472.CAN-09-3301.

62. Liu, L.; Lian, J.; Zhang, H.; Tian, H.; Liang, M.; Yin, M.; Sun, F. MicroRNA-302a sensitizes testicular embryonal carcinoma cells to cisplatin-induced cell death. *J. Cell. Physiol.* **2013**, *228*, 2294–2304, doi:10.1002/jcp.24394.

63. Singh, R.; Fazal, Z.; Freemantle, S.J.; Spinella, M.J. Mechanisms of cisplatin sensitivity and resistance in testicular germ cell tumors. *Cancer Drug Resist.* **2019**, *2*, 580–594, doi:10.20517/cdr.2019.19.

64. Lobo, J.; Jerónimo, C.; Henrique, R. Cisplatin Resistance in Testicular Germ Cell Tumors: Current Challenges from Various Perspectives. *Cancers* **2020**, *12, doi:*10.3390/cancers12061601.

65. Chen, H.H.W.; Kuo, M.T. Role of glutathione in the regulation of Cisplatin resistance in cancer chemotherapy. *Met. Based Drugs* **2010**, *2010, doi:*10.1155/2010/430939.

66. Masters, J.R.; Thomas, R.; Hall, A.G.; Hogarth, L.; Matheson, E.C.; Cattan, A.R.; Lohrer, H. Sensitivity of testis tumour cells to chemotherapeutic drugs: role of detoxifying pathways. *Eur. J. Cancer* **1996**, *32A*, 1248–1253, doi:10.1016/0959-8049(96)00033-0.

67. Srivastava, A.K.; Han, C.; Zhao, R.; Cui, T.; Dai, Y.; Mao, C.; Zhao, W.; Zhang, X.; Yu, J.; Wang, Q.-E. Enhanced expression of DNA polymerase eta contributes to cisplatin resistance of ovarian cancer stem cells. *Proc. Natl. Acad. Sci. U. S. A.* **2015**, *112*, 4411–4416, doi:10.1073/pnas.1421365112.

68. Rudolph, C.; Melau, C.; Nielsen, J.E.; Vile Jensen, K.; Liu, D.; Pena-Diaz, J.; Rajpert-De Meyts, E.; Rasmussen, L.J.; Jørgensen, A. Involvement of the DNA mismatch repair system in cisplatin sensitivity of testicular germ cell tumours. *Cell. Oncol. (Dordr)* **2017**, *40*, 341–355, doi:10.1007/s13402-017-0326-8.

69. Honecker, F.; Wermann, H.; Mayer, F.; Gillis, A.J.M.; Stoop, H.; van Gurp, R.J.L.M.; Oechsle, K.; Steyerberg, E.; Hartmann, J.T.; Dinjens, W.N.M.; et al. Microsatellite instability, mismatch repair deficiency, and BRAF mutation in treatment-resistant germ cell tumors. *J. Clin. Oncol.* **2009**, *27*, 2129–2136, doi:10.1200/JCO.2008.18.8623.

70. Bassett, E.; Vaisman, A.; Tropea, K.A.; McCall, C.M.; Masutani, C.; Hanaoka, F.; Chaney, S.G. Frameshifts and deletions during in vitro translesion synthesis past Pt-DNA adducts by DNA polymerases beta and eta. *DNA Repair (Amst)* **2002**, *1*, 1003–1016, doi:10.1016/S1568-7864(02)00150-7.

71. Shachar, S.; Ziv, O.; Avkin, S.; Adar, S.; Wittschieben, J.; Reissner, T.; Chaney, S.; Friedberg, E.C.; Wang, Z.; Carell, T.; et al. Two-polymerase mechanisms dictate error-free and error-prone translesion DNA synthesis in mammals. *EMBO J.* **2009**, *28*, 383–393, doi:10.1038/emboj.2008.281.

72. Kersemaekers, A.-M.F.; Mayer, F.; Molier, M.; van Weeren, P.C.; Oosterhuis, J.W.; Bokemeyer, C.; Looijenga, L.H.J. Role of P53 and MDM2 in treatment response of human germ cell tumors. *J. Clin. Oncol.* **2002**, *20*, 1551–1561, doi:10.1200/JCO.2002.20.6.1551.

73. Michaud, W.A.; Nichols, A.C.; Mroz, E.A.; Faquin, W.C.; Clark, J.R.; Begum, S.; Westra, W.H.; Wada, H.; Busse, P.M.; Ellisen, L.W.; et al. Bcl-2 blocks cisplatin-induced apoptosis and predicts poor outcome following chemoradiation treatment in advanced oropharyngeal squamous cell carcinoma. *Clin. Cancer Res.* **2009**, *15*, 1645–1654, doi:10.1158/1078-0432.CCR-08-2581.

74. Juliachs, M.; Muñoz, C.; Moutinho, C.A.; Vidal, A.; Condom, E.; Esteller, M.; Graupera, M.; Casanovas, O.; Germà, J.R.; Villanueva, A.; et al. The PDGFRβ-AKT pathway contributes to CDDP-acquired resistance in testicular germ cell tumors. *Clin. Cancer Res.* **2014**, *20*, 658–667, doi:10.1158/1078-0432.CCR-13-1131.

75. Koster, R.; Di Pietro, A.; Timmer-Bosscha, H.; Gibcus, J.H.; van den Berg, A.; Suurmeijer, A.J.; Bischoff, R.; Gietema, J.A.; Jong, S. de. Cytoplasmic p21 expression levels determine cisplatin resistance in human testicular cancer. *J. Clin. Invest.* **2010**, *120*, 3594–3605, doi:10.1172/JCI41939.

76. Selfe, J.; Goddard, N.C.; McIntyre, A.; Taylor, K.R.; Renshaw, J.; Popov, S.D.; Thway, K.; Summersgill, B.; Huddart, R.A.; Gilbert, D.C.; et al. IGF1R signalling in testicular germ cell tumour cells impacts on cell survival and acquired cisplatin resistance. *J. Pathol.* **2018**, *244*, 242–253, doi:10.1002/path.5008.

77. Noel, E.E.; Yeste-Velasco, M.; Mao, X.; Perry, J.; Kudahetti, S.C.; Li, N.F.; Sharp, S.; Chaplin, T.; Xue, L.; McIntyre, A.; et al. The association of CCND1 overexpression and cisplatin resistance in testicular germ cell tumors and other cancers. *Am. J. Pathol.* **2010**, *176*, 2607–2615, doi:10.2353/ajpath.2010.090780.

78. Ren, J.-H.; He, W.-S.; Nong, L.; Zhu, Q.-Y.; Hu, K.; Zhang, R.-G.; Huang, L.-L.; Zhu, F.; Wu, G. Acquired cisplatin resistance in human lung adenocarcinoma cells is associated with enhanced autophagy. *Cancer Biother. Radiopharm.* **2010**, *25*, 75–80, doi:10.1089/cbr.2009.0701.

79. Koul, S.; McKiernan, J.M.; Narayan, G.; Houldsworth, J.; Bacik, J.; Dobrzynski, D.L.; Assaad, A.M.; Mansukhani, M.; Reuter, V.E.; Bosl, G.J.; et al. Role of promoter hypermethylation in Cisplatin treatment response of male germ cell tumors. *Mol Cancer* **2004**, *3*, 16, doi:10.1186/1476-4598-3-16.

80. Port, M.; Glaesener, S.; Ruf, C.; Riecke, A.; Bokemeyer, C.; Meineke, V.; Honecker, F.; Abend, M. Micro-RNA expression in cisplatin resistant germ cell tumor cell lines. *Mol Cancer* **2011**, *10*, 52, doi:10.1186/1476-4598-10-52.

81. Bakardjieva-Mihaylova, V.; Skvarova Kramarzova, K.; Slamova, M.; Svaton, M.; Rejlova, K.; Zaliova, M.; Dobiasova, A.; Fiser, K.; Stuchly, J.; Grega, M.; et al. Molecular Basis of Cisplatin Resistance in Testicular Germ Cell Tumors. *Cancers* **2019**, *11, doi:*10.3390/cancers11091316.

82. Loveday, C.; Litchfield, K.; Proszek, P.Z.; Cornish, A.J.; Santo, F.; Levy, M.; Macintyre, G.; Holryod, A.; Broderick, P.; Dudakia, D.; et al. Genomic landscape of platinum resistant

and sensitive testicular cancers. *Nat Commun* **2020**, *11*, 2189, doi:10.1038/s41467-020-15768-x.

83. Schmidtova, S.; Kalavska, K.; Gercakova, K.; Cierna, Z.; Miklikova, S.; Smolkova, B.; Buocikova, V.; Miskovska, V.; Durinikova, E.; Burikova, M.; et al. Disulfiram Overcomes Cisplatin Resistance in Human Embryonal Carcinoma Cells. *Cancers* **2019**, *11, doi:*10.3390/cancers11091224.

84. Cierna, Z.; Mego, M.; Miskovska, V.; Machalekova, K.; Chovanec, M.; Svetlovska, D.; Hainova, K.; Rejlekova, K.; Macak, D.; Spanik, S.; et al. Prognostic value of programmed-death-1 receptor (PD-1) and its ligand 1 (PD-L1) in testicular germ cell tumors. *Ann. Oncol.* **2016**, *27*, 300–305, doi:10.1093/annonc/mdv574.

85. Adra, N.; Einhorn, L.H.; Althouse, S.K.; Ammakkanavar, N.R.; Musapatika, D.; Albany, C.; Vaughn, D.; Hanna, N.H. Phase II trial of pembrolizumab in patients with platinum refractory germ-cell tumors: a Hoosier Cancer Research Network Study GU14-206. *Ann. Oncol.* **2018**, *29*, 209–214, doi:10.1093/annonc/mdx680.

86. Mego, M.; Svetlovska, D.; Chovanec, M.; Rečkova, M.; Rejlekova, K.; Obertova, J.; Palacka, P.; Sycova-Mila, Z.; Giorgi, U. de; Mardiak, J. Phase II study of avelumab in multiple relapsed/refractory germ cell cancer. *Invest. New Drugs* **2019**, *37*, 748–754, doi:10.1007/s10637-019-00805-4.

87. Schönberger, S.; Kraft, D.; Nettersheim, D.; Schorle, H.; Casati, A.; Craveiro, R.B.; Mohseni, M.M.; Calaminus, G.; Dilloo, D. Targeting EpCAM by a Bispecific Trifunctional Antibody Exerts Profound Cytotoxic Efficacy in Germ Cell Tumor Cell Lines. *Cancers* **2020**, *12, doi:*10.3390/cancers12051279.

88. Jostes, S.; Nettersheim, D.; Schorle, H. Epigenetic drugs and their molecular targets in testicular germ cell tumours. *Nat. Rev. Urol.* **2019**, *16*, 245–259, doi:10.1038/s41585-019-0154-x.

89. Jostes, S.; Nettersheim, D.; Fellermeyer, M.; Schneider, S.; Hafezi, F.; Honecker, F.; Schumacher, V.; Geyer, M.; Kristiansen, G.; Schorle, H. The bromodomain inhibitor JQ1 triggers growth arrest and apoptosis in testicular germ cell tumours in vitro and in vivo. *J Cell Mol Med* **2017**, *21*, 1300–1314, doi:10.1111/jcmm.13059.

90. Nettersheim, D.; Jostes, S.; Fabry, M.; Honecker, F.; Schumacher, V.; Kirfel, J.; Kristiansen, G.; Schorle, H. A signaling cascade including ARID1A, GADD45B and DUSP1 induces apoptosis and affects the cell cycle of germ cell cancers after romidepsin treatment. *Oncotarget* **2016**, *7*, 74931–74946, doi:10.18632/oncotarget.11647.

91. Müller, M.R.; Burmeister, A.; Skowron, M.A.; Stephan, A.; Bremmer, F.; Wakileh, G.A.; Petzsch, P.; Köhrer, K.; Albers, P.; Nettersheim, D. Therapeutical interference with the epigenetic landscape of germ cell tumors: a comparative drug study and new mechanistical insights. *Clin. Epigenetics* **2022**, *14*, 5, doi:10.1186/s13148-021-01223-1.

92. Albany, C.; Hever-Jardine, M.P.; Herrmann, K.M. von; Yim, C.Y.; Tam, J.; Warzecha, J.M.; Shin, L.; Bock, S.E.; Curran, B.S.; Chaudhry, A.S.; et al. Refractory testicular germ cell tumors are highly sensitive to the second generation DNA methylation inhibitor guadecitabine. *Oncotarget* **2017**, *8*, 2949–2959, doi:10.18632/oncotarget.13811.

93. Albany, C.; Fazal, Z.; Singh, R.; Bikorimana, E.; Adra, N.; Hanna, N.H.; Einhorn, L.H.; Perkins, S.M.; Sandusky, G.E.; Christensen, B.C.; et al. A phase 1 study of combined guadecitabine and cisplatin in platinum refractory germ cell cancer. *Cancer Med.* **2021**, *10*, 156–163, doi:10.1002/cam4.3583.

94. Oing, C.; Hentrich, M.; Lorch, A.; Gläser, D.; Rumpold, H.; Ochsenreither, S.; Richter, S.; Dieing, A.; Zschäbitz, S.; Pereira, R.R.; et al. Treatment of refractory germ-cell tumours with single-agent cabazitaxel: a German Testicular Cancer Study Group case series. *J. Cancer Res. Clin. Oncol.* **2020**, *146*, 449–455, doi:10.1007/s00432-019-03071-2.

95. Fenner, M.; Oing, C.; Dieing, A.; Gauler, T.; Oechsle, K.; Lorch, A.; Hentrich, M.; Kopp, H.-G.; Bokemeyer, C.; Honecker, F. Everolimus in patients with multiply relapsed or cisplatin refractory germ cell tumors: results of a phase II, single-arm, open-label multicenter trial (RADIT) of the German Testicular Cancer Study Group. *J. Cancer Res. Clin. Oncol.* **2019**, *145*, 717–723, doi:10.1007/s00432-018-2752-z.

96. Necchi, A.; Lo Vullo, S.; Giannatempo, P.; Raggi, D.; Calareso, G.; Togliardi, E.; Crippa, F.; Pennati, M.; Zaffaroni, N.; Perrone, F.; et al. Pazopanib in advanced germ cell tumors after chemotherapy failure: results of the open-label, single-arm, phase 2 Pazotest trial. *Ann. Oncol.* **2017**, *28*, 1346–1351, doi:10.1093/annonc/mdx124.

97. Giorgi, U. de; Schepisi, G.; Gurioli, G.; Pisano, C.; Basso, U.; Lolli, C.; Petracci, E.; Casadei, C.; Cecere, S.C.; Attademo, L.; et al. Olaparib as salvage treatment for advanced germ cell tumors after chemotherapy failure: Results of the open-label, single-arm, IGG-02 phase II trial. *JCO* **2020**, *38*, 5058, doi:10.1200/JCO.2020.38.15_suppl.5058.

98. Mego, M.; Svetlovska, D.; Reckova, M.; de Angelis; Kalavska, K.; Obertova, J.; Palacka, P.; Rejlekova, K.; Sycova-Mila, Z.; Chovanec, M.; et al. Gemcitabine, carboplatin and veliparib in multiple relapsed/refractory germ cell tumours: The GCT-SK-004 phase II trial. *Invest. New Drugs* **2021**, *39*, 1664–1670, doi:10.1007/s10637-021-01130-5.

99. Schönberger, S.; van Beekum, C.; Götz, B.; Nettersheim, D.; Schorle, H.; Schneider, D.T.; Casati, A.; Craveiro, R.B.; Calaminus, G.; Dilloo, D. Brentuximab vedotin exerts profound antiproliferative and pro-apoptotic efficacy in CD30-positive as well as cocultured CD30-negative germ cell tumour cell lines. *J Cell Mol Med* **2018**, *22*, 568–575, doi:10.1111/jcmm.13344.

100. Albany, C.; Einhorn, L.; Garbo, L.; Boyd, T.; Josephson, N.; Feldman, D.R. Treatment of CD30-Expressing Germ Cell Tumors and Sex Cord Stromal Tumors with Brentuximab Vedotin: Identification and Report of Seven Cases. *Oncologist* **2018**, *23*, 316–323, doi:10.1634/theoncologist.2017-0544.

101. Necchi, A.; Anichini, A.; Raggi, D.; Giannatempo, P.; Magazzù, D.; Nicolai, N.; Colecchia, M.; Paolini, B.; Coradeschi, E.; Tassi, E.; et al. Brentuximab Vedotin in CD30-Expressing Germ Cell Tumors After Chemotherapy Failure. *Clin. Genitourin. Cancer* **2016**, *14*, 261-264.e4, doi:10.1016/j.clgc.2016.03.020.

102. Skowron, M.A.; Vermeulen, M.; Winkelhausen, A.; Becker, T.K.; Bremmer, F.; Petzsch, P.; Schönberger, S.; Calaminus, G.; Köhrer, K.; Albers, P.; et al. CDK4/6 inhibition presents as a therapeutic option for paediatric and adult germ cell tumours and induces cell cycle arrest and apoptosis via canonical and non-canonical mechanisms. *Br J Cancer* **2020**, *123*, 378–391, doi:10.1038/s41416-020-0891-x.

103. Vaughn, D.J.; Hwang, W.-T.; Lal, P.; Rosen, M.A.; Gallagher, M.; O'Dwyer, P.J. Phase 2 trial of the cyclin-dependent kinase 4/6 inhibitor palbociclib in patients with retinoblastoma protein-expressing germ cell tumors. *Cancer* **2015**, *121*, 1463–1468, doi:10.1002/cncr.29213.

104. Damjanov, I.; Horvat, B.; Gibas, Z. Retinoic acid-induced differentiation of the developmentally pluripotent human germ cell tumor-derived cell line, NCCIT. *Lab. Invest.* **1993**, *68*, 220–232.

105. Josephson, R.; Ording, C.J.; Liu, Y.; Shin, S.; Lakshmipathy, U.; Toumadje, A.; Love, B.; Chesnut, J.D.; Andrews, P.W.; Rao, M.S.; et al. Qualification of embryonal carcinoma 2102Ep as a reference for human embryonic stem cell research. *Stem Cells* **2007**, *25*, 437–446, doi:10.1634/stemcells.2006-0236.

106. Simões, P.D.; Ramos, T. Human pluripotent embryonal carcinoma NTERA2 cl.D1 cells maintain their typical morphology in an angiomyogenic medium. *J. Negat. Results Biomed.* **2007**, *6*, 5, doi:10.1186/1477-5751-6-5.

107. Hochberg, A.; Rachmilewitz, J.; Eldar-Geva, T.; Salant, T.; Schneider, T.; de Groot, N. Differentiation of Choriocarcinoma Cell Line (JAr). *Cancer Res.* **1992**, 3713–3717.

108. Eckert, D.; Nettersheim, D.; Heukamp, L.C.; Kitazawa, S.; Biermann, K.; Schorle, H. TCam-2 but not JKT-1 cells resemble seminoma in cell culture. *Cell Tissue Res* **2008**, *331*, 529–538, doi:10.1007/s00441-007-0527-y.

109. Oechsle, K.; Honecker, F.; Cheng, T.; Mayer, F.; Czaykowski, P.; Winquist, E.; Wood, L.; Fenner, M.; Glaesener, S.; Hartmann, J.T.; et al. Preclinical and clinical activity of sunitinib in patients with cisplatin-refractory or multiply relapsed germ cell tumors: a Canadian Urologic Oncology Group/German Testicular Cancer Study Group cooperative study. *Ann. Oncol.* **2011**, *22*, 2654–2660, doi:10.1093/annonc/mdr026.

110. Fichtner, A.; Bohnenberger, H.; Elakad, O.; Richter, A.; Lenz, C.; Oing, C.; Ströbel, P.; Kueffer, S.; Nettersheim, D.; Bremmer, F. Proteomic profiling of cisplatin-resistant and cisplatin-sensitive germ cell tumour cell lines using quantitative mass spectrometry. *World J. Urol.* **2022**, *40*, 373–383, doi:10.1007/s00345-022-03936-1.

111. Nettersheim, D.; Schorle, H. The plasticity of germ cell cancers and its dependence on the cellular microenvironment. *J Cell Mol Med* **2017**, *21*, 1463–1467, doi:10.1111/jcmm.13082.

112. Nettersheim, D.; Gillis, A.J.M.; Looijenga, L.H.J.; Schorle, H. TGF-β1, EGF and FGF4 synergistically induce differentiation of the seminoma cell line TCam-2 into a cell type resembling mixed non-seminoma. *Int. J. Androl.* **2011**, *34*, e189-203, doi:10.1111/j.1365-2605.2011.01172.x.

113. Nettersheim, D.; Jostes, S.; Sharma, R.; Schneider, S.; Hofmann, A.; Ferreira, H.J.; Hoffmann, P.; Kristiansen, G.; Esteller, M.B.; Schorle, H. BMP Inhibition in Seminomas Initiates Acquisition of Pluripotency via NODAL Signaling Resulting in Reprogramming to an Embryonal Carcinoma. *PLoS Genet.* **2015**, *11*, e1005415, doi:10.1371/journal.pgen.1005415.

114. Nettersheim, D.; Heimsoeth, A.; Jostes, S.; Schneider, S.; Fellermeyer, M.; Hofmann, A.; Schorle, H. SOX2 is essential for in vivo reprogramming of seminoma-like TCam-2 cells to an embryonal carcinoma-like fate. *Oncotarget* **2016**, *7*, 47095–47110, doi:10.18632/oncotarget.9903.

115. Constantin, T.A.; Greenland, K.K.; Varela-Carver, A.; Bevan, C.L. Transcription associated cyclin-dependent kinases as therapeutic targets for prostate cancer. *Oncogene* **2022**, *41*, 3303–3315, doi:10.1038/s41388-022-02347-1.

116. Vervoort, S.J.; Devlin, J.R.; Kwiatkowski, N.; Teng, M.; Gray, N.S.; Johnstone, R.W. Targeting transcription cycles in cancer. *Nat Rev Cancer* **2022**, *22*, 5–24, doi:10.1038/s41568-021-00411-8.

117. Fant, C.B.; Taatjes, D.J. Regulatory functions of the Mediator kinases CDK8 and CDK19. *Transcription* **2019**, *10*, 76–90, doi:10.1080/21541264.2018.1556915.

118. Larochelle, S.; Amat, R.; Glover-Cutter, K.; Sansó, M.; Zhang, C.; Allen, J.J.; Shokat, K.M.; Bentley, D.L.; Fisher, R.P. Cyclin-dependent kinase control of the initiation-to-elongation switch of RNA polymerase II. *Nat Struct Mol Biol* **2012**, *19*, 1108–1115, doi:10.1038/nsmb.2399.

119. Nilson, K.A.; Guo, J.; Turek, M.E.; Brogie, J.E.; Delaney, E.; Luse, D.S.; Price, D.H. THZ1 Reveals Roles for Cdk7 in Co-transcriptional Capping and Pausing. *Mol. Cell* **2015**, *59*, 576–587, doi:10.1016/j.molcel.2015.06.032.

120. Noe Gonzalez, M.; Sato, S.; Tomomori-Sato, C.; Conaway, J.W.; Conaway, R.C. CTD-dependent and -independent mechanisms govern co-transcriptional capping of Pol II transcripts. *Nat Commun* **2018**, *9*, 3392, doi:10.1038/s41467-018-05923-w.

121. Fisher, R.P. Cdk7: a kinase at the core of transcription and in the crosshairs of cancer drug discovery. *Transcription* **2019**, *10*, 47–56, doi:10.1080/21541264.2018.1553483.

122. Olson, C.M.; Jiang, B.; Erb, M.A.; Liang, Y.; Doctor, Z.M.; Zhang, Z.; Zhang, T.; Kwiatkowski, N.; Boukhali, M.; Green, J.L.; et al. Pharmacological perturbation of CDK9 using selective CDK9 inhibition or degradation. *Nat. Chem. Biol.* **2018**, *14*, 163–170, doi:10.1038/nchembio.2538.

123. Vos, S.M.; Farnung, L.; Urlaub, H.; Cramer, P. Structure of paused transcription complex Pol II-DSIF-NELF. *Nature* **2018**, *560*, 601–606, doi:10.1038/s41586-018-0442-2.

124. Ebmeier, C.C.; Erickson, B.; Allen, B.L.; Allen, M.A.; Kim, H.; Fong, N.; Jacobsen, J.R.; Liang, K.; Shilatifard, A.; Dowell, R.D.; et al. Human TFIIH Kinase CDK7 Regulates Transcription-Associated Chromatin Modifications. *Cell Reports* **2017**, *20*, 1173–1186, doi:10.1016/j.celrep.2017.07.021.

125. Dubbury, S.J.; Boutz, P.L.; Sharp, P.A. CDK12 regulates DNA repair genes by suppressing intronic polyadenylation. *Nature* **2018**, *564*, 141–145, doi:10.1038/s41586-018-0758-y.

126. Krajewska, M.; Dries, R.; Grassetti, A.V.; Dust, S.; Gao, Y.; Huang, H.; Sharma, B.; Day, D.S.; Kwiatkowski, N.; Pomaville, M.; et al. CDK12 loss in cancer cells affects DNA damage response genes through premature cleavage and polyadenylation. *Nat Commun* **2019**, *10*, 679, doi:10.1038/s41467-019-09703-y.

127. Pirngruber, J.; Shchebet, A.; Schreiber, L.; Shema, E.; Minsky, N.; Chapman, R.D.; Eick, D.; Aylon, Y.; Oren, M.; Johnsen, S.A. CDK9 directs H2B monoubiquitination and controls

replication-dependent histone mRNA 3'-end processing. *EMBO Rep.* **2009**, *10*, 894–900, doi:10.1038/embor.2009.108.

128. Chou, J.; Quigley, D.A.; Robinson, T.M.; Feng, F.Y.; Ashworth, A. Transcription-Associated Cyclin-Dependent Kinases as Targets and Biomarkers for Cancer Therapy. *Cancer Discov* **2020**, *10*, 351–370, doi:10.1158/2159-8290.CD-19-0528.

129. Zhang, M.; Zhang, L.; Hei, R.; Li, X.; Cai, H.; Wu, X.; Zheng, Q.; Cai, C. CDK inhibitors in cancer therapy, an overview of recent development. *Am. J. Cancer Res.* **2021**, *11*, 1913–1935.

130. Mayer, F.; Mueller, S.; Malenke, E.; Kuczyk, M.; Hartmann, J.T.; Bokemeyer, C. Induction of apoptosis by flavopiridol unrelated to cell cycle arrest in germ cell tumour derived cell lines. *Invest. New Drugs* **2005**, *23*, 205–211, doi:10.1007/s10637-005-6728-x.

131. Rathkopf, D.; Dickson, M.A.; Feldman, D.R.; Carvajal, R.D.; Shah, M.A.; Wu, N.; Lefkowitz, R.; Gonen, M.; Cane, L.M.; Dials, H.J.; et al. Phase I study of flavopiridol with oxaliplatin and fluorouracil/leucovorin in advanced solid tumors. *Clin. Cancer Res.* **2009**, *15*, 7405–7411, doi:10.1158/1078-0432.CCR-09-1502.

132. Chen, X.-X.; Xie, F.-F.; Zhu, X.-J.; Lin, F.; Pan, S.-S.; Gong, L.-H.; Qiu, J.-G.; Zhang, W.-J.; Jiang, Q.-W.; Mei, X.-L.; et al. Cyclin-dependent kinase inhibitor dinaciclib potently synergizes with cisplatin in preclinical models of ovarian cancer. *Oncotarget* **2015**, *6*, 14926–14939, doi:10.18632/oncotarget.3717.

133. Mita, M.M.; Joy, A.A.; Mita, A.; Sankhala, K.; Jou, Y.-M.; Zhang, D.; Statkevich, P.; Zhu, Y.; Yao, S.-L.; Small, K.; et al. Randomized Phase II Trial of the Cyclin-Dependent Kinase Inhibitor Dinaciclib (MK-7965) Versus Capecitabine in Patients With Advanced Breast Cancer. *Clinical Breast Cancer* **2014**, *14*, 169–176, doi:10.1016/j.clbc.2013.10.016.

134. Flynn, J.; Jones, J.; Johnson, A.J.; Andritsos, L.; Maddocks, K.; Jaglowski, S.; Hessler, J.; Grever, M.R.; Im, E.; Zhou, H.; et al. Dinaciclib is a novel cyclin-dependent kinase inhibitor with significant clinical activity in relapsed and refractory chronic lymphocytic leukemia. *Leukemia* **2015**, *29*, 1524–1529, doi:10.1038/leu.2015.31.

135. Ghia, P.; Scarfò, L.; Perez, S.; Pathiraja, K.; Derosier, M.; Small, K.; McCrary Sisk, C.; Patton, N. Efficacy and safety of dinaciclib vs ofatumumab in patients with relapsed/refractory chronic lymphocytic leukemia. *Blood* **2017**, *129*, 1876–1878, doi:10.1182/blood-2016-10-748210.

136. Zhang, T.; Kwiatkowski, N.; Olson, C.M.; Dixon-Clarke, S.E.; Abraham, B.J.; Greifenberg, A.K.; Ficarro, S.B.; Elkins, J.M.; Liang, Y.; Hannett, N.M.; et al. Covalent targeting of

remote cysteine residues to develop CDK12 and CDK13 inhibitors. *Nat Chem Biol* **2016**, *12*, 876–884, doi:10.1038/nchembio.2166.

137. Shyamsunder, P.; Sridharan, S.P.; Madan, V.; Dakle, P.; Zeya, C.; Kanojia, D.; Chng, W.-J.; Ong, S.T.; Koeffler, H.P. THZ531 Induces a State of BRCAness in Multiple Myeloma Cells: Synthetic Lethality with Combination Treatment of THZ 531 with DNA Repair Inhibitors. *IJMS* **2022**, *23, doi:*10.3390/ijms23031207.

138. Hu, S.; Marineau, J.J.; Rajagopal, N.; Hamman, K.B.; Choi, Y.J.; Schmidt, D.R.; Ke, N.; Johannessen, L.; Bradley, M.J.; Orlando, D.A.; et al. Discovery and Characterization of SY-1365, a Selective, Covalent Inhibitor of CDK7. *Cancer Res.* **2019**, *79*, 3479–3491, doi:10.1158/0008-5472.CAN-19-0119.

139. Rimel, J.K.; Poss, Z.C.; Erickson, B.; Maas, Z.L.; Ebmeier, C.C.; Johnson, J.L.; Decker, T.-M.; Yaron, T.M.; Bradley, M.J.; Hamman, K.B.; et al. Selective inhibition of CDK7 reveals high-confidence targets and new models for TFIIH function in transcription. *Genes Dev.* **2020**, *34*, 1452–1473, doi:10.1101/gad.341545.120.

140. Olson, C.M.; Liang, Y.; Leggett, A.; Park, W.D.; Li, L.; Mills, C.E.; Elsarrag, S.Z.; Ficarro, S.B.; Zhang, T.; Düster, R.; et al. Development of a Selective CDK7 Covalent Inhibitor Reveals Predominant Cell-Cycle Phenotype. *Cell Chemical Biology* **2019**, *26*, 792-803.e10, doi:10.1016/j.chembiol.2019.02.012.

141. Zhou, L.; Jiang, Y.; Luo, Q.; Li, L.; Jia, L. Neddylation: A novel modulator of the tumor microenvironment. *Mol Cancer* **2019**, *18*, 28557, doi:10.1186/s12943-019-0979-1.

142. Bano, I.; Malhi, M.; Zhao, M.; Giurgiulescu, L.; Sajjad, H.; Kieliszek, M. A review on cullin neddylation and strategies to identify its inhibitors for cancer therapy. *3 Biotech* **2022**, *12*, 103, doi:10.1007/s13205-022-03162-x.

143. Baek, K.; Krist, D.T.; Prabu, J.R.; Hill, S.; Klügel, M.; Neumaier, L.-M.; Gronau, S. von; Kleiger, G.; Schulman, B.A. NEDD8 nucleates a multivalent cullin-RING-UBE2D ubiquitin ligation assembly. *Nature* **2020**, *578*, 461–466, doi:10.1038/s41586-020-2000-y.

144. Enchev, R.I.; Schulman, B.A.; Peter, M. Protein neddylation: beyond cullin-RING ligases. *Nat. Rev. Mol. Cell Biol.* **2015**, *16*, 30–44, doi:10.1038/nrm3919.

145. Jones, T.M.; Carew, J.S.; Bauman, J.E.; Nawrocki, S.T. Targeting NEDDylation as a Novel Approach to Improve the Treatment of Head and Neck Cancer. *Cancers* **2021**, *13, doi:*10.3390/cancers13133250.

146. Brown, J.S.; Jackson, S.P. Ubiquitylation, neddylation and the DNA damage response. *Open Biol.* **2015**, *5*, 150018, doi:10.1098/rsob.150018.

147. Zeng, Y.; Iv, Y.-S.; Pan, Q.-H.; Zhou, Y.-G.; Li, H. An overactive neddylation pathway serves as a therapeutic target and MLN4924 enhances the anticancer activity of cisplatin in pancreatic cancer. *Oncol. Lett.* **2019**, *18*, 2724–2732, doi:10.3892/ol.2019.10596.

148. Li, L.; Wang, M.; Yu, G.; Chen, P.; Li, H.; Wei, D.; Zhu, J.; Xie, L.; Jia, H.; Shi, J.; et al. Overactivated neddylation pathway as a therapeutic target in lung cancer. *J. Natl. Cancer Inst.* **2014**, *106*, dju083, doi:10.1093/jnci/dju083.

149. Naik, S.K.; Lam, E.W.-F.; Parija, M.; Prakash, S.; Jiramongkol, Y.; Adhya, A.K.; Parida, D.K.; Mishra, S.K. NEDDylation negatively regulates ERRβ expression to promote breast cancer tumorigenesis and progression. *Cell Death Dis.* **2020**, *11*, 703, doi:10.1038/s41419-020-02838-7.

150. Wang, Y.; Wu, J.; Chen, H.; Yang, Y.; Xiao, C.; Yi, X.; Shi, C.; Zhong, K.; He, H.; Li, Y.; et al. Genome-wide CRISPR-Cas9 screen identified KLF11 as a druggable suppressor for sarcoma cancer stem cells. *Sci. Adv.* **2021**, *7, doi:*10.1126/sciadv.abe3445.

151. Ramaker, R.C.; Hardigan, A.A.; Gordon, E.R.; Wright, C.A.; Myers, R.M.; Cooper, S.J. Pooled CRISPR screening in pancreatic cancer cells implicates co-repressor complexes as a cause of multiple drug resistance via regulation of epithelial-to-mesenchymal transition. *BMC Cancer* **2021**, *21*, 632, doi:10.1186/s12885-021-08388-1.

152. Joung, J.; Konermann, S.; Gootenberg, J.S.; Abudayyeh, O.O.; Platt, R.J.; Brigham, M.D.; Sanjana, N.E.; Zhang, F. Genome-scale CRISPR-Cas9 knockout and transcriptional activation screening. *Nat. Protoc.* **2017**, *12*, 828–863, doi:10.1038/nprot.2017.016.

153. Huber, W.; Carey, V.J.; Gentleman, R.; Anders, S.; Carlson, M.; Carvalho, B.S.; Bravo, H.C.; Davis, S.; Gatto, L.; Girke, T.; et al. Orchestrating high-throughput genomic analysis with Bioconductor. *Nat Methods* **2015**, *12*, 115–121, doi:10.1038/nmeth.3252.

154. Cock, P.J.A.; Antao, T.; Chang, J.T.; Chapman, B.A.; Cox, C.J.; Dalke, A.; Friedberg, I.; Hamelryck, T.; Kauff, F.; Wilczynski, B.; et al. Biopython: Freely available Python tools for computational molecular biology and bioinformatics. *Bioinformatics* **2009**, *25*, 1422–1423, doi:10.1093/bioinformatics/btp163.

155. Chapman, B.; Chang, J. Biopython. *SIGBIO Newsl.* **2000**, *20*, 15–19, doi:10.1145/360262.360268.

156. Wingett, S.W.; Andrews, S. FastQ Screen: A tool for multi-genome mapping and quality control. *F1000Research* **2018**, *7*, 1338.

157. Carbon, S.; Douglass, E.; Good, B.M.; Unni, D.R.; Harris, N.L.; Mungall, C.J.; Basu, S.; Chisholm, R.L.; Dodson, R.J.; Hartline, E.; et al. The Gene Ontology resource: Enriching a GOld mine. *Nucleic Acids Research* **2021**, *49*, D325-D334, doi:10.1093/nar/gkaa1113.

158. Kim, D.; Langmead, B.; Salzberg, S.L. HISAT: A fast spliced aligner with low memory requirements. *Nat. Methods* **2015**, *12*, 357–360, doi:10.1038/nmeth.3317.

159. Kanehisa, M. KEGG: Kyoto Encyclopedia of Genes and Genomes. *Nucleic Acids Research* **2000**, *28*, 27–30, doi:10.1093/nar/28.1.27.

160. van Rossum, G. *Python reference manual*, 1995.

161. R Core Team. *R;* R Foundation for Statistical Computing: Vienna, Austria: Vienna, Austria, 2021.

162. Gillespie, M.; Jassal, B.; Stephan, R.; Milacic, M.; Rothfels, K.; Senff-Ribeiro, A.; Griss, J.; Sevilla, C.; Matthews, L.; Gong, C.; et al. The reactome pathway knowledgebase 2022. *Nucleic Acids Research* **2022**, *50*, D687-D692, doi:10.1093/nar/gkab1028.

163. RStudio Team. *RStudio: Integrated Development for R.;* RStudio, PBC: Boston, MA, USA: Boston, MA, USA, 2020.

164. Szklarczyk, D.; Franceschini, A.; Wyder, S.; Forslund, K.; Heller, D.; Huerta-Cepas, J.; Simonovic, M.; Roth, A.; Santos, A.; Tsafou, K.P.; et al. STRING v10: Protein–protein interaction networks, integrated over the tree of life. *Nucleic Acids Research* **2015**, *43*, D447-D452, doi:10.1093/nar/gku1003.

165. Pertea, M.; Pertea, G.M.; Antonescu, C.M.; Chang, T.-C.; Mendell, J.T.; Salzberg, S.L. StringTie enables improved reconstruction of a transcriptome from RNA-seq reads. *Nat. Biotechnol.* **2015**, *33*, 290–295, doi:10.1038/nbt.3122.

166. Martin, M. Cutadapt removes adapter sequences from high-throughput sequencing reads. *EMBnet j.* **2011**, *17*, 10, doi:10.14806/ej.17.1.200.

167. Oliveros, J.C. Venny. An Interactive Tool for Comparing Lists with Venn's Diagrams. 2007-2015. Available online: https://bioinfogp.cnb.csic.es/tools/venny/index.html (accessed on 24 October 2022).

168. Love, M.I.; Huber, W.; Anders, S. Moderated estimation of fold change and dispersion for RNA-seq data with DESeq2. *Genome Biol.* **2014**, *15*, 550, doi:10.1186/s13059-014-0550-8.

169. Ashburner, M.; Ball, C.A.; Blake, J.A.; Botstein, D.; Butler, H.; Cherry, J.M.; Davis, A.P.; Dolinski, K.; Dwight, S.S.; Eppig, J.T.; et al. Gene Ontology: Tool for the unification of biology. *Nat Genet* **2000**, *25*, 25–29, doi:10.1038/75556.

170. Schwill, M.; Tamaskovic, R.; Gajadhar, A.S.; Kast, F.; White, F.M.; Plückthun, A. Systemic analysis of tyrosine kinase signaling reveals a common adaptive response program in a HER2-positive breast cancer. *Sci. Signal.* **2019**, *12, doi:*10.1126/scisignal.aau2875.

171. Nettersheim, D.; Berger, D.; Jostes, S.; Skowron, M.; Schorle, H. Deciphering the molecular effects of romidepsin on germ cell tumours: DHRS2 is involved in cell cycle arrest but not apoptosis or induction of romidepsin effectors. *J Cell Mol Med* **2019**, *23*, 670–679, doi:10.1111/jcmm.13971.

172. Jacobsen, C.; Honecker, F. Cisplatin resistance in germ cell tumours: Models and mechanisms. *Andrology* **2015**, *3*, 111–121, doi:10.1111/andr.299.

173. Caggiano, C.; Cavallo, F.; Giannattasio, T.; Cappelletti, G.; Rossi, P.; Grimaldi, P.; Feldman, D.R.; Jasin, M.; Barchi, M. Testicular Germ Cell Tumors Acquire Cisplatin Resistance by Rebalancing the Usage of DNA Repair Pathways. *Cancers* **2021**, *13, doi:*10.3390/cancers13040787.

174. Sun, X.; Wang, S.; Gai, J.; Guan, J.; Li, J.; Li, Y.; Zhao, J.; Zhao, C.; Fu, L.; Li, Q. SIRT5 Promotes Cisplatin Resistance in Ovarian Cancer by Suppressing DNA Damage in a ROS-Dependent Manner via Regulation of the Nrf2/HO-1 Pathway. *Front. Oncol.* **2019**, *9*, 560, doi:10.3389/fonc.2019.00754.

175. Fotouhi, O.; Kjellin, H.; Juhlin, C.C.; Pan, Y.; Vesterlund, M.; Ghaderi, M.; Yousef, A.; Andersson-Sand, H.; Kharaziha, P.; Caramuta, S.; et al. Proteomics identifies neddylation as a potential therapy target in small intestinal neuroendocrine tumors. *Oncogene* **2019**, *38*, 6881–6897, doi:10.1038/s41388-019-0938-8.

176. Chen, X.; Li, Y.; Dai, H.; Zhang, H.; Wan, D.; Zhou, X.; Situ, C.; Zhu, H. Cyclin-dependent kinase 7 is essential for spermatogenesis by regulating retinoic acid signaling pathways and the STAT3 molecular pathway. *IUBMB Life* **2021**, *73*, 1446–1459, doi:10.1002/iub.2574.

177. Liang, S.; Hu, L.; Wu, Z.; Chen, Z.; Liu, S.; Xu, X.; Qian, A. CDK12: A Potent Target and Biomarker for Human Cancer Therapy. *Cells* **2020**, *9, doi:*10.3390/cells9061483.

178. Hu, Q.; Poulose, N.; Girmay, S.; Helevä, A.; Doultsinos, D.; Gondane, A.; Steele, R.E.; Liu, X.; Loda, M.; Liu, S.; et al. Inhibition of CDK9 activity compromises global splicing in

prostate cancer cells. *RNA Biol.* **2021**, *18*, 722–729, doi:10.1080/15476286.2021.1983287.

179. Tellier, M.; Zaborowska, J.; Neve, J.; Nojima, T.; Hester, S.; Furger, A.; Murphy, S. CDK9 and PP2A regulate RNA polymerase II transcription termination and coupled RNA maturation. *bioRxiv* **2021**, 2021.06.21.449289, doi:10.1101/2021.06.21.449289.

180. Zhang, H.; Christensen, C.L.; Dries, R.; Oser, M.G.; Deng, J.; Diskin, B.; Li, F.; Pan, Y.; Zhang, X.; Yin, Y.; et al. CDK7 Inhibition Potentiates Genome Instability Triggering Anti-tumor Immunity in Small Cell Lung Cancer. *Cancer Cell* **2020**, *37*, 37-54.e9, doi:10.1016/j.ccell.2019.11.003.

181. Kalan, S.; Amat, R.; Schachter, M.M.; Kwiatkowski, N.; Abraham, B.J.; Liang, Y.; Zhang, T.; Olson, C.M.; Larochelle, S.; Young, R.A.; et al. Activation of the p53 Transcriptional Program Sensitizes Cancer Cells to Cdk7 Inhibitors. *Cell Reports* **2017**, *21*, 467–481, doi:10.1016/j.celrep.2017.09.056.

182. Zeng, M.; Kwiatkowski, N.P.; Zhang, T.; Nabet, B.; Xu, M.; Liang, Y.; Quan, C.; Wang, J.; Hao, M.; Palakurthi, S.; et al. Targeting MYC dependency in ovarian cancer through inhibition of CDK7 and CDK12/13. *eLife* **2018**, *7*, 387, doi:10.7554/eLife.39030.

183. Karimian, A.; Ahmadi, Y.; Yousefi, B. Multiple functions of p21 in cell cycle, apoptosis and transcriptional regulation after DNA damage. *DNA Repair (Amst)* **2016**, *42*, 63–71, doi:10.1016/j.dnarep.2016.04.008.

184. Park, M.H.; Kim, S.Y.; Kim, Y.J.; Chung, Y.-H. ALS2CR7 (CDK15) attenuates TRAIL induced apoptosis by inducing phosphorylation of survivin Thr34. *Biochem. Biophys. Res. Commun.* **2014**, *450*, 129–134, doi:10.1016/j.bbrc.2014.05.070.

185. Arrouchi, H.; Lakhlili, W.; Ibrahimi, A. A review on PIM kinases in tumors. *Bioinformation* **2019**, *15*, 40–45, doi:10.6026/97320630015040.

186. Henninger, E.E.; Pursell, Z.F. DNA polymerase ε and its roles in genome stability. *IUBMB Life* **2014**, *66*, 339–351, doi:10.1002/iub.1276.

187. Fouad, S.; Wells, O.S.; Hill, M.A.; D'Angiolella, V. Cullin Ring Ubiquitin Ligases (CRLs) in Cancer: Responses to Ionizing Radiation (IR) Treatment. *Front. Physiol.* **2019**, *10*, 1144, doi:10.3389/fphys.2019.01144.

188. Hu, X.; Meng, Y.; Xu, L.; Qiu, L.; Wei, M.; Su, D.; Qi, X.; Wang, Z.; Yang, S.; Liu, C.; et al. Cul4 E3 ubiquitin ligase regulates ovarian cancer drug resistance by targeting the antiapoptotic protein BIRC3. *Cell Death Dis.* **2019**, *10*, 104, doi:10.1038/s41419-018-1200-y.

189. Bitter, E.E.; Townsend, M.H.; Erickson, R.; Allen, C.; O'Neill, K.L. Thymidine kinase 1 through the ages: a comprehensive review. *Cell Biosci.* **2020**, *10*, 138, doi:10.1186/s13578-020-00493-1.

190. Hu, Q.; Hu, X.; Zhao, Y.; Zhang, L.; Yang, Y.; li, l. *Upregulation of SGOL2 Predicts Poor Prognosis and Facilitates Hepatocellular Carcinoma Progression via Dysregulating the Cell Cycle by Directly Activating MAD2*, 2021.

191. Agorreta, J.; Hu, J.; Liu, D.; Delia, D.; Turley, H.; Ferguson, D.J.P.; Iborra, F.; Pajares, M.J.; Larrayoz, M.; Zudaire, I.; et al. TRAP1 regulates proliferation, mitochondrial function, and has prognostic significance in NSCLC. *Mol. Cancer Res.* **2014**, *12*, 660–669, doi:10.1158/1541-7786.MCR-13-0481.

192. Zhang, X.; Dong, Y.; Gao, M.; Hao, M.; Ren, H.; Guo, L.; Guo, H. Knockdown of TRAP1 promotes cisplatin-induced apoptosis by promoting the ROS-dependent mitochondrial dysfunction in lung cancer cells. *Mol. Cell. Biochem.* **2021**, *476*, 1075–1082, doi:10.1007/s11010-020-03973-7.

193. Lin, S.; Shang, Z.; Li, S.; Gao, P.; Zhang, Y.; Hou, S.; Qin, P.; Dong, Z.; Hu, T.; Chen, P. Neddylation inhibitor MLN4924 induces G2 cell cycle arrest, DNA damage and sensitizes esophageal squamous cell carcinoma cells to cisplatin. *Oncol. Lett.* **2018**, *15*, 2583–2589, doi:10.3892/ol.2017.7616.

194. Zeng, Y.; Zou, M.; Liu, Y.; Que, K.; Wang, Y.; Liu, C.; Gong, J.; You, Y. Keratin 17 Suppresses Cell Proliferation and Epithelial-Mesenchymal Transition in Pancreatic Cancer. *Front. Med. (Lausanne)* **2020**, *7*, 572494, doi:10.3389/fmed.2020.572494.

195. Kuzmichev, A.N.; Kim, S.-K.; D'Alessio, A.C.; Chenoweth, J.G.; Wittko, I.M.; Campanati, L.; McKay, R.D. Sox2 acts through Sox21 to regulate transcription in pluripotent and differentiated cells. *Curr. Biol.* **2012**, *22*, 1705–1710, doi:10.1016/j.cub.2012.07.013.

196. Loehr, A.R.; Pierpont, T.M.; Gelsleichter, E.; Galang, A.M.D.; Fernandez, I.R.; Moore, E.S.; Guo, M.Z.; Miller, A.D.; Weiss, R.S. Targeting Cancer Stem Cells with Differentiation Agents as an Alternative to Genotoxic Chemotherapy for the Treatment of Malignant Testicular Germ Cell Tumors. *Cancers* **2021**, *13*, 2045, doi:10.3390/cancers13092045.

7. Appendix

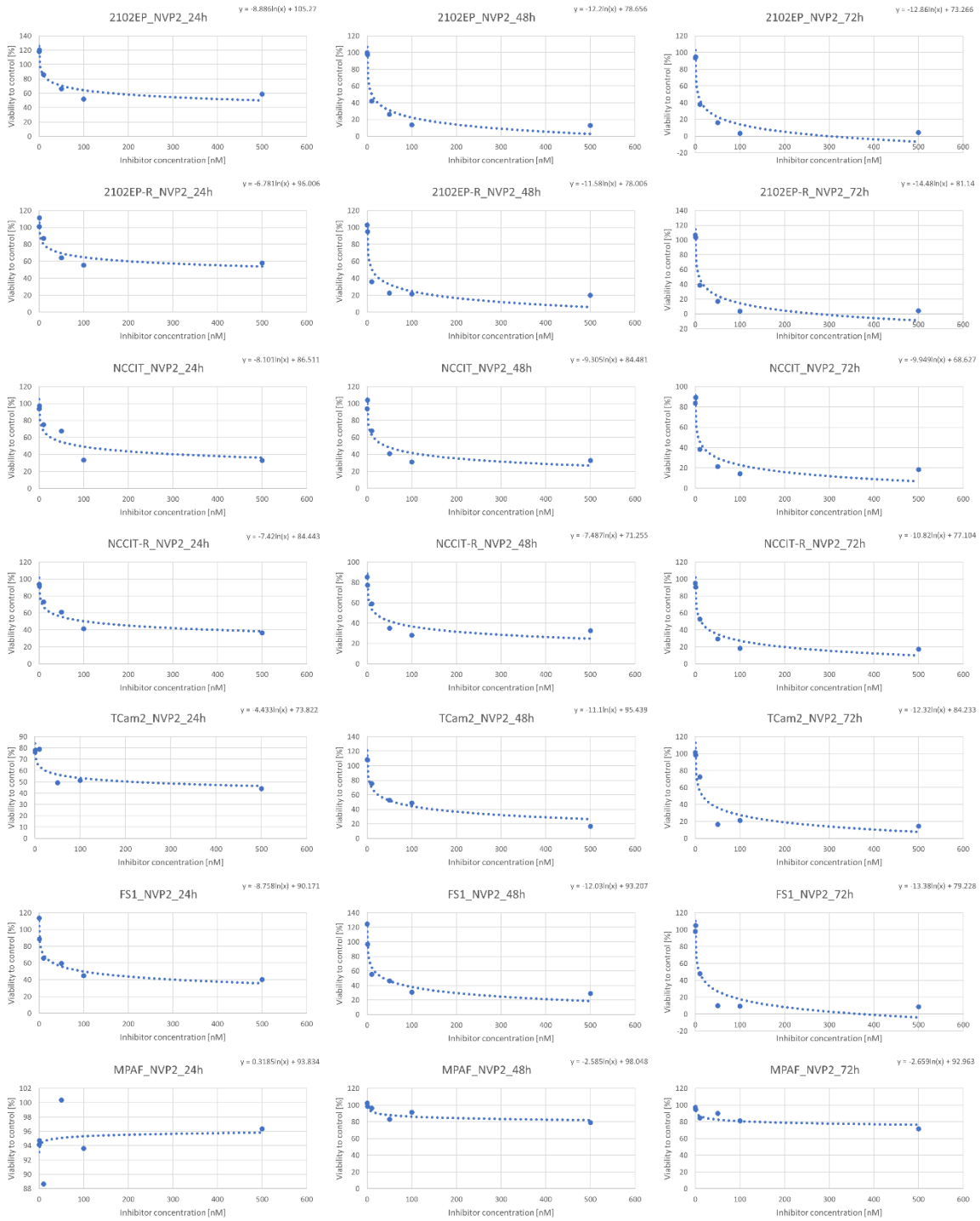

Appendix Figure 1: Application of logarithmic regression model on XTT viability assay generated data (Figure 8) for calculation of NVP2 IC50 values. Reprinted from [1].

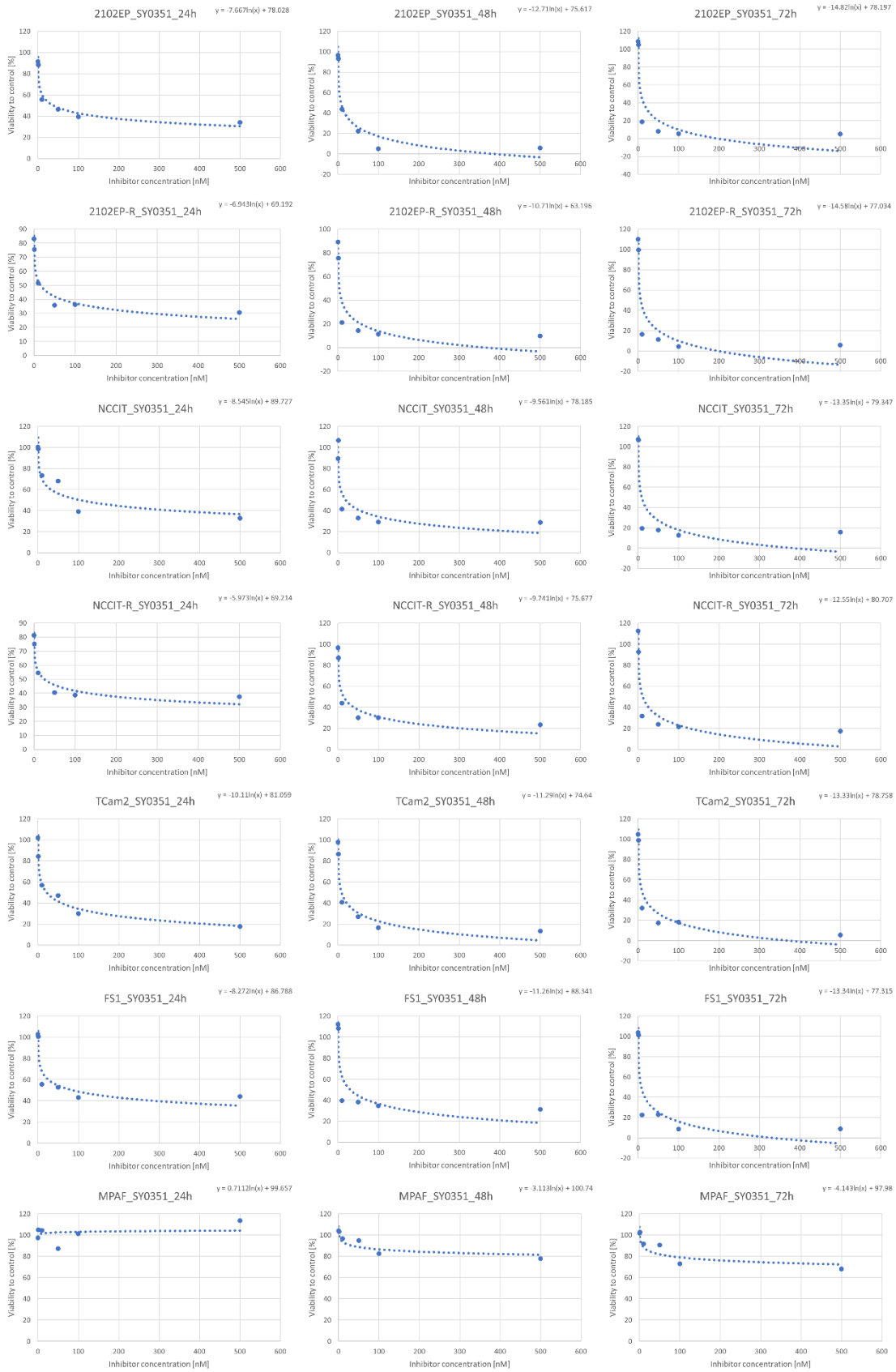

Appendix Figure 2: Application of logarithmic regression model on XTT viability assay generated data (Figure 8) for calculation of SY0351 IC50 values. Reprinted from [1].

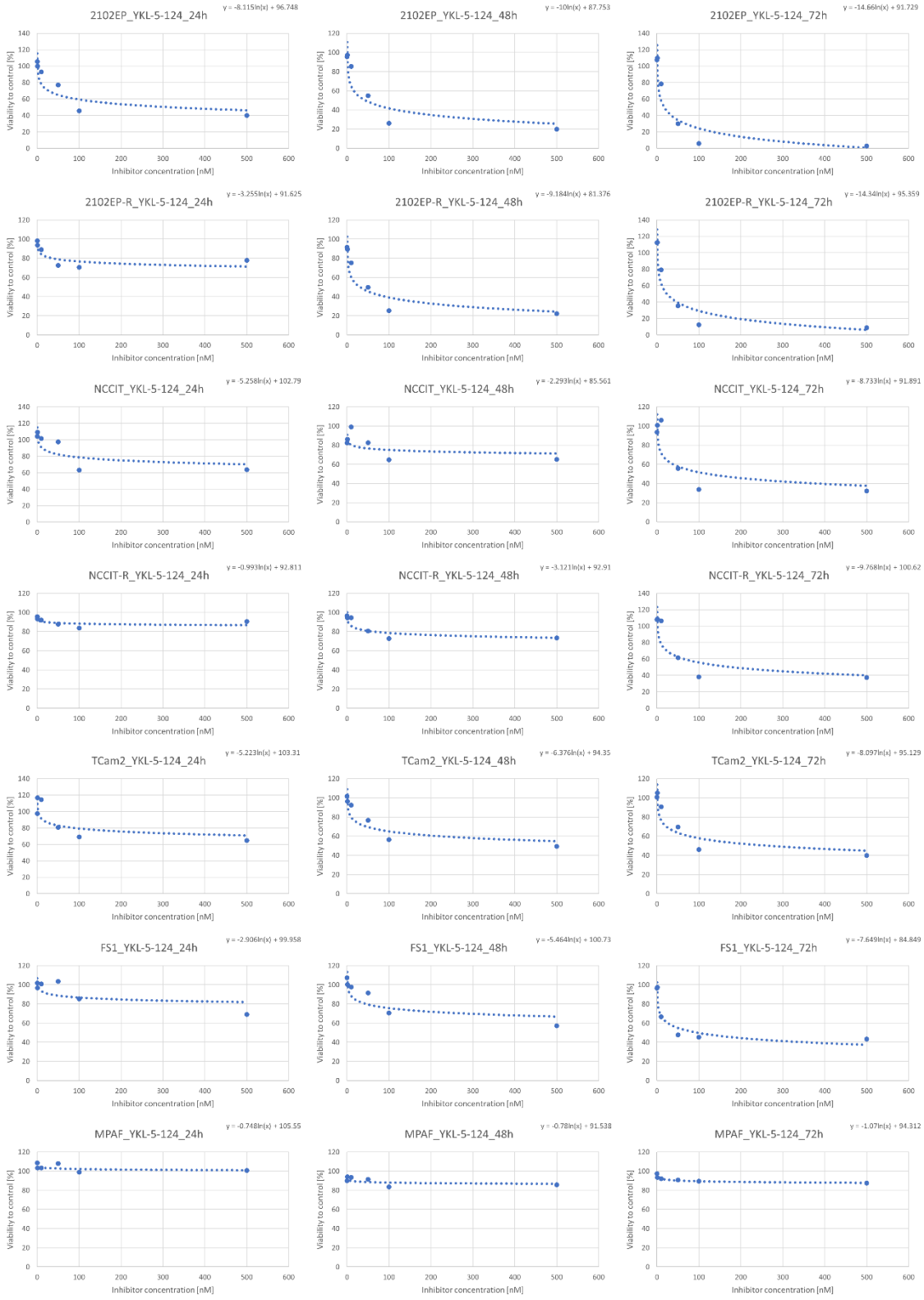

Appendix Figure 3: Application of logarithmic regression model on XTT viability assay generated data (Figure 8) for calculation of YKL-5-124 IC50 values. Reprinted from [1].

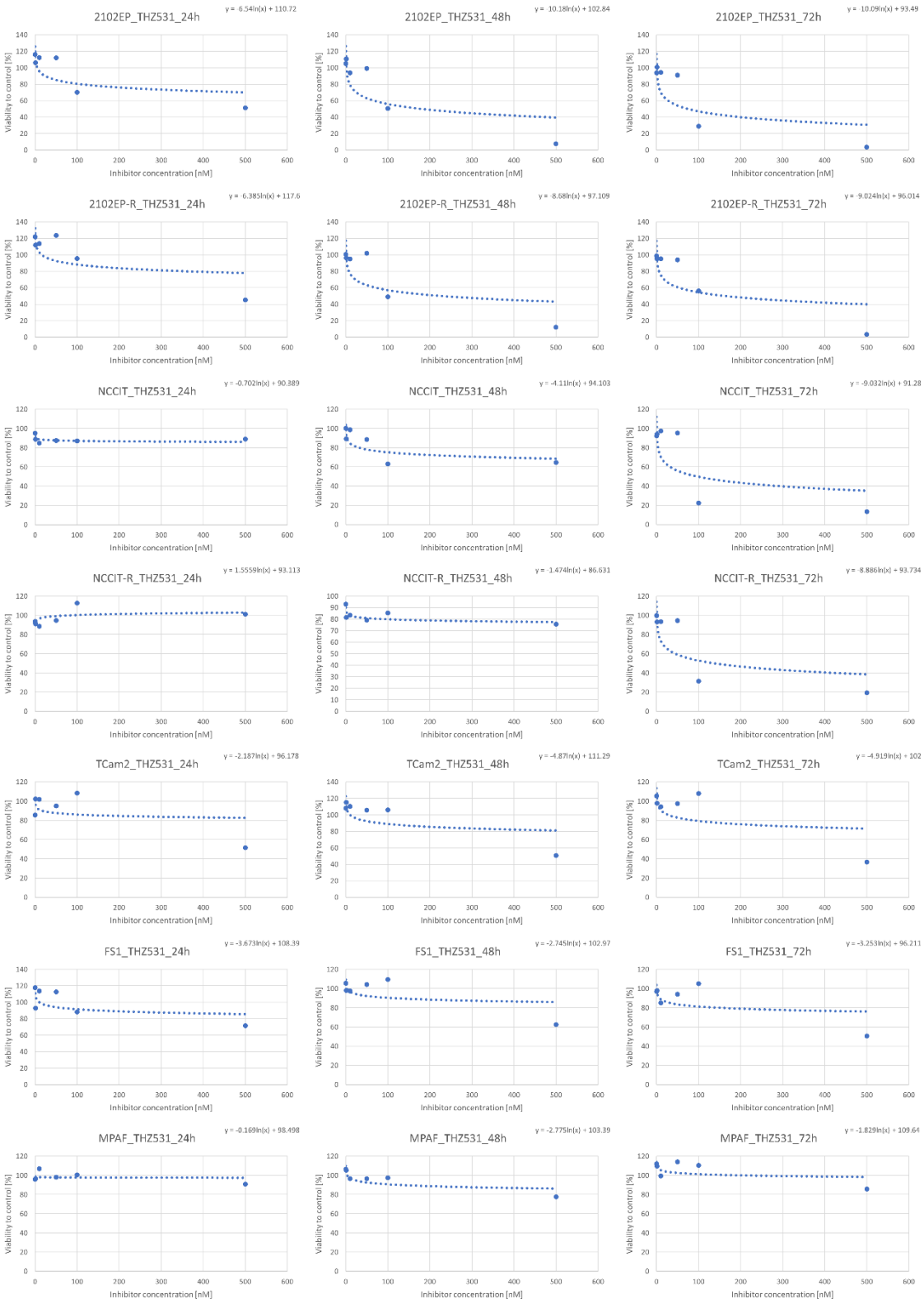

Appendix Figure 4: Application of logarithmic regression model on XTT viability assay generated data (Figure 8) for calculation of THZ531 IC50 values. Reprinted from [1].

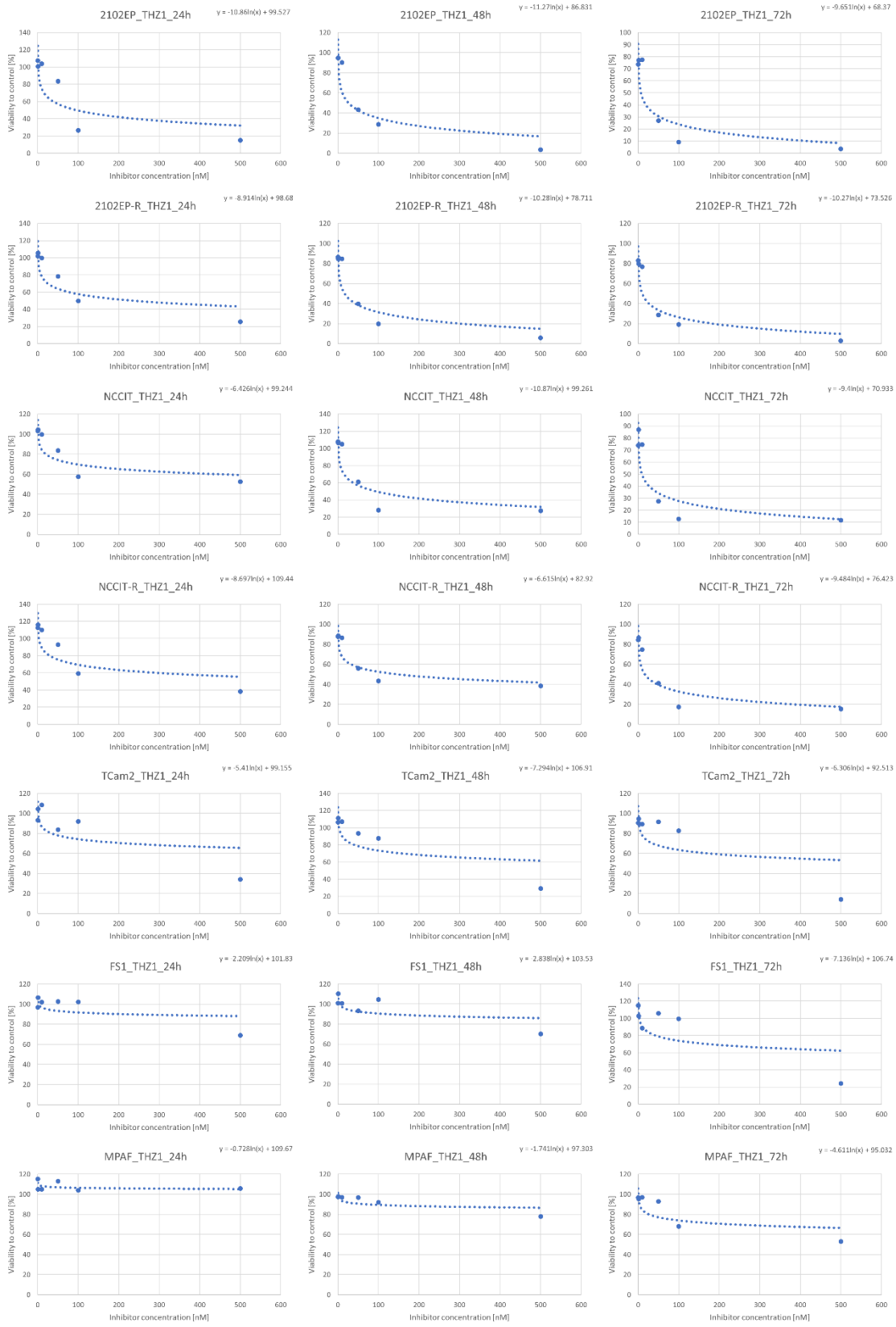

Appendix Figure 5: Application of logarithmic regression model on XTT viability assay generated data (Figure 9) for calculation of THZ1 IC50 values. Reprinted from [1].

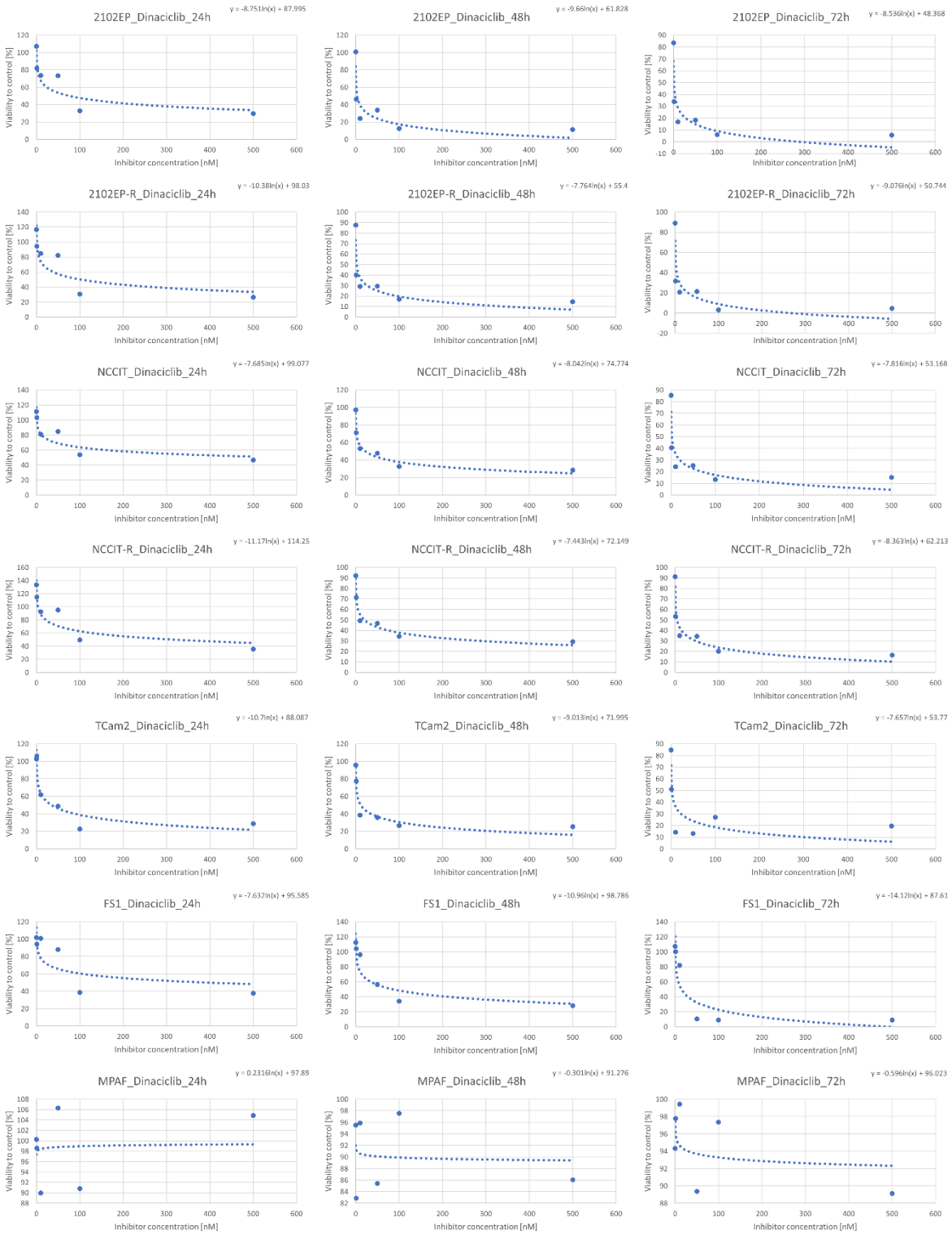

Appendix Figure 6: Application of logarithmic regression model on XTT viability assay generated data (Figure 9) for calculation of Dinaciclib IC50 values. Reprinted from [1].

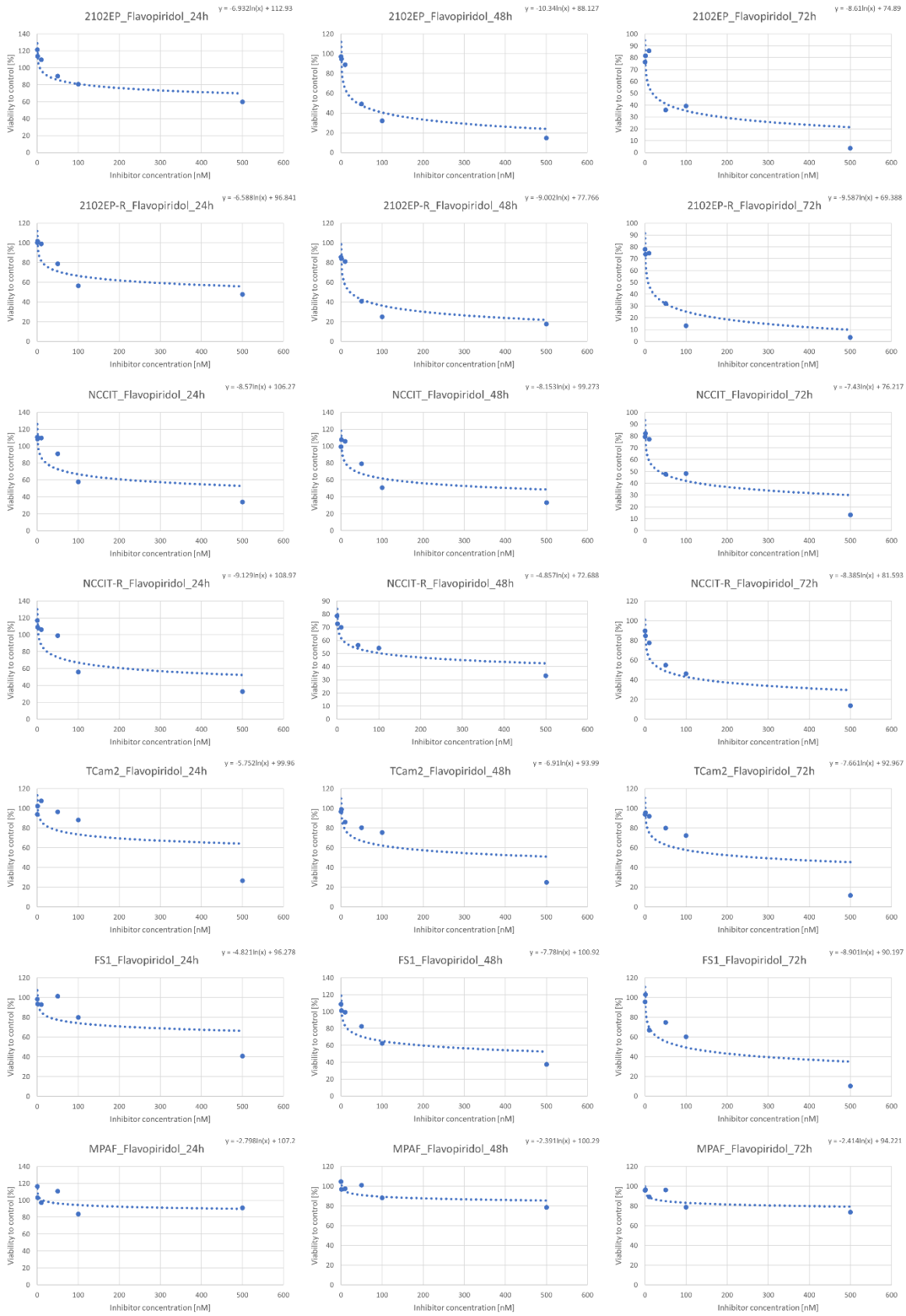

Appendix Figure 7: Application of logarithmic regression model on XTT viability assay generated data (Figure 9) for calculation of Flavopiridol IC50 values. Reprinted from [1].

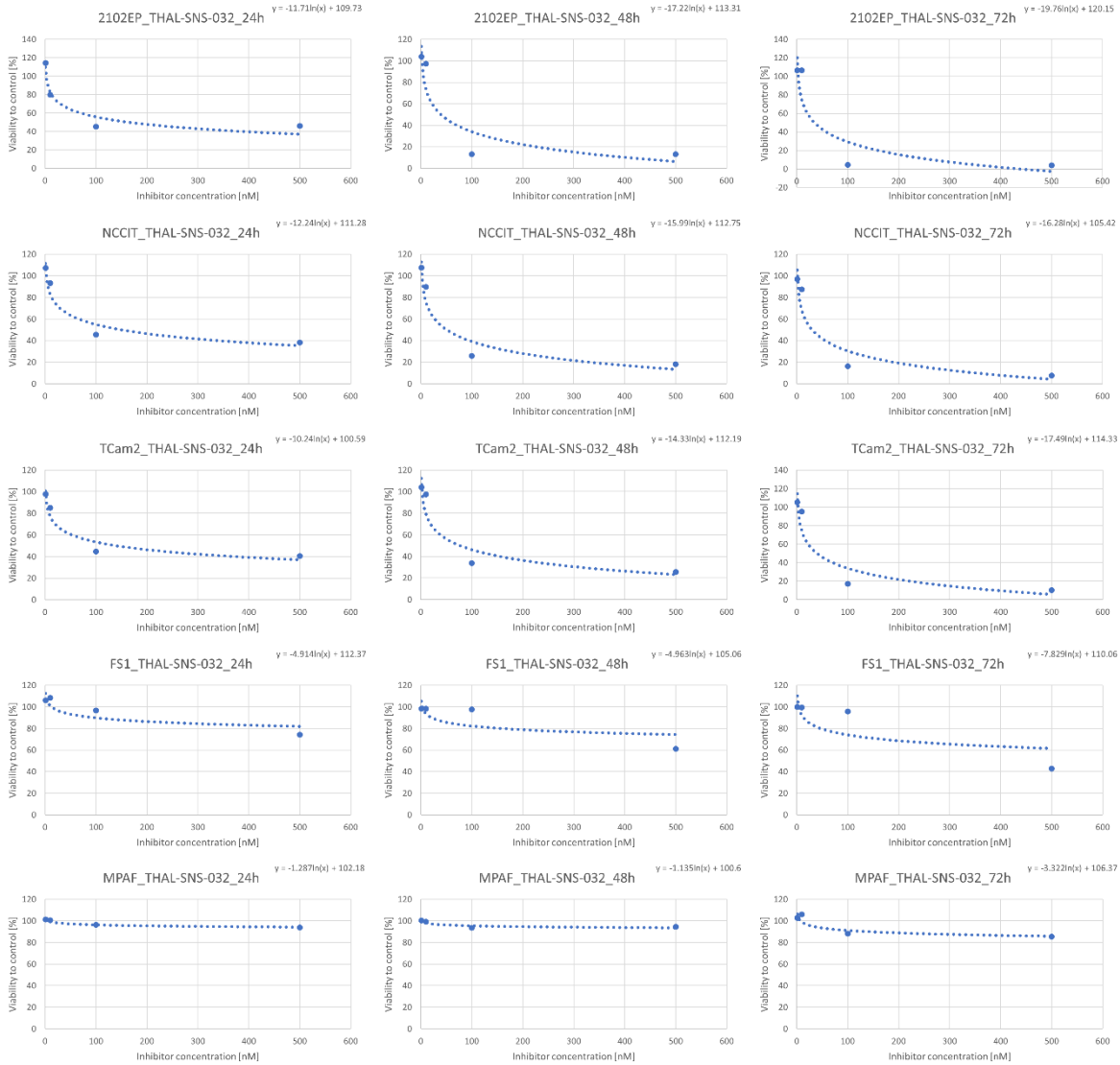

Appendix Figure 8: Application of logarithmic regression model on XTT viability assay generated data (Figure 9) for calculation of THAL-SNS-032 IC50 values. Reprinted from [1].

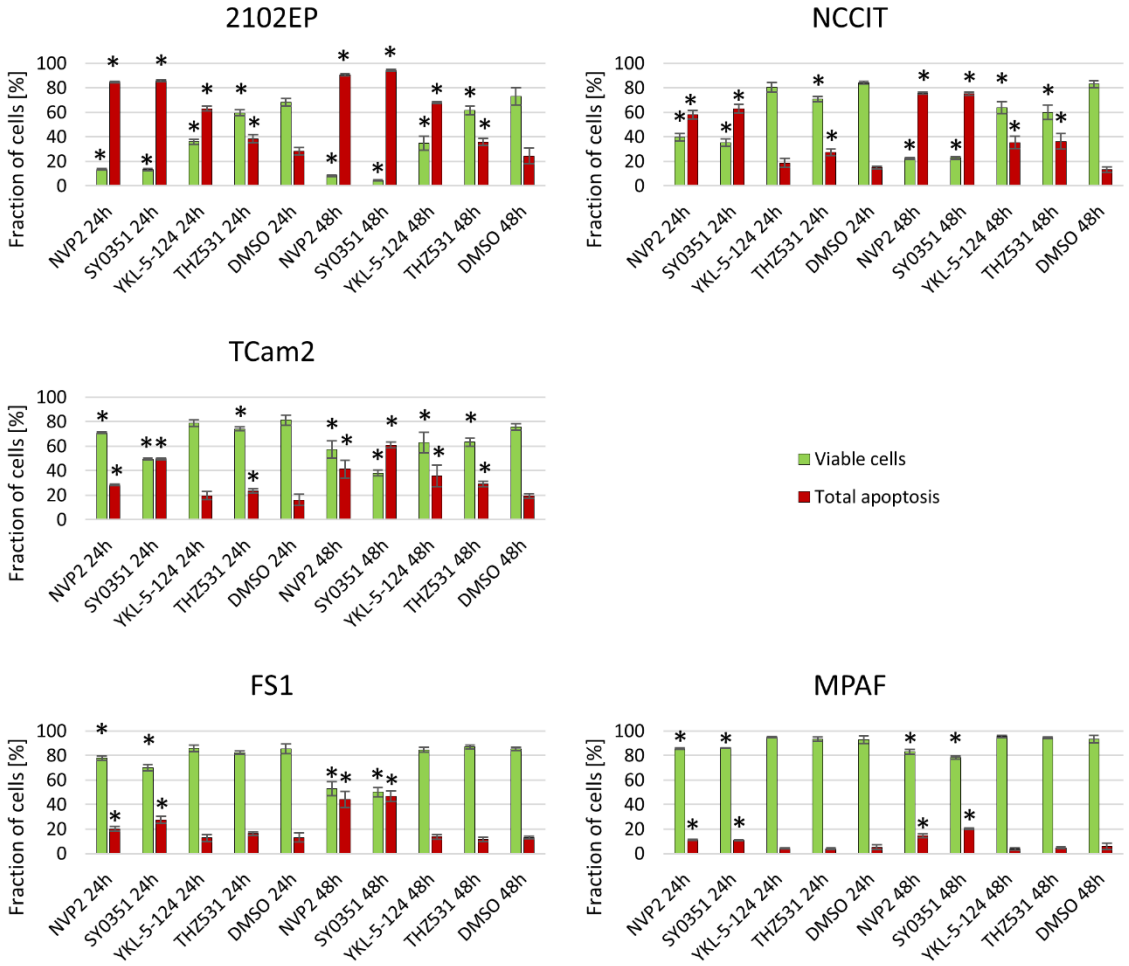

Appendix Figure 9: FACS-based apoptosis analysis of TGCT and control cells. Modified from [1]. 2102EP, NCCIT, TCam2, FS1 and MPAF cells were treated with CDK inhibitors (NVP2/SY0351: 10 nM; YKL-5-124/THZ531: 100 nM) or DMSO control (0.0002%) for 24 h and 48 h. For detection of apoptotic and viable cells 7AAD/PE AnnexinV FACS analysis was performed. Significance was calculated by comparing the treated samples to the control sample using the two-tailed student's t-test. Asterisks indicate significant difference (* $p<0.05$). *n*=3-6.

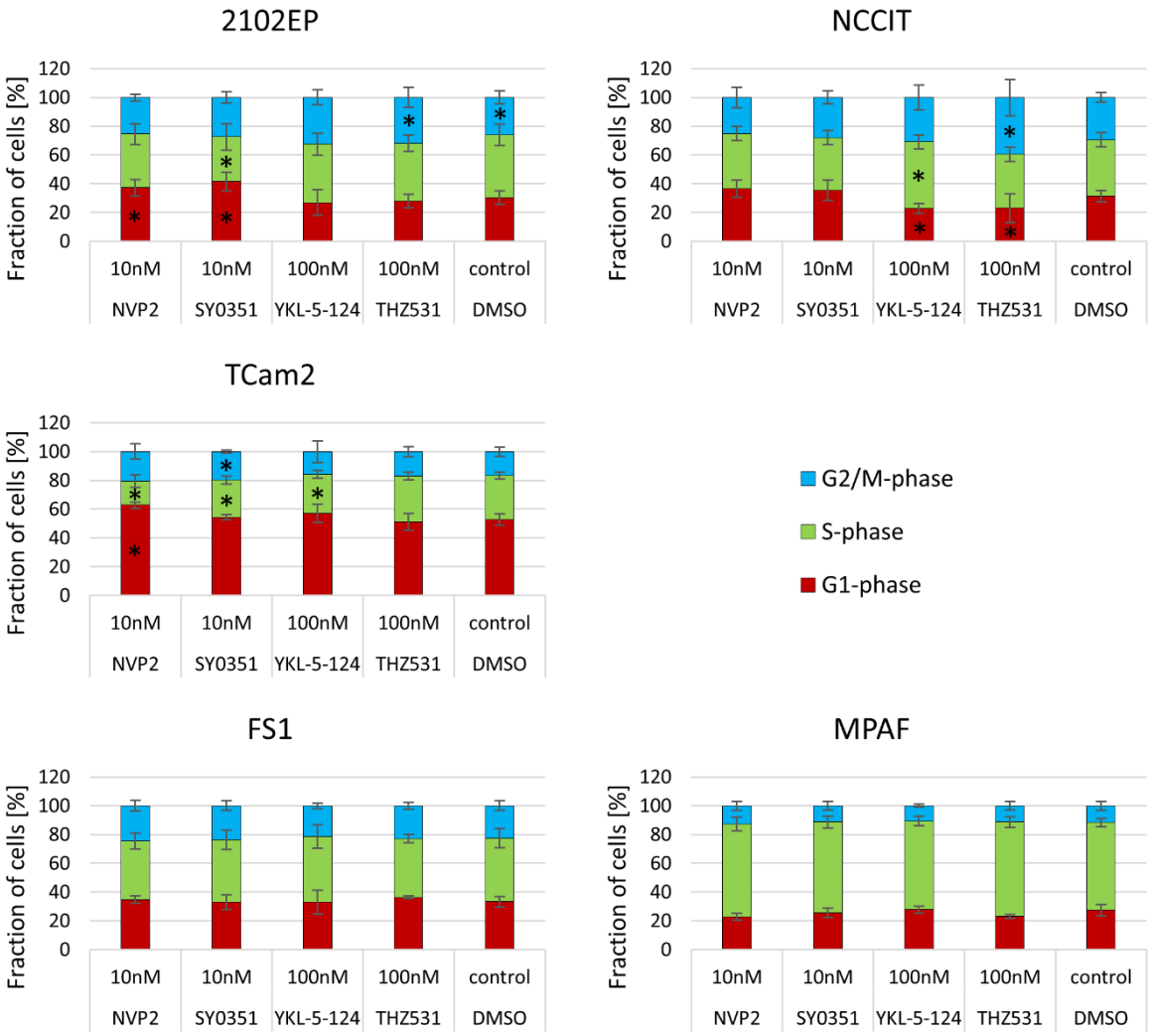

Appendix Figure 10: FACS-based cell cycle analysis of TGCT and control cells. Modified from [1]. 2102EP, NCCIT, TCam2, FS1 and MPAF cells were treated with CDK inhibitors or DMSO control (0.0002%) for 20 h. Hoechst-33342 based FACS analysis was performed to detect DNA content, indicating cell cycle phase. Significance was calculated by comparing each treated cell fraction to the corresponding control sample cell fraction using the two-tailed student's t-test. Asterisks indicate significant difference (* $p<0.05$). *n*=3-6.

Appendix Table 1: List of candidate genes for cisplatin resistance. Reprinted from [2]. A genome scale CRIPR/Cas9 based activation screen in 2102EP and JAR cells revealed candidate genes responsible for cisplatin resistance (read count >10000).

Activation Screen (MPHv2SAMv2) – Candidate Genes								
2102EP			JAR					
Rank	Gene name	read counts	Rank	Gene name	read counts	Rank	Gene name	read counts
1	TRAP1	8044032	1	CYP2R1	4248699	36	TRAP1	36686
2	TK1	7803883	2	LEKR1	4084952	37	OR8B3	36487
3	DDB1	6841409	3	CCL1	2230750	38	TK1	34429
4	ENSA	1590607	4	LHB	1223512	39	ARAF	30934
5	IFNW1	656648	5	WBP2NL	1066313	40	NAT14	30356
6	AKT3	531280	6	OR2W1	331952	41	NT5C3A	29223
7	PIR	499632	7	PLEKHF1	307083	42	KLK5	28747
8	AK1	496415	8	NAE1	179370	43	ING1	28599
9	KIF27	489821	9	CLDND2	171947	44	SGOL2	28571
10	GMNC	483723	10	ANGPTL1	167831	45	APOM	27737
11	CYP27A1	478347	11	CELF1	164345	46	DDB1	27734
12	PERP	462899	12	SOAT1	106411	47	CDC37	26990
13	MGAT4A	458608	13	AGPAT2	105646	48	SNRK	26934
14	ZC3H14	420023	14	EFR3B	95494	49	PAPD5	24778
15	CLEC2D	413240	15	TLCD1	94701	50	FBXO18	24447
16	DPP10	374926	16	KCNJ12	92110	51	NUP133	23166
17	C17orf103	359665	17	ALDH3B1	89330	52	ZNF676	20759
18	DDX10	295925	18	MDN1	87298	53	RHOBTB1	20123
19	KLHL36	230245	19	ALKBH3	81611	54	LOC441155	19573
20	SPDYC	224181	20	RNF165	76285	55	UNC79	19160
21	PP2D1	204439	21	CRY2	73850	56	SVOPL	18118
22	MTRNR2L6	186447	22	IRF2BP2	56826	57	OR6C1	17054
23	MTMR11	172159	23	CASC10	53587	58	LRRC43	16162
24	DNAJB6	149516	24	NPIPA7	53418	59	GPD2	13226
25	GCC1	125790	25	LEPROTL1	53049	60	EEF2K	13037
26	FAM115A	124352	26	CALCOCO2	50726	61	TGIF1	12622
			27	SCAND1	49872	62	BMF	12391
			28	RUNX1	48367	63	IGSF10	12082
			29	FADS1	45803	64	PHGR1	12035
			30	POLE4	43866	65	DHRS12	11884
			31	CPT1C	42620	66	C1orf189	11776
			32	ITSN1	42605	67	CEP350	11669
			33	ANK1	40835	68	LDLRAD4	11262
			34	HTR3E	40078	69	HESX1	11134
			35	KRT71	36909	70	USP6NL	10717

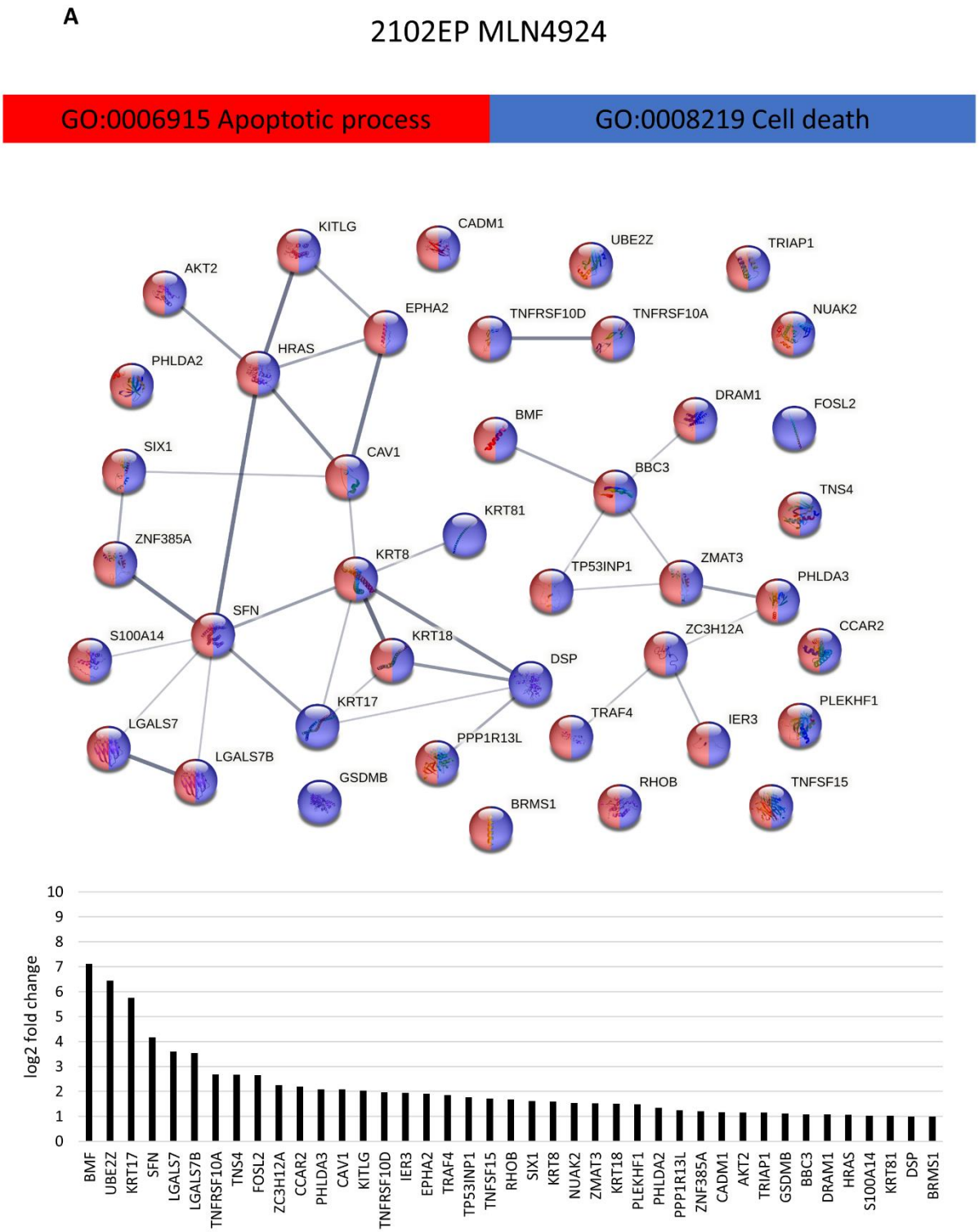

Appendix Figure 11: Comprehensive overview of all differentially upregulated genes associated with apoptosis and cell death after neddylation inhibition and cisplatin treatment in 2102EP cells. Reprinted from [2]. STRING interaction network with all connected and non-connected genes involved in apoptosis and cell death (GO analysis) as well as corresponding log2 fold changes of differentially upregulated genes. 3'mRNA sequencing was performed 48 h after (**A**) MLN4924 (0.25 µM), (**B**) cisplatin (2.5 µM) and (**C**) MLN4924/cisplatin combination (0.25 µM/2.5 µM) treatment. *n*=3.

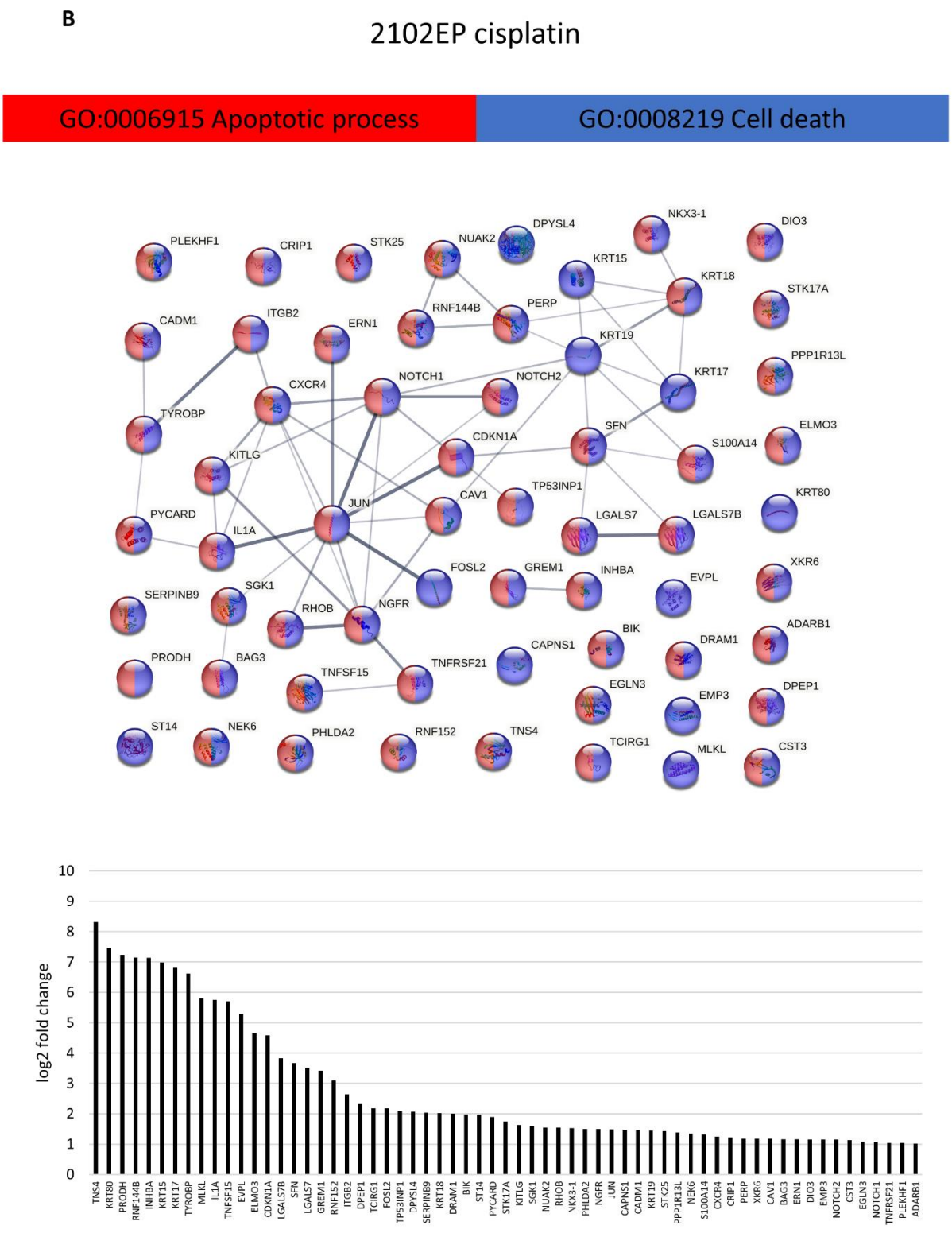

Appendix Figure 11: Comprehensive overview of all differentially upregulated genes associated with apoptosis and cell death after neddylation inhibition and cisplatin treatment in 2102EP cells. Reprinted from [2]. STRING interaction network with all connected and non-connected genes involved in apoptosis and cell death (GO analysis) as well as corresponding log2 fold changes of differentially upregulated genes. 3'mRNA sequencing was performed 48 h after (**A**) MLN4924 (0.25 µM), (**B**) cisplatin (2.5 µM) and (**C**) MLN4924/cisplatin combination (0.25 µM/2.5 µM) treatment. *n*=3.

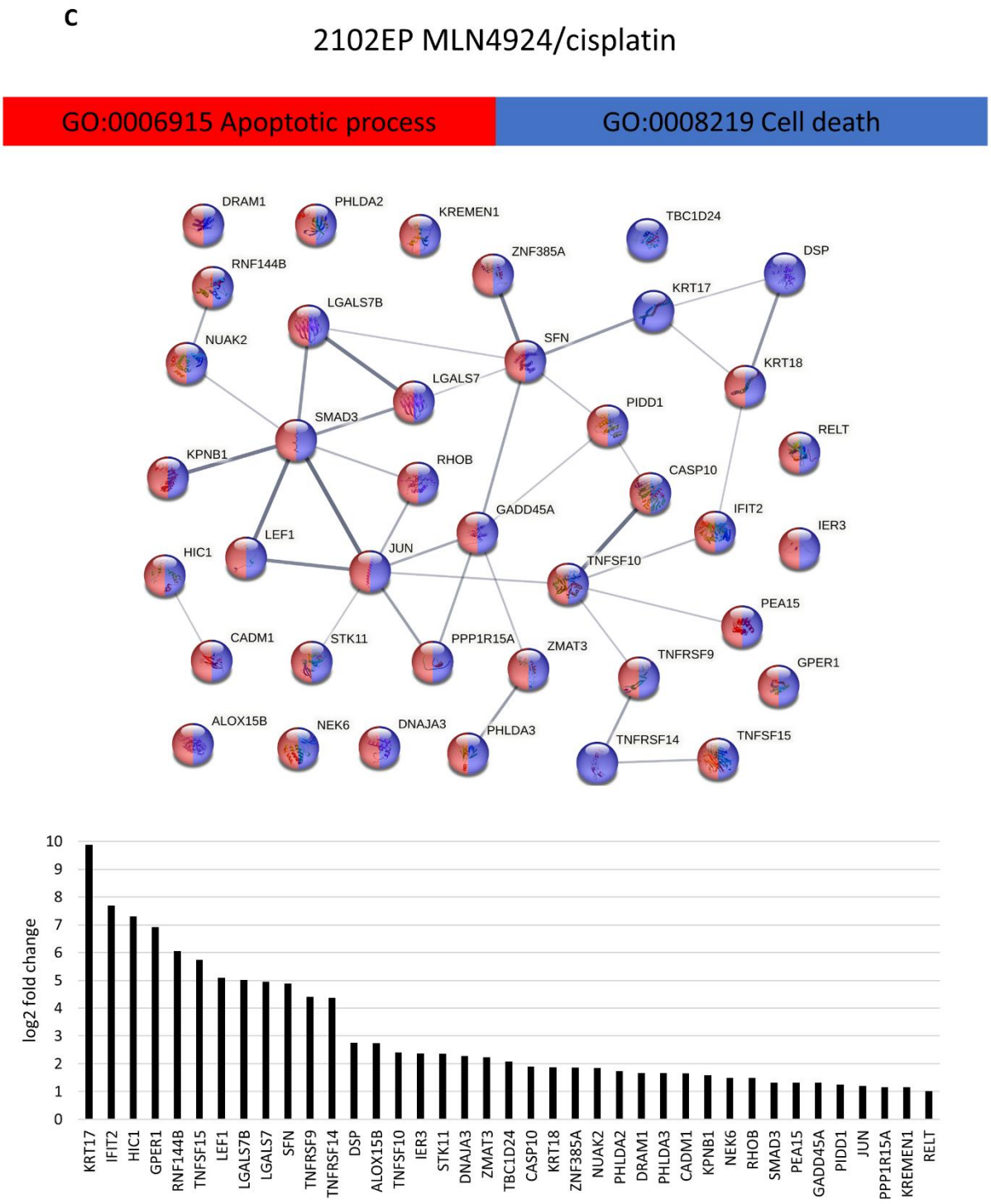

Appendix Figure 11: Comprehensive overview of all differentially upregulated genes associated with apoptosis and cell death after neddylation inhibition and cisplatin treatment in 2102EP cells. Reprinted from [2]. STRING interaction network with all connected and non-connected genes involved in apoptosis and cell death (GO analysis) as well as corresponding log2 fold changes of differentially upregulated genes. 3'mRNA sequencing was performed 48 h after (**A**) MLN4924 (0.25 µM), (**B**) cisplatin (2.5 µM) and (**C**) MLN4924/cisplatin combination (0.25 µM/2.5 µM) treatment. *n*=3.

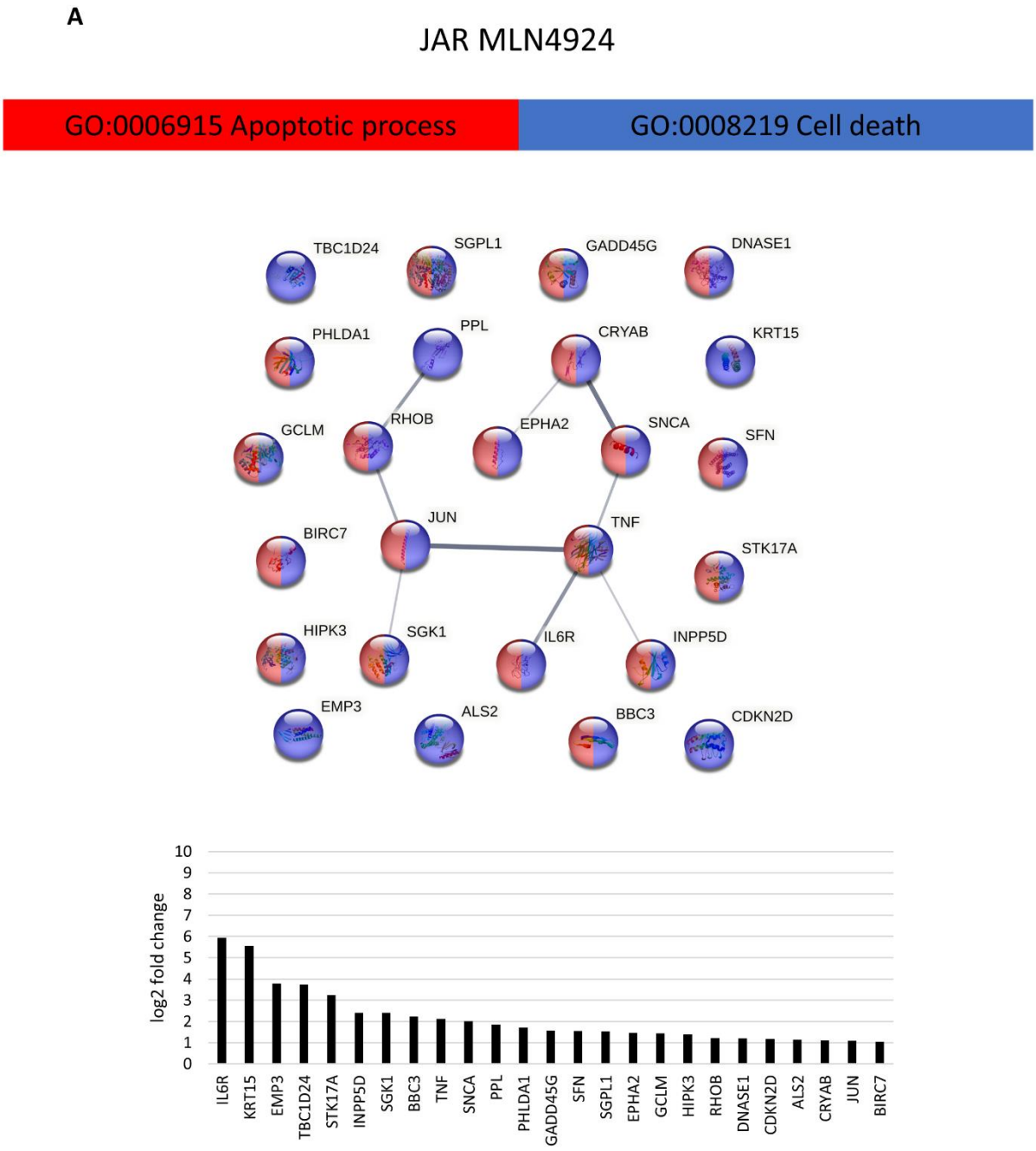

Appendix Figure 12: Comprehensive overview of all differentially upregulated genes associated with apoptosis and cell death after neddylation inhibition and cisplatin treatment in JAR cells. Reprinted from [2]. STRING interaction network with all connected and non-connected genes involved in apoptosis and cell death (GO analysis) as well as corresponding log2 fold changes of differentially upregulated genes. 3'mRNA sequencing was performed 48 h after (**A**) MLN4924 (1 µM), (**B**) cisplatin (4 µM) and (**C**) MLN4924/cisplatin combination (1 µM/4 µM) treatment. *n*=3.

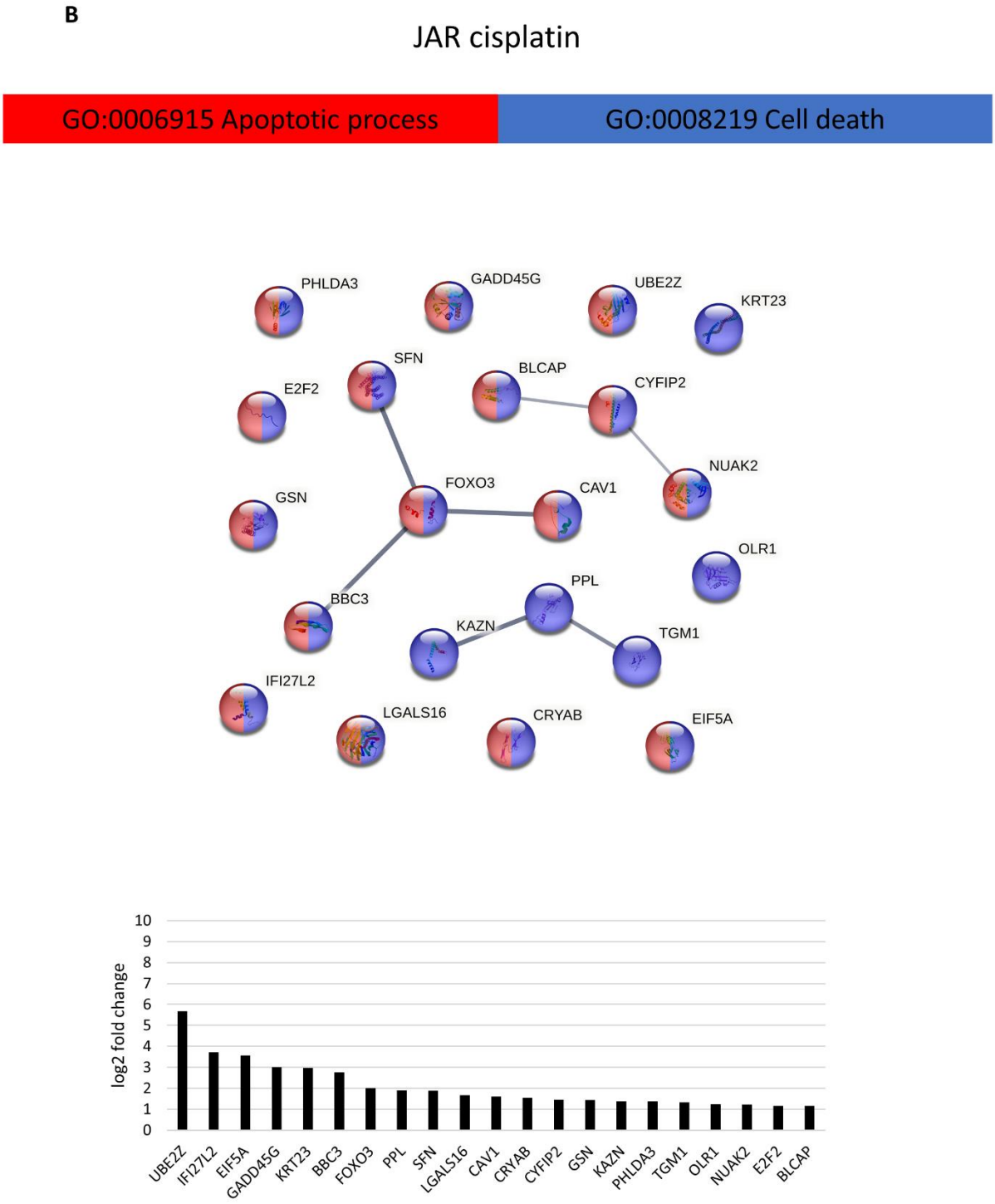

Appendix Figure 12: Comprehensive overview of all differentially upregulated genes associated with apoptosis and cell death after neddylation inhibition and cisplatin treatment in JAR cells. Reprinted from [2]. STRING interaction network with all connected and non-connected genes involved in apoptosis and cell death (GO analysis) as well as corresponding log2 fold changes of differentially upregulated genes. 3'mRNA sequencing was performed 48 h after (**A**) MLN4924 (1 µM), (**B**) cisplatin (4 µM) and (**C**) MLN4924/cisplatin combination (1 µM/4 µM) treatment. *n*=3.

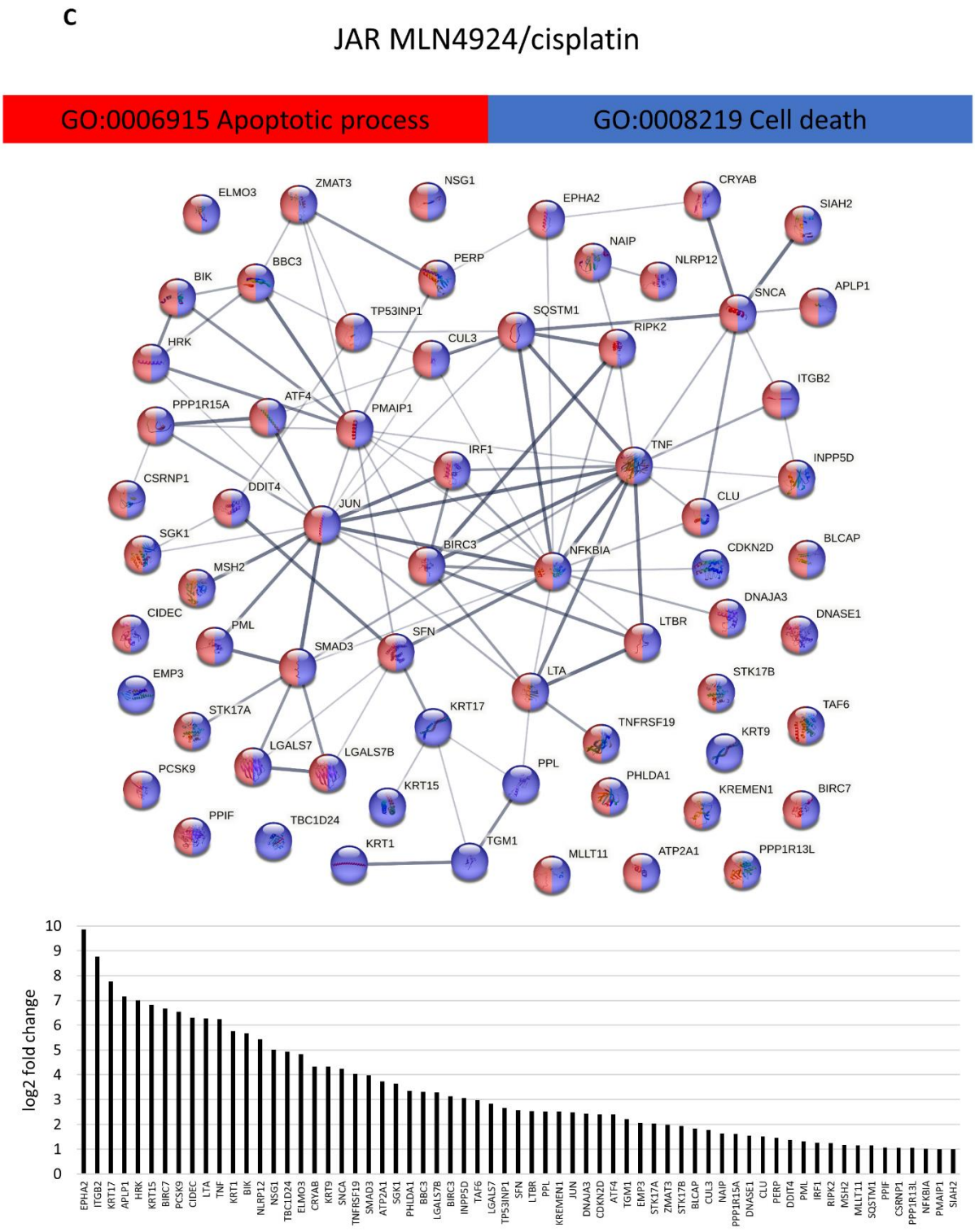

Appendix Figure 12: Comprehensive overview of all differentially upregulated genes associated with apoptosis and cell death after neddylation inhibition and cisplatin treatment in JAR cells. Reprinted from [2]. STRING interaction network with all connected and non-connected genes involved in apoptosis and cell death (GO analysis) as well as corresponding log2 fold changes of differentially upregulated genes. 3'mRNA sequencing was performed 48 h after (**A**) MLN4924 (1 µM), (**B**) cisplatin (4 µM) and (**C**) MLN4924/cisplatin combination (1 µM/4 µM) treatment. *n*=3.

A

2102EP MLN4924

GO:0030154 Cell differentiation

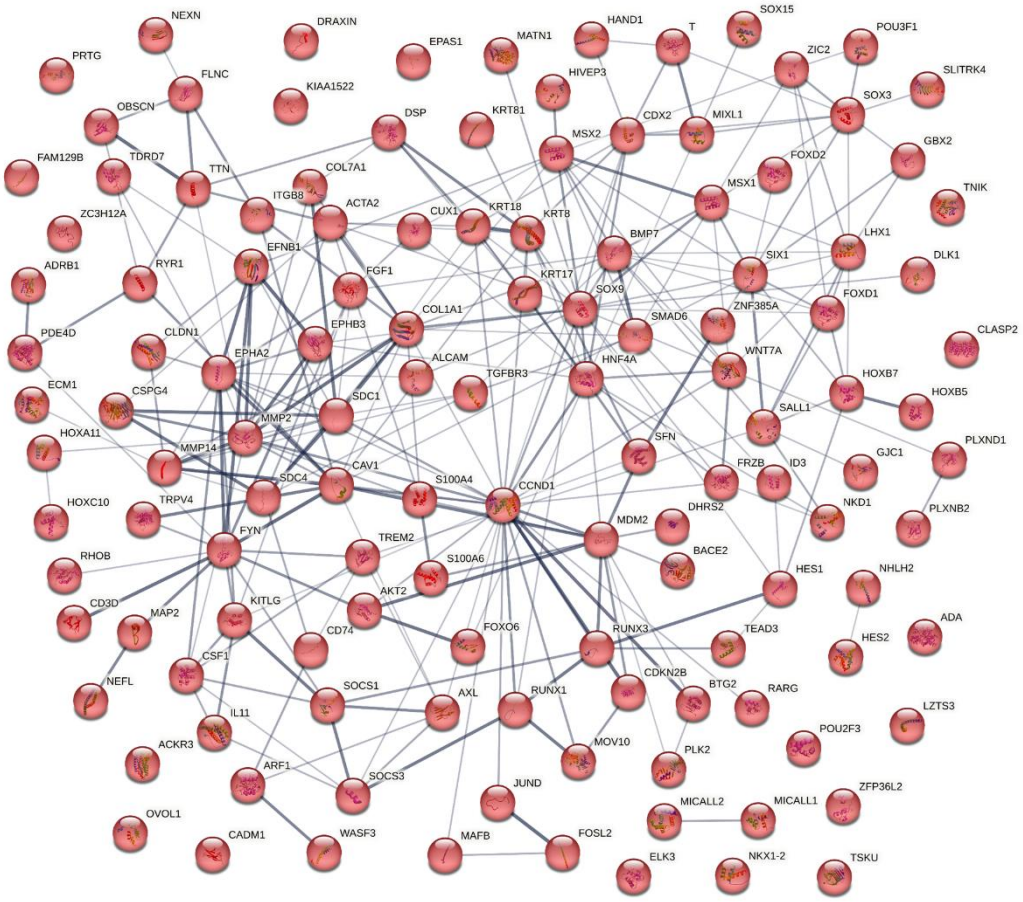

Appendix Figure 13: Comprehensive overview of all differentially upregulated genes associated with cell differentiation after neddylation inhibition and cisplatin treatment in 2102EP cells. Reprinted from [2]. STRING interaction network with all connected and non-connected genes involved in cell differentiation (GO analysis). 3'mRNA sequencing was performed 48 h after (**A**) MLN4924 (0.25 µM), (**B**) cisplatin (2.5 µM) and (**C**) MLN4924/cisplatin combination (0.25 µM/2.5 µM) treatment. *n*=3.

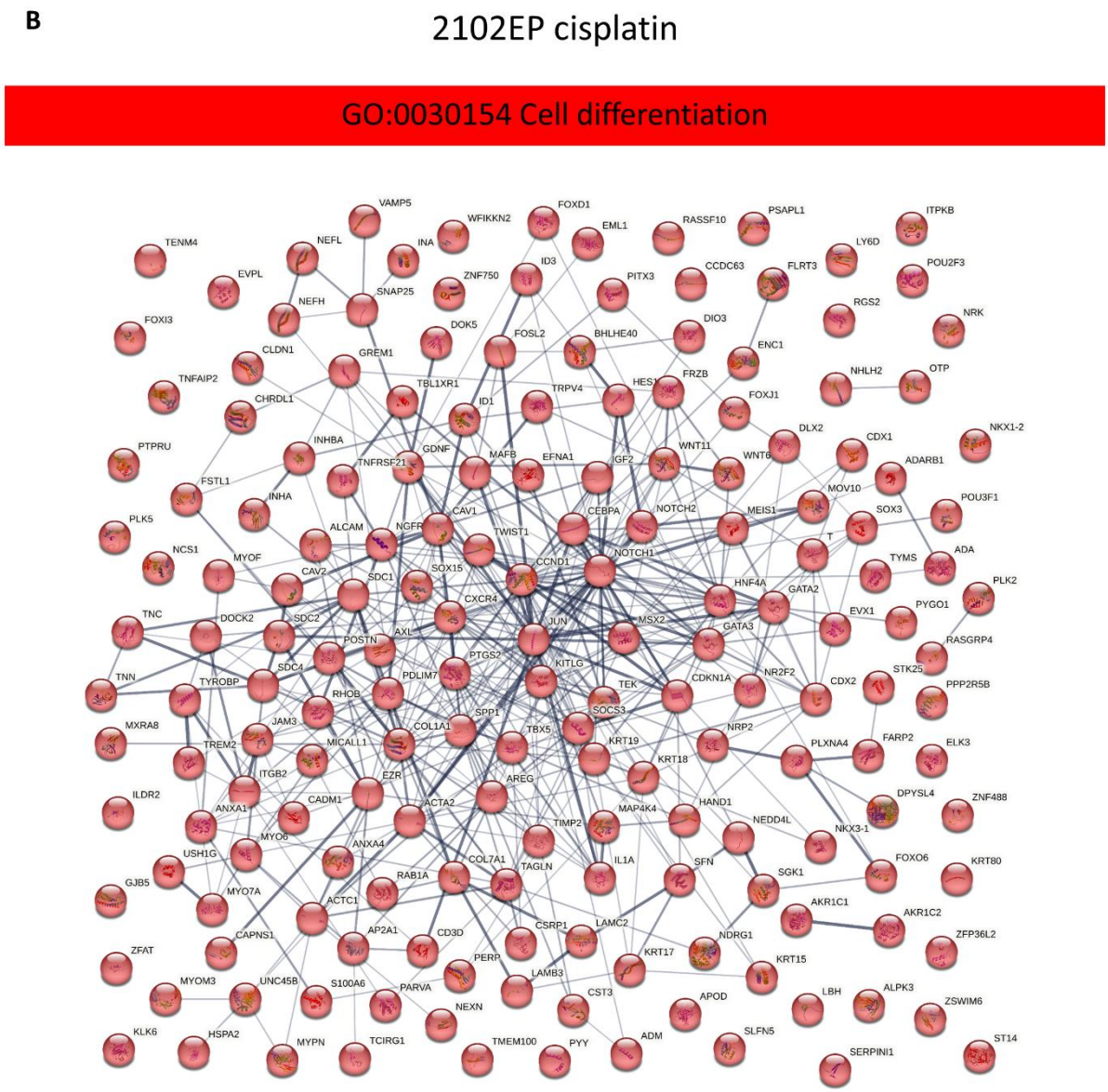

Appendix Figure 13: Comprehensive overview of all differentially upregulated genes associated with cell differentiation after neddylation inhibition and cisplatin treatment in 2102EP cells. Reprinted from [2]. STRING interaction network with all connected and non-connected genes involved in cell differentiation (GO analysis). 3'mRNA sequencing was performed 48 h after (**A**) MLN4924 (0.25 µM), (**B**) cisplatin (2.5 µM) and (**C**) MLN4924/cisplatin combination (0.25 µM/2.5 µM) treatment. *n*=3.

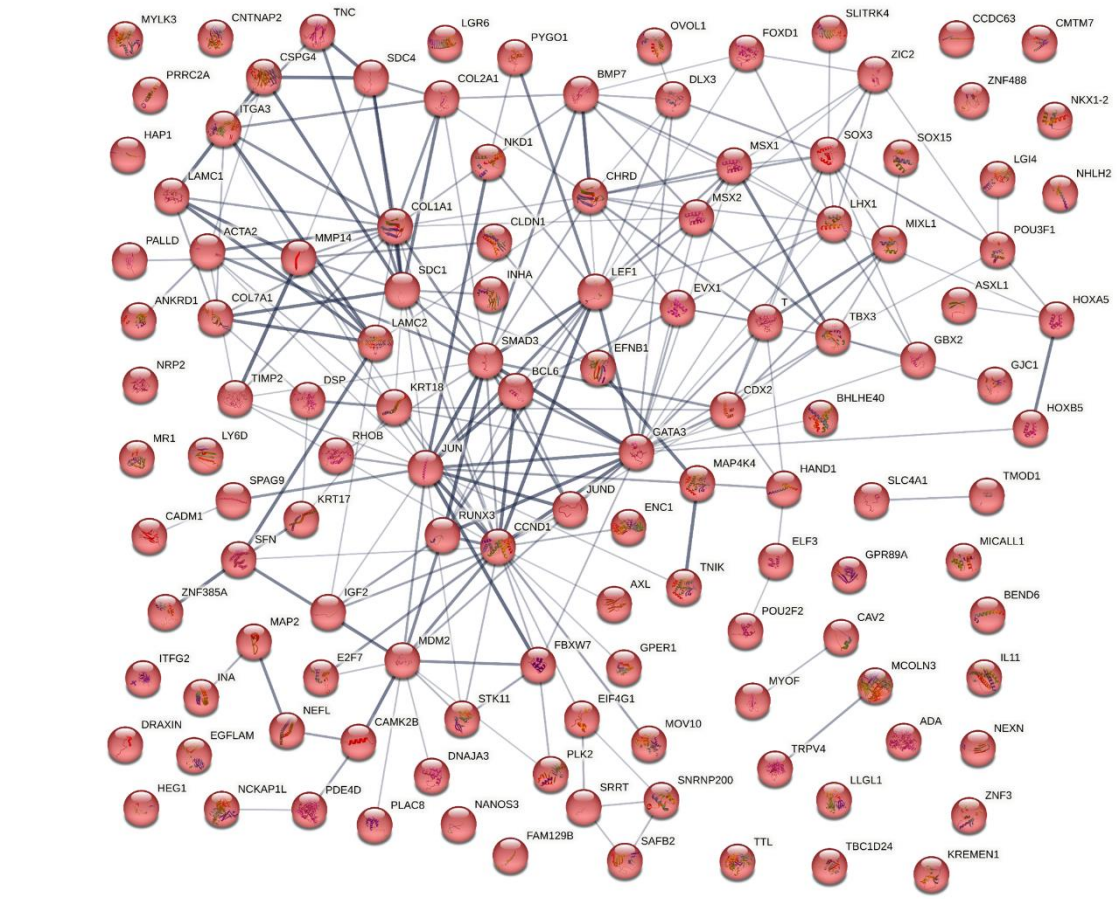

Appendix Figure 13: Comprehensive overview of all differentially upregulated genes associated with cell differentiation after neddylation inhibition and cisplatin treatment in 2102EP cells. Reprinted from [2]. STRING interaction network with all connected and non-connected genes involved in cell differentiation (GO analysis). 3'mRNA sequencing was performed 48 h after (**A**) MLN4924 (0.25 µM), (**B**) cisplatin (2.5 µM) and (**C**) MLN4924/cisplatin combination (0.25 µM/2.5 µM) treatment. *n*=3.

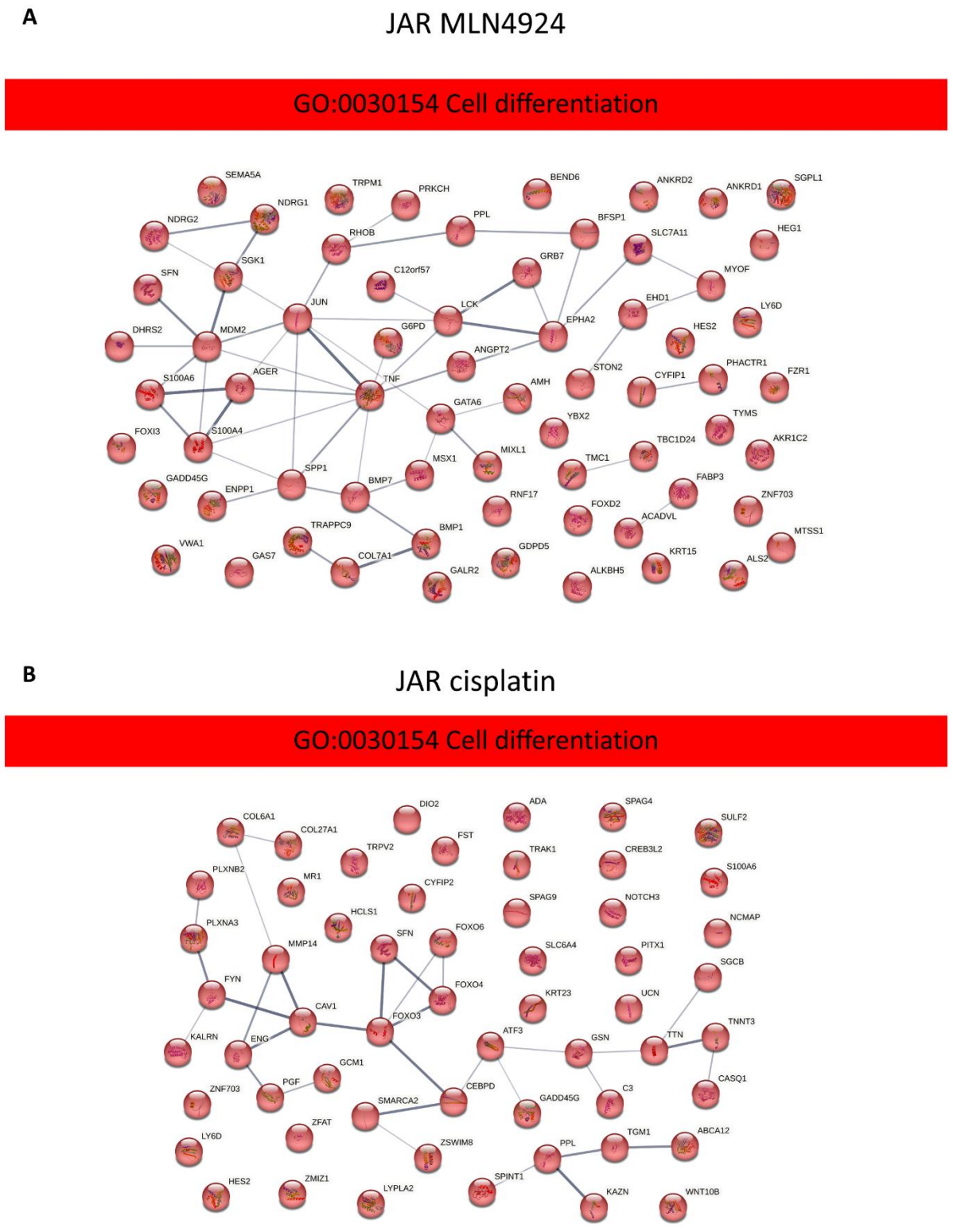

Appendix Figure 14: Comprehensive overview of all differentially upregulated genes associated with cell differentiation after neddylation inhibition and cisplatin treatment in JAR cells. Reprinted from [2]. STRING interaction network with all connected and non-connected genes involved in cell differentiation (GO analysis). 3'mRNA sequencing was performed 48 h after (**A**) MLN4924 (1 µM), (**B**) cisplatin (4 µM) and (**C**) MLN4924/cisplatin combination (1 µM/4 µM) treatment. *n*=3.

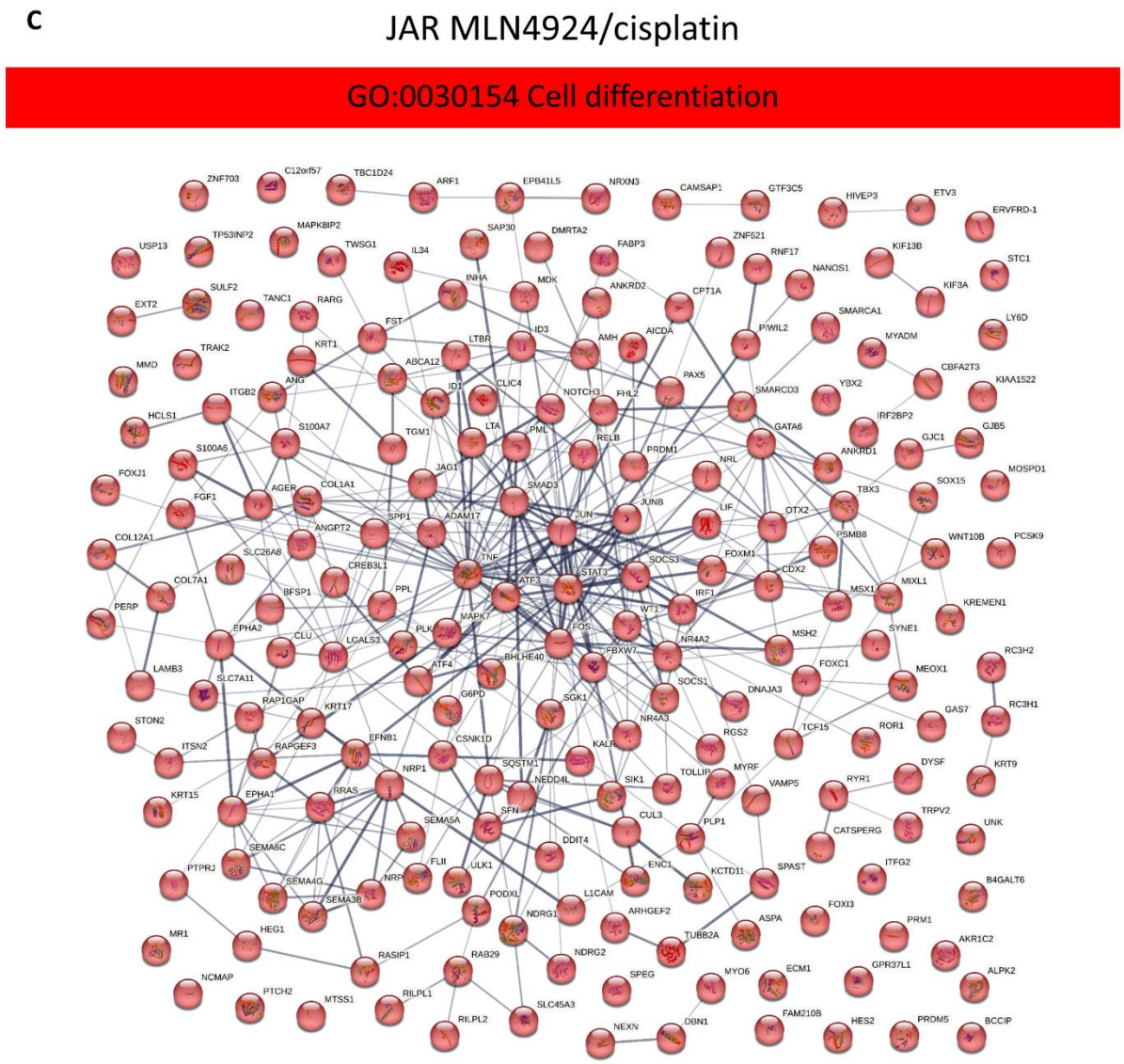

Appendix Figure 14: Comprehensive overview of all differentially upregulated genes associated with cell differentiation after neddylation inhibition and cisplatin treatment in JAR cells. Reprinted from [2]. STRING interaction network with all connected and non-connected genes involved in cell differentiation (GO analysis). 3'mRNA sequencing was performed 48 h after (**A**) MLN4924 (1 µM), (**B**) cisplatin (4 µM) and (**C**) MLN4924/cisplatin combination (1 µM/4 µM) treatment. *n*=3.

8. Acknowledgements

Am Ende dieser Arbeit möchte ich gerne „Danke“ sagen. Es gibt einige Menschen, die mich auf verschiedenste Art und Weise auf meinem Weg als Doktorand unterstützt und begleitet haben.

Zu allererst möchte ich mich bei meinem Doktorvater Prof. Dr. Hubert Schorle bedanken, der mir zunächst die Möglichkeit gab in seiner Arbeitsgruppe meine Masterarbeit anzufertigen und mir danach anbot für meine Promotion zu bleiben. Er hat mich während dieser Zeit nicht nur fachlich gefördert und vorangebracht, sondern war auch in persönlicher Hinsicht ein Mentor mich, der mich bei wichtigen Entscheidungen, wie zum Beispiel meiner weiteren Karriereplanung unglaublich unterstützt hat.

Weiterhin möchte ich Herrn Prof. Dr. Oliver Gruß, Herrn PD. Dr. Reinhard Bauer und Prof. Dr. Matthias Geyer als Mitglieder meiner Promotionskommission danken.

Ein besonderer Dank gilt auch Dr. Simon Schneider, der immer ein offenes Ohr für mich hatte und mir sowohl fachlich als auch persönlich mit Rat und Tat zur Seite stand. Besonders möchte ich mich für das Korrekturlesen meiner Dissertation bedanken.

Ich möchte außerdem meine ehemaligen und derzeitigen Kollegen aus der AG Schorle (Gaby Beine, Dr. Sina Jostes, Dr. Simon Schneider, Dr. Jan Langkabel, Gina Merges, Dr. Lena Arévalo, Aylin Hansen, Andjela Kovacevic, Christoph Wiesejahn, Andrea Jäger, Angela Egert) erwähnen. Ich danke euch allen von Herzen für eine unglaublich schöne Zeit und eine freundschaftliche Atmosphäre in der ich mich wohlfühlen konnte. Ich erinnere mich immer gerne an die gemeinsamen Laborausflüge, Mittagessen und Gespräche zurück.

Auch unseren Kollaborationspartnern Prof. Dr. Daniel Nettersheim, Prof. Dr. Valentin Stein, Prof. Dr. Matthias Geyer, Dr. Robert Düster und Dr. Ulf Einsfelder möchte ich für den regen wissenschaftlicheren Austausch sowie für die gute Zusammenarbeit danken.

Zuletzt danke ich meiner Familie, insbesondere meinen Eltern und meiner Partnerin für Ihre fortwährende und bedingungslose Unterstützung. Ohne Euch hätte ich es niemals bis hierhin geschafft.